ADAPTIVE CONTROL TO REDUCE THE DYNAMIC RESPONSE OF BRIDGES CONSIDERING PARAMETRIC CHANGES

A Dissertation

by

RACHEL WYSARD SOARES

Submitted to the Office of Graduate and Professional Studies of
Texas A&M University
in partial fulfillment of the requirements for the degree of

DOCTOR OF PHILOSOPHY

Chair of Committee,	Luciana R. Barroso
Committee Members,	Mary Beth Hueste
	John Niedzwecki
	Alan Palazzolo
Head of Department,	Robin Autenrieth

August 2019

Major Subject: Civil Engineering

ABSTRACT

Parametric variations occur throughout bridges service life as a result of temperature fluctuations, cracking, localized damage and fatigue. Likewise, bridges parameters are difficult to estimate precisely; implemented control schemes may perform unsatisfactorily depending on their sensitivity to parametric changes. Adaptive control may present an alternative to control bridge structures, as adaptive schemes are able to calculate control gains that vary over time based on sensed responses. As a result, adaptive control strategies are able to sustain performance and deal with parametric variations. In this research, adaptive control schemes are developed and implemented to control bridges considering different types of structural configurations. The controllers' ability in mitigating excessive seismic response and sustaining performance, the sensitivity of structural configuration and modeling considerations for control design and implementation on bridge structures are investigated. Initially, an adaptive control approach is developed to control two different highway bridges having as main control algorithm the simple adaptive control strategy. As a preliminary investigation, the control scheme is implemented and designed aiming to mitigate seismic responses of a three-span highway bridge considering realistic implementation and operation conditions. Following the initial investigation, a parametric study is conducted considering a two-span skewed highway bridge in order to assess the robustness of the control approach. Sequentially, adaptive semi-active control schemes are developed to control a cable-stayed bridge having as main control algorithms the simple adaptive control and the neuro-fuzzy control strategies. The bridge is subjected to

parametric changes in order to assess the robustness of the control approaches. The effects of multi-support excitation with different angles of incidence are investigated. Lastly, earthquake records matched to the site's design spectra effects are examined. The results indicate the adaptive schemes proposed in this research are a viable alternative to improve robustness to structural control of bridges. The developed adaptive control schemes are suitable to control large bridge structures, as they are able to reduce dynamic responses and offer robustness improvement when compared to nonadaptive schemes.

DEDICATION

To Igor, my husband and best friend.

ACKNOWLEDGEMENTS

I would like to thank my committee chair, Dr. Barroso, for all the support, valuable advice, and kindness. This research would not have been possible without her guidance. I also would like to express my gratitude to my committee members, Dr. Hueste, Dr. Niedzwecki, and Dr. Palazzolo for their contributions to this research and also for adding so much to my overall academic and professional knowledge.

I also wish to express my gratitude for the Brazilian National Council for Scientific and Technological Development (CNPq) for the financial support. Also, I would like to thank my research team at Texas A&M for all the discussions and shared knowledge. Thanks also to my Professors from UFRJ for making it possible for me to have this unimaginable experience. Thanks to my amazing Brazilian friends that helped this journey to be full of laughter, joy, and support.

Thanks to all my family members for all the support and encouragement. I want to express gratitude especially to my mother Sueli that made always a huge effort so my sister and I could have a good education. Deborah, Rafa, and Biel, thanks for the friendship; I could not possibly do this without our many chats and shared laughter. Maria Rita and Juarez, thanks for all the years of friendship. Lastly, I want to thank Clarinha for the companionship and also my dear husband Igor. I am undeserving of your love, kindness, friendship, encouragement, and support. Thank you for joining me in this journey and for leaving everything behind to be by my side; I will be forever grateful to you.

CONTRIBUTORS AND FUNDING SOURCES

Contributors

This work was supervised by a dissertation committee consisting of Professor Luciana R. Barroso (advisor), Professor Mary Beth Hueste and Professor John Niedzwecki of the Department of Civil Engineering and Professor Alan Palazzolo of the Department of Mechanical Engineering.

All work for the thesis was completed independently by the student.

Funding Sources

Graduate study was supported by the Brazilian National Council for Scientific and Technological Development (CNPq). Its contents are solely the responsibility of the authors and do not necessarily represent the official views of the CNPq.

TABLE OF CONTENTS

Page

LIST OF FIGURES

Page

LIST OF TABLES

Page

1. INTRODUCTION

As materials science and engineering field develops materials with increased strength, civil structures are allowed to become every day more flexible and more sensitive to dynamic loads. Modern bridges have become slender structures and able to carry significantly long spans. The more flexible and lowly damped these structures are, the more complex dynamic behavior they present, which increases their susceptibility to dynamic events.

Bridge collapse is likely to result in loss of lives; in 1986, the collapse of the Amarube Railroad Bridge in Kasumi (Japan) resulted in the death of 6 people. In 1989, the Cypress Street Viaduct located in Oakland-CA collapsed after Loma Prieta earthquake and resulted in the death 42 people. The collapsed street viaduct is shown in Fig. 1.1. In 2001, the collapse of the Hintze Ribeiro bridge, in Castelo de Paiva (Portugal) resulted in 59 deaths. In 2011, the collapse of the Kutai Kartanegara Bridge in Kalimantan (Indonesia) killed at least 20 and injured 40 people. Recently, in 2018, the collapse of the Morandi bridge, in Genoa (Italy) resulted in the death of 43 people.

In the fortunate event when no lives are lost, bridge collapse still carries the potential to bring a great amount of distress to a region. The economic losses due to infrastructure damage are likely to be massive; after 1995 Kobe (Japan) earthquake, 60% of the bridges were severely damaged and the estimated direct cost is around $4.6 billion (Chung 1996). In addition to the direct economic losses, bridge collapse typically complicates the implementation of recovery plans. Bridges are usually essential

connections between regions as they are often the only way for a terrestrial mean of transportation to access a certain area. Prevention of bridge collapse not only avoids the consequences of the collapse itself, but it can likewise facilitate access to a region that experienced the event, speeding up the recovery process. Bridge collapse or excessive damage after a major extreme event most likely delays help and supplies from reaching the affected area.

[https://pubs.usgs.gov/dds/dds-29/screens/022sr.jpeg]

Fig. 1.1: Street Viaduct, Oakland-CA after Loma Prieta Earthquake, reprinted from United States Geological Survey (1999).

Structural dynamic control is a modern alternative to alleviate excessive dynamic vibrations and enhance performance of civil engineering structures. Control strategies and devices are a viable alternative to limit bridge excessive responses and avoid collapse or excessive damage. Control may also provide the means to increase the flexibility of civil structures and reduce material usage, while ensuring an acceptable level of comfort and serviceability to bridge users.

Structural control can be categorized as passive, active, or semi-active control. Passive control is a type of control that does not introduce energy to the system, and consequently do not introduce instability. One drawback of this control solution is that passive control has often a frequency range limitation and its parameters once defined cannot be changed. Passive control may be a good alternative to control civil structures as it is known for being able to reduce dynamic induced responses. However, passive control is not a very versatile type of control due to the aforementioned frequency range limitation and consequent inability to deal with parametric and excitations uncertainties. Examples of purely passive control commonly implemented are tuned mass dampers (TMD) and base isolation.

In active control, control commands can be obtained through closed-loop schemes. The control forces are related to the level of excitation, the expected reference response, and sensed structural dynamic responses. A control algorithm is responsible for the calculation of the control commands, based on a defined control law. The control commands are translated into control forces that are actively introduced into the system by control devices. Therefore, active control introduces energy to the system and it has the

potential of introducing instability. Another drawback of active control is that active control requires a great amount of power for the generation of forces necessary to control large structures. These forces are generally massive and would call for a great amount of electricity to be generated. Electricity is likely to be unavailable during major extreme events, which would require fairly large batteries to guarantee the functionally of the control scheme. Some examples of active control devices are hydraulic actuators, and active mass dampers (AMD).

Semi-active control brings together some advantages of both passive and active control. This type of control can be seen as an adjustable passive control, where resisting forces are compatible with a given control command. In semi-active control, the control command may be obtained through closed-loop schemes. The control command can be calculated through a control algorithm, based on the level of excitation, expected reference response, and structural responses. As the forces on semi-active control are reactive, the scheme does not introduce energy into the system. Since the resisting level is adjustable, it has the versatility of active control. Some examples of semi-active control devices are magnetorheological dampers (MR dampers), resettable dampers, and electrorheological dampers (ER dampers).

Control algorithms or strategies calculate the control command that is given to the device, based on a control law and sensor-measured responses. In feedback control, most control laws are functions of the actual structure responses and desired predefined reference responses. Some examples of control algorithms are the classical PID control, H-infinity, pole placement, model reference adaptive control, fuzzy logic control, neural-

networks, and genetic algorithms. Control strategies can be categorized as adaptive and non-adaptive. Non-adaptive strategies have their parameters predefined during the design phase and these parameters do not change after that. Adaptive control strategies have the ability of adjusting its own parameters based on observation of the system behavior. They may or may not explicitly estimate structural parameters. The adaptive strategies that estimate structural parameters explicitly are called indirect adaptive control strategies; the strategies that do not explicitly calculate structural parameters are called direct adaptive control strategies.

Structural parameters of an existing bridge may differ from the estimated during control design for several reasons. Engineering modeling simplifications and assumptions, changes during construction, any level of damage, cracking, temperature fluctuations, localized damage, deterioration, accumulation of snow, all are factors that lead to existing parameters that are different from previously estimated ones. A controller designed based on any estimated parameters may present an unsatisfactory performance, and has the potential to even worsen the dynamic performance of the bridge. As previously stated, adaptive control algorithms have the ability to adapt its characteristics based on the actual behavior of the structure. The controller performance can be then guaranteed even when in face of the great amount of uncertainties that involve the estimation of bridge parameters. This research intends to develop and implement adaptive control schemes, and evaluate their ability in mitigating excessive response of bridge structures under varying parametric conditions. To achieve this goal, the adaptive control schemes are developed and implemented to control bridges considering different types of structural

parameters configurations. The controllers' ability in dealing with parametric changes while mitigating excessive responses is assessed. Realistic operation and implementation conditions are considered, and the importance and sensitivity of structural modeling considerations for control design and implementation on bridge structures are investigated.

2. BACKGROUND

In this section, a brief summary of the background of the field of structural control relevant specifically to control of bridges structures is presented. Structural control is the application of control theory to dynamic systems in order to stabilize and reduce responses of these systems induced by dynamic events. For bridge structures, control theory can be applied to bound structural responses to acceptable levels and guarantee satisfactory structural performance. Excessive responses may lead to a great amount of discomfort to users and to local and/or global damage that may ultimately lead to collapse. This section presents initially the theoretical background and subsequently the control applications available in literature that are found to be of relevance to the development of this research.

2.1. Theoretical Background

Structural control is an emerging alternative to alleviate dynamic responses of civil structures in order to protect them from damage and guarantee an acceptable level of comfort. Based on their operational mechanisms, control solutions can be categorized into passive, active, semi-active, and hybrid control. A state-of-the-art review and description of brief description of each of these control alternatives, as well as the advantages and disadvantages brought by each of them can be found in Saaed et al. (2015).

One control mechanism commonly implemented to control bridge structures is the passive control. This mechanism does not require external sources of energy as it is reactive to the motion of the structure. Passive control frequently presents itself as a good

alternative to control civil structures, as it is known for being able to reduce dynamic induced responses in cases where the sources of the dynamic loads are well known and there are not many uncertainties involved. This type of control is unable to destabilize the structure, generally it is simple to design, install, and typically are of low cost. However, passive control does not provide much versatility once designed and implemented. This control solution has a frequency range limitation and its parameters once defined cannot be changed. Consequently, the scheme may perform poorly in face of parametric variations and uncertain excitations.

One example of passive control is base isolation, which consists in isolating the upper portion of the structure with rubber bearings or sliding isolation in order to reduce accelerations transmitted from the ground. Another example of passive control is obtained by setting up passive devices, such as viscous dampers or friction dampers, which are able to dissipate energy that would otherwise be applied to the structure. Another passive control system is obtained with tuned-mass dampers (TMD); these devices are composed of a combination of a solid mass, springs, and dampers. This system is able to shift the fundamental period of the main structure and reduce its response under certain dynamic load. TMD were studied as a solution to control bridge structures in many publications, such as (Battista and Pfeil 2000, Ubertini and Materazzi 2009). In cases where the excitation is broadband or the structure does not have a majorly predominant frequency passive control is not the most appropriate control solution.

Active control overcomes the lack of versatility of passive control. Active systems can operate through closed-loop control schemes such as feedback control. In feedback

control, structural responses are measured by sensors and fed to a control system. A control algorithm calculates the required control command based on a control law which leads the actuation system. These devices then apply the necessary forces to the structure. A diagram of a generic feedback system is given by Fig. 2.1.

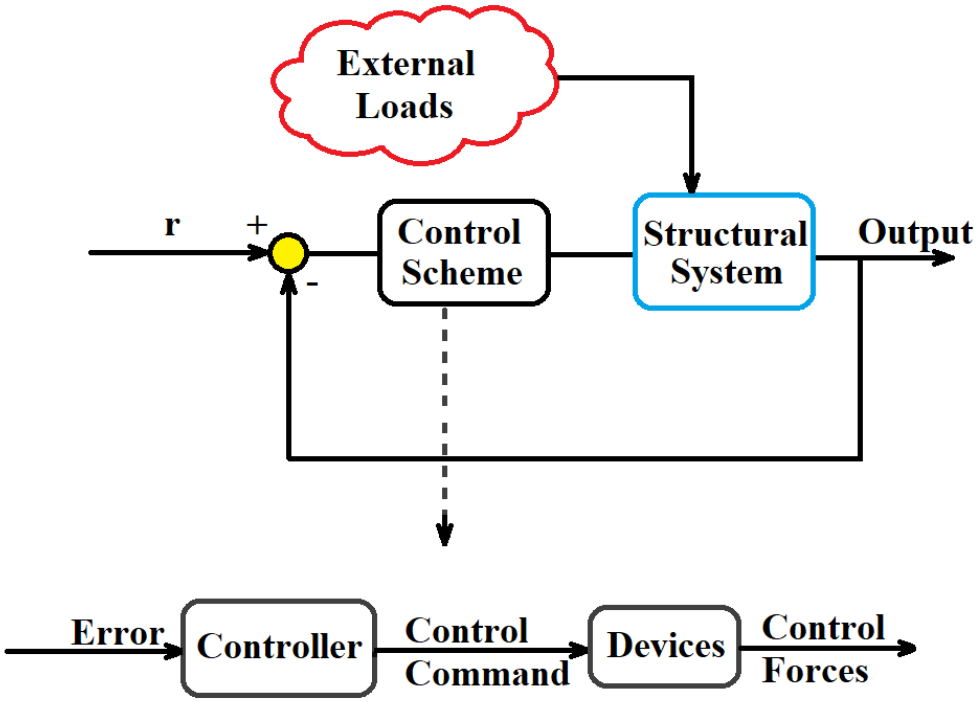

Fig. 2.1: General representation of a feedback control system under disturbances.

Active control systems are generally very effective when it comes to reducing dynamic response. However, these systems present some drawbacks. They are generally highly sensitive to structural parameters variations and may introduce instability to a system. Additionally, they need great power sources to generate high forces. Power is likely to be unavailable during major extreme events and massive batteries are needed to guarantee the system remains operational. Hydraulic actuators are examples of commonly

implemented active control devices; their dynamic behavior is thoroughly discussed in (De Silva 2015, Dyke et al. 1995, Sivaselvan et al. 2008). Hydraulic actuators operate through highly pressurized liquid hydraulic power. They are able to provide high forces and require significantly high power sources. One disadvantage of these devices is the high nonlinearity of fluid power systems (De Silva 2015).

Semi-active control brings together some of the advantages from active and passive control systems and addresses some of their disadvantages. It is a versatile type of control scheme, given its ability to generate control forces based on closed-loop control. It requires low amounts of energy to operate, which means small batteries are enough for the mechanism to remain operational. Since it is a form of controllable passive scheme, it only generates resisting forces. Hence, semi-active control does not introduce energy into the system and cannot destabilize it.

Some examples of semi-active control devices are magnetorheological dampers (MR), resettable dampers, electrorheological damper (ER), and piezoelectric dampers. Piezoelectric friction dampers are adjustable friction dampers. The material that composes these devices can generate strains with the application of an electric field. This feature gives the possibility of adjusting the contact pressure through closed-loop control schemes. These devices are successfully utilized for structural control of buildings in Lu (2009), Xu (2008). ER dampers are devices filled with a controllable fluid that has the ability of changing its properties once subjected to an electric field. This feature gives the possibility of adjusting control forces based on feedback control with a low level of energy consumption. MR dampers, are dampers filled with a fluid that can have its properties

changed through the application of a magnetic field. MR dampers also have the advantage allowing for closed-loop control application for the adjustment of control forces and requiring low energy consumption levels. One of the major advantages of MR dampers to control large structures when compared to ER dampers is the large yield stress it is able to achieve. The MR fluid yield stress is an order of magnitude greater than ER fluid, while both fluids have comparable viscosity. This impacts the device size and dynamic range, given the minimum amount of fluid necessary in a controllable device is proportional to the viscosity and inversely proportional to the maximum yield stress squared. Therefore, the amount of fluid needed for a MR fluid to operate is about two orders of magnitude smaller than an ER damper with the same maximum capacity. Additionally, while the power requirements for MR and ER devices are roughly similar, only MR dampers can be sourced by common low-voltage batteries. MR dampers are also less susceptible to dielectric breakdown, contamination and extreme temperatures than ER dampers (Spencer and Sain 1997).

Many publications refer to the dynamic modeling and behavior of MR dampers. In Spencer Jr et al. (1997), a review of different dynamic models for MR dampers are presented. The Bingham (Stanway et al. 1985), the Gamota and Filisko (Gamota and Filisko 1991), and the Bouc-Wen (Wen 1976) models are thoroughly described. The authors then propose a modification to the Bouc-Wen model, establishing a different dynamic model for MR dampers. The different dynamic models are displayed in Fig. 2.2. In Yang et al. (2002), a dynamic model for large scale MR dampers is developed and the results are compared to experimental results. In this study, parameters are determined

experimentally for large scale MR dampers. Jung (2004) presents detailed state-of-the-art for MR dampers as mechanisms implemented to control civil engineering structures. Tsang et al. (2006) presents simplified inverse models for MR dampers, which allows for voltage calculations based on control command.

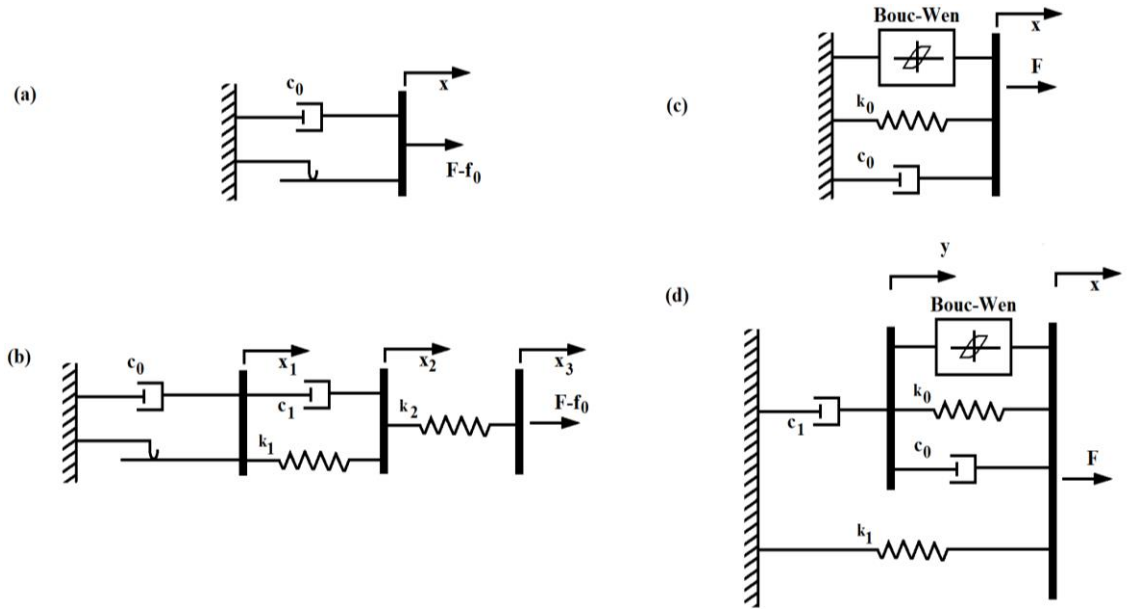

Fig. 2.2: Dynamic models for MR dampers: (a) Bingham; (b) Gamota and Filisko; (c) Bouc-Wen; (d) Modified Bouc-Wen, adapted from Spencer Jr et al. (1997).

Resettable devices are semi-active energy dissipation devices composed by a two-way piston and a valve. Whenever this valve is closed, the fluid inside the cylinder is compressed by the motion of the piston. Once the valve is open, the energy stored in the fluid is dissipated. There are available pneumatic and hydraulic versions of the resettable devices (Jabbari and Bobrow 2002). These devices have been successfully applied for multi-level seismic hazard mitigation of steel moment frames and were able to successfully reduce permanent deflections in Barroso et al. (2003) .

Another closed-loop control component are the control algorithms. Control algorithms are responsible for the calculation of the control command based on a control law. The control command dictates the control forces to be generated by the devices and applied to the structure. Control algorithms can be adaptive and non-adaptive. In non-adaptive control algorithms, the control gains are previously designed and do not change over time. Some examples of optimal non-adaptive strategies are the clipped-optimal control, and the linear quadratic regulator. Adaptive control strategies are able to calculate the control gains in real-time based on the observation of the dynamic behavior of the system. Adaptive strategies are direct when the structural parameters are not obtained explicitly, and indirect when the parameters are obtained explicitly. Examples of adaptive control techniques are the model reference adaptive control (MRAC), the simple adaptive control strategy (SAC), and the neuro-fuzzy adaptive control.

SAC is an adaptive control technique based on the classical MRAC. The idea for SAC was first introduced by Sobel et al. (1982), and it has been developed over a series of studies (Barkana 2005, 2008, 2013, 2014, 2016a, c, 1987, Barkana and Guez 1990, Barkana and Kaufman 1993). The idea behind SAC is to overcome limitations of the classic model reference adaptive control for multiple-input multiple-output (MIMO) systems, such as requiring full-state feedback or full-order observers, and instability caused by unmodeled dynamics. Fig. 2.3 shows the general block diagram for the method.

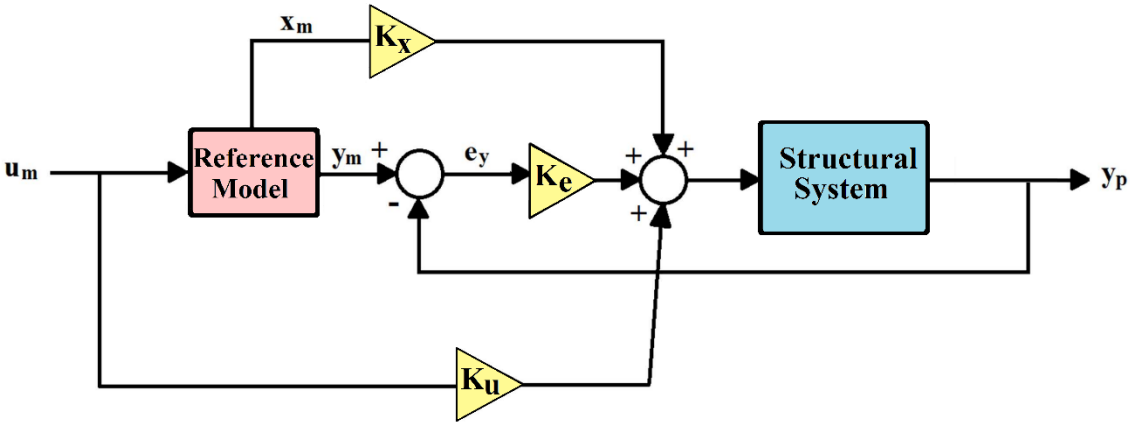

Fig. 2.3: SAC's block diagram.

In Barkana (2014), a survey is presented containing the method's latest developments. In this study, a review and stability proof under ideal conditions of the MRAC. Provided the system is stable and the full state vector is available, the MRAC satisfy a strict positive realness condition and it is proven stable. However, it is pointed out that unmodeled dynamics that occur when the actual structural system is of higher order than the model reference have the potential to lead to instability in the presence of disturbances or noise. SAC can be implemented with a significantly reduced order model reference when compared to the actual structural system, and it is applicable to systems that are prone to present instability. Moreover, SAC is proven to guarantee perfect tracking asymptotically, and it successfully avoids the need of estimators.

In Barkana (2016c), some of the concerns regarding the divergence of adaptive gains under the presence of disturbances are addressed. Up to the development of the aforementioned study, a sigma term had been used to guarantee stability under

disturbances. However, this term had the potential to eliminate perfect tracking and lead to chaotic-like phenomena. In Barkana (2016c), Lyapunov's proof of stability is combined to other techniques and a parallel feedforward term is introduced to SAC's formulation to guarantee perfect tracking and robustness under disturbances and non-ideal scenarios. Since its first development, SAC was applied successfully in a handful of examples available in the literature, including civil structures. The results from these studies indicate the control method is promising in dealing with changes in parameters, disturbances, and noise.

Another control technique that may potentially deal with parametric uncertainties is the adaptive neuro-fuzzy control. This technique combines fuzzy controllers and learning neural networks. Fuzzy logic is logic that involves not only true and false statements, but also partially true or partially false statements; fuzzy controllers apply fuzzy logic to generate control command. Neural networks consist of a computational model that have the ability of adapting and learning from training patterns or data. The combination of neural networks to the fuzzy control gives the possibility of training the fuzzy controller to achieve a certain target and become more adaptable. In a type of neuro-fuzzy control called ANFIS (adaptive neuro-fuzzy inference system), a set of if-then rules are defined through a process of data collection to create a fuzzy inference system (FIS) with tunable membership function parameters that is able to emulate experts' decisions (Jang et al. 1997). First a target controller is defined and input and output of this controller are collected, then the neural-fuzzy controller training process begins. It uses the neural networks to build a map of the input and the output sets based on the target controller data

collected (Schurter and Roschke 2001b). The training process is continued until the error function has reached an acceptable level. Fig. 2.4 gives a general schematics of the training process of the neuro-fuzzy control.

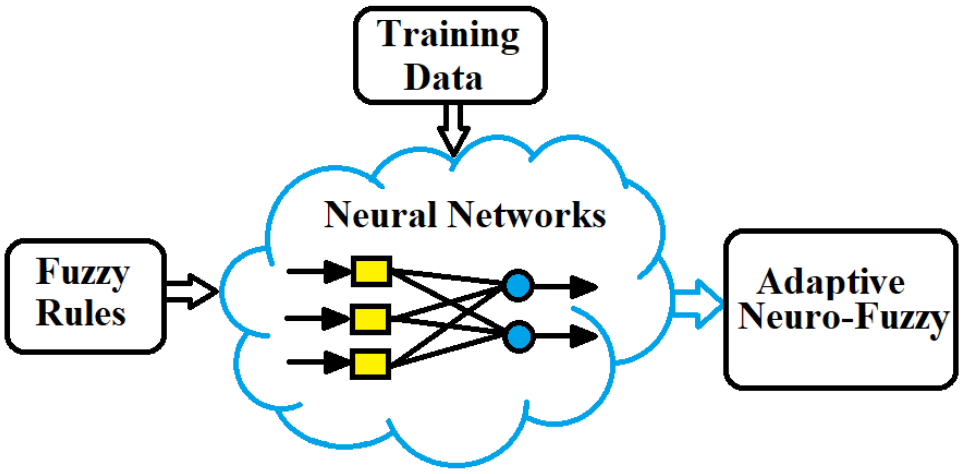

Fig. 2.4: Neuro-Fuzzy control training schematics.

2.2. Control Applications

In Erkus et al. (2002), semi-active control of an elevated highway bridge is implemented and its performance is compared to the performances of active and passive control. The semi-active control scheme is composed of MR dampers and LQR-based clipped optimal control. The passive system is composed of rubber bearings, and the active is composed of ideal actuators controlled by LQR. The bridge is modeled as a two-degree-of-freedom system and the analysis performed is linear. Three design goals are set: reduction of pier response, reduction of bearing response, and reduction of both pier and bearing. The study concludes the performance of the semi-active control is similar to the passive system for reduction of pier response. The semi-active control's performance is

similar to the ideal active control for reduction of bearing response. For reduction of both pier and bearing responses all strategies (active, passive, and semi-active) exhibit similar performances.

The second generation benchmark for structural control of cable-stayed bridges is developed by Caicedo et al. (2003), based on the drawings of the Bill Emerson Memorial Bridge. The bridge was built in 2003 in Cape Girardeau, Missouri. A three-dimensional linear structural model is developed and equations of motion are given by the study, based on the deformed equilibrium position. The study is as a guide for investigation of control applications to cable-stayed bridges subjected to seismic excitations; it accounts for multi-support and transverse excitations effects, presents evaluation criteria, and control constraints.

Jung et al. (2003) proposes a control scheme for the benchmark cable-stayed bridge combining MR dampers and clipped-optimal control algorithm focusing on the effects of control-structure interaction. The control scheme is composed of 5 accelerometers, 4 displacement transducers, and 24 MR dampers. In the study, it is concluded that the Bouc-Wen and the modified Bouc- Wen model are more efficient in representing the behavior of the MR damper than the Bingham model. The performance of the proposed control is similar to that of the ideal active control system. The semi-active control strategy is able to reduce the peak and normed response for several earthquakes, however, it increased the deck peak shear. The semi-active control presents improved performance for the historical earthquakes when those are scaled down, but presented mixed performance for unscaled records when compared to the passive strategy (passive-

on). The study concludes that although MR dampers showed some promising results for seismic control of cable-stayed bridges, more thoroughly studies are necessary to validate their performance.

A fuzzy control technique to control MR dampers to improve the performance of cable-stayed bridges is presented in Ok et al. (2007). This technique overcomes the need for a primary controller to determine the control force and a secondary one to modulate voltage, given the fuzzy logic controller is able to determine the voltage directly. This technique is implemented on the benchmark control problem for cable stayed bridges. The performance of the controller is compared to H_2/LQG control with ideal actuators, semi-active clipped optimal control, and hybrid control for a set of two earthquakes (Mexico City and El Centro). The proposed technique shows satisfactory performance and it is able to mitigate excessive responses under imposed seismic loads.

In Agrawal et al. (2009), Tan and Agrawal (2009) is presented the problem definition and sample control benchmark problem for seismically excited highway bridges. The problem is based on a highway overcrossing located in Southern California, USA. The study intends to set a standardized model for comparative evaluation of control strategies. The structural model developed for this study considers material nonlinearities of central piers and isolation bearings, as well as soil structure interaction.

A decentralized model reference controller is developed in Ningsu (1999), to mitigate excessive transverse vibration of a cable-stayed beam under seismic loading. The controller design is developed based on the sliding mode control technique, which sustains performance under uncertainties and disturbances. The controller performance is

evaluated and it is shown that the vibrations of the bridge deck are significantly attenuated by the proposed controller, when compared to the uncontrolled case.

In Gattulli and Romeo (2000), an integrated procedure is proposed to identify and control a multi-degree of freedom (MDOF) structure. The effectiveness of the adaptive control algorithm sliding mode control and MRAC integrated to an online parameter identification procedure based on tracking errors are investigated. Numerical simulations are performed in a three degree of freedom (DOF) shear building-type structure. The study shows that the proposed method is successful in identifying the changes in parameters and control excessive vibrations; the method stability is proven even when abrupt parametric changes are introduced.

In the study developed by Schurter and Roschke (2001a), a neuro-fuzzy strategy is implemented with acceleration feedback to control buildings with MR dampers. The accelerations of the building are defined as the controller input and the MR damper voltage command were the controller output. A single degree of freedom (SDOF) and a MDOF systems are subjected to different earthquake records and the performance of the semi-active scheme is compared to the performance of purely passive control. The passive control is more effective in reducing the acceleration response of the SDOF. On the other hand, semi-active control shows to be more effective for the MDOF building response reduction.

In Chu (2009), a real-time model reference adaptive identification technique is proposed in order to incorporate online system identification to the MRAC algorithm. The law used for parameter estimate is based on Lyapunov's direct method, and the energy

function is considered by assembling weighted response tracking error and parameter estimates error. A numerical simulation for a SDOF time-invariant system is performed where the system is subjected to two different sets of earthquake loads. The control proposed shows to be effective, as the parameters of the system are successfully identified and excessive vibrations attenuated.

In Bitaraf et al. (2010), SAC is implemented with semi-active and active devices to control a three-story building. The study investigates the ability of the method to deal with changes in structural parameters. A change in stiffness is introduced to some stories of the building, which is then subjected to different load scenarios. The objective is to guarantee that the controlled damaged structure performs in a similar fashion as the controlled undamaged one. For comparison, three different designs are considered: the nominal uncontrolled structure, nominal active-controlled structure, and nominal semi-active-controlled structure. The results indicated that the controlled responses are significantly smaller in comparison to the uncontrolled. After damage is imposed, the damaged controlled structure performs similarly as the undamaged one for both types of control devices (active and semi-active).

SAC is also applied successfully to mitigate excessive response of civil structures under seismic excitation in further studies by Bitaraf and Hurlebaus (2013), Bitaraf et al. (2012). The former study applies SAC and MR dampers to control a three-story building, considering damaged and undamaged configurations. The performance is compared to a hydraulic actuation active control system. The control method shows effectiveness even in the presence of noise and damage, for the three suites of earthquakes applied. However,

the hydraulic actuator introduces unwanted behavior to the structure. The latter study applies SAC and MR dampers to control a 20-story building considering nonlinear behavior; SAC's performance is compared to other control methods (passive-on and clipped optimal control). The method is successful in mitigating excessive responses for the four different suites of earthquakes considered.

A method based on SAC for nonlinear and nonstationary systems is developed by Ulrich and Sasiadek (2014). The technique proposes a decentralization of the adaptation law mechanism. The decentralized method considers only the diagonal of the gain matrices, reducing the number of parameters to be considered. The scheme is successfully proven stable using Lyapunov's direct method and Lassalle's invariance principle, and its effectiveness in tracking trajectory is shown.

In Javanbakht (2016), SAC is implemented with acceleration feedback and MR dampers to reduce seismic response of a 20-story tall building, accounting for material nonlinearities. SAC controls effectively the structure and permanent damage effects are mitigated. A modification to the classical MRAC to include the possibility of different damping levels and account for multi-hazard occurrence is proposed in Venanzi et al. (2017). The method is applied to control a tall building subjected to extreme loading (earthquake and wind). It successfully reduces the responses and tracks the model reference. The proposed scheme displays a slightly worse performance when compared to the classical MRAC, however, the control forces required by the modified method are smaller than the forces required by the classical MRAC method.

3. MOTIVATION AND SIGNIFICANCE

Extreme dynamic events have the potential to bring a bridge to structural failure, which can lead to numerous losses in lives. Furthermore, bridges are often essential to dislocate between areas and frequently are the only way for a terrestrial mean of transportation to access a certain region. Prevention of bridge collapse or excessive damage possibly facilitates the access to the region that experienced the major extreme event, which may expedite help and supplies access and ease the implementation of recovery plans. Likewise, the direct and indirect economic losses due to infrastructure damage subsequent to an extreme event is typically massive. Bridges generally present little redundancy and complex dynamic behavior. These structures are often prone to present substantial responses when subjected to dynamic loading. Materials technology recent advances led to the development of high strength materials, which made possible for modern bridges to carry substantially long and slender spans. This increase in flexibility leads to further complexity of dynamic behavior and susceptibility to dynamic events. Control strategies and devices present themselves as useful solutions to limit bridges excessive responses and avoid collapse or excessive damage. Control can ensure an acceptable level of comfort and serviceability and offer the designer the possibility of increasing the flexibility of bridge structures, therefore lessening material usage.

Furthermore, bridges are structures that are exposed to the environment and are subjected to extreme changes in temperature, cracking, corrosion, snow accumulation, extreme loading and fatigue. Engineering modeling simplifications, estimates, and

assumptions can also result in parameters that are different from those that are existent in the actual structure. A controller designed based on the estimated structural parameters may perform poorly in the case where the controller does not present enough robustness in face of parametric uncertainties. On the other hand, a control approach that is dependable and robust has the potential to guarantee performance limits and impact how structures are designed in the future.

Adaptive control algorithms are known for having the ability of maintaining performance even when in presence of changes in parameters. Adaptive control schemes are able to calculate control specifications in real-time based on the actual observed structural behavior. Adaptive control is presented in this research as a suitable control alternative to deal with the many uncertainties related to the prediction of bridge structural parameters. Adaptive control techniques have not yet been fully investigated as a control solution for bridge structures, and this research intends to address this research gap. For this matter, adaptive control schemes are developed and implemented and their ability in mitigating excessive response of bridge structures and potentially deal with parametric variations is evaluated. The concepts of the control strategies simple adaptive control and neural-fuzzy adaptive control are employed to develop the control schemes for bridges considering different types of structural configurations. The controllers' ability in dealing with parametric changes while mitigating excessive responses is assessed. Realistic operation and implementation conditions are considered; the importance and sensitivity of structural modeling considerations for control design and implementation on bridge structures are investigated.

3.1. Objectives

The goal of this research is to develop, implement, design and assess adaptive control schemes to mitigate excessive response of bridges under varying parametric conditions.

The objectives of this research are to:

(1) Develop adaptive control schemes based on the concepts of the simple adaptive control and the neural-fuzzy control strategies, and investigate their effectiveness in reducing excessive dynamic responses of bridge structures;

(2) Implement, design and evaluate the performance of the developed control in face of parametric changes while considering different types of structural configurations and realistic operation conditions;

(3) Investigate the importance and sensitivity of structural modeling considerations for implementation and design of control specifically related to bridge structures.

3.2. Research Overview

In section 1, 2 and 3 are presented the introduction, background, motivation, significance and objectives of the research. In section 4, bridges dynamic analysis, structural characterization and modeling assumptions are presented and discussed. Model reduction techniques are presented, implemented and validated for the cable-stayed bridge. Section 5 discusses and presents the theoretical basis necessary for the development of bridges structural control schemes developed in this research.

In section 6, adaptive control approaches are developed to control two different highway bridges. An initial investigation where a control scheme based on the SAC algorithm is developed and implemented, aiming to mitigate seismic responses of a three-span highway bridge. Following the initial investigation, a comprehensive parametric study is conducted considering a two-span skewed highway bridge.

In section 7, semi-active adaptive control schemes based in SAC and neuro-fuzzy adaptive control are proposed. A case-study is conducted considering a cable-stayed bridge as the main structural configuration to be controlled. The two adaptive schemes are implemented to control the cable-stayed bridge, considering multi-support excitations and different angles of incidence. Lastly, the adaptive control schemes are implemented for the cable-stayed bridge considering earthquakes matched to the site design spectra, following AASHTO (2017) provisions.

4. BRIDGES' STRUCTURAL MODELING AND DYNAMIC ANALYSIS

In this section, dynamic analysis theoretical and methodological bases necessary to the development of this research are briefly explained, followed by the structural and modeling considerations related to the initial investigation, the parametric and the case study. Lastly, model reduction techniques are presented and discussed. There are numerous assumptions and design simplifications adopted during this stage preceding control design/implementation that are essential to make the analysis computationally feasible. The aforementioned factors affect the parameters to be considered for the dynamic analysis, control design and implementation phases.

The structural models of the bridges are developed in the finite elements software SAP2000® (Computers and Structures 2016), considering the three-dimensional character of the structures, as well as the geometric and material properties of the structural members. The masses are lumped at strategic places to simplify the analysis with careful consideration, in order to capture the dynamic behavior of the structures. The mass and stiffness matrices are exported to MATLAB® (The Mathworks 2017a) environment, where they are assembled and mapped. Lastly, the control schemes are modeled, designed, and analyzed in SIMULINK® (The Mathworks 2017b) environment.

4.1. Dynamic Analysis

The equation of motion for a multi-degree of freedom (MDOF) system subjected to ground motion is given by Equation (4.1), where $\ddot{x}_g$ is the ground acceleration, $\mathbf{E}$ is

the earthquake mapping vector composed of zeros and ones, $\ddot{\mathbf{x}}$ is the system relative acceleration vector, $\mathbf{M}$ is the mass matrix, $\mathbf{C}$ is the damping matrix, $\dot{\mathbf{x}}$ is the relative velocity vector, $\mathbf{K}$ is the stiffness matrix, and $\mathbf{x}$ is the system relative displacement vector. The structural responses are taken as relative with respect to the ground. The mass, stiffness, and damping matrices are square matrices with a size correspondent to the system's degrees of freedom (DOFs) number.

$$\mathbf{M}\ddot{\mathbf{x}} + \mathbf{C}\dot{\mathbf{x}} + \mathbf{K}\mathbf{x} = -\mathbf{M}\mathbf{E}\ddot{x}_g \tag{4.1}$$

Given that Equation (4.1) is a second-order differential equation and there are many numerical methods available to solve first-order differential equations, it is convenient to convert this system to state-space representation. State-space representation consists of representing a n^{th} order differential equation as n first-order differential equations. The MDOF system in state-space representation is given by Equations (4.2)-(4.5), where $\mathbf{z}$ is the state vector, $\mathbf{0}$ and $\mathbf{I}$ are null and identity matrices, respectively, with sizes that are correspondent to the number of the system's DOFs.

$$\dot{\mathbf{z}} = \mathbf{A}\mathbf{z} + \mathbf{B}\ddot{x}_g \tag{4.2}$$

$$\mathbf{z} = \begin{Bmatrix} \mathbf{x} \\ \dot{\mathbf{x}} \end{Bmatrix} \tag{4.3}$$

$$\mathbf{A} = \begin{bmatrix} \mathbf{0} & \mathbf{I} \\ -\mathbf{M}^{-1}\mathbf{K} & -\mathbf{M}^{-1}\mathbf{C} \end{bmatrix} \tag{4.4}$$

$$\mathbf{B} = \begin{bmatrix} \mathbf{0} \\ -\mathbf{E} \end{bmatrix} \tag{4.5}$$

By including the control system into the state-space formulation, Equation (4.2) becomes Equation (4.6), where $\mathbf{f_c}$ is the control forces vector. $\mathbf{B_c}$ is defined by Equation (4.7), where $\mathbf{J}$ is a matrix containing the placement and inclination information of the control devices.

$$\dot{\mathbf{z}} = \mathbf{A}\mathbf{z} + \mathbf{B}\ddot{x}_g + \mathbf{B_c}\mathbf{f_c} \tag{4.6}$$

$$\mathbf{B_c} = \begin{bmatrix} \mathbf{0} \\ \mathbf{M}^{-1}\mathbf{J} \end{bmatrix} \tag{4.7}$$

The output Equation is a set of equations chosen to contain responses or forces that are wished to be explicitly obtained:

$$\mathbf{Y} = \mathbf{C}\mathbf{z} + \mathbf{D}\mathbf{u} \tag{4.8}$$

For example, in order to output displacements and velocities, the output equation becomes:

$$\mathbf{C} = \mathbf{I} \tag{4.9}$$

$$\mathbf{D} = \mathbf{0} \tag{4.10}$$

The numerical solution of the dynamic system is performed using MATLAB/SIMULINK® version 2017a software package (The Mathworks 2017a, b). The majority of the differential equations are solved using ODE45 routine, which is a variable step solver that uses an explicit Runge-Kutta formula for numerical integration, the Dormand-Prince pair (Dormand and Prince 1980). The method is recommended to solve most non-stiff ordinary differential equations. ODE15s routine is used whenever the differential equation presents stiff behavior. ODE15s is an implicit variable step solver that computes the model's state at the next time step using variable-order numerical differentiation formulas.

The damping matrix of civil structures is not calculated directly from structural dimensions, member sizes, or material properties. Damping properties of different elements and materials is not well established and are very difficult to measure, since most damping comes from concrete cracks or friction at steel connections, for example. When classical damping is assumed, the damping matrix can be diagonalized using the undamped mode shapes. The damping can be directly specified by a modal damping ratio (modal damping), or through a linear combination of the mass and stiffness matrices (mass

proportional damping, stiffness proportional damping, Rayleigh damping, or Caughey damping).

It is important to point out that, when proportional damping is assumed, there is a mathematical relationship with either mass or stiffness matrices, and variation of these parameters would affect the damping matrix as well. However, the damping prediction is already very much simplified and contains a great amount of imprecision. In reality, physical structures or systems are generally comprised of many substructures tied together in various fashions. These substructures can be made-up of a variety of materials. Furthermore, these substructures may be connected to one another by rivets, bolts, screws, dampers, springs, welds, friction, etc. Also, the spatial geometry of the structure may be very complicated. This invariably means that the damping in the system is not proportional to the distribution of the mass and/or stiffness of the system. The many uncertainties embedded in the prediction of damping on civil structures calls again for the need of a control solution that is robust when in face of parametric variations, given it is somewhat difficult to predict it, and to predict its variations as well. In this work, the damping is assumed to remain the same throughout all the parametric variation scenarios.

4.2. Structural Characterization- Three-span Highway Bridge

The three-span highway bridge considered as the preliminary study of this research (section 6.1) is described in Dicleli et al. (2005). It is an existing continuous bridge located in Jackson County, Illinois. The bridge is 11.5m wide and carries two traffic lanes. It has two 16.36m long side spans and a 19.2m long midspan. The superstructure is

composed 6 W33x130 steel beams supporting a reinforced concrete deck; the total weight of the superstructure is approximately 4.4MN. The beams are supported by two heavy wall piers; at both abutments there are roller bearings supporting the beams and fixed bearings on both piers.

Fig. 4.1 shows the bridge dimensions and geometry. The bridge structural model is developed in SAP2000® and displayed in Fig. 4.2. The bridge structural members are represented by three-dimensional beam elements. For simplicity, the soil-structure interaction is not accounted for in the development of this structural model. The deck and piers masses are lumped in a way that captures the dynamic characteristics of the complete model but also reduces computational effort; singularities are removed by static condensation. The simplified model has a total of 31 DOFs. The mass and stiffness nodal values are directly extracted from the FE software. The mass and stiffness matrices are assembled in MATLAB® environment and the control schemes are added to the system. Rayleigh damping is assumed with 2% ratio for the first 2 modes.

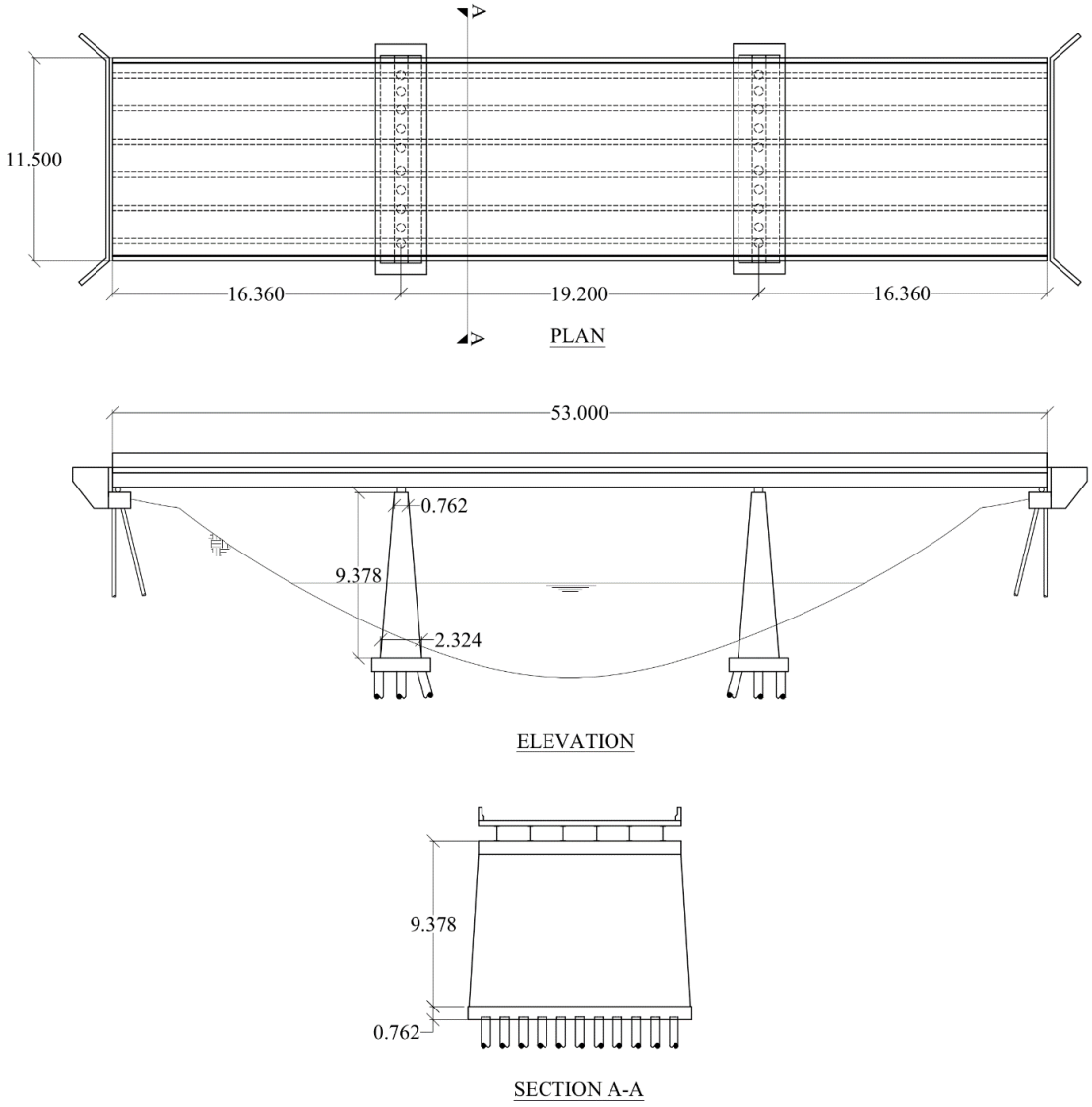

Fig. 4.1: Elevation and plan view of the highway bridge, adapted from Dicleli et al. (2005).

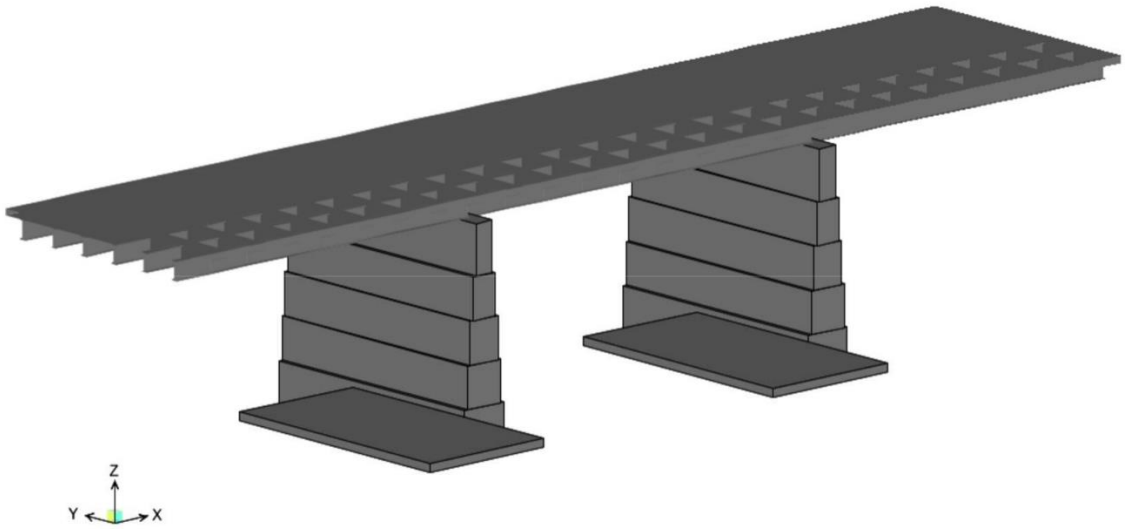

Fig. 4.2: FE model of the three-span bridge in SAP2000®.

4.3. Structural Characterization- Two-span Highway Bridge

The two-span highway bridge considered on the parametric study of this research (section 6.2) is described as the problem definition and sample control benchmark problem for seismically excited highway bridges (Agrawal et al. 2009, Tan and Agrawal 2009). The problem statement is based on an existing highway overcrossing located in Orange County, Southern California. The bridge is displayed in Fig. 4.3. The study intends to set a standardized structural model and characterization for highway bridges seismic control-related research. The bridge consists of a continuous two-span prestressed concrete box-girder bridge. It spans a four-lane highway, with two 58.5m long spans. The abutments are skewed at 30° and the deck is 12.95m wide, as shown in Fig. 4.4. The cross section of the deck consists of three cells supported by a 31.4m long and 6.9m high prestressed

outrigger and 6.9m high columns. The system rests on two pile groups, each consisting of 49 driven concrete friction piles. The cross section of the bridge along the transverse beam and a plan view of the pile group are shown in Fig. 4.5.

Fig. 4.3: Highway 91/5 over-crossing, located in Orange County- CA, reprinted from Agrawal et al. (2009).

Fig. 4.6 shows the three dimensional finite-element model of the bridge developed in SAP2000®. The bridge superstructure is represented by three dimensional beam elements and rigid links are used to model the abutments and deck-ends. The effects of soil–structure interaction at the end abutments/approach embankments are included by frequency-independent springs and dashpots according to the parameters defined by Makris and Zhang (2004), given in Table 4.2. The masses of the non-structural elements are included in the model and their stiffness contributions are neglected.

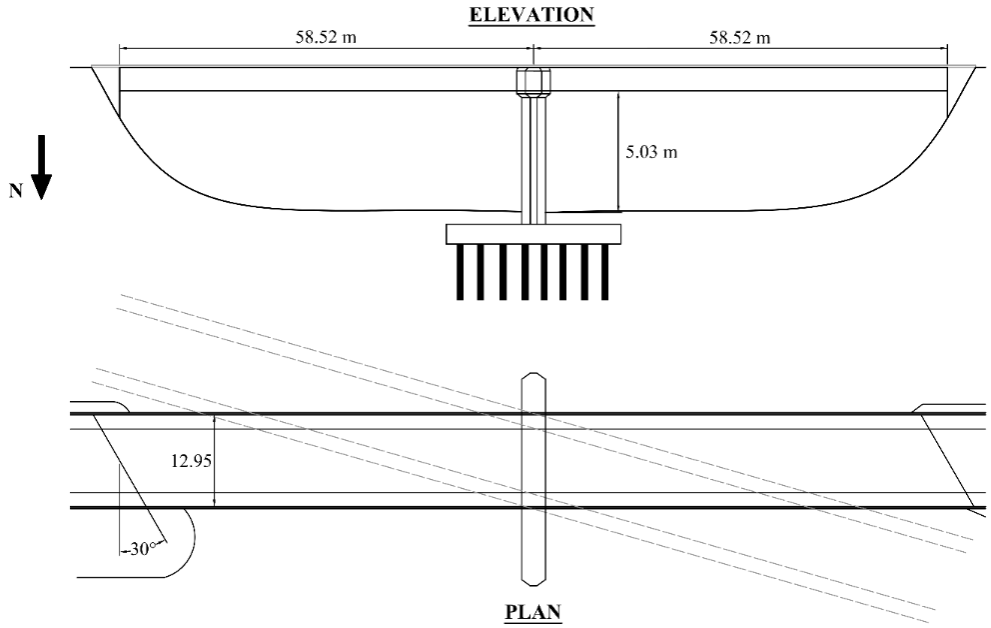

Fig. 4.4: Elevation and plan view of the highway bridge, adapted from Agrawal et al. (2009).

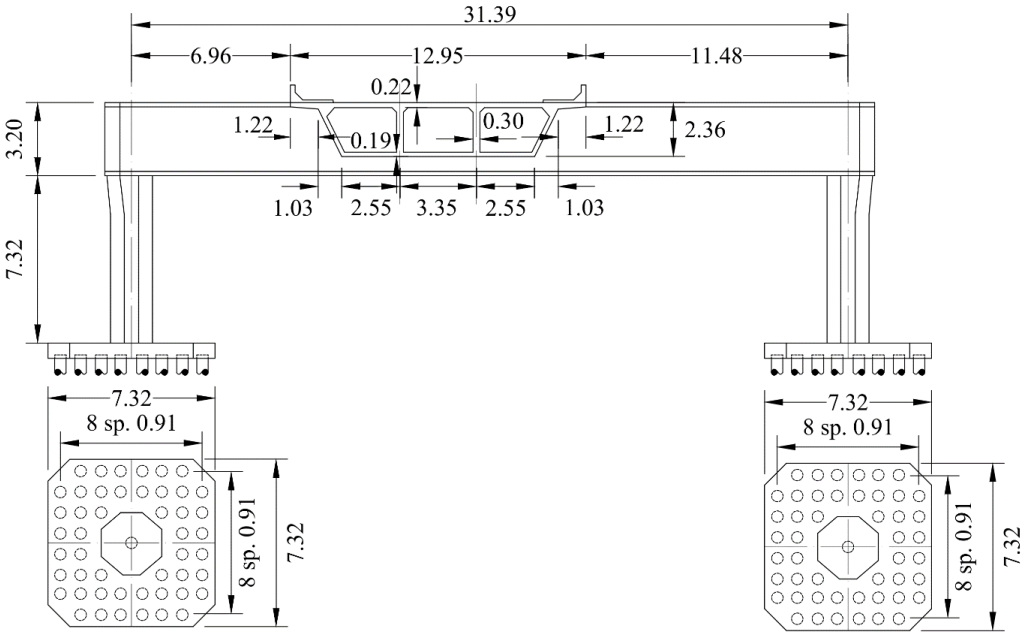

Fig. 4.5: Cross section along center bent of highway bridge, adapted from Agrawal et al. (2009).

The total weight of the deck is approximately 25MN. All element mass matrices and initial elastic element stiffness matrices are extracted from the finite element model and summed at nodal masses, to assemble global stiffness and mass matrices within MATLAB® environment. The inherent damping of the superstructure is assumed to be a function of the mass and initial elastic stiffness matrix of the superstructure. The Raleigh damping parameters are computed by assuming a 2% modal damping ratio in the first and second mode (Agrawal et al. 2009). Table 4.1 summarizes the modal properties of the bridge. More details on the benchmark control problem can be found in Agrawal et al. (2009) and Tan and Agrawal (2009).

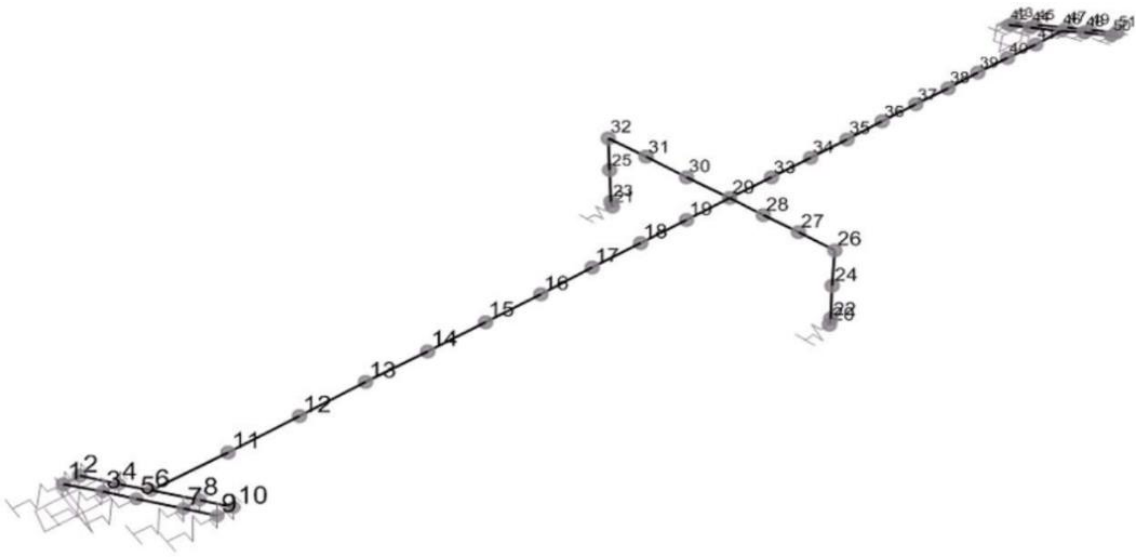

Fig. 4.6: FE model of the benchmark highway bridge.

Table 4.1: Modal properties of the benchmark highway bridge.

Mode	Frequency (Hz)	Period (s)	Description
# 1	1.250	0.800	Torsional
# 2	1.280	0.780	Torsional and Vertical
# 3	1.520	0.660	Vertical
# 4	1.680	0.590	Transverse
# 5	1.710	0.580	Vertical
# 6	3.240	0.310	Transverse

Table 4.2: Spring and dashpot values that approximate the presence of the approach embankments and pile foundation of the highway bridge, reprinted from Makris and Zhang (2004).

Parameters	Values
	Embankment + pile foundations
K_x (MN/m)	119+292 (119+271)*
K_y (MN/m)	119+293 (119+272)*
K_z (MN/m)	451+1,135 (451+1,058)*
C_x (MN.s/m)	11+28 (11+24)*
C_y (MN.s/m)	11+22 (11+17)*
C_z (MN.s/m)	14+128 (14+101)*
	Pile foundations of center bent
K_x, K_y (MN/m)	492.0
K_r (MN.m/rad)	31,739.0
K_{xr}, K_{yr} (MN/rad)	-811.0
K_z (MN.s/m)	1,452.0
C_x, C_y (MN.s/m)	14.5
C_z (MN.s/m)	54.3

*values in parenthesis are correspondent to the west abutment

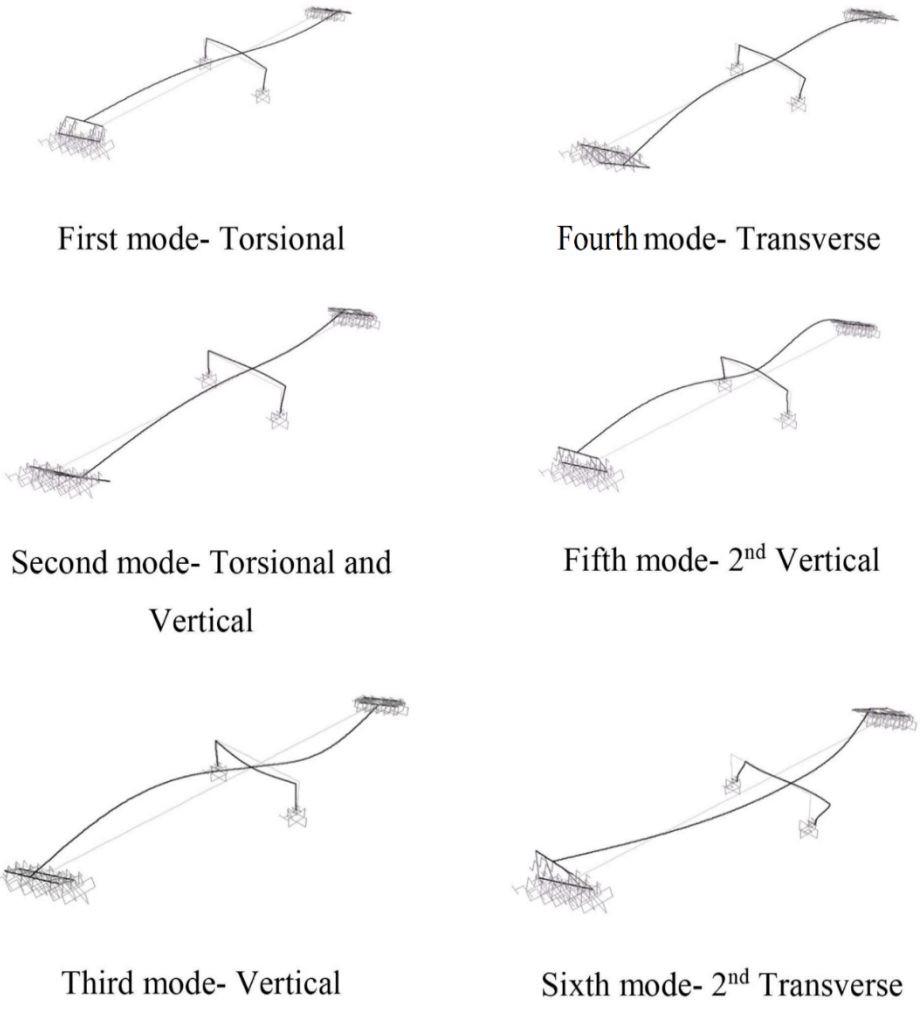

Fig. 4.7: Mode shapes of the benchmark highway bridge.

4.4. Structural Characterization- Cable-Stayed Bridge

The cable-stayed bridge considered as the case study of this research (section 7) is described as the second generation benchmark problem for control of cable-stay bridges (Caicedo et al. 2003). The cable-stayed bridge spans the Mississippi River (on Missouri 74–Illinois 146) near Cape Girardeau, Missouri, as displayed in Fig. 4.8. Seismic activity

is expected given the bridge location being near the New Madrid seismic zone. Soil-structure interaction is not considered in the analysis since the foundations of the main bridge are attached to bedrock and it is likely soil-structure interaction is not an issue for this particular structure (Caicedo et al. 2003).

The bridge is composed of two towers, 128 cables, and 12 additional piers in the approach bridge from the Illinois side. It has a total length of 1205.8m, the main span has 350.6m in length, the side spans have 142.7m in length, and the approach on the Illinois side is 570m long. The bridge has four lanes plus two narrower bicycle lanes, which gives a total width of 29.3m. The deck is composed of steel beams and prestressed concrete slabs. The beams are composed of ASTM A709 grade 50W steel, with a yield strength of 344MPa. The concrete slabs are composed of prestressed concrete with a compressive strength of 41.36MPa. The 128 cables are made of high–strength, low–relaxation steel (ASTM A882 grade 270). The cable area ranges from 28.5cm^2 to 76.3cm^2, and they are encased in polyethylene piping for corrosion resistance. The H-shaped towers are 102.4m high at pier 2 and 108.5m high at pier 3, and each tower supports a total 64 cables. The towers are composed of reinforced concrete with 37.92MPa compressive strength, and their cross section is variable over their height. Fig. 4.9 shows a lateral view of the bridge, Fig. 4.10 a cross section of the deck, and Fig. 4.11 a cross section of the towers.

Fig. 4.8: Second Generation Benchmark problem for cable-stayed bridges, located in Cape Girardeau, MO. Reprinted from Caicedo and Dyke (2004).

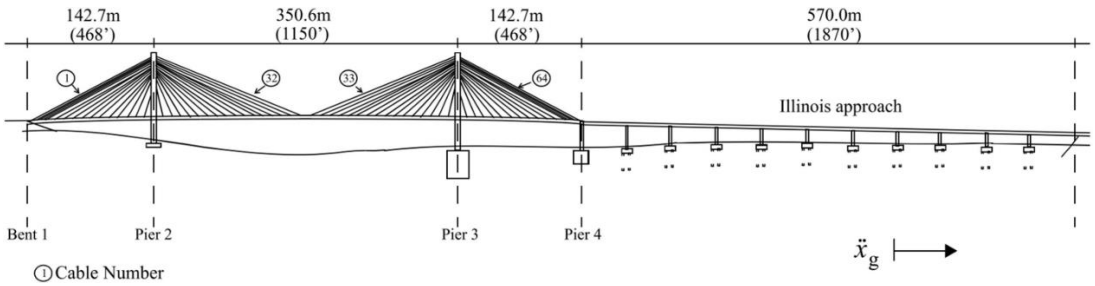

Fig. 4.9: Bill Emerson Memorial Bridge, Cape Girardeau- MO. Reprinted from Caicedo et al. (2003).

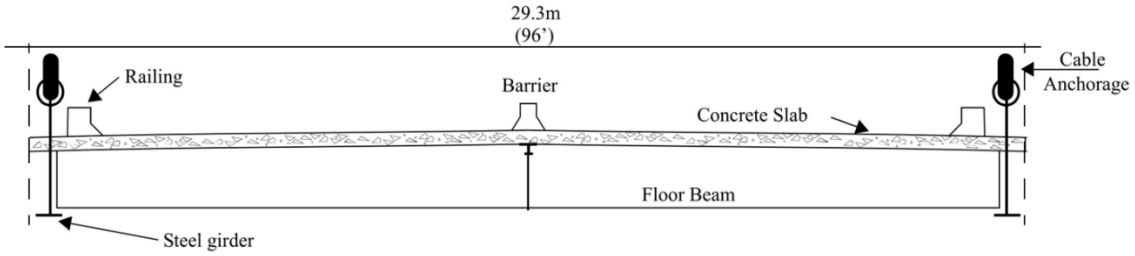

Fig. 4.10: Cross section of the deck, reprinted from Caicedo et al. (2003).

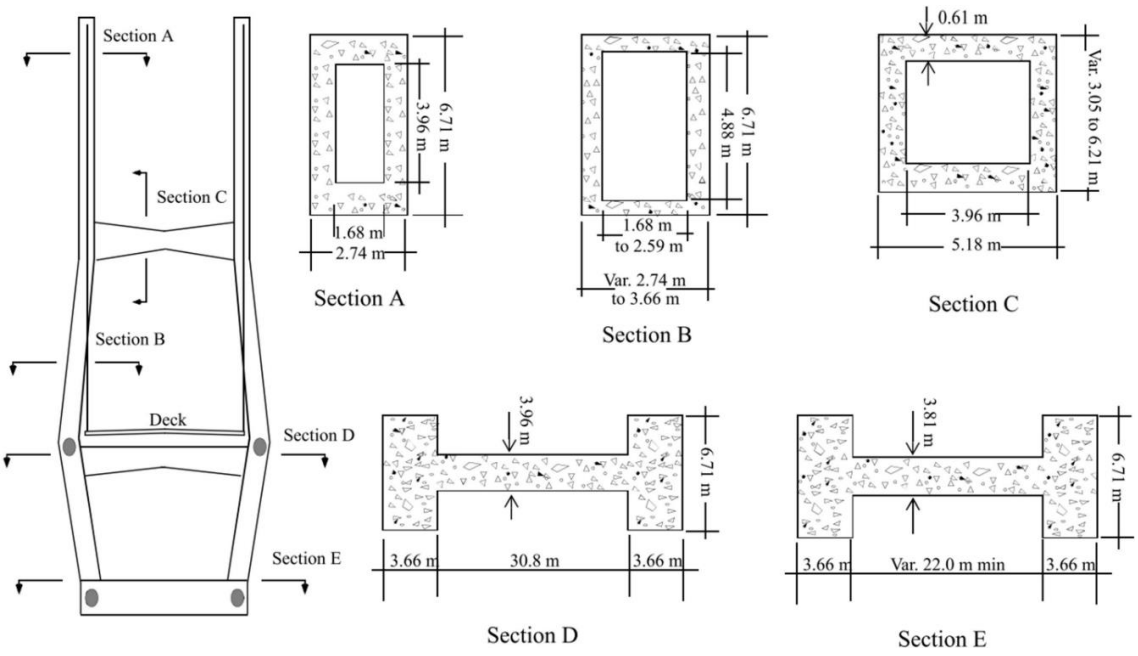

Fig. 4.11: Cross section of the towers, reprinted from Caicedo et al. (2003).

A three-dimensional finite elements model is developed in SAP2000®, based on the structural characterization of the bridge. Nonlinearities are not accounted for in the dynamic analysis. Nonetheless, the stiffness matrix extracted from the software is determined after nonlinear static analysis and are correspondent to the deformed state of the bridge due to the action of dead loads (Wilson and Gravelle 1991). The finite element

model is built with beam elements, truss elements, and rigid links. The nominal tension for each cable is applied in the FE model. The element mass matrices and element stiffness matrices obtained through the finite element model are summed at nodal masses to assemble global stiffness and mass matrices within MATLAB® environment. For the variable cross-sections, the average value among subsequent elements is considered. At bending 1, longitudinal displacements (*X*) and rotations about *Y* and *Z* axes motions are restricted in the model. The bearings at pier 4 do not restrict the longitudinal motion or rotation about the *X* axis (Caicedo et al. 2003). For the cables modeling, the catenary shape variation is considered by introducing the equivalent elastic modulus for each cable:

$$E_{eq} = \frac{E_c}{1+\left[\frac{(wL_x)^2 A_c E_c}{12T_c^{\,3}}\right]} \tag{4.11}$$

Where A_c is the area of the cable cross-section, T_c is the tension in the cable, w is its unit weight, L_x is the cable length projected in the *X*-*Z* plane, and E_c is the modulus of elasticity of the cable material. The stiffness of the cable is only considered where the cable is under tension. The deck modeling follows the recommendations from Wilson and Gravelle (1991); the deck is a massless central beam called a “spine”. The deck masses are lumped and linked to the spine by rigid links to capture the deck’s torsional response to lateral loads (Fig. 4.12). The deck is treated as a C-shaped section and the concrete slab is converted to an equivalent area of steel, considering the ratio between steel and concrete elastic moduli. The area of the equivalent section is 1.844m^2, the moments of inertia about

the vertical and transverse axes are: I_{yy}=160.67m^4, I_{zz}=0.6077m^4, and J_{eq}=0.0677m^4. The neutral axis position is of 1.77m above the bottom extremity of the steel beam. The total mass of the deck per meter is 2,645.7kg/m, which gives a total weight of approximately 17MN. Modal damping is assumed for the bridge, assigning 3% of critical damping for each mode (Caicedo et al. 2003).

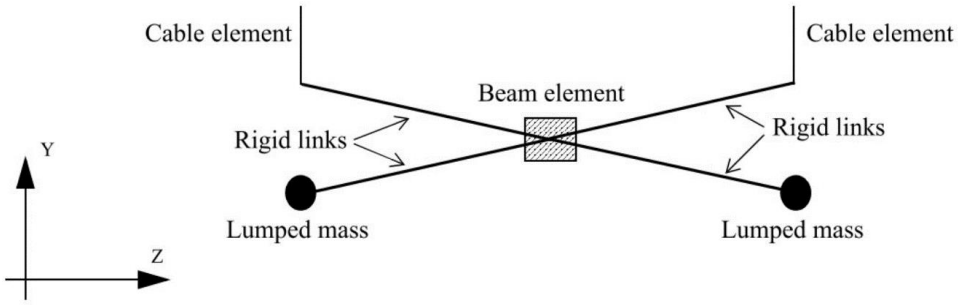

Fig. 4.12: Model scheme cross-section of the deck, reprinted from Caicedo et al. (2003).

Fig. 4.13 shows the mode shapes obtained for the cable-stayed bridge and Table 4.3 gives its the modal properties. In this study, a linear model of the cable-stayed bridge is considered for the dynamic analysis. However, geometric nonlinearities effects are not completely dismissed, given the stiffness matrices are obtained through nonlinear static analysis considering the deformed shape after dead loads' action. More information regarding the bridge geometry and structural modeling is available in Caicedo et al. (2003).

Table 4.3: Modal properties of the cable-stayed bridge.

Mode	Frequency (Hz)	Period (s)	Description
# 1	0.296	3.375	Vertical
# 2	0.306	3.272	Vertical
# 3	0.427	2.340	Torsion
# 4	0.506	1.977	Torsion
# 5	0.597	1.675	Vertical
# 6	0.616	1.623	Lateral + Torsion

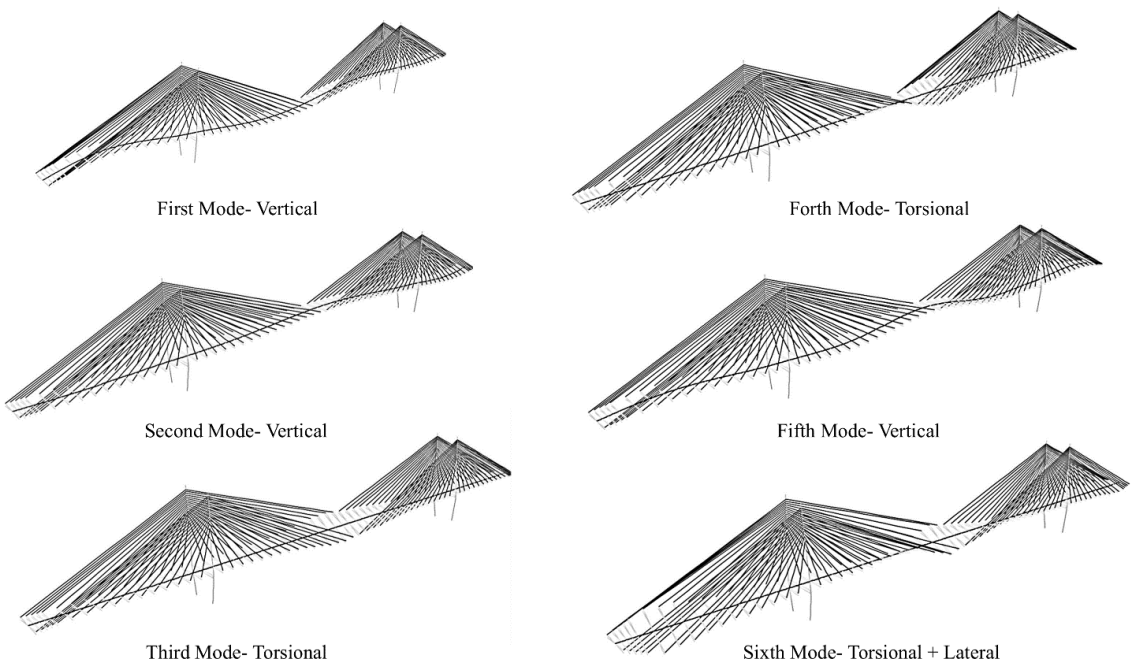

Fig. 4.13: Mode shapes of the benchmark cable-stayed bridge.

4.5. Model Reduction Techniques

The complex nature and size of bridge structures leads to the need of developing large finite elements models in order to capture the dynamic behavior of the bridge accurately. Even though modern computers present a substantial increase in efficiency, storage capacity and speed of processing, there is a good chance that directly adopting the full size finite elements model in simulations is computationally intensive and time-consuming. It is necessary to represent the structural model in an accurate but also efficient way in order to reduce computer storage and solving time requirements. The computational effort of a numerical simulation is approximately proportional to the cubic of the size of the problem, which means it is reduced significantly when the size of the problem is reduced (Qu 2013). In this subsection, selected model reduction techniques are presented and discussed. Subsequently, model reduction is implemented and discussed for the case study's cable-stayed bridge to find the most efficient and accurate model reduction method before the implementation of the developed control techniques.

4.5.1. Mass Lumping

The mass of continuous elements of the bridge may be idealized as concentrated lumps that are representative of the summed masses of a portion of the structure. This procedure is often enough to reduce computational effort for dynamic analysis of smaller bridges, as for example is the case for the highway bridges studied in section 6. This technique requires careful evaluation and considerations regarding the dynamic behavior of the structure, in order to avoid suppression of vibrational modes that are of important

contribution to its dynamic behavior. Static condensation can be applied to eliminate singularities caused by massless nodes that contribute to the stiffness properties of the structure (Chopra 2012).

4.5.2. Static Condensation (Guyan Condensation)

Static condensation is a model reduction method that can be applied to eliminate DOFs with no masses and avoid singularities. The equation of motion for an undamped MDOF system assuming there are no applied forces at the DOFs with zero mass can be represented as follows, where the DOFs with zero mass are represented by the subscript **0** and the DOFs with mass are represented by the subscript **t**:

$$\begin{bmatrix} \mathbf{m}_{tt} & \mathbf{0} \\ \mathbf{0} & \mathbf{0} \end{bmatrix} \begin{Bmatrix} \ddot{\mathbf{x}}_t \\ \ddot{\mathbf{x}}_0 \end{Bmatrix} + \begin{bmatrix} \mathbf{k}_{tt} & \mathbf{k}_{t0} \\ \mathbf{k}_{0t} & \mathbf{k}_{00} \end{bmatrix} \begin{Bmatrix} \mathbf{x}_t \\ \mathbf{x}_0 \end{Bmatrix} = \begin{Bmatrix} \mathbf{p}_t(\mathbf{t}) \\ \mathbf{0} \end{Bmatrix} \tag{4.12}$$

The first portion of equation of motion can be rewritten as:

$$\mathbf{m}_{tt}\ddot{\mathbf{x}}_t + \hat{\mathbf{k}}_{tt}\mathbf{x}_t = \mathbf{p}_t(\mathrm{t}) \tag{4.13}$$

$$\hat{\mathbf{k}}_{tt} = \mathbf{k}_{tt} - \mathbf{k}_{0t}{}^{\mathbf{T}}\mathbf{k}_{00}{}^{-1}\mathbf{k}_{0t} \tag{4.14}$$

Where $\hat{\mathbf{k}}_{tt}$ is the condensed stiffness matrix. Static condensation can be extrapolated to reduce further the system, eliminating DOFs with masses. In this case, the method is only exact for static problems. The full model is separated into master/active DOFs and slave/dependent DOFs. Although not exact, it may represent the system within

suitable precision. The error of the method depends on the cut frequency considered, and the accuracy may be improved by including inertia effects, by optimal selection of master DOFs, and by increasing the number of master DOFs (Qu 2013). Assuming there are no forces in the dependent DOFs, the static equation is represented as follows, where the master DOFs are represented by the subscript **a** and the slave DOFs are represented by the subscript **d**:

$$\begin{bmatrix} \mathbf{k}_{aa} & \mathbf{k}_{ad} \\ \mathbf{k}_{da} & \mathbf{k}_{dd} \end{bmatrix} \begin{Bmatrix} \mathbf{u}_a \\ \mathbf{u}_d \end{Bmatrix} = \begin{Bmatrix} \mathbf{p}_a \\ \mathbf{0} \end{Bmatrix} \tag{4.15}$$

The second portion of the equation can be separated:

$$\mathbf{k}_{da}\mathbf{u}_a + \mathbf{k}_{dd}\mathbf{u}_d = \mathbf{0} \tag{4.16}$$

And the displacement for the dependent DOF may be written as:

$$\mathbf{u}_d = -\mathbf{k}_{dd}^{-1}\mathbf{k}_{da}\mathbf{u}_a \tag{4.17}$$

Taking the first portion of the equation and substituting the displacements for the slave DOFs gives:

$$\mathbf{k}_{aa}\mathbf{u}_a + \mathbf{k}_{ad} - \mathbf{k}_{dd}^{-1}\mathbf{k}_{da}\mathbf{u}_a = \mathbf{p}_a \tag{4.18}$$

Which leads to the transformation matrix, the reduced stiffness and mass matrices:

$$\mathbf{T} = \begin{bmatrix} \mathbf{I} \\ -\mathbf{k}_{dd}^{-1}\mathbf{k}_{da} \end{bmatrix} \tag{4.19}$$

$$\mathbf{K}_{red} = \mathbf{T}^{T}\mathbf{K}\mathbf{T} \tag{4.20}$$

$$\mathbf{M}_{red} = \mathbf{T}^{T}\mathbf{M}\mathbf{T} \tag{4.21}$$

The eigenproblem then becomes:

$$(\mathbf{K}_{red} - \lambda\mathbf{M}_{red})\Phi = \mathbf{0} \tag{4.22}$$

The dependent DOFs displacements may be obtained by:

$$\begin{Bmatrix} \mathbf{u}_a \\ \mathbf{u}_d \end{Bmatrix} = \mathbf{T}\mathbf{u}_a \tag{4.23}$$

The displacements and rotations of the complete model can be easily retrieved:

$$\mathbf{x}_d = -\mathbf{K}_{dd}^{-1}\mathbf{K}_{da}\mathbf{x}_a \tag{4.24}$$

It is important to point out that the eigenvalues of the reduced system are always higher than those of the original system; the quality of the eigenvalue approximation depends highly on the location of points preserved in the reduced model and decreases as the mode number increases. The magnitude of the error depends on the properties of the model and on which and how many DOFs are selected as the masters.

4.5.3. Quasistatic Condensation (Eigenvalue Shift Technique)

This technique can be applied whenever it is desired to improve the accuracy of a specific mode of interest. When this method is applied, the mode closest to the shifting value ends up with the highest accuracy and the error found for the other modes increases. Therefore, its application is found to be appropriate for structures where predominant modes contribute considerably to the response. The eigenproblem for the reduced model is defined by:

$$(\bar{\mathbf{K}} - \bar{\lambda}\mathbf{M})\boldsymbol{\Phi} = \mathbf{0} \tag{4.25}$$

And the dynamic stiffness matrix and eigenvalue with shift **q** are:

$$\bar{\mathbf{K}} = \mathbf{K} - \mathbf{q}\mathbf{M} \tag{4.26}$$

$$\bar{\lambda} = \lambda - \mathbf{q} \tag{4.27}$$

Separating active (master) and dependent (slave) DOFs leads to the following:

$$\left(\begin{bmatrix} \bar{\mathbf{k}}_{aa} & \bar{\mathbf{k}}_{ad} \\ \bar{\mathbf{k}}_{da} & \bar{\mathbf{k}}_{dd} \end{bmatrix} - \bar{\lambda} \begin{bmatrix} \mathbf{m}_{aa} & \mathbf{m}_{ad} \\ \mathbf{m}_{da} & \mathbf{m}_{dd} \end{bmatrix} \right) \begin{Bmatrix} \boldsymbol{\Phi}_a \\ \boldsymbol{\Phi}_d \end{Bmatrix} = \begin{Bmatrix} \mathbf{0} \\ \mathbf{0} \end{Bmatrix} \tag{4.28}$$

The second portion of the equation leads to:

$$\boldsymbol{\Phi}_d = -(\bar{\mathbf{k}}_{dd} - \bar{\lambda}\mathbf{m}_{dd})^{-1}(\bar{\mathbf{k}}_{da} - \bar{\lambda}\mathbf{m}_{da})\boldsymbol{\Phi}_a \tag{4.29}$$

Letting $\bar{\lambda} = \mathbf{0}$ leads to the transformation matrix $\hat{\mathbf{T}}$ and the reduced stiffness and mass matrices:

$$\hat{\mathbf{R}}_G = -(\bar{\mathbf{k}}_{dd})^{-1}\bar{\mathbf{k}}_{da} = -(\mathbf{k}_{dd} - q\mathbf{m}_{dd})^{-1}(\mathbf{k}_{da} - q\mathbf{m}_{da}) \tag{4.30}$$

$$\hat{\mathbf{T}} = \begin{bmatrix} \mathbf{I} \\ \hat{\mathbf{R}}_G \end{bmatrix} \tag{4.31}$$

$$\hat{\mathbf{K}}_{red} = \hat{\mathbf{T}}^T \mathbf{K} \hat{\mathbf{T}} \tag{4.32}$$

$$\hat{\mathbf{M}}_{red} = \hat{\mathbf{T}}^T \mathbf{M} \hat{\mathbf{T}} \tag{4.33}$$

4.5.4. Generalized Guyan Condensation

The condensation matrix obtained through Guyan condensation is independent of the stiffness portion concerning the active DOFs. The generalized Guyan condensation implements all elements of the stiffness matric into the condensation matrix in an attempt of improving the accuracy of the model reduction. Letting the matrices $\mathbf{K_a}$ and $\mathbf{K_d}$ be defined as:

$$\mathbf{K}_a = \begin{bmatrix} \mathbf{k}_{aa} \\ \mathbf{k}_{da} \end{bmatrix} \tag{4.34}$$

$$\mathbf{K_d} = \begin{bmatrix} \mathbf{k_{ad}} \\ \mathbf{k_{dd}} \end{bmatrix} \tag{4.35}$$

Equations (4.15)-(4.18) can be rewritten as:

$$\mathbf{K_a u_a} + \mathbf{K_d u_d} = \mathbf{p} \tag{4.36}$$

$$\mathbf{u_d} = (\mathbf{K_d}^T \mathbf{K_d})^{-1} \mathbf{K_d}^T \mathbf{K_a u_a} \tag{4.37}$$

$$\mathbf{R_G} = (\mathbf{K_d}^T \mathbf{K_d})^{-1} \mathbf{K_d}^T \mathbf{K_a} \tag{4.38}$$

This leads to the reduced stiffness and mass matrices:

$$\mathbf{K_{red}} = \mathbf{k_{aa}} + \mathbf{R_G}^T \mathbf{k_{da}} + \mathbf{k_{ad}} \mathbf{R_G} + \mathbf{R_G}^T \mathbf{k_{dd}} \mathbf{R_G} \tag{4.39}$$

$$\mathbf{M_{red}} = \mathbf{m_{aa}} + \mathbf{R_G}^T \mathbf{m_{da}} + \mathbf{m_{ad}} \mathbf{R_G} + \mathbf{R_G}^T \mathbf{m_{dd}} \mathbf{R_G} \tag{4.40}$$

As observed for Guyan condensation, the frequencies resulting from the reduced model are higher than those from the full model. Recent research shows that the generalized Guyan condensation can have lower accuracy than Guyan condensation due to truncations during the computation of the generalized inverse (Qu 2013).

4.5.5. Common Inverse Two-Step Method

A prediction-correction scheme is utilized in order to increase the accuracy of Guyan condensation in this method. The prediction stage is obtained by Guyan condensation, and the correction stage is obtained by application of Kidder's mode expansion (Kidder 1973) to estimate the mode shapes for the dependent DOFs. Assuming the active DOFs eigenvalues and their corresponding eigenvectors are computed, the eigenvectors at the dependent DOFs can be obtained by:

$$\boldsymbol{\varphi}_{id} \approx -(\mathbf{k}_{dd}^{-1} + \lambda_i \mathbf{k}_{dd}^{-1}\mathbf{m}_{dd}\mathbf{k}_{dd}^{-1})(\mathbf{k}_{da}^{-1} - \lambda_i \mathbf{m}_{da})\boldsymbol{\varphi}_{ia} \tag{4.41}$$

The eigenproblem of the reduced model defined by Guyan condensation is given by:

$$(\mathbf{K}_G - \lambda \mathbf{M}_G)\boldsymbol{\Phi}_m = \mathbf{0} \tag{4.42}$$

$$\mathbf{M}_G^{-1}\mathbf{K}_G\boldsymbol{\Phi}_m = \lambda\boldsymbol{\Phi}_m \tag{4.43}$$

Introducing this into Equation (4.41):

$$\boldsymbol{\varphi}_{id} \approx [-\mathbf{k}_{dd}^{-1}\mathbf{k}_{da}^{-1} + \mathbf{k}_{dd}^{-1}(\mathbf{m}_{da} - \mathbf{m}_{aa}\mathbf{k}_{dd}^{-1}\mathbf{k}_{da})\mathbf{M}_G^{-1}\mathbf{K}_G]\boldsymbol{\varphi}_{ia} \tag{4.44}$$

Defining the dynamic condensation matrix ***R*** as:

$$\boldsymbol{\Phi}_{id} = \mathbf{R}\boldsymbol{\Phi}_{ia} \tag{4.45}$$

$$\mathbf{R} = \mathbf{R}_G + \mathbf{K}_{dd}^{-1}[(\mathbf{M}_{da} - \mathbf{M}_{aa}\mathbf{K}_{dd}^{-1}\mathbf{K}_{da})\mathbf{M}_G^{-1}\mathbf{K}_G] \tag{4.46}$$

Leads to the transformation matrix, the reduced stiffness and mass matrices:

$$\mathbf{T} = \begin{bmatrix} \mathbf{I} \\ \mathbf{R} \end{bmatrix} \tag{4.47}$$

$$\mathbf{K}_{red} = \mathbf{T}^T\mathbf{K}\mathbf{T} \tag{4.48}$$

$$\mathbf{M}_{red} = \mathbf{T}^T\mathbf{M}\mathbf{T} \tag{4.49}$$

When it comes to predicting mode shapes and frequencies, the accuracy of the method of this method is shown to be higher than of the Guyan condensation, although extra computational effort is required to formulate the dynamic condensation matrix. The method is also more accurate than the generalized Guyan condensation, given there is no computation of the generalized inverse that leads to loss of accuracy.

4.5.6. Model Reduction for the Cable-Stayed Bridge

The cable stayed-bridge complete finite elements structural model developed in SAP2000® results in a total of 2532 DOFs. It is desired to reduce the number of DOFs considered for the dynamic analysis to remove singularities and for it to become computationally manageable. Fig. 4.14 displays the cable-stayed bridge model active nodes considered in this research. The choice of active and dependent nodes follows

careful evaluation and considerations regarding the dynamic behavior of the structure, and its vibrational modes contribution and shapes. A total of four aforementioned reduction methods are used to reduce the size of the of the bridge: Guyan condensation, quasistatic condensation, generalized Guyan condensation, and common inverse method. The reduced model has a total of 231 DOFs.

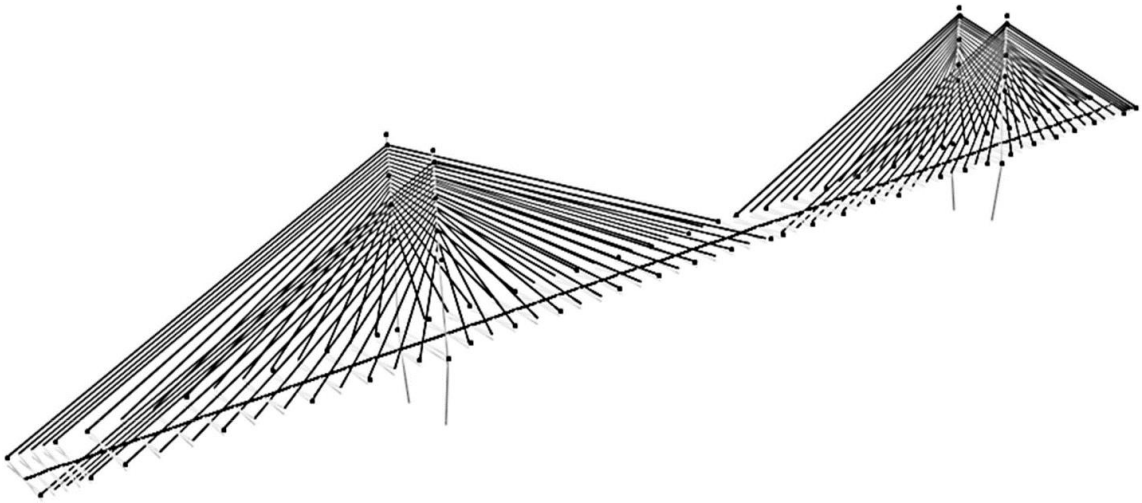

Fig. 4.14: Active nodes considered for the cable-stayed bridge model reduction.

The solution of the eigenproblem for reduced and complete model is displayed in Table 4.4 for the first 6 modes, along with the percentage error between the complete and reduced model found for each method. The common inverse model reduction method provided the least error when considering the modal frequencies, followed by Guyan with shift (quasistatic), and Guyan condensation. The generalized Guyan technique provided unsatisfactory results, reaching a maximum percentage error of 84.5%. This is attributed to the numerical truncation errors accumulated during the computation of the generalized inverse $(\mathbf{K_d}^{\mathbf{T}}\mathbf{K_d})^{-1}$. Due to this great discrepancy between the reduced and the complete

model, this method is discarded as a viable method for model reduction of the cable-stayed bridge.

Table 4.4: Eigenvalues and percentage error for model reduction methods.

Mode	Freq. (Hz)	Error (%)	Mode	Freq. (Hz)	Error (%)
Guyan			Quasistatic Condensation		
# 1	0.296	0.008%	# 1	0.296	0.006%
# 2	0.306	0.020%	# 2	0.306	0.014%
# 3	0.432	1.139%	# 3	0.432	0.989%
# 4	0.521	3.103%	# 4	0.520	2.805%
# 5	0.597	0.123%	# 5	0.597	0.113%
# 6	0.631	2.449%	# 6	0.630	2.308%
Generalized Guyan			Common Inverse		
# 1	0.337	13.589%	# 1	0.296	0.000%
# 2	0.487	59.471%	# 2	0.306	0.000%
# 3	0.634	48.335%	# 3	0.427	0.000%
# 4	0.935	84.929%	# 4	0.506	0.002%
# 5	0.935	56.732%	# 5	0.597	0.000%
# 6	0.951	54.331%	# 6	0.616	0.001%

For further investigation of the accuracy of the methods, the complete and reduced model by Guyan condensation, Guyan with shift, and common inverse are subjected to 3 different earthquake records: El Centro (1940), Chi-Chi (1999), and Landers (1992). Fig. 4.15 and Fig. 4.16 display, respectively, tower 1 longitudinal (*X* direction, along the deck) displacements and velocities time-histories of the complete and the reduced model compared. Table 4.5 shows the maximum percentage error between the complete and reduced models displacements, velocity, and accelerations of tower 1.

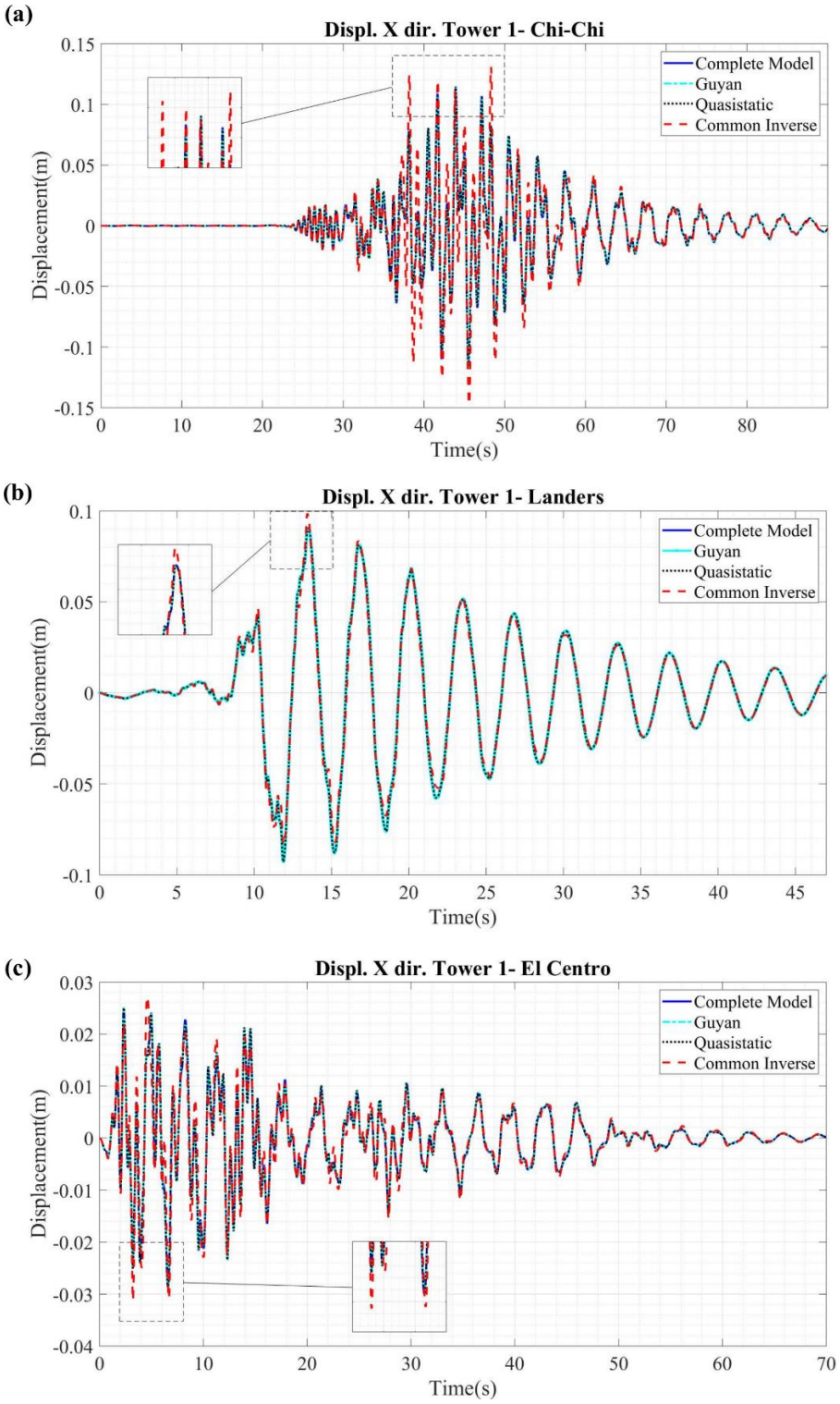

Fig. 4.15: Cable-stayed bridge tower 1 displacements: complete model and model after 3 different model reduction techniques. (a) Chi-Chi (b) Landers (c) El Centro.

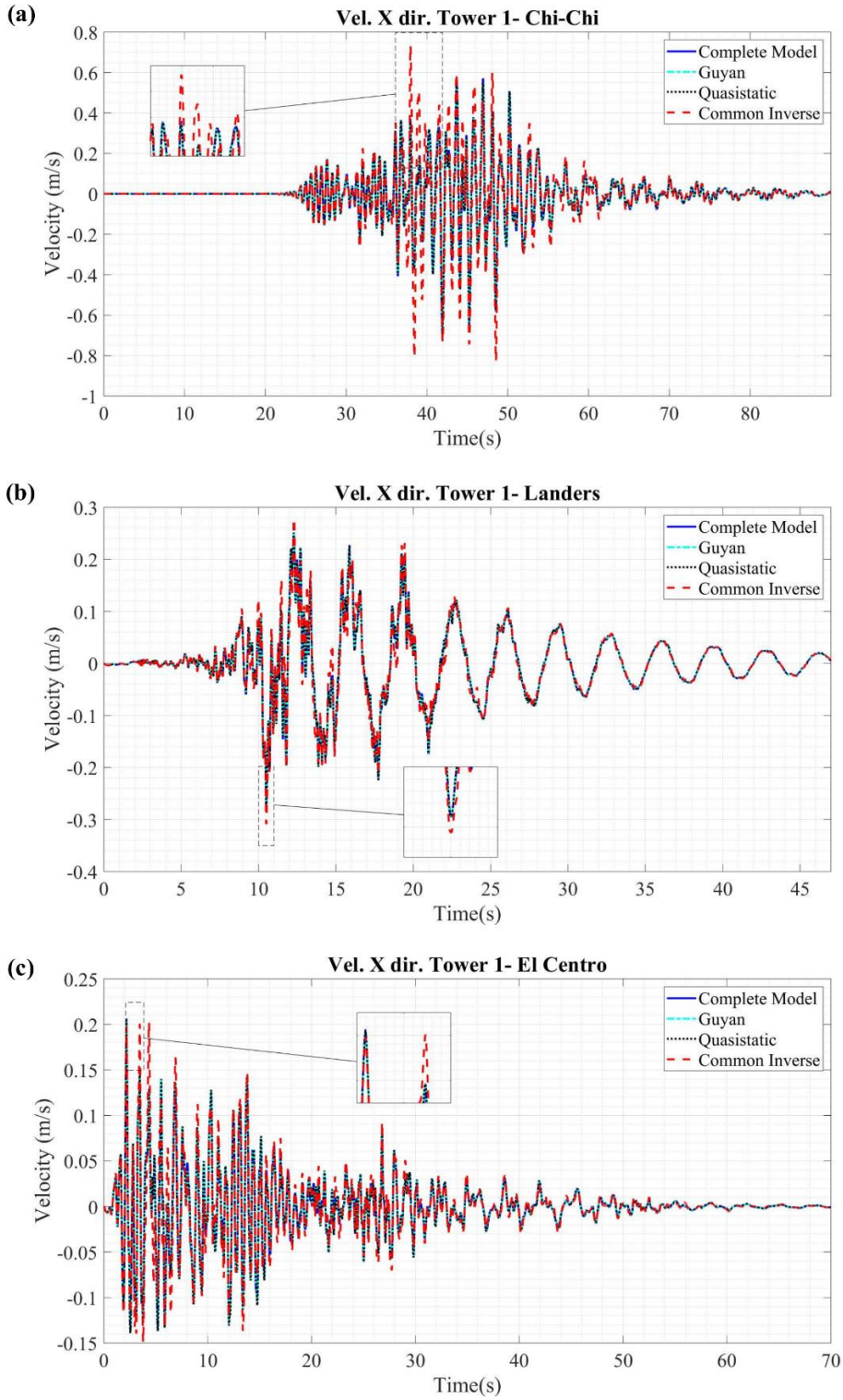

Fig. 4.16: Cable-stayed bridge tower 1 velocities: complete model and model after 3 different model reduction techniques. (a) Chi-Chi (b) Landers (c) El Centro.

Table 4.5: Maximum percentage error between complete and reduced model.

Earthquake	Displacements	Velocities
	Guyan Condensation	
Chi-Chi	3.4%	3.4%
Landers	1.4%	4.3%
El Centro	5.2%	6.2%
	Quasistatic Condensation	
Chi-Chi	3.4%	3.4%
Landers	1.4%	4.2%
El Centro	5.2%	6.3%
	Common Inverse Two-step Method	
Chi-Chi	57.2%	65.2%
Landers	13.2%	26.7%
El Centro	38.6%	45.0%

Guyan condensation with shift gave the least error for computation of responses under seismic loading, followed by Guyan condensation. The results for both techniques are very similar but Guyan condensation is of simpler formulation. For simplicity, Guyan condensation technique is chosen for the model reduction of the cable-stayed bridge. The reduced model by Guyan condensation is found to exhibit satisfactory estimation of modal properties and seismic response.

4.6. Considerations Regarding Modeling Assumptions and Simplifications

Bridges are usually substantial in size and structurally complex; as a consequence, many simplifications are necessary to guarantee the dynamic analyses of bridges are computationally feasible. Additionally, a number of modeling assumptions and simplifications are presumed when developing a structural model for dynamic analysis and control design. Consideration of kinematic constraints, the mass lumping approach's

choice, the choice of active nodes, the choice of a model reduction method, damping considerations and material properties approximations precede the development of a representative structural model. Careful investigation and validations are followed by a decision-making process that leads to the acceptance of the model as structurally representative of the bridge. Also, bridges undergo localized damage and deterioration, fatigue, accumulation of snow and cracking over the course of their service life. All the aforementioned factors will lead to bridge actual parameters being discrepant in comparison to the parameters considered during control design. Therefore, parametric estimates considering the nominal structure are likely to differ from actual existing structural parameters.

The development of a control scheme that presents satisfactory performance when considering the nominal structure and presents a predictable behavior and enough robustness in face of parametric variations is fundamental for its successful operation. A system that does not offer these characteristics require extensive instrumentation of the existing structure, continuous monitoring and model identification to guarantee the control strategy remains effective and it does not worsen the dynamic performance of the bridge. The adaptive schemes proposed in this research are therefore presented as a potential control scheme that is able to provide the necessary predictability and robustness to bridge control.

5. STRUCTURAL CONTROL

In this section, the structural dynamic control theoretical and methodological bases necessary to the development of this research are described and discussed. In section 5.1, control devices dynamic behavior and modeling particularities are presented. Control devices are the physical materialization of the structural control scheme, which are responsible for either actively introducing the control forces or for resisting and dissipating energy. In section 5.2, the control strategies theoretical basis, modeling, and implementation details are presented. The control strategies are responsible for calculating the control command, which is conveyed to the control device so the structure achieves an acceptable dynamic performance.

5.1. Control Devices

Control devices dynamic behavior and modeling particularities are presented in this portion of the research. The particular control devices utilized during the development of this work and to be discussed in this section are the MR dampers and resettable dampers, which are semi-active control devices; and the hydraulic actuators, which are active control devices.

5.1.1. Magneto-Rheological (MR) Dampers

The MR damper is a semi-active controllable damper that provides dependable functionality with considerably low power requirements. These devices present the

advantage of becoming passive dampers in case there is any malfunction, which guarantees a basic level of functionality (Spencer Jr et al. 1997). These dampers are filled with magnetorheological fluid, which is capable of changing its rheological behavior when subjected to an electromagnetic field. This phenomenon gives the dampers the ability of changing its resistance capacity. Magnetorheological fluids are composed of a liquid and soft iron particles, 20-40% in volume; some liquids used in manufacturing of MR dampers are glycol, water, mineral or synthetic oil. The major advantages of using MR dampers to control civil structures are: the large yield stress it is able to achieve, which impacts the device size and dynamic range; being able to be sourced by low-voltage batteries; being less susceptible to dielectric breakdown, contamination and extreme temperatures than other semi-active devices such as ER dampers (Spencer and Sain 1997). According to Spencer and Nagarajaiah (2003), these devices have the advantage of being mechanically simple given they do not contain any moving parts except the piston. Fig. 5.1 gives a simple schematics of MR dampers typical components and Fig. 5.2 shows an example of a commercially available MR damper.

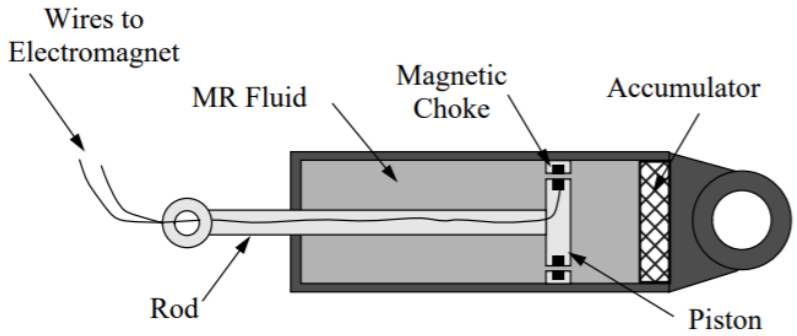

Fig. 5.1: MR damper typical components, adapted from Spencer Jr et al. (1997).

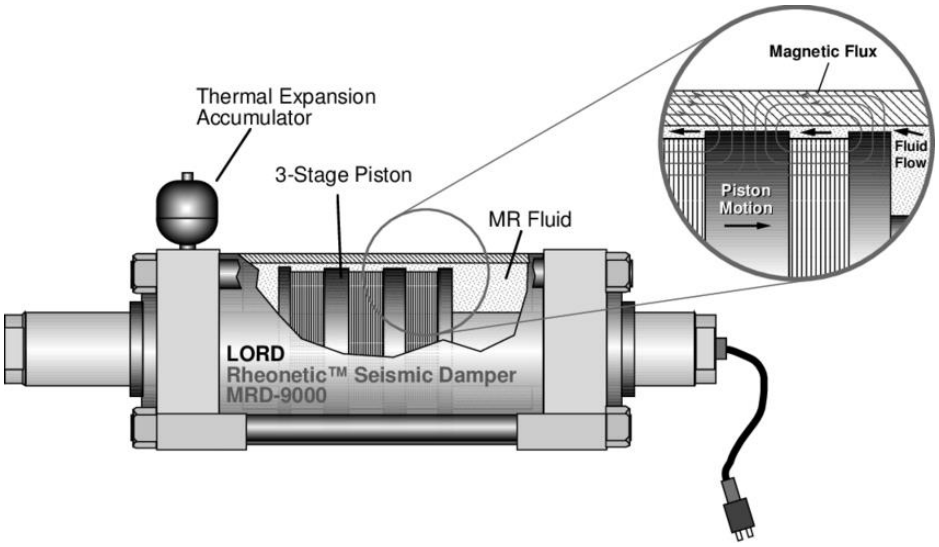

Fig. 5.2: Example of a MR damper.

There are many models available in the literature that may be adopted to model the dynamics of the MR dampers. In this research, the simple Bouc-Wen model is chosen to develop the dynamic model of the MR dampers, given its general satisfactory prediction of the force-displacement and force-velocity diagrams in comparison to experimental data (Spencer Jr et al. 1997) and its simplicity. In the simple Bouc-Wen model, the dynamic behavior of the device is represented by the hysteresis of the Bouc-Wen model (Wen, 1976) and a viscous damper acting in parallel, as shown in Fig. 5.3.

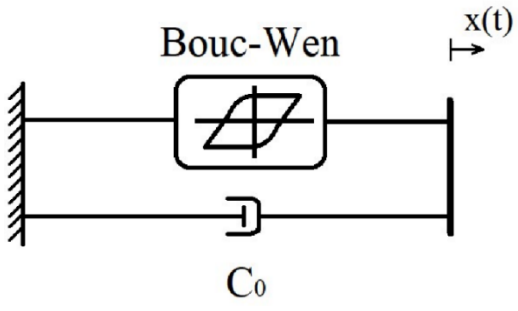

Fig. 5.3: Simple Bouc-Wen Model.

The damper force is obtained by Equation (5.1), where $\dot{x}$ is the velocity and C_0 is obtained by Equation (5.2), where α is obtained by Equation (5.3), C_{0a} and C_{0b} are constants. The input voltage *u* can be obtained by the inverse model described by Equation (5.4), where *f* is the controller output. The input voltage can be obtained by the first order filter given by Equation (5.5), where *v* is the output voltage. The evolutionary variable *z* is responsible for representing the hysteretic behavior; the evolutionary variable is obtained by Equation (5.6), where γ, β, *A*, and *n* are constants.

$$f = C_0\dot{x} + \alpha z \tag{5.1}$$

$$C_0 = C_{0a} + C_{0b}u \tag{5.2}$$

$$\alpha = \alpha_a + \alpha_b u \tag{5.3}$$

$$u = \frac{f - C_{0a}\dot{x} - \alpha_a z}{C_{0b}\dot{x} - \alpha_b z} \tag{5.4}$$

$$v = u + \frac{\dot{u}}{\eta} \tag{5.5}$$

$$\dot{z} = -\gamma|\dot{x}|z|z|^{(n-1)} - \beta\dot{x}|z|^n + A\dot{x} \tag{5.6}$$

Table 5.1 presents the parameters of the 1000 kN (224.8 kips) MR damper used on this research, retrieved from Jung et al. (2003). In this research, MR dampers also are set to work as purely passive devices. The following schemes are considered: the passive-off scheme, which accounts for the case where the device is working with zero voltage; the passive-on scheme, which accounts for the case where the device is working with its maximum voltage.

Table 5.1: MR damper parameters.

Parameter	Value	Parameter	Value
C_{0a}	105.4 (kN.s/m)	α_b	29.1 (kN/m/V)
C_{0b}	131.6 (kN.s/m/V)	β	141.0 (m^{-2})
α_a	26 (kN/m)	γ	141.0 (m^{-2})
V_{max}	10 (V)	n	2
A	2074.5	η	100 (s^{-1})

5.1.2. Resettable Dampers

Resettable dampers are semi-active devices composed by a two-way piston and a valve. Whenever the valve is closed, the fluid inside the cylinder is compressed by the motion of the piston; once the valve is open, the energy stored in the fluid is dissipated. These devices have been successfully applied to multi-level seismic hazard mitigation of steel moment frames and were proven capable of reducing permanent deflections (Barroso et al. 2003). Resettable dampers work as pneumatic spring devices that change the stiffness of the system and dissipate energy. They are feasible in both pneumatic and hydraulic versions, and are capable of producing large resisting forces (Jabbari and Bobrow 2002).

Fig. 5.4 shows the general schematics of the device. When the device valve is closed and the device is compressed (or extended) energy is stored in the piston. As the energy storage rate is stationary, the valve is quickly opened and shut, releasing the energy from the system (Barroso et al. 2003). The forces of the piston are dependent on the piston area, stroke, and fluid bulk modulus, and it is possible to create devices with output forces in the megaton range (Jabbari and Bobrow 2002). Since the dynamics is considerably faster than most structures dynamics, no additional dynamics analysis is needed beyond the resetting of the valve. Testing performed by Jabbari and Bobrow (2002) showed a resetting time of 20-30ms, which implicates the dynamics of the device is not significant for frequencies up to 20 Hz. Considering that most civil engineering structures operate in frequencies smaller than this, it is safe to justify the approximation for the behavior of the device as a linear spring.

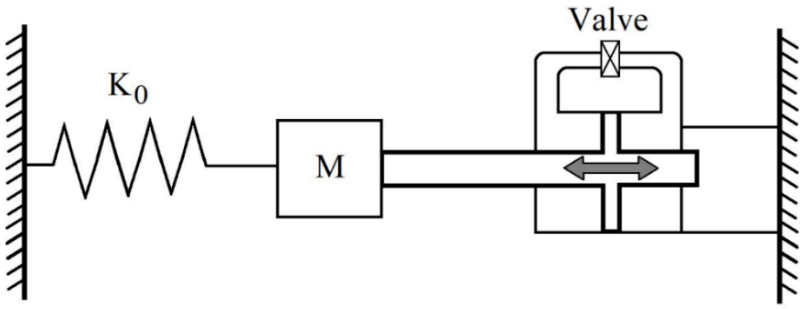

Fig. 5.4: Schematics of a resettable damper device.

The device resisting force is obtained by Equation (5.7), where A is the piston area, β is the fluid bulk modulus, and s is the cylinder stroke length. The equation of motion for a MDOF system controlled by a resettable device is given by Equation (5.8). The rate of change in the energy can be obtained by taking the time derivative of the energy stored in the device given by Equation (5.9), which leads to Equation (5.10). The device stores energy if $\dot{U} > 0$; as soon as the device resets, the energy is released and $\dot{U} = 0$. The control law for the device can be defined then by Equation (5.11), it ensures that the device always removes energy from the system. Table 5.2 gives the parameters for the device considered in this research (Jabbari and Bobrow 2002). The device considered in this study has the maximum control force of 1000kN.

$$F(x) = -\frac{4A\beta}{s}x \tag{5.7}$$

$$\mathbf{M}\ddot{\mathbf{x}} + \mathbf{C}\dot{\mathbf{x}} + \mathbf{K}\mathbf{x} + \sum_i \left(-\frac{4A\beta}{s} \right)_i (\mathbf{x} - \mathbf{x_{s,i}}) = \mathbf{0} \tag{5.8}$$

$$U = \frac{1}{2}\sum_i (x - x_{s,i})^T K_i (x - x_{s,i}) \tag{5.9}$$

$$\dot{U} = \dot{x}^T K_i (x - x_{s,i}) \tag{5.10}$$

$$\text{set } x_{s,i} = x \text{ whenever } \dot{U}_i = 0 \tag{5.11}$$

Table 5.2: Resettable damper parameters.

Parameter	Value
β	1723.7 (MPa)
s	10.16 (cm)
A	12.9 (cm^2)

5.1.3. Hydraulic Actuators

Hydraulic actuators are active control devices that operate through highly pressurized hydraulic power. These devices are able to provide high forces, while requiring very high power sources. In these actuators, the AC motor turns electrical power into mechanical power so the hydraulic fluid inside their chamber gets pumped and pressurized. The hydraulic fluid can be composed of mineral oils or oil in water emulsion. A relief valve and an accumulator are responsible for regulating and stabilizing the pressure; a servo valve controls the fluid rate and the pressure into the actuator. Through a feedback control system based on the sensed response, the servo valve manages the actuator in order to achieve the desired load. One disadvantage of this device is the high nonlinearity commonly observed in fluid power systems (De Silva 2015).

The actuator force is obtained by the first order differential Equation (5.12), where f is the actuator force, $\dot{x}$ is the velocity, u_v is the servo-valve input. The constants α_1, α_2 and α_3 are obtained by Equations (5.13)-(5.15), where β is the fluid bulk modulus, A_{HA} is the cross sectional area of the actuator, k_q is the flow gain, V_t is the total volume of the actuator chamber, and k_c is the flow pressure coefficient. A PID control is implemented to calculate the input command and stabilize the actuator through a feedback scheme.

Table 5.3 shows the parameters considered in this study which correspond to a 1000 kN hydraulic actuator. Fig. 5.5 shows the block diagram of the hydraulic actuator system.

$$\dot{f} = \alpha_1 u_v - \alpha_2 \dot{x} - \alpha_3 f \tag{5.12}$$

$$\alpha_1 = \frac{4\beta A_{HA} k_q}{V_t} \tag{5.13}$$

$$\alpha_2 = \frac{4\beta A_{HA}^{\ 2}}{V_t} \tag{5.14}$$

$$\alpha_3 = \frac{4\beta k_c}{V_t} \tag{5.15}$$

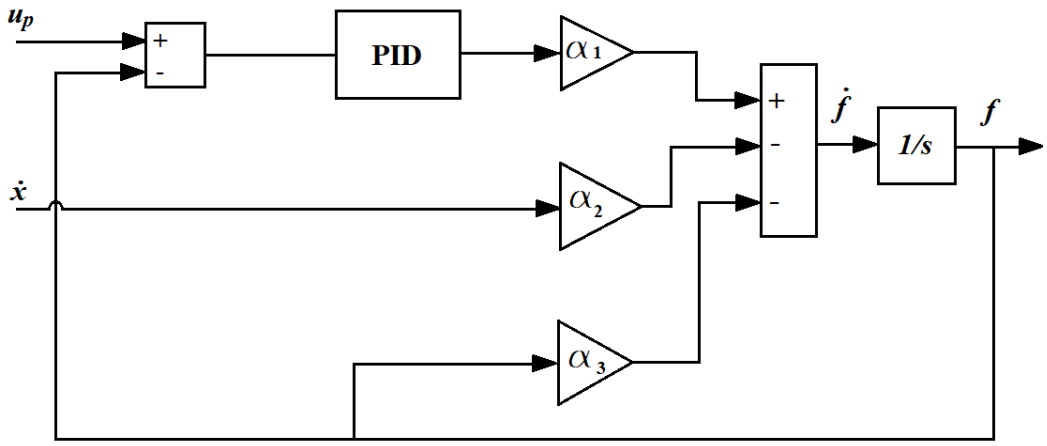

Fig. 5.5: Hydraulic actuator system block diagram

Table 5.3: Hydraulic actuator parameters.

Parameter	Value
α_1	5.81×10^6 (kN/ms)
α_2	5.46×10^3 (kN/m)
α_3	1.62×10^3 (s^{-1})

5.2. Control Strategies

Control strategies theoretical basis, modeling, and implementation details are presented in this portion of the research. The particular control strategies utilized during the development of this work and to be discussed in this section are the optimal control linear quadratic regulator (LQR), the simple adaptive control (SAC) and the neuro-fuzzy adaptive control.

5.2.1. Optimal Control

Optimal control is obtained when a control law is found to satisfy a criterion of optimality. The criterion defined as optimal is established by the designer in the form a mathematical scale that quantifies the best choice for the object of the design in question.

5.2.1.1. Linear Quadratic Regulator (LQR)

The LQR is an optimal control strategy that pursues a suitable control solution with minimum cost. A regulator control problem seeks to return to the equilibrium position a system initially displaced by minimizing a performance index. The LQR control law gives an optimal control solution for a linear system by minimizing the quadratic performance

index **J** given by Equation (5.16), where **z**(t) are the states for the system, **Q** is a symmetric semi-definite matrix and **R** is symmetric and positive definite. Changing matrices **Q** and **R** are the way to tune the controller. A very small **R**, for example, means fast convergence and high control efforts.

$$\mathbf{J} = \int_0^{t_f} \left[\mathbf{z}(t)^T \mathbf{Q} \mathbf{z}(t) + \mathbf{u}(t)^T \mathbf{R} \mathbf{u}(t) \right] \mathbf{dt} \tag{5.16}$$

The control law for the strategy is given by Equation (5.17) and the gain **K** is obtained by Equation (5.18). **P** is the unique solution of the non-linear matrix Riccatti Equation (5.19). The solution for this equation can be obtained by matrix factorizations, by iterative processes or eigen decomposition. One broadly adopted method to solve these types of equations was developed by Arnold and Laub (1984). LQR stability is easily guaranteed if all the states in the system are available for feedback (full-feedback), and the model of the system is well defined. The feedback control scheme for a system controlled by the LQR strategy with full feedback is given by Fig. 5.6.

$$\mathbf{u}(t) = \mathbf{K} \mathbf{z}(t) \tag{5.17}$$

$$\mathbf{K} = \mathbf{R}^{-1} \mathbf{B}^T \mathbf{P} \tag{5.18}$$

$$\mathbf{A}^T \mathbf{P} + \mathbf{P} \mathbf{A} - \mathbf{B} \mathbf{P} \mathbf{R}^{-1} \mathbf{B}^T \mathbf{P} + \mathbf{Q} = \mathbf{0} \tag{5.19}$$

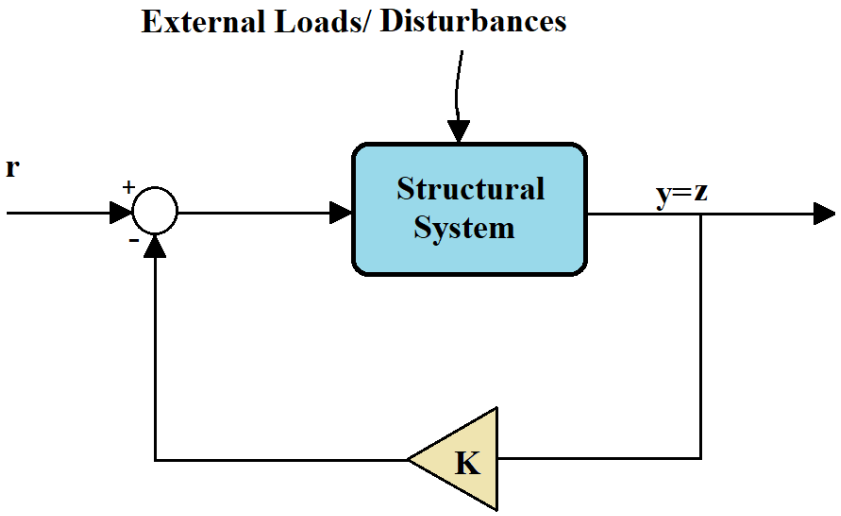

Fig. 5.6: LQR-controlled system with full-feedback.

5.2.1.2. Linear Quadratic Estimator

In the case where it is not possible to measure directly all states from the system, it is necessary to introduce an observer to reconstruct them based on measurable outputs. One way of estimating the states is the implementation of an optimal Linear Quadratic Estimator (LQE). The LQE optimally estimates the state in the presence of Gaussian noises present in the output measurements. Given a system with white process noise **w** and white measurement noise **v** that are zero-mean stochastic Gaussian processes, uncorrelated in time and with each other:

$$\dot{\mathbf{x}} = \mathbf{A}\mathbf{x} + \mathbf{B}\mathbf{u} + \mathbf{G}\mathbf{w} \tag{5.20}$$

$$\mathbf{y} = \mathbf{C}\mathbf{x} + \mathbf{u} + \mathbf{H}\mathbf{w} + \mathbf{v} \tag{5.21}$$

Defining the zero-mean stochastic Gaussian processes covariance:

$$E(\mathbf{w}\mathbf{w}^T) = W \tag{5.22}$$

$$E(\mathbf{v}\mathbf{v}^T) = V \tag{5.23}$$

$$E(\mathbf{w}\mathbf{v}^T) = S \tag{5.24}$$

The objective is to construct an estimate for the states that minimizes the steady-state error covariance:

$$P = \lim_{t\to\infty} E\left[(\mathbf{x} - \hat{\mathbf{x}})(\mathbf{x} - \hat{\mathbf{x}})^{\mathbf{T}}\right] \tag{5.25}$$

The LQE can be designed as given by Equation (5.26), where $\hat{\mathbf{x}}$ is the state estimate, **L** is the observer gain matrix given by Equation (5.27)-(5.29) and **P** is the solution of the corresponding Algebraic Riccatti Equation (5.30). Fig. 5.7 gives the block diagram for implementation of the observer.

$$\dot{\hat{\mathbf{x}}} = \mathbf{A}\hat{\mathbf{x}} + \mathbf{B}\mathbf{u} + \mathbf{L}(\mathbf{y} - \mathbf{C}\hat{\mathbf{x}}) \tag{5.26}$$

$$\mathbf{L} = (\mathbf{P}\,\mathbf{C}^{\mathbf{T}}\bar{\mathbf{S}})\bar{\mathbf{V}}^{-1} \tag{5.27}$$

$$\bar{\mathbf{V}} = \mathbf{V} + \mathbf{HS} + \mathbf{S}^{\mathrm{T}}\mathbf{H}^{\mathrm{T}} + \mathbf{HWH}^{\mathrm{T}} \tag{5.28}$$

$$\bar{\mathbf{S}} = \mathbf{G}\left(\mathbf{WH}^{\mathrm{T}} + \mathbf{S}\right) \tag{5.29}$$

$$\mathbf{AP} + \mathbf{PA}^{\mathrm{T}} - (\mathbf{PC}^{\mathrm{T}}\bar{\mathbf{S}})\bar{\mathbf{V}}^{-1}\mathbf{C}^{\mathrm{T}}\mathbf{P} + \mathbf{W} = \mathbf{0} \tag{5.30}$$

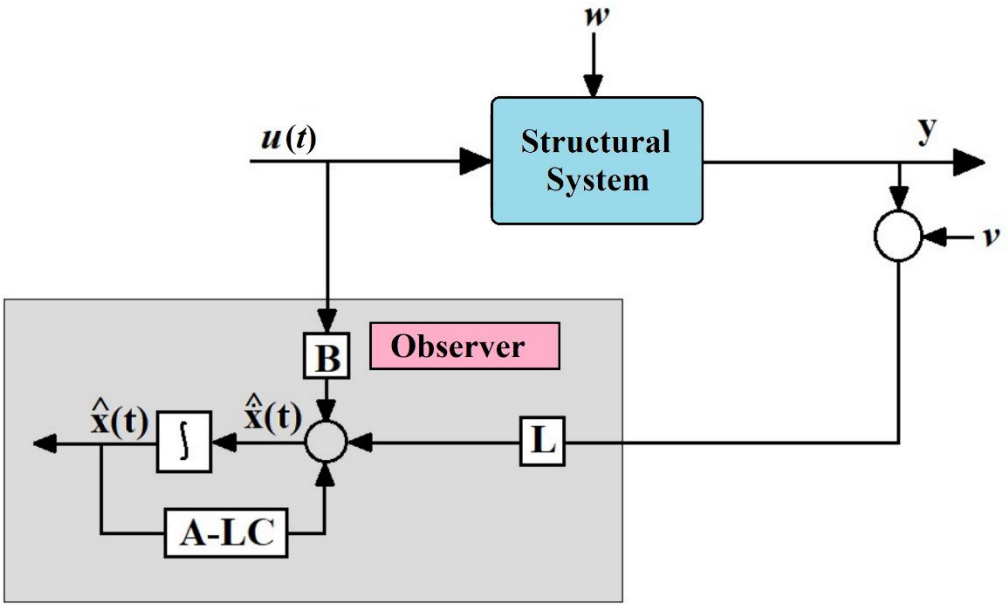

Fig. 5.7: Block diagram of LQE's implementation.

5.2.2. Simple Adaptive Control

Model reference control is a type of control that operates to match the response of a system to a reference system, which responds accordingly to a desirable design specification. The control command of a model reference control drives the structural system to behave as the model reference. The design of this system and computation of

control gains would require previous knowledge of the system parameters, which leads to the need of adaptation in order to deal with parametric uncertainty. Adaptive techniques are categorized into explicit (indirect) or implicit (direct). The indirect methods require the explicit estimation of the structural parameters for development of the adaptation process. The direct methods develop the adaptation process without explicit computation of structural parameters. The adaptation process is carried out based solely on the errors between the actual structure and the model reference outputs, leading them to tend to zero asymptotically. The direct methods are appealing for implementation given they eliminate the need of designing complex and efficient online identifiers.

The simple adaptive control (SAC) is an implicit, or direct, model reference adaptive control. SAC was first introduced in (Sobel et al. 1982) and it has been developed over the last decades through a series of studies (Barkana 1987, Barkana and Guez 1990, Barkana and Kaufman 1993, Barkana 2005, 2008, 2013, 2014, 2016a, c, b). The method is based on the classical model reference adaptive control (MRAC) as an attempt to overcome many of its drawbacks when it comes to its implementation for MIMO systems. Since SAC is a direct adaptive control method, it does not explicitly calculate the actual structural parameters in order to compute control gains. SAC does not require full identification of the parameters of the actual structure, and also allows the choice of a model reference of lower order than the system. The method is appealing to be applied in large scale structures because its implementation is simple and successful in tracking the behavior of the reference. SAC gives the possibility of adopting a significantly reduced order model reference even for complex and large structural systems, and it is applicable

to unstable systems. SAC is proven to guarantee perfect tracking asymptotically and it does not require full-state feedback or the use of identifiers or observers (Barkana 2016c). Since its early developments, SAC was applied successfully to control a handful of structures, including civil structures. The results indicate the control method is promising in overcoming parametric changes, disturbances, and noise.

The governing state-space representation for the structural system and the model reference are defined by Equations (5.31)-(5.34). In the equations, $\mathbf{A_p}$, $\mathbf{B_p}$, and $\mathbf{C_p}$ are the state, input, and output matrices for the actual structural system, respectively. $\mathbf{A_m}$, $\mathbf{B_m}$, and $\mathbf{C_m}$ are the state, input, and output matrices for the model reference, respectively. $\mathbf{d_i}(t)$ and $\mathbf{d_0}(t)$ are input and output disturbances.

$$\dot{\mathbf{x}}_\mathbf{p}(t) = \mathbf{A_p}\mathbf{x_p}(t) + \mathbf{B_p}\mathbf{u_p}(t) + \mathbf{d_i}(t) \tag{5.31}$$

$$\mathbf{y_p}(t) = \mathbf{C_p}\mathbf{x_p}(t) + \mathbf{d_0}(t) \tag{5.32}$$

$$\mathbf{x_m}(t) = \mathbf{A_m}\mathbf{x_m}(t) + \mathbf{B_m}\mathbf{u_m}(t) + \mathbf{d_i}(t) \tag{5.33}$$

$$\mathbf{y_m}(t) = \mathbf{C_m}\mathbf{x_m}(t) \tag{5.34}$$

SAC's control law is given by Equation (5.35), where $\mathbf{r}(t)$ is a matrix composed by the error between the output of the model reference and the measured outputs $\mathbf{e_y}$, the model reference states and input $\mathbf{x_m}$, and $\mathbf{u_m}$, respectively. The time-varying control gain

matrix $\mathbf{K}(t)$ defined by Equation (5.36) is calculated by solving the differential Equations (5.38)-(5.40).

$$\mathbf{u_p}(t) = \mathbf{K}(t)\,\mathbf{r}(t) \tag{5.35}$$

$$\mathbf{K}(t) = [\mathbf{K_e}(t),\quad \mathbf{K_x}(t),\quad \mathbf{K_u}(t)] \tag{5.36}$$

$$\mathbf{r}^{\mathbf{T}}(t) = [\mathbf{e_y}(t)\quad \mathbf{x_m}^{\mathbf{T}}(t)\quad \mathbf{u_m}^{\mathbf{T}}(t)] \tag{5.37}$$

$$\dot{\mathbf{K}}_{\mathbf{e}}(t) = \mathbf{e_y}(t)\mathbf{e_y}(t)^{\mathbf{T}}\boldsymbol{\Gamma}_{\mathbf{e}} \tag{5.38}$$

$$\dot{\mathbf{K}}_{\mathbf{x}}(t) = \mathbf{e_y}(t)\mathbf{x_m}(t)^{\mathbf{T}}\boldsymbol{\Gamma}_{\mathbf{x}} \tag{5.39}$$

$$\dot{\mathbf{K}}_{\mathbf{u}}(t) = \mathbf{e_y}(t)\mathbf{u_m}(t)^{\mathbf{T}}\boldsymbol{\Gamma}_{\mathbf{u}} \tag{5.40}$$

SAC guaranteed stability depends on the system transfer function being almost strictly positive real (ASPR), which many real-world systems cannot be guaranteed to satisfy. A system is defined as ASPR when exists a gain in a closed-loop system that can guarantee the system is strictly positive real (SPR). In SAC's early formulations, a sigma term had been used to guarantee stability under disturbances; however, it has been observed that this term could eliminate perfect tracking, and lead to chaotic-like phenomena. A parallel feedforward (PFC) term was introduced in Barkana (2016c) to guarantee perfect tracking and robustness under disturbances and non-ideal scenarios,

eliminating the sigma term. The parallel feedforward configuration added guaranteed ASPR conditions. Fig. 5.8 shows the detailed block diagram of SAC.

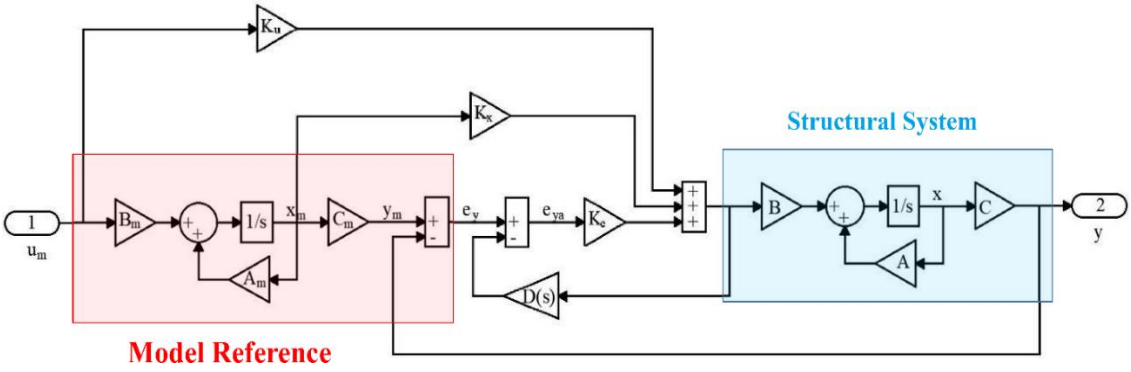

Fig. 5.8: Block diagram for SAC strategy.

5.2.3. Neuro-Fuzzy Adaptive Control

Neural-Fuzzy adaptive controllers are the combination of the two intelligent controllers fuzzy inference systems (FIS) and learning neural networks (ANN) to build a hybrid intelligent system. Neural networks adjust the membership functions of the fuzzy system, giving it a higher adaptation capability. Fuzzy logic is defined as logic that involves not only true and false statements as Boolean logic, but also includes partially true or partially false statements. This allows for logical reasoning by the introduction of imprecise statements. The statements are built following experts' knowledge that are translated in the form of fuzzy logic rules sets. These rules sets are a combination of "if-then" statements and membership functions that correlate the input and the output. FIS apply fuzzy logic to generate control command.

The process of converting numerical values into fuzzy values is called fuzzification, where the input is converted into a number ranging from 0 to 1. The membership functions link the input to the fuzzy scale. The development of the membership functions sets requires defining a data universe based on expert's knowledge; these functions are the key elements of the decision making process: the knowledge base. Fig. 5.9 gives an example of the fuzzification process. After the input passes through the fuzzification process and the knowledge base lead to the decision making, it is time for the defuzzification, where the fuzzy outputs are transformed in order to be expressed in terms of well-defined values, or crisp values. Fig. 5.10 shows the general functioning process of the FIS.

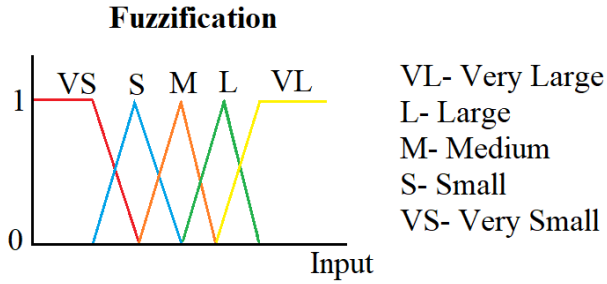

Fig. 5.9: Fuzzification of the input variable.

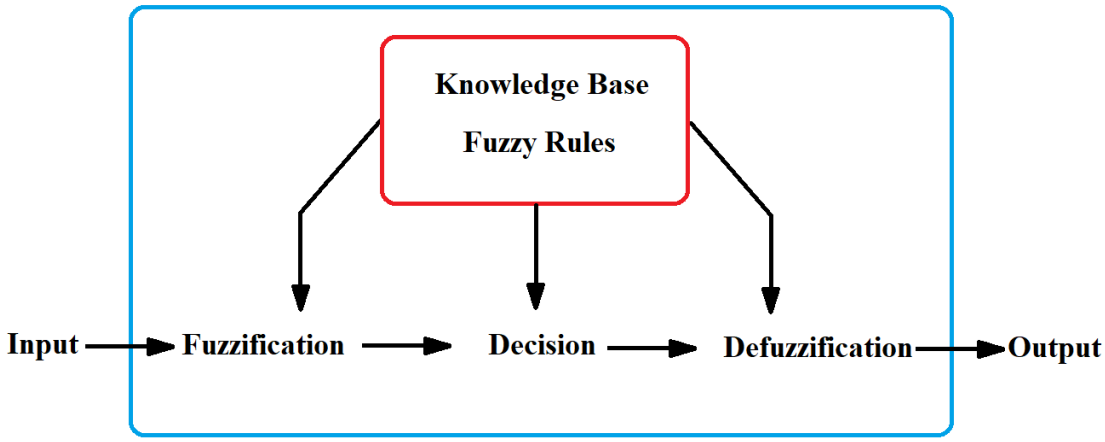

Fig. 5.10: General schematics of a FIS.

The membership functions are any chosen function responsible for stablishing the relationship, or degree of membership, between the input and a range from 0 to 1. The functions set can be of any shape that satisfies the design needs. They can be triangular, as given by Fig. 5.9, trapezoidal, bell-shaped, or Gaussian. The fuzzy rule sets are responsible for stablishing the decision making inside a fuzzy controller in the form of "if-then" rules. The main difference between fuzzy logic and Boolean logic rules is that in the latter case it is necessary to define precisely the value to be set as a threshold. For example: *"if the accelerations are greater than 3m/s^2 then set the actuator to work with maximum capacity"*. In fuzzy logic, the threshold does not need to be defined precisely, it can be a vague concept: *"if the accelerations are high then set the actuator to maximum working capacity"*. The method described so far is called the Mamdani FIS method (Mamdani and Assilian 1999).

The Takagi-Sugeno method (Sugeno 1985) is another largely implemented FIS method. This method is similar to the Mamdani, however in the Takagi-Sugeno method

the output membership functions are either linear or constant, and the final output is obtained by weighting all the outputs. Although Mamdani's method is more intuitive for human operation, Takagi-Sugeno method is more computationally efficient. For this reason, the method is more suitable for implementation of optimization routines and adaptive techniques.

Neural networks, or artificial neural networks (ANN), are built to process information inspired in the human brain's operation. This system is able to process information that is complex and nonlinear; it has the ability to deal with a great amount of information and to solve a variety of tasks. Neural networks are highly interconnected systems of simple operating components which process a great amount of information to change their internal state and produce an output, depending on the input content and activation function. A neuron is the unit internal component of ANN and is responsible for processing the information through an activation process. Fig. 5.11 shows the basic components of ANN's unit, the neuron.

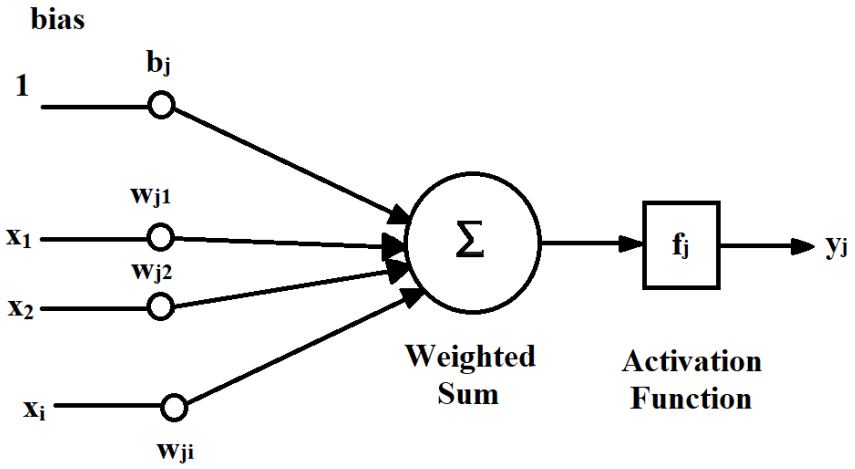

Fig. 5.11: Artificial neural network neuron/unit.

The weighted sum $s_j(t)$ is given by:

$$s_j(t) = \sum_{i=1}^{n} (w_{ji} x_i) + b_j \tag{5.41}$$

Where w_{ji} is the weight for neuron *j* and input *i*, x_i are the inputs, and b_j is a bias. The activation function $f(s_j)$ can give many shapes to the output y_j. These functions are responsible for mapping the input values and fitting them into a desired range. Some examples of activation functions are the unit step function, given by Equation (5.42), the sigmoid function, given by Equation (5.43) and the hyperbolic tangent function, given by Equation (5.44). The choice of a nonlinear activation function turns possible capturing nonlinear patterns. Fig. 5.12 shows the aforementioned activation functions graphically.

$$f(s) = \begin{cases} 0 & s < 0 \\ 1 & s \geq 0 \end{cases} \tag{5.42}$$

$$f(s) = \frac{1}{1 - e^{-s}} \tag{5.43}$$

$$f(s) = \tanh(s) = \frac{e^{s} - e^{-s}}{e^{s} + e^{-s}} \tag{5.44}$$

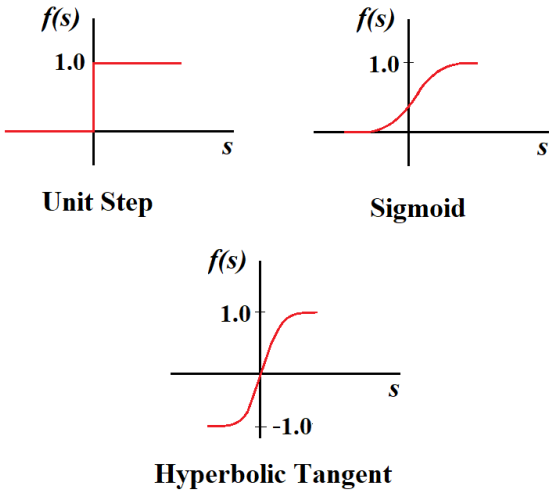

Fig. 5.12: Examples of activation functions.

The architecture of the ANN generally consists of three different layers: the input layer, which receives the input data, the hidden layer, and the output layer. In the feedforward architecture, data move in one direction only. Consequently, the output of each layer does not have any influence on the previous layer. Fig. 5.13 shows a feedforward ANN typical architecture. Recurring architecture, on the other hand, contain feedback paths.

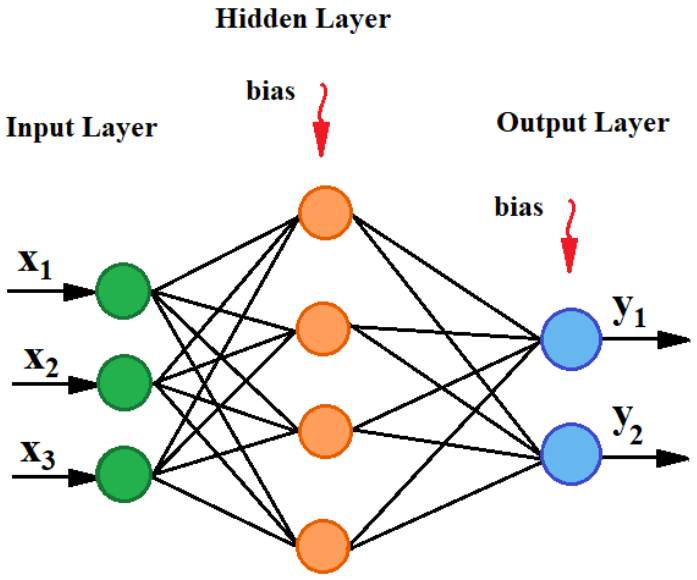

Fig. 5.13: Feedforward artificial neural network architecture.

The ANN's learning process consists of modifying the weights and biases until the output is in accordance with the desired output. There are different learning algorithms available and they can be classified into:

a) Supervised learning: the network is provided as a range of data that represents the input possibilities and the associated outputs and the weights are adjusted until an acceptable level of error is reached.

b) Unsupervised learning: there is no feedback information given to adjust the weights. No guidelines or target output is provided to the network.

The combination of ANN and FIS gives the possibility of training the FIS to achieve a certain level of expertise. Through a process of data collection, a set of if-then rules are defined to create a fuzzy inference system (FIS) with tunable membership

function parameters that is able to emulate an expert's decisions. The adaptive network based fuzzy inference system (ANFIS) is a neuro-fuzzy controller obtained with the combination of ANN and Takagi-Sugeno FIS. In this method, the ANN is used to adjust the membership functions for the FIS. First a target controller is defined and input and output of this controller are collected; then the training of the neural-fuzzy controller begins. ANFIS uses the neural networks to build a mapping of the input/ output set based on the target controller (Schurter and Roschke 2001b). The training is continued until the error function is within an acceptable range. Fig. 5.14 gives diagram showing ANFIS' architecture.

Assuming there are two inputs x_1 and x_2 and one output f, as given in Fig. 5.14. The "if-then" rules for the Takagi-Sugeno model are:

a) **If** x_1 is A_1 and x_2 is B_1 **Then** $f_1 = p_1 x_1 + q_1 x_1 + r_1$

b) **If** x_1 is A_2 and x_2 is B_2 **Then** $f_2 = p_2 x_2 + q_2 x_2 + r_2$ ...

c) **If** x_1 is A_n and x_2 is B_n **Then** $f_n = p_n x_2 + q_n x_2 + r_n$

Where A and B are membership functions and p, q and r are constants. The first layer has the adaptive nodes that require an initial suitable membership function:

$$y_{1,i} = \mu_{Ii}(x_i) \tag{5.45}$$

The second layer starts a product or T-norm operation:

$$y_{2,i} = \mu_{Ai}(x_1)\mu_{Bi}(x_2)...\mu_{pi}(x_n) \quad i = 1,2...,n \tag{5.46}$$

The third layer calculates the firing strength ratio of the rules:

$$y_{3,i} = \bar{w}_i = \frac{w_i}{\sum_i w_i} \tag{5.47}$$

Layer 4 generates the "if-then" rules, and Layer 5 calculates the sum of all signals:

$$y_{5,i} = \bar{w}_i = \frac{\sum_i w_i f_i}{\sum_i w_i} \tag{5.48}$$

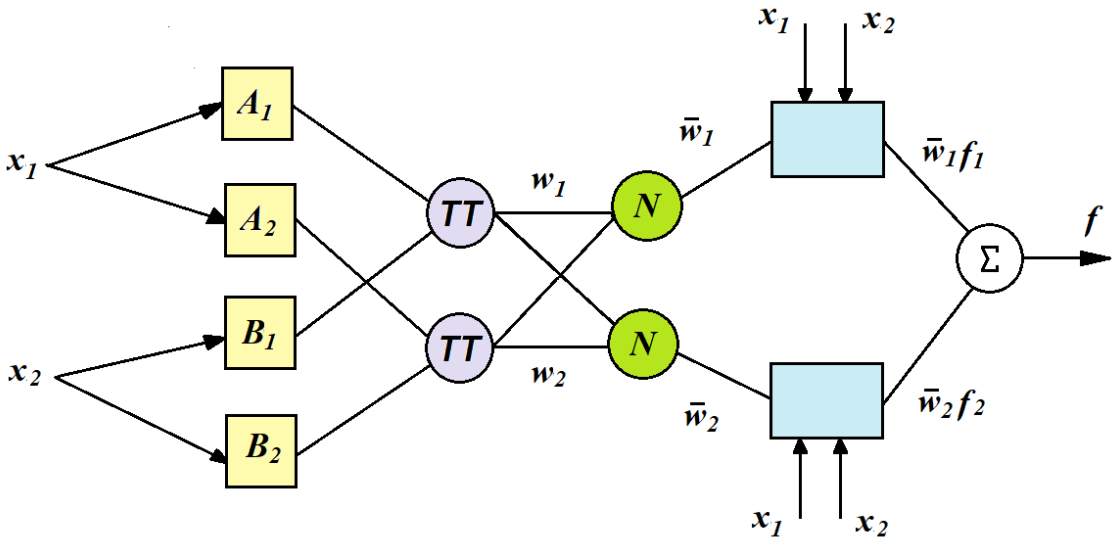

Fig. 5.14: ANFIS' architecture.

5.3. Controllability and Observability

In this section, two important concepts for multivariable systems control are introduced, controllability and observability. A system is controllable if exists a control input $\mathbf{u}(t)$ that can transfer the system from any initial state $\mathbf{x}(t_0)$ to some final state $\mathbf{x}(t_f)$ in a finite time interval. For a system represented in state-space format, the sufficient

condition for complete state controllability is that the n x n matrix given by Equation (5.49) contains n linearly independent row or column vectors, that is the matrix is nonsingular and of rank n.

$$\mathbf{M} = \left[\mathbf{B}\ \mathbf{AB} \ldots \mathbf{A}^{n-1}\mathbf{B} \right] \tag{5.49}$$

A system is observable if at a time t_0, the system state $\mathbf{x}(t_0)$ can be determined exactly from observation of the output $\mathbf{y}(t)$ over a finite time interval. A system is observable if the n x n matrix defined by Equation (5.50) contains n linearly independent row or column vectors, that is the matrix is nonsingular and of rank n.

$$\mathbf{N} = \left[\mathbf{C}^{\mathbf{T}}\ \mathbf{A}^{\mathbf{T}}\mathbf{C}^{\mathbf{T}} \ldots \left(\mathbf{A}^{\mathbf{T}}\right)^{\mathbf{n-1}} \mathbf{C}^{\mathbf{T}} \right] \tag{5.50}$$

6. HIGHWAY BRIDGES ADAPTIVE CONTROL CONSIDERING PARAMETRIC VARIATIONS

In this section, adaptive control schemes are proposed to control two different highway bridges considering parametric variations. The main objective of the control approach is to provide a guaranteed level of robustness when the structure is subjected to different parametric variations. In the first portion of this section, the preliminary study is presented, where an adaptive scheme is developed to control the three-span highway bridge described in section 4.2. The bridge is subjected to seismic excitation and the performance of the scheme is evaluated before and after a reduction in stiffness is introduced. In the second portion, the parametric study is presented where an adaptive scheme is developed to control the two-span highway bridge described in section 4.3. The bridge is subjected to seismic excitation and to systematic parametric variations. Semi-active and active devices are realistically implemented and white noise is introduced to measurements to evaluate the proposed control scheme operational performance.

6.1. Three-span Highway Bridge

An adaptive scheme is developed to control a three-span highway bridge subjected to seismic excitation. The performance of the scheme is evaluated when in face of parametric variation by introducing a 20% reduction in stiffness to the bridge piers. The structural characterization of the bridge is given in section 4.2.

6.1.1. Earthquake Suite

In order to evaluate the effectiveness of the proposed adaptive scheme, three different sets of earthquakes are applied to the bridge in the transverse direction (*y* direction, refer to Fig. 4.2). The earthquakes selected are LA ground motions from the SAC project (Sommerville 1997), and each carry different intrinsic characteristics. The earthquakes acceleration time histories are shown in Fig. 6.1, and their acceleration response spectra is given by Fig. 6.2. Table 6.1 gives a summary of the basic characteristics of the ground motions.

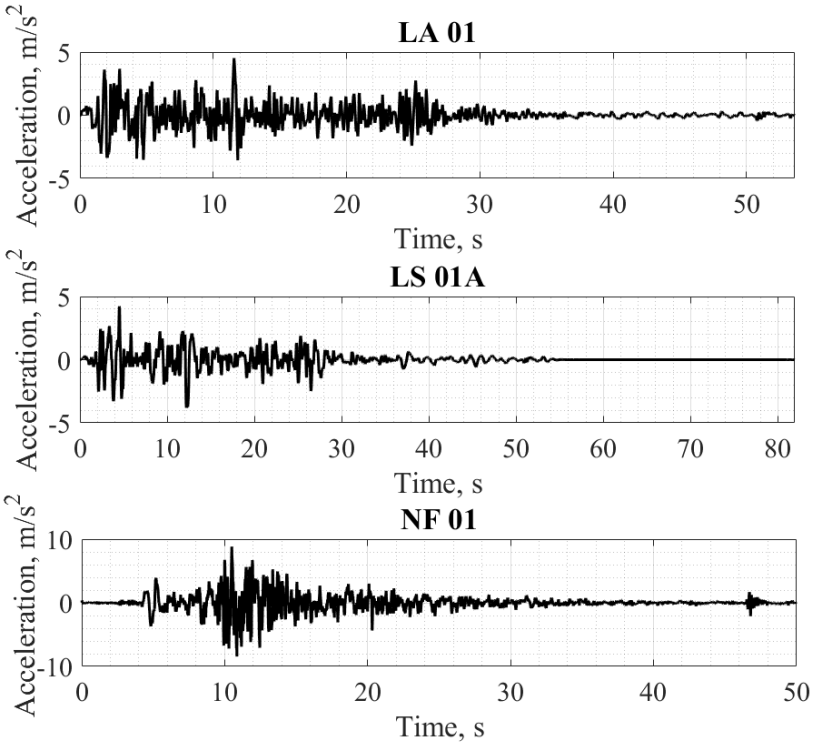

Fig. 6.1: Acceleration time history of the ground motions applied to the three-span highway bridge.

Table 6.1: LA ground motions applied to the three-span highway bridge.

Name	Record	Description	Duration (s)	PGA (m/s^2)	Sampling Rate (s)
LA01	Imperial Valley 1940, El Centro	10% probability of exceedance in 50 years	53.62	4.52	0.02
LS01A	40-IVIR, Soil Type 1	Soft Soil, 10% probability of exceedance in 50 years	81.94	4.23	0.02
NF01	Sep 1978, Tabas Station	Near Fault	50.02	8.83	0.02

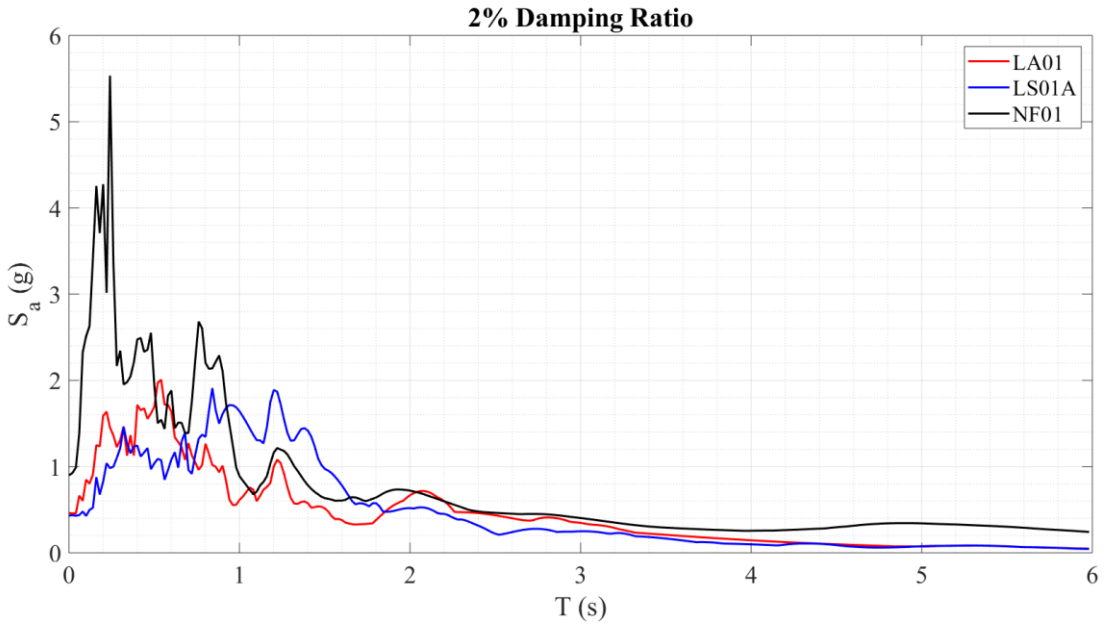

Fig. 6.2: Acceleration response spectra for the ground motions applied to the three-span highway bridge, 2% damping ratio.

6.1.2. Control Scheme Design and Implementation

The control scheme developed for the highway bridge is composed of sensors measuring transverse displacements at both abutments, piers and midspans. There are 4 control devices acting in the transverse direction attached to each bridge ends and abutments, totalizing 8 devices. Fig. 6.3 gives the schematics of the devices distribution for each bridge end.

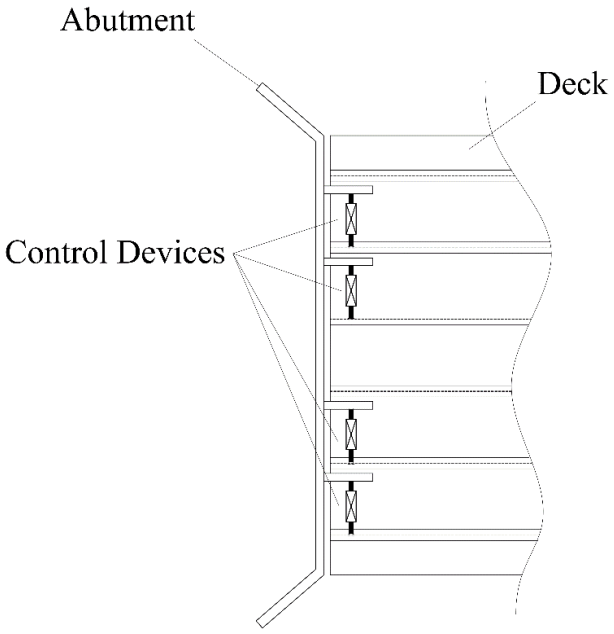

Fig. 6.3: Schematics of the devices distribution on the three-span highway bridge.

The main control strategy adopted for this adaptive control scheme is based in the SAC algorithm. Ideal active devices are considered as the control operators in order to tune the controller, find the adequate model reference and control gains. The first model reference adopted is the uncontrolled bridge, considering the nominal parameters.

The adaptive gains constants are taken as:

$\Gamma_e = 10^{10}$

$\Gamma_x = 10^{10}$

$\Gamma_u = 10^{10}$

The displacements of the bridge end 1 and top of bridge pier 1 are given for all three earthquakes in Fig. 6.4 and Fig. 6.5, respectively. The displacements shown are associated to the bridge controlled by the adaptive scheme, for the nominal structure and after the stiffness reduction is introduced. Table 6.2 gives the maximum error between the responses of the controlled structure, before and after the stiffness is reduced. It is noticeable that the controlled nodes (bridge ends) follow the model reference, which shows that the scheme is well-designed for reference tracking purposes. The uncontrolled nodes present greater relative error. However, the overall response of the structure based on the ideal design is very similar to the response after the stiffness reduction. The controller holds performance after parametric change and the design is considered satisfactory for reference tracking requirements.

Table 6.2: Maximum percentage relative error between the responses of the SAC-controlled structure considering the ideal design and after the piers stiffness is reduced in 20%.

Location	Maximum percentage error					
	LA01		LS01		NF01	
	Displacement	Velocity	Displacement	Velocity	Displacement	Velocity
End 1	0.3%	1.8%	0%	4%	0%	1%
Pier 1	13.0%	13.7%	13%	12%	14%	15%
Pier 2	8.7%	14.6%	7%	13%	12%	15%
End 2	0.4%	1.3%	0%	2%	1%	1%

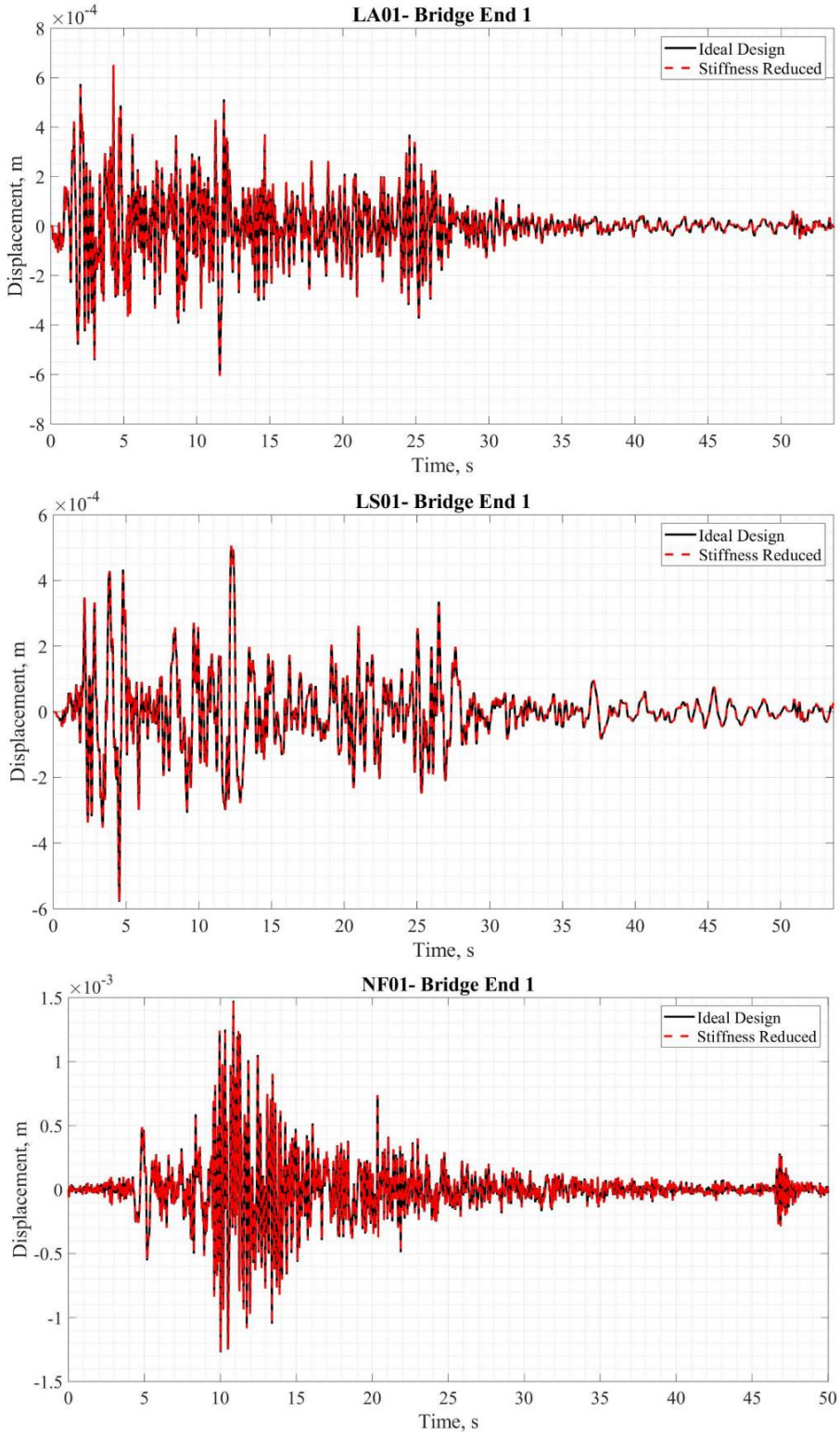

Fig. 6.4: Reference tracking considering all three earthquakes- top of the bridge end 1.

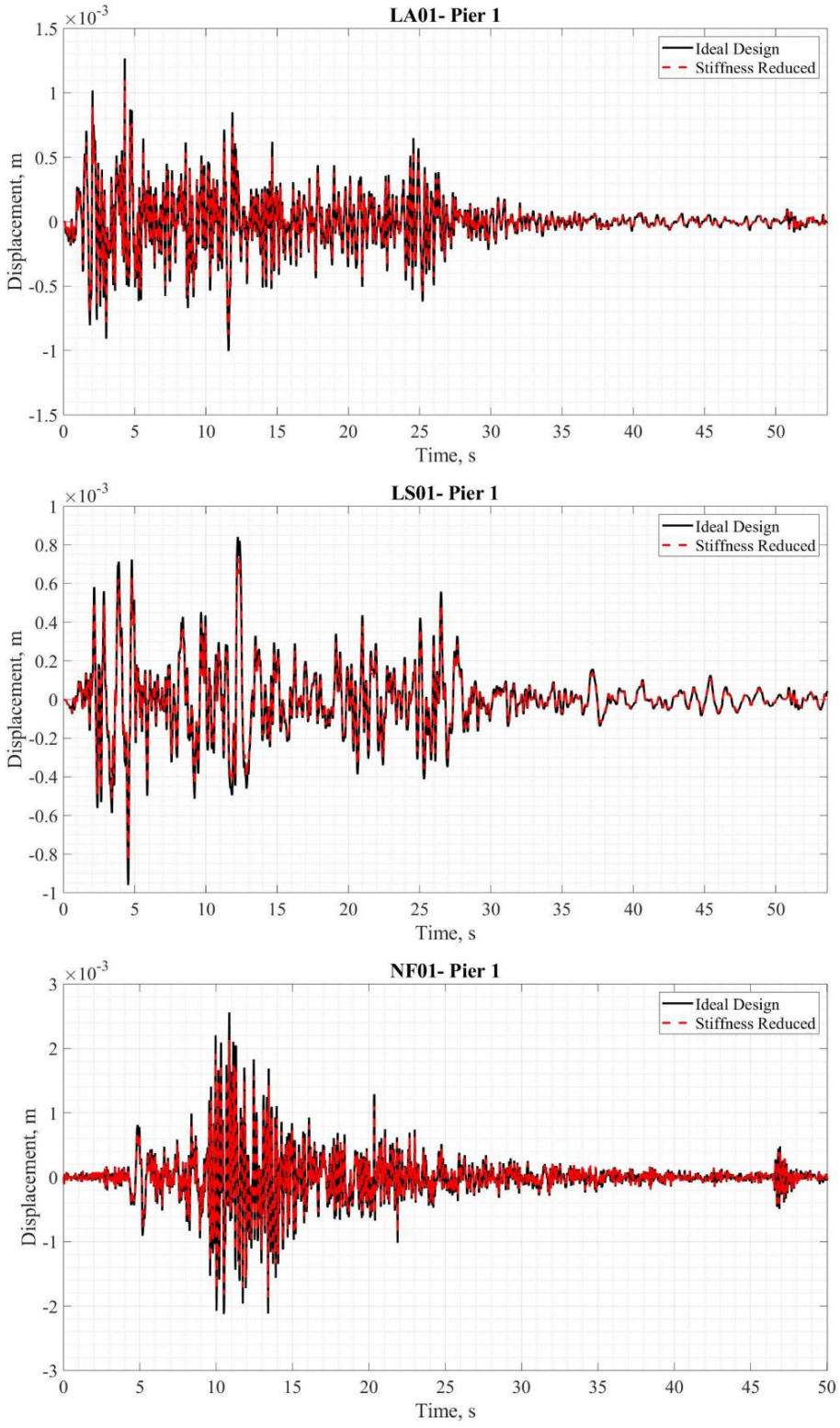

Fig. 6.5: Reference tracking considering all three earthquakes- top of the bridge pier 1.

At this point, a slightly different model reference is taken to also reach response reduction along with reference tracking. The model reference is taken as the nominal bridge subjected to the earthquake records and responding with a 50% displacements reduction. The objective is to track the behavior of the nominal uncontrolled bridge and mitigate excessive displacements and velocities. The bridge ends displacements are given for all three earthquakes in Fig. 6.6, for the nominal structure and after the parametric change when controlled by the adaptive scheme.Table 6.3Table 6.3 gives the maximum error between the responses of the controlled structure, before and after the stiffness is reduced. It is noticeable that the controlled nodes (bridge ends) still follow really well the model reference. The uncontrolled nodes present slightly larger relative error, but the overall response of the nominal structure is very similar to the response of the structure after stiffness reduction. The controller not only holds performance after parametric change but it is able to reduce overall responses. In the next subsection realistic operational conditions are accounted for by including devices dynamics and control forces saturation.

Table 6.3: Maximum percentage relative error between the responses of the SAC-controlled structure considering the ideal design and after the piers stiffness is reduced in 20%.

Location	Maximum percentage error					
	LA01		LS01		NF01	
	Displac.	Velocity	Displac.	Velocity	Displac.	Velocity
End 1	0.3%	2.2%	0.2%	4.4%	0.4%	1.3%
Pier 1	19.2%	14.9%	20.3%	13.0%	18.2%	16.3%
Pier 2	8.6%	13.3%	6.8%	12.0%	11.5%	14.1%
End 2	0.5%	1.2%	0.1%	2.1%	0.7%	1.3%

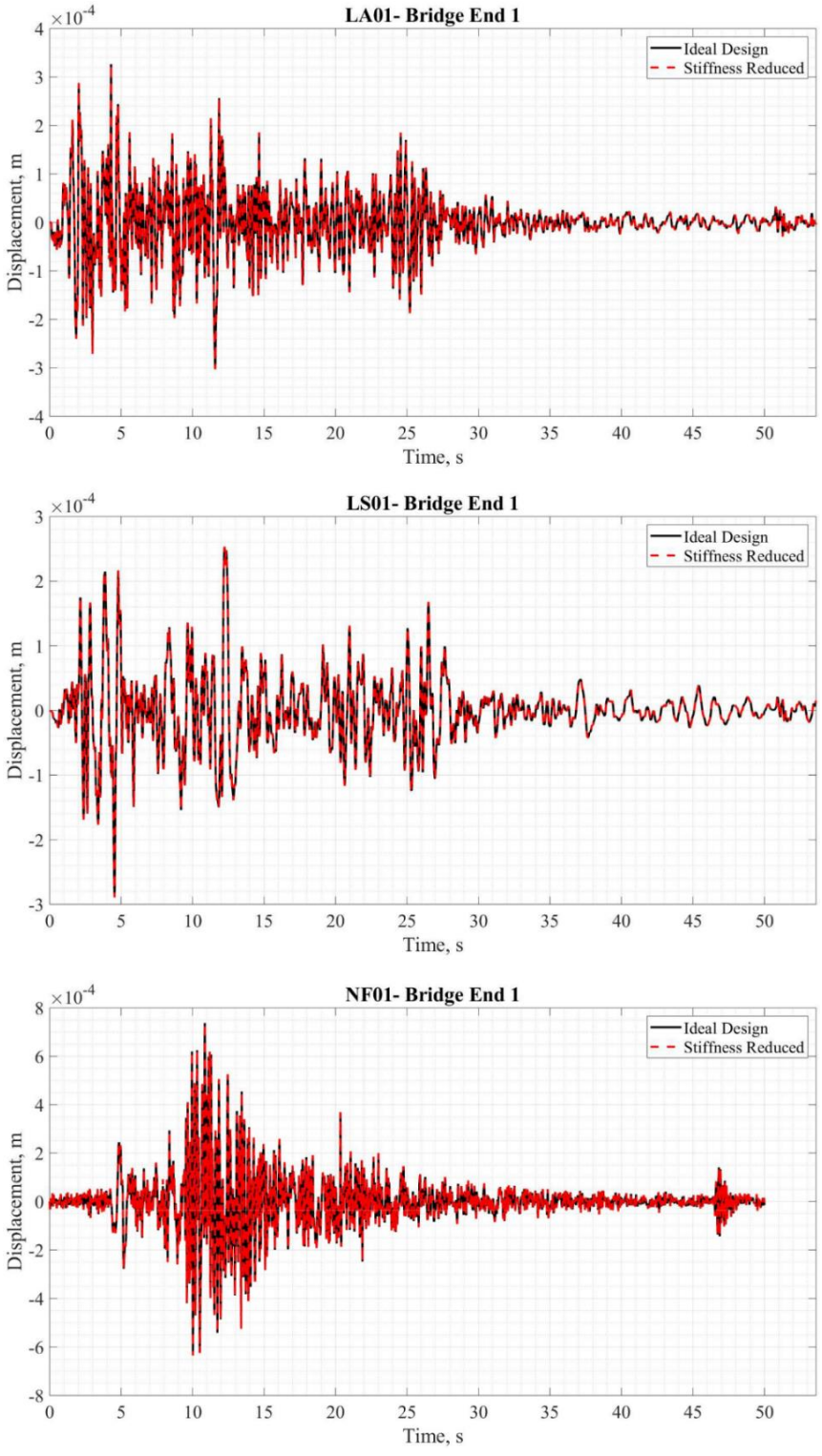

Fig. 6.6: Reference tracking for the second model reference considering all three earthquakes- bridge end 1.

6.1.3. Results and Discussion

In this section, active hydraulic actuators and semi-active MR dampers are modeled as the control devices for the scheme developed previously. The overall goal of the control scheme is to reduce the seismic responses and also guarantee that the bridge behaves as predicted during the design phase, even when in the presence of parametric changes. The performance of the control scheme is assessed by comparing the response of the bridge controlled by the adaptive scheme to the response of the bridge controlled by purely passive linear dampers and to the uncontrolled responses. Two parametric scenarios are considered, the nominal structure and the structure with both piers subjected to a 20% stiffness reduction.

Fig. 6.7 gives the displacements at the bridge end 1 for the uncontrolled and controlled cases, before and after the stiffness is reduced. Fig. 6.8 gives the displacements at the bridge pier 1 for the uncontrolled and controlled cases, before and after the stiffness is reduced. Table 6.4 gives the percentage peak response reduction associated to each control strategy, before and after the stiffness reduction. Table 6.5 gives the control schemes peak control forces and Table 6.6 gives the maximum percentage relative error between the nominal structure and after the piers stiffness reduction responses.

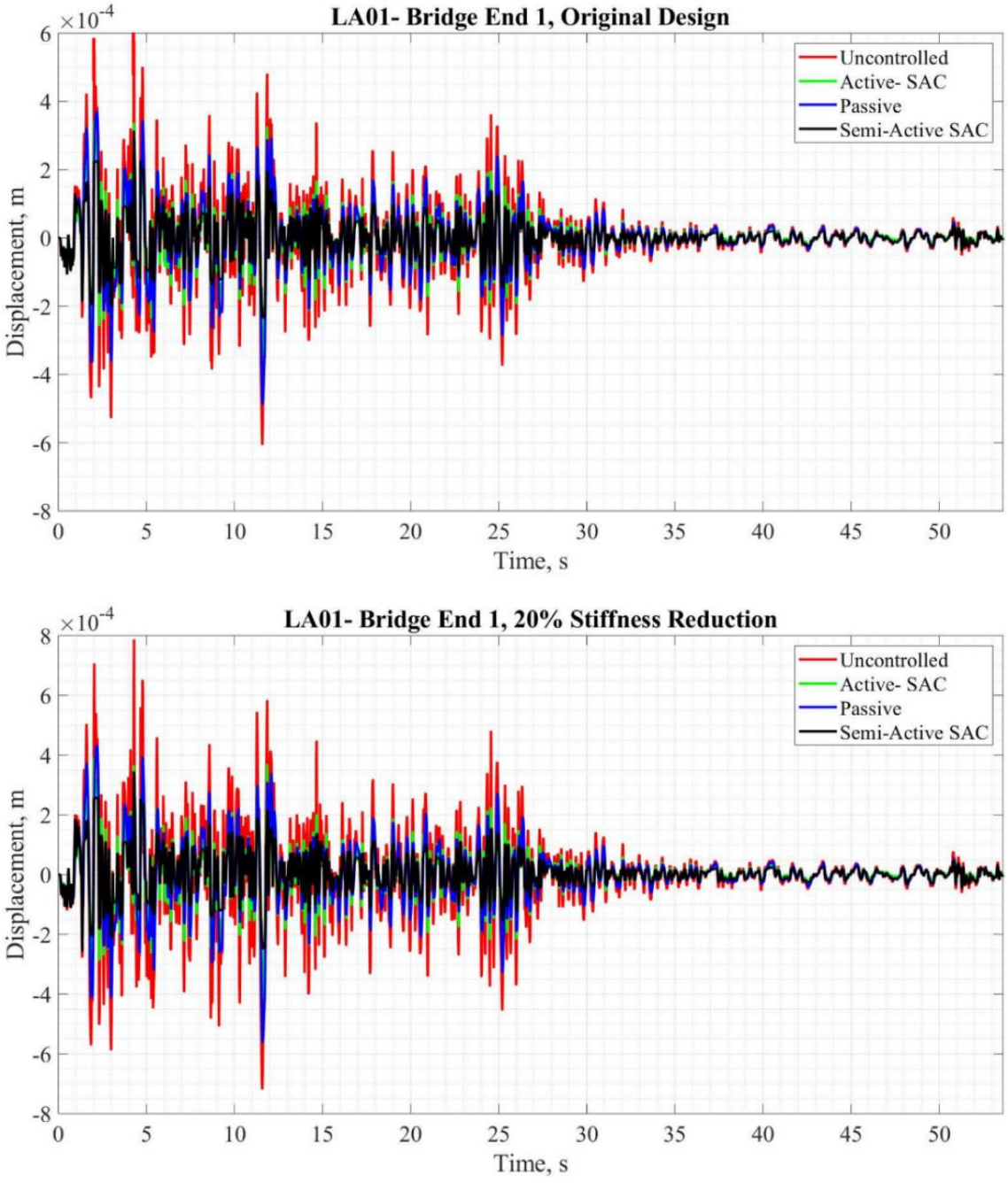

Fig. 6.7: Displacements at the bridge end 1 for the uncontrolled and controlled cases, before and after the stiffness reduction.

Table 6.4: Peak response reduction percentage for all control strategies, before and after the stiffness reduction.

Peak Response Reduction (%)							
Nominal Structure							
Location	Control Scheme	LA01		LS01		NF01	
		Displac.	Velocity	Displac.	Velocity	Displac.	Velocity
End 1	Passive	43.5%	76.3%	17.9%	51.4%	54%	83%
	SAC HA	42.3%	66.2%	34.0%	53.8%	44%	64%
	SAC MR	58.1%	83.2%	54.2%	72.0%	56%	81%
Pier 1	Passive	59.5%	90.5%	28.8%	71.1%	73%	94%
	SAC HA	52.6%	64.2%	44.4%	54.9%	54%	63%
	SAC MR	73.0%	86.6%	71.8%	74.0%	68%	83%
Pier 2	Passive	57.9%	88.5%	24.3%	65.8%	70%	91%
	SAC HA	52.2%	71.2%	41.2%	56.5%	59%	76%
	SAC MR	67.6%	85.2%	61.9%	72.4%	68%	85%
End 2	Passive	70.9%	95.9%	34.8%	80.2%	83%	97%
	SAC HA	64.6%	80.5%	54.9%	68.9%	71%	84%
	SAC MR	80.8%	94.4%	77.2%	89.7%	81%	94%
Piers 20% Bending Stiffness Reduction							
Location	Control Scheme	LA01		LS01		NF01	
		Displac.	Velocity	Displac.	Velocity	Displac.	Velocity
End 1	Passive	36.8%	71.7%	22.2%	60.3%	60.3%	84.7%
	SAC HA	36.7%	63.4%	38.5%	57.8%	50.8%	68.3%
	SAC MR	53.0%	82.8%	57.4%	72.5%	60.5%	81.6%
Pier 1	Passive	55.0%	89.3%	32.5%	75.6%	75.9%	94.1%
	SAC HA	47.5%	58.5%	48.9%	60.4%	59.3%	67.9%
	SAC MR	69.1%	84.9%	73.6%	74.8%	71.3%	84.9%
Pier 2	Passive	49.1%	84.5%	30.4%	74.1%	76.5%	93.0%
	SAC HA	45.8%	66.0%	45.9%	61.7%	65.3%	80.3%
	SAC MR	62.3%	82.6%	65.4%	75.1%	74.0%	87.9%
End 2	Passive	64.4%	94.3%	40.3%	85.6%	86.2%	97.6%
	SAC HA	59.9%	77.1%	58.5%	72.7%	75.5%	86.8%
	SAC MR	77.9%	93.8%	79.4%	90.5%	84.3%	94.9%

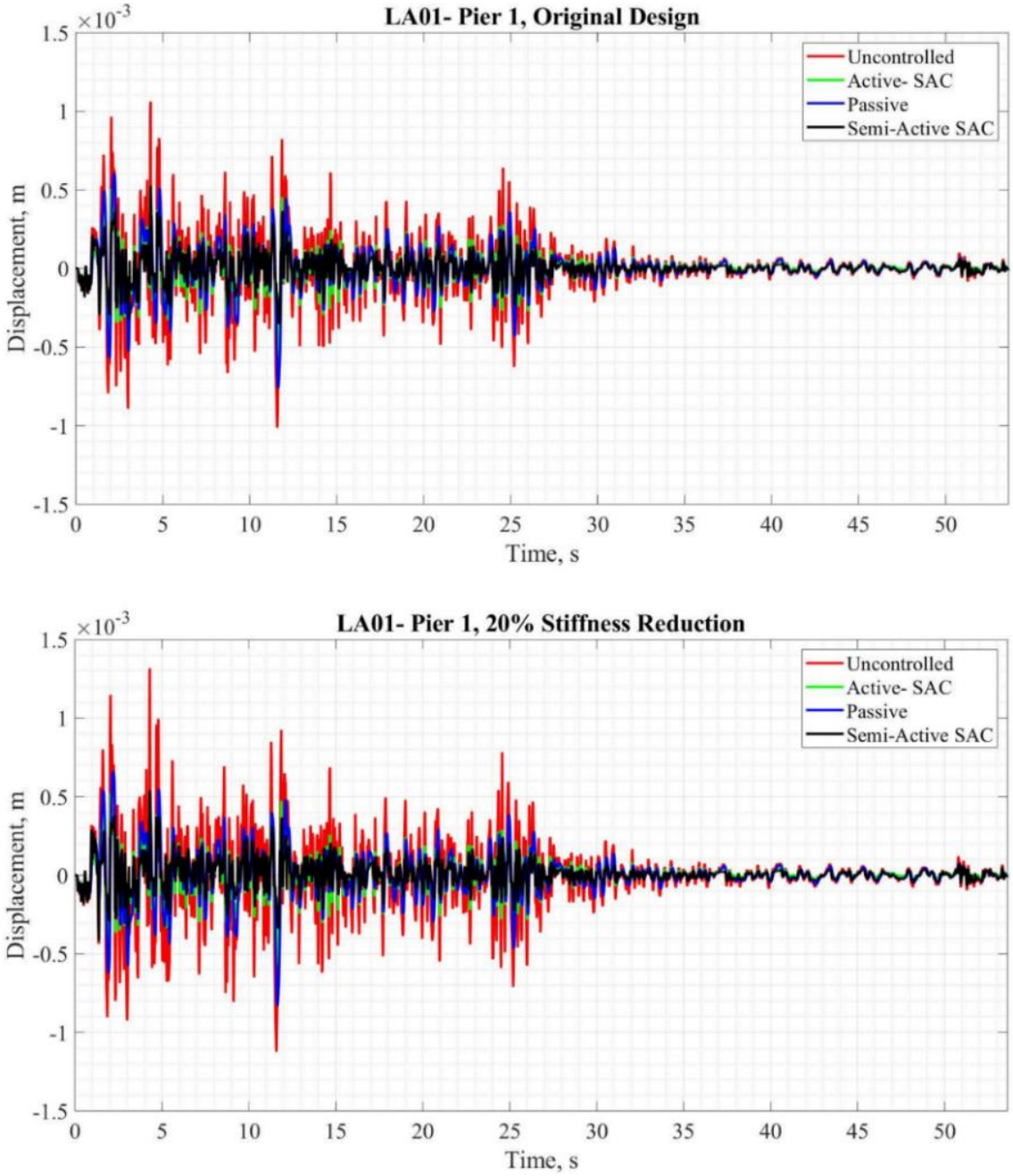

Fig. 6.8: Displacements at the bridge pier 1 for the uncontrolled and controlled cases, before and after the stiffness reduction.

Table 6.5: Peak control force for all control strategies for all three earthquakes, before and after the stiffness reduction.

Peak Control Force (kN)			
Nominal Structure			
Control Scheme	LA01	LS01	NF01
Passive	357.48	267.45	655.00
SAC HA	729.62	515.36	1,000.00
SAC MR	613.56	314.44	1,000.00
Piers 20% Bending Stiffness Reduction			
Control Scheme	LA01	LS01	NF01
Passive	396.09	303.61	754.10
SAC HA	782.20	563.44	1,000.00
SAC MR	641.85	349.51	1,000.00

Table 6.6: Maximum percentage relative error between nominal design and 20% stiffness reduction responses.

Maximum percentage error							
Location	Control Scheme	LA01		LS01		NF01	
		Displac.	Velocity	Displac.	Velocity	Displac.	Velocity
End 1	Uncontrolled	19.1%	7.9%	19.1%	22.7%	11.5%	4.5%
	Passive	12.0%	7.3%	14.3%	10.9%	12.6%	7.4%
	SAC HA	10.6%	9.3%	9.9%	15.3%	11.2%	8.8%
	SAC MR	9.3%	3.5%	10.2%	14.8%	12.4%	3.1%
Pier 1	Uncontrolled	13.1%	6.9%	12.7%	15.9%	9.6%	2.1%
	Passive	8.2%	5.5%	9.7%	7.8%	8.5%	5.4%
	SAC HA	3.8%	0.2%	3.5%	4.6%	3.5%	0.9%
	SAC MR	3.6%	1.6%	6.0%	5.5%	7.3%	2.3%

The results indicate the adaptive strategy is the most successful in mitigating excessive seismic responses when compared to the passive strategy. Additionally, the adaptive technique performance is the least affected by the reduction in stiffness. The semi-active adaptive control strategy gives better results in terms of response reduction when compared to the active adaptive control. It can be concluded from observation of the

results that the adaptive schemes provide satisfactory overall performance when it comes to mitigation of seismic responses while successfully holds performance when the parametric change is introduced.

6.2. Two-span Highway Bridge

This section presents a parametric study conducted to investigate with further depth the performance of the adaptive control of bridge structures in face of systematic parametric variations. An adaptive control approach is developed aiming to reduce seismic responses of bridges considering realistic operational conditions. The control approach is implemented and designed to control a seismically excited two-span highway bridge; its effectiveness is assessed considering parametric variations. The scheme is designed and implemented to provide control command to MR dampers and to hydraulic actuators installed at the bridge ends. The scheme is assessed by subjecting the bridge to a set of 11 earthquakes, while stiffness and mass parameters are varied systematically. The performance of the adaptive control scheme is compared to non-adaptive passive control and optimal control, taking into account the effects of noise and device dynamics. The structural characterization and modeling of the bridge utilized in the development of this portion of the work is found in section 4.3.

6.2.1. Earthquake Suite

The earthquake suite is chosen as an attempt to cover a full range of different earthquakes characteristics. The earthquake loads applied to the bridge act in the

transverse direction. The set of 11 earthquakes comprehends far and near field earthquakes, different values of moment magnitude, different peak accelerations and velocities. Table 6.7 summarizes the characteristics of the earthquakes suite and Fig. 6.9 gives their acceleration response spectra.

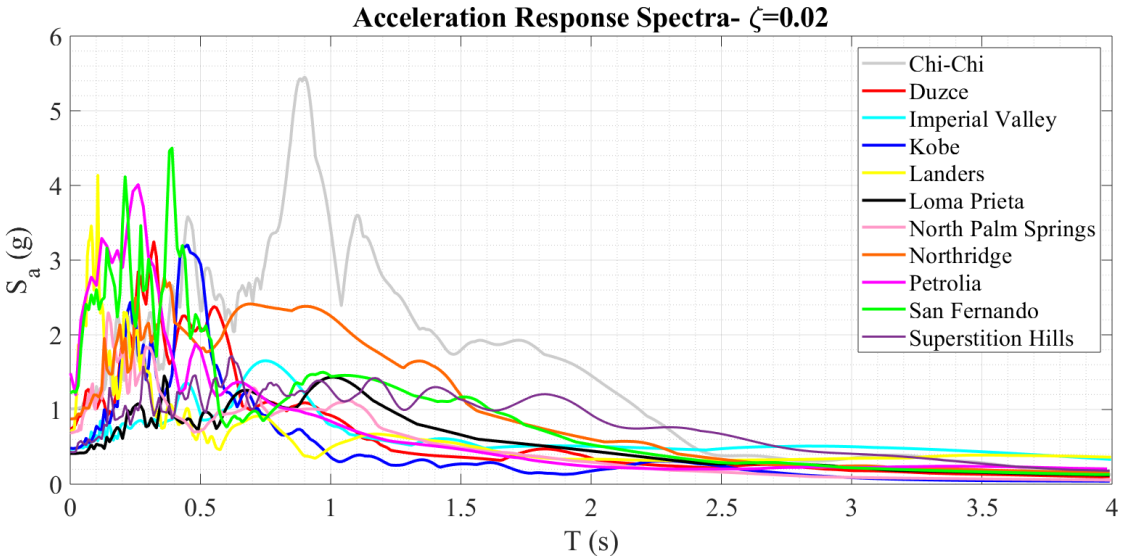

Fig. 6.9: Acceleration response spectra for the earthquake suite.

Table 6.7: Earthquake suite characteristics

Earthquake	Record Station	Magnitude (M_w)	Dist. to Fault (km)	PGA (g)	PGV (m/s)	Duration (s)
Chi-Chi, Taiwan (1999)	TCU084	7.6	10.4	1.16	1.15	90
Duzce, Turkey (1999)	Bolu	7.1	17.6	0.73	0.56	56
Imperial Valley (1979)	El Centro Array #7	6.4	29.4	0.46	1.13	36.5
Kobe, Japan (1995)	Nishi-Akashi	6.9	11.1	0.51	0.37	41
Landers (1992)	Lucerne Valley	7.3	42	0.71	1.26	47
Loma Prieta (1989)	Los Gatos	7	6.1	0.56	0.95	39
Palm Springs (1986)	North Palm Springs	6	7.3	0.49	0.73	10
Northridge (1994)	Rinaldi	6.7	7.1	0.84	1.66	13
Petrolia (1992)	Cape Mendocino	7	3.8	1.50	1.25	17
San Fernando (1971)	Pacoima Dam	6.6	8.5	1.17	1.14	9
Superstition Hills (1987)	Parachute Test Site	6.6	7.2	0.45	0.99	15

6.2.2. Control Scheme Design and Implementation

The model reference choice is one of the major challenges when it comes to reference tracking control of large structure. It is important to choose a model reference that is well-behaved enough so the controller is robust and able to mitigate excessive responses. It is equally important that this model reference present lower order than the actual structure, which guarantees the control solution is computational feasible and manageable. In the proposed approach, a reduced order model reference is taken with monitored nodes as shown in Fig. 6.10 (a). The possibility of taking a model reference of

lower order than the actual structure is one of the advantages of implementing SAC algorithm for large structures. The selected nodes are assumed to have zero displacements when subjected to any external disturbances are taken as the model reference. It is desired that the control scheme induces the bridge to a stationary position as fast as possible during the occurrence of a major extreme event. It is important to point out that the reference tracking in this case is not going to be perfect, since the earthquakes generate strong forces and the devices have physical force limitations. However, the reference tracking is not the most important feature when it comes to civil structures. It is important that the control scheme is able to mitigate excessive responses and present enough robustness when it comes to parametric variations.

The gains for SAC obtained after design are:

$$\Gamma_e = 10^6$$
$$\Gamma_x = 10^3$$
$$\Gamma_u = 10^3$$

A total of 16 control devices, 8 at each bridge end, are placed between abutments and the deck controlling the transverse and longitudinal directions. The main devices considered are MR dampers and hydraulic actuators. The MR dampers working with no external power (passive-off) and with constant maximum external power (passive-on) are also considered. For the adaptive scheme, a total of 10 sensors measure displacements as shown in Fig. 6.10 (a). LQR requires full-state feedback or the reconstruction of the states through an estimator; however, for the reconstruction of the states to be of quality, it is necessary that the system is observable. A total of 10 sensors measuring displacements, as adopted for the adaptive strategy, leads to a non-observable system, therefore indicating

the reconstruction of the states is not guaranteed to be accurate. The LQR+LQE operating with 10 sensors is examined in this study anyway for comparison purposes. Nevertheless, an observable system composed of LQR+LQE operating with a total of 41 sensors measuring displacements is also considered, as given in Fig. 6.10 (b). White noise is introduced to the measured outputs given that such measurements are likely to be imperfect.

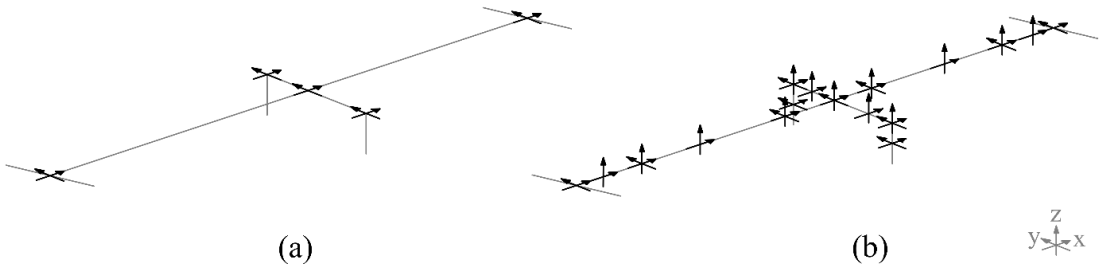

Fig. 6.10: Sensors schematics: (a) SAC and LQR non-observable system- 10 sensors; (b) LQR observable system- 41 sensors.

6.2.3. Parametric Variations Scenarios

The following scenarios of parametric variations are considered: overall mass increase of 10% and 5%, overall mass reduction of 10% and 5%, overall stiffness increase of 25% and 20%, overall stiffness reduction of 20% and 25%. Additionally, it is considered a combination of overall stiffness increase of 25% and overall mass reduction of 10%, a combination of overall stiffness increase of 25% and overall mass increase of 10%, a combination of overall stiffness reduction of 25% and overall mass reduction of

10%, and a combination of overall stiffness reduction of 25% and overall mass increase of 10%.

6.2.4. Performance Evaluation Criteria

The performance evaluation criteria selected for this study are defined by Equations (6.1) to (6.6) and are selected from the criteria defined by Agrawal et al. (2009). J_3 criteria evaluates normalized peak displacement, J_4 criteria evaluates normalized peak acceleration, J_{11} criteria evaluates normed displacements, J_{15} criteria evaluates peak control force, and J_{20} criteria evaluates the number of sensors.

$$J_3 = \max\left\{\max\left|\frac{y_m(t)}{y_{0m}{}^{\max}}\right|\right\} \tag{6.1}$$

$$J_4 = \max\left\{\max\left|\frac{\ddot{y}_m(t)}{\ddot{y}_{0m}{}^{\max}}\right|\right\} \tag{6.2}$$

$$\|\bullet\| = \sqrt{\frac{1}{t_f}\int_0^{t_f}(\bullet)^2} \tag{6.3}$$

$$J_{11} = \max\left\{\max\frac{\|y_m(t)\|}{\|y_{0m}{}^{\max}\|}\right\} \tag{6.4}$$

$$J_{15} = \max\left\{\max\left|\frac{f_l(t)}{W}\right|\right\} \tag{6.5}$$

$$J_{20} = \text{number of sensors} \tag{6.6}$$

6.2.5. Active Control

In this section, the results obtained in the parametric study for the adaptive active control scheme are presented and discussed. In this scheme, hydraulic actuators are the physical control devices utilized and controlled by the proposed SAC scheme. The performance of the control scheme is assessed by comparing to an active LQR+LQE scheme with the sensors distribution displayed in Fig. 6.10 (b) (41 sensors, observable scheme), and to passive-on/passive-off cases. All responses displayed correspond to the midspan transverse direction (*y* axis direction, refer to Fig. 6.10).

Fig. 6.11, Fig. 6.12 and Fig. 6.13 show a three-dimensional plot of J_3, J_4 and J_{11} for different mass and stiffness variations due to earthquake Chi-Chi. The three-dimensional plots for the other earthquakes are available in Appendix A. Fig. 6.14 gives the displacement time histories for the active adaptive scheme and the active LQR the nominal structure and the bridge with reduced stiffness in 25% and an increase in mass of 10% for the earthquake Chi-Chi. Fig. 6.15 gives the maximum performance criteria J_3, J_4 and J_{11} due to earthquake Chi-Chi, for the parametric variations scenarios considered. Table 6.8 gives the maximum values obtained for the performance criteria J_3, J_4 and J_{11} of the different control schemes, for all earthquakes.

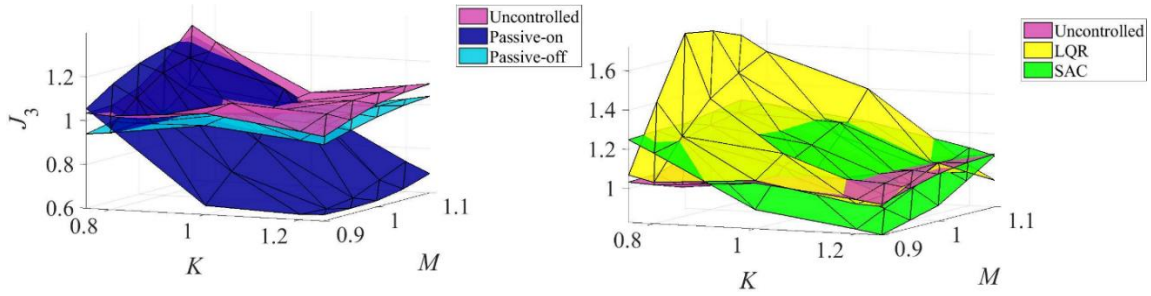

Fig. 6.11: J_3 for different mass and stiffness ratios: Chi-Chi.

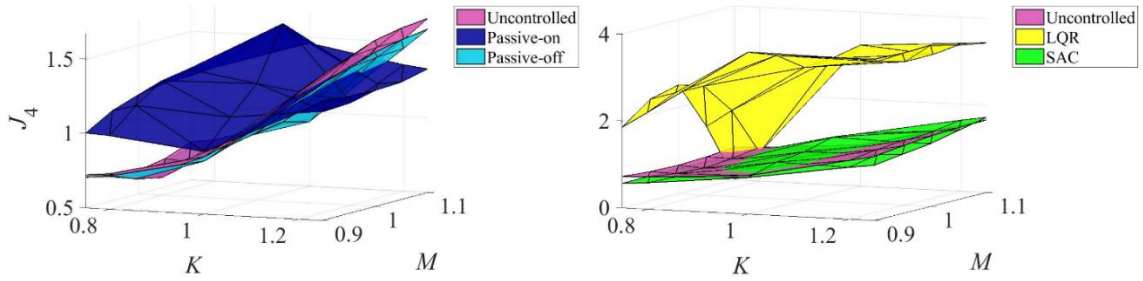

Fig. 6.12: J_4 for different mass and stiffness ratios: Chi-Chi.

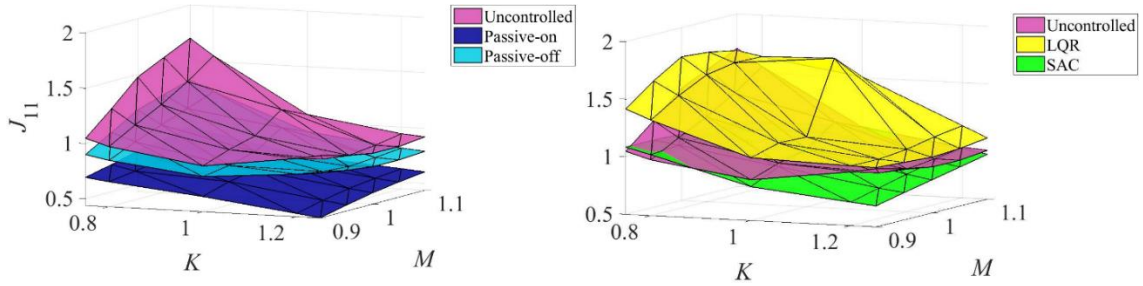

Fig. 6.13: J_{11} for different mass and stiffness ratios: Chi-Chi.

Table 6.8: Maximum performance criteria J_3, J_4 and J_{11} for the parametric variations cases considered.

Control	Chi-Chi	Duzce	Imp. Val.	Kobe	Land.	Loma Prieta	Palm Spr.	Nort.	Petr.	San Fern.	Sup. Hills
						Max J_3					
Uncont.	1.668	1.304	1.333	1.551	1.219	1.433	1.292	1.645	1.299	1.397	1.542
P. on	1.639	1.413	1.409	1.757	1.305	2.665	1.348	1.809	1.569	1.859	1.427
P. off	1.596	1.277	1.280	1.489	1.071	1.297	1.180	1.598	1.336	1.287	1.400
LQR(b)	1.719	1.650	1.219	2.745	1.776	1.330	1.715	1.062	1.096	2.023	2.008
SAC	1.309	1.064	1.569	2.161	0.938	1.018	1.052	1.028	1.025	1.351	1.113
						Max J_4					
Uncont.	1.308	1.066	1.634	1.348	1.289	1.523	1.093	1.263	1.165	1.129	1.217
P. on	1.261	1.064	1.452	2.013	1.510	1.372	1.033	1.163	1.032	1.879	1.138
P. off	1.187	1.045	1.545	1.273	1.140	1.294	1.046	1.214	1.126	1.010	1.085
LQR(b)	3.728	5.628	11.843	11.783	10.542	15.171	7.133	6.698	4.545	7.398	10.599
SAC	1.722	1.175	1.771	2.519	1.127	1.316	1.194	1.395	1.414	1.438	1.465
						Max J_{11}					
Uncont.	1.702	1.106	1.338	1.227	1.574	1.275	1.009	1.361	1.531	1.551	1.150
P. on	0.900	1.002	1.032	1.277	1.404	1.051	0.592	1.522	1.325	1.725	0.839
P. off	1.323	0.870	0.971	0.971	0.990	0.829	0.739	1.079	1.126	1.142	0.866
LQR(b)	2.282	5.816	1.921	3.235	2.489	1.836	2.348	2.376	2.519	7.940	3.112
SAC	1.084	1.809	3.671	1.478	1.014	0.875	0.978	1.067	1.155	1.450	0.978

Table 6.9: Performance criteria J_{15}, and J_{20} for the different control schemes.

Performance Criteria	Passive-on	Passive-off	SAC+HA	LQR(b)+HA
J_{15}	0.039	0.001	0.039	0.039
J_{20}	-	-	10	41

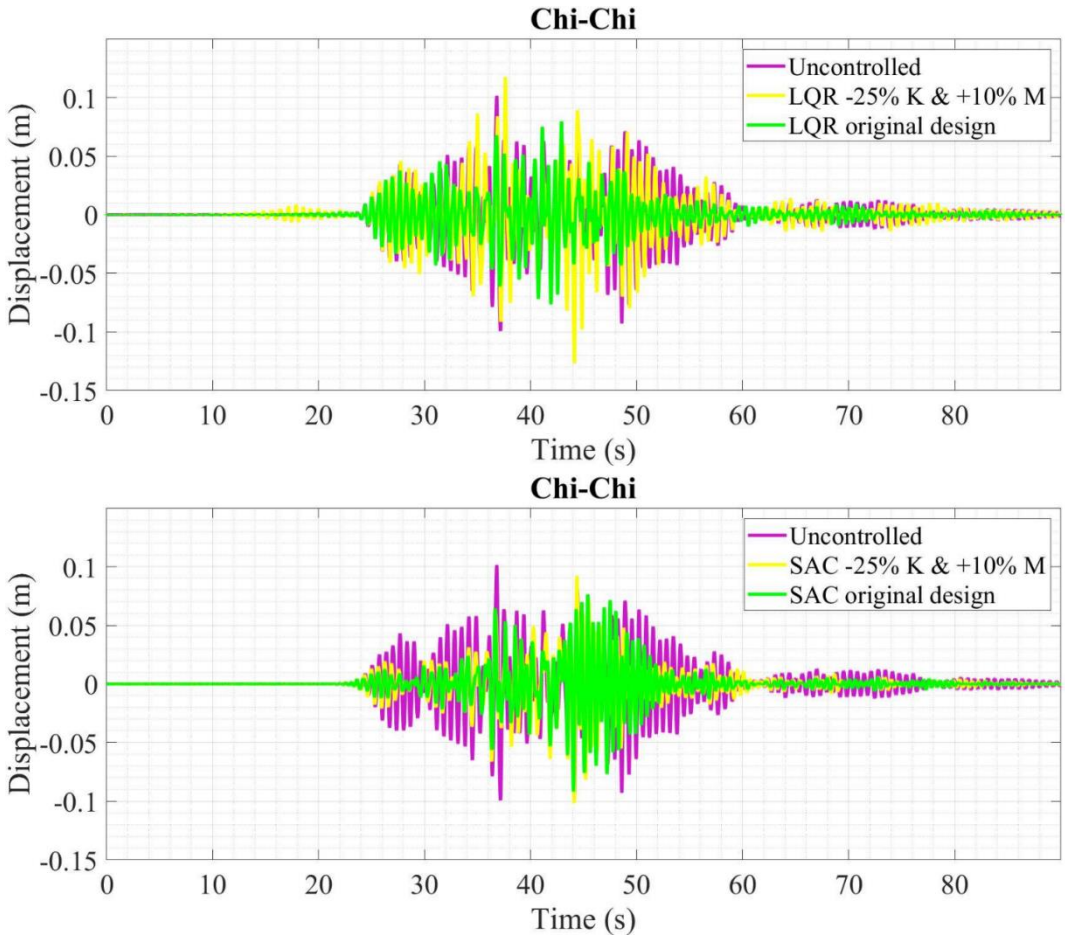

Fig. 6.14: Displacement for uncontrolled, SAC and LQR- controlled for nominal structure and after 25% stiffness reduction and 10% mass increase: Chi-Chi.

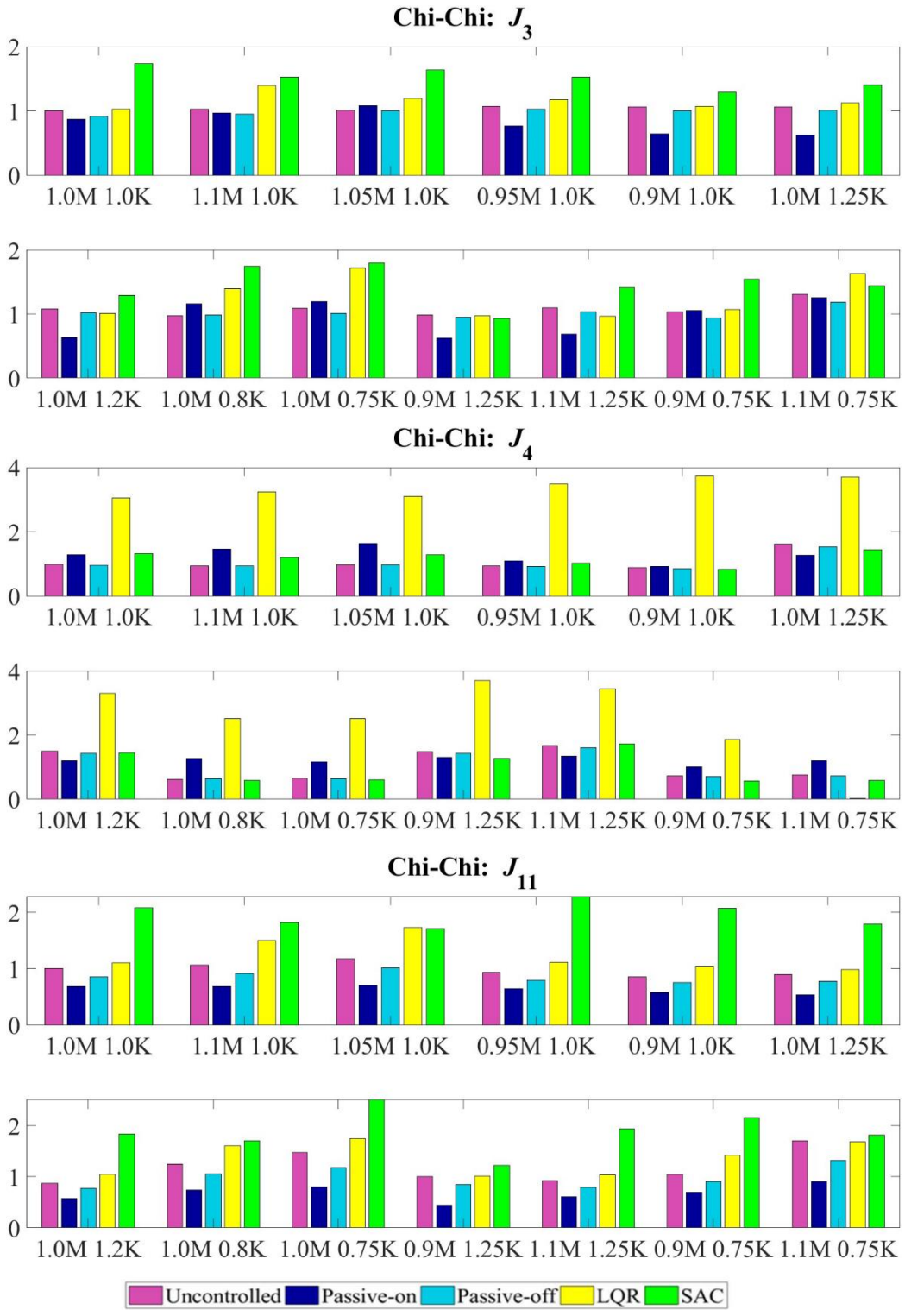

Fig. 6.15: Maximum J_3, J_4 and J_{11} for different parametric variations scenarios-earthquake Chi-Chi.

The hydraulic actuator introduces unwanted behavior for both feedback control algorithms when parametric changes are introduced. The accelerations and displacements are particularly worsened for the LQR+LQE active-controlled bridge case, but are also worsened for some SAC active- controlled cases. For some earthquakes the hydraulic actuator worsened the responses even for the nominal structural parameters. This observed behavior may be due to the dynamic force control present in the actuator model, which will be further discussed in subsection 6.2.7.

6.2.6. Semi-Active Control

In this section, the results obtained in the parametric study for the adaptive semi-active control scheme are presented and discussed. For this portion of the study, MR dampers are the physical control devices utilized and controlled by the proposed SAC scheme. The performance of the control scheme is assessed by comparing to passive-on and passive-off cases, and to a semi-active LQR+LQE scheme considering both distribution of sensors displayed in Fig. 6.10 (observable and non-observable cases). The responses displayed are for the midspan in the transverse direction (*y* axis direction, refer to Fig. 6.10).

Table 6.10 gives J_{15}, and J_{20} performance criteria values for the different control schemes. Fig. 6.16, Fig. 6.17 and Fig. 6.18 show a three-dimensional plot of J_3, J_4 and J_{11} for different mass and stiffness ratios due to earthquake Chi-Chi. The three-dimensional plots with maximum performance criteria J_3, J_4 and J_{11} for different control strategies due to the other earthquakes are available in Appendix A. Table 6.11 gives the maximum

performance criteria J_3, J_4 and J_{11} obtained from the different control schemes, for all earthquakes considered in this analysis. Table 6.12 gives the standard deviation among the different parametric variations scenarios of the performance criteria J_3, J_4 and J_{11} for the different control schemes.

Table 6.10: Performance criteria J_{15}, and J_{20} for the different control schemes.

Performance Criteria	Passive-on	Passive-off	SAC	LQR (a)	LQR (b)
J_{15}	0.039	0.001	0.039	0.039	0.039
J_{20}	-	-	10	10	41

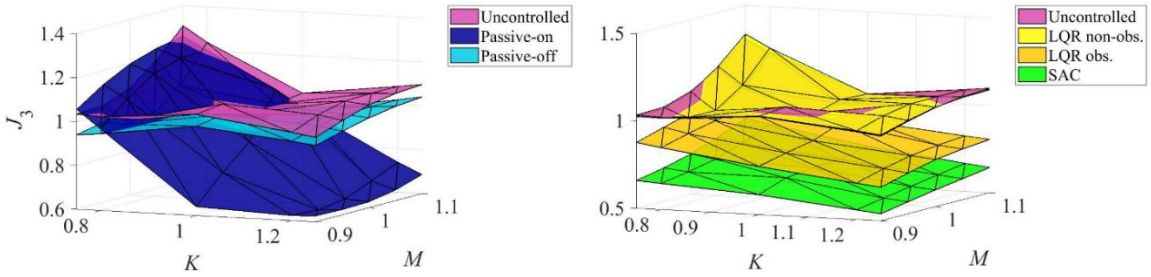

Fig. 6.16: J_3 for different scenarios of mass and stiffness ratios, earthquake Chi-Chi.

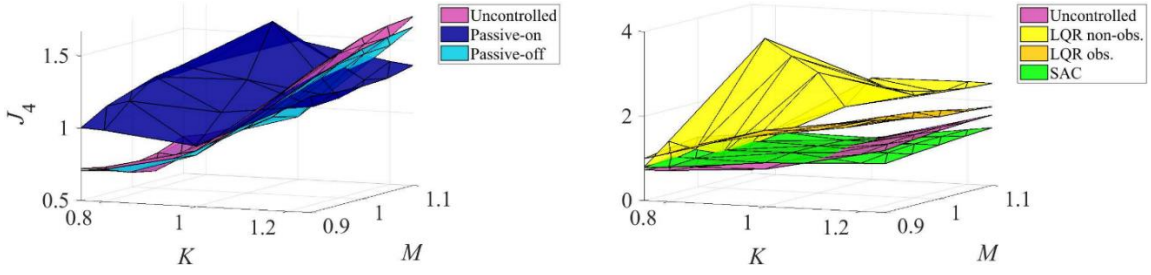

Fig. 6.17: J_4 for different scenarios of mass and stiffness ratios, earthquake Chi-Chi.

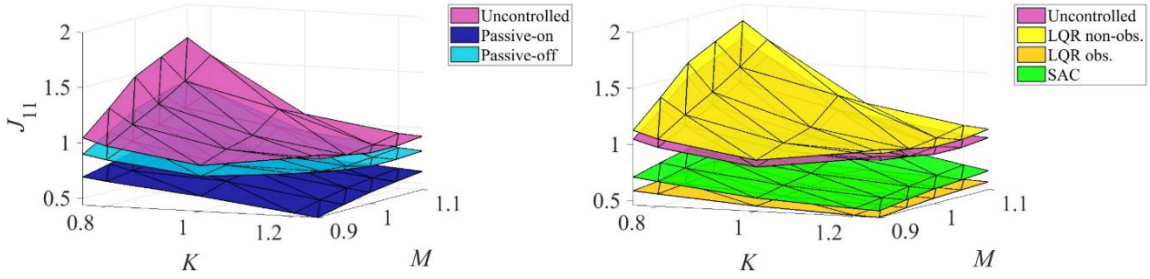

Fig. 6.18: J_{11} for different scenarios of mass and stiffness ratios, earthquake Chi-Chi.

SAC and LQR+LQE (b) (41 sensors, observable system) present the best performances in terms of reduction of peak displacements (J_3). Both strategies are able to reduce the overall peak displacement and sustain well the performance when in face of parametric variations. In terms of normalized RMS displacements (J_{11}), LQR+LQE (b) provides the best overall performance, followed by SAC. Passive-off strategy is able to reduce overall peak and RMS displacements (J_3 and J_{11}), but the strategy is not able to sustain performance well, and the reduction is not significant. LQR+LQE (a) (10 sensors, non-observable system) does not give an overall satisfactory performance. This poor performance is expected, given that states of the system are not well reconstructed due to the lack of observability. Results in term of J_3 and J_{11} performance criteria indicate that the passive-on strategy is able to reduce peak and RMS displacements for some earthquakes, while it worsens the peak displacements for others. For some parametric change scenarios, passive-on strategy increased significantly the midspan RMS and peak displacements (J_3 and J_{11}). This poor performance is attributed to excessive stiffness introduced by the devices on the bridge ends when operating with maximum voltage.

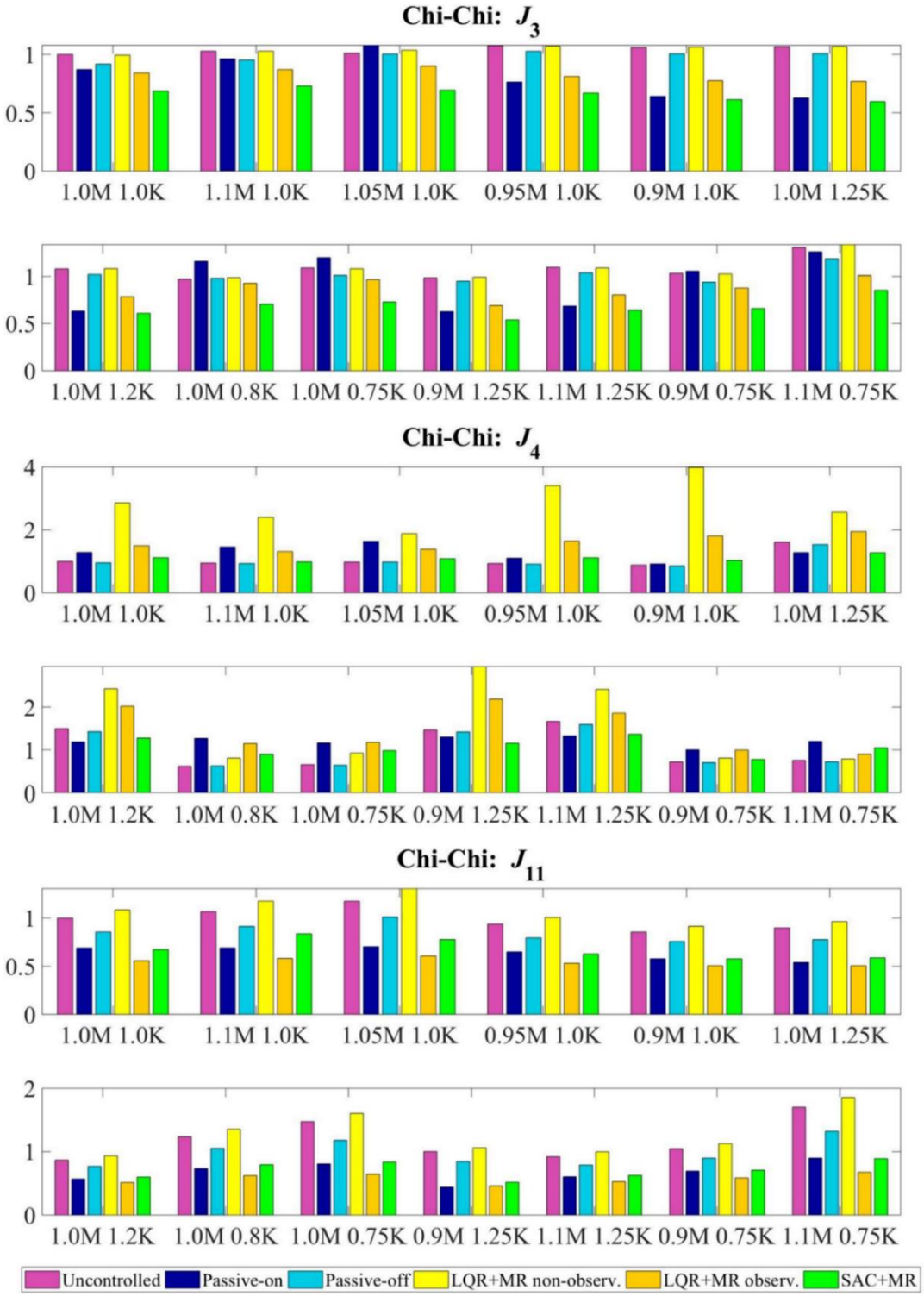

Fig. 6.19: Maximum J_3, J_4 and J_{11} for different parametric variations scenarios-earthquake Chi-Chi.

Table 6.11: Maximum performance criteria J_3, J_4 and J_{11} for the parametric variations scenarios.

Control	Chi-Chi	Duzce	Imp. Val.	Kobe	Land.	Loma Prieta	Palm Spr.	Nort.	Petr.	San Fern.	Sup. Hills
						J_3					
Uncont.	1.308	1.066	1.634	1.348	1.289	1.523	1.093	1.263	1.165	1.129	1.217
P. On	1.261	1.064	1.452	2.013	1.510	1.372	1.033	1.163	1.032	1.879	1.138
P. Off	1.187	1.045	1.545	1.273	1.140	1.294	1.046	1.214	1.126	1.010	1.085
LQR (a)	1.336	1.052	1.482	1.377	1.348	1.643	1.114	1.162	1.093	1.123	1.270
LQR (b)	1.009	0.648	1.158	1.095	0.940	0.934	0.903	1.111	1.066	1.588	0.781
SAC	0.853	0.715	1.132	1.070	0.988	1.172	1.051	0.959	0.966	1.186	0.806
						J_4					
Uncont.	1.668	1.304	1.333	1.551	1.219	1.433	1.292	1.645	1.299	1.397	1.542
P. On	1.639	1.413	1.409	1.757	1.305	2.665	1.348	1.809	1.569	1.859	1.427
P. Off	1.596	1.277	1.280	1.489	1.071	1.297	1.180	1.598	1.336	1.287	1.400
LQR (a)	3.984	3.259	7.728	6.344	6.572	9.121	4.940	3.722	2.869	3.570	5.127
LQR (b)	2.190	1.796	2.945	2.692	2.592	3.573	1.701	1.920	1.912	1.877	2.166
SAC (a)	1.365	1.094	1.761	1.543	1.017	1.827	1.214	1.481	1.582	1.219	1.515
						J_{11}					
Uncont.	1.702	1.106	1.338	1.227	1.574	1.275	1.009	1.361	1.531	1.551	1.150
P. On	0.900	1.002	1.032	1.277	1.404	1.051	0.592	1.522	1.325	1.725	0.839
P. Off	1.323	0.870	0.971	0.971	0.990	0.829	0.739	1.079	1.126	1.142	0.866
LQR (a)	1.856	1.317	1.780	1.391	2.110	1.651	1.088	1.147	1.602	1.761	1.282
LQR (b)	0.676	0.423	0.557	0.658	0.645	0.474	0.404	0.830	0.670	1.073	0.501
SAC (a)	0.892	0.461	0.742	0.664	0.747	0.607	0.641	0.804	0.669	0.980	0.549

Table 6.12: Performance criteria J_3, J_4 and J_{11} standard deviation among the parametric variation scenarios.

Control	Chi-Chi	Duzce	Imp. Val.	Kobe	Land.	Loma Prieta	Palm Spr.	Nort.	Petr.	San Fern.	Sup. Hills
	Standard Deviation - J_3										
Uncont.	0.084	0.059	0.282	0.095	0.148	0.239	0.052	0.161	0.104	0.074	0.155
P. On	0.241	0.088	0.219	0.366	0.263	0.148	0.014	0.162	0.038	0.322	0.142
P. Off	0.067	0.061	0.268	0.089	0.110	0.203	0.077	0.145	0.087	0.065	0.130
LQR (a)	0.089	0.062	0.272	0.098	0.167	0.216	0.074	0.118	0.054	0.067	0.159
LQR (b)	0.088	0.058	0.115	0.089	0.113	0.105	0.023	0.116	0.019	0.201	0.195
SAC (a)	0.078	0.031	0.102	0.085	0.082	0.190	0.110	0.109	0.024	0.172	0.084
	Standard Deviation - J_4										
Uncont.	0.373	0.182	0.312	0.265	0.223	0.228	0.240	0.282	0.215	0.199	0.317
P. On	0.185	0.269	0.238	0.242	0.211	0.597	0.333	0.308	0.367	0.217	0.291
P. Off	0.348	0.181	0.289	0.250	0.194	0.202	0.209	0.279	0.216	0.170	0.284
LQR (a)	3.001	2.388	5.797	4.553	4.881	6.858	3.761	2.738	2.234	2.705	5.139
LQR (b)	1.469	1.395	0.934	1.567	0.987	1.441	0.123	0.283	0.354	0.320	0.580
SAC (a)	0.161	0.119	0.293	0.099	0.110	0.200	0.121	0.209	0.276	0.097	0.202
	Standard Deviation – J_{11}										
Uncont.	0.252	0.131	0.274	0.082	0.176	0.217	0.126	0.223	0.197	0.222	0.084
P. On	0.119	0.167	0.135	0.198	0.088	0.163	0.058	0.216	0.187	0.160	0.134
P. Off	0.175	0.091	0.174	0.066	0.072	0.118	0.049	0.159	0.117	0.109	0.059
LQR (a)	0.281	0.149	0.369	0.067	0.287	0.275	0.110	0.169	0.183	0.263	0.103
LQR (b)	0.063	0.044	0.051	0.074	0.052	0.042	0.029	0.089	0.036	0.103	0.194
SAC (a)	0.120	0.033	0.069	0.042	0.019	0.029	0.042	0.124	0.016	0.085	0.029

In terms of normalized peak acceleration performance criterion (J_4), it can be observed that LQR+LQE (a) and (b) increase the transverse accelerations of the midspan. Evaluation criteria J_{15} indicates that peak control forces necessary for the passive-off strategy are the lowest amongst all schemes; the other schemes reach the same maximum control force that corresponds to the maximum device capacity. Lastly, J_{20} performance criterion indicates that LQR+LQE (b) scheme requires a considerable amount of sensors (41), while the SAC scheme requires a significantly lower amount of sensors (10), which is a strong advantage of the adaptive scheme.

6.2.7. Discussion

The results obtained in the parametric study conducted to assess the adaptive control approach to mitigate seismic responses of a two-span highway bridge considering realistic implementation are discussed herein. The scheme allows the choice of a model reference of significantly low order and it does not require full-state feedback or the use of observers. Adaptive control is presented as an alternative to control bridge structures since it is able to calculate control gains that vary over time based on sensed responses, which potentially gives the controlled system an improved capability to sustain performance when in face of parametric variations. The effectiveness of the control approach is investigated when controlling a seismically excited skewed two-span highway bridge considering systematic parametric variations. The performances of the active and semi-active adaptive control schemes are compared to non-adaptive control schemes when the structure is subjected to a set of 11 earthquakes.

The hydraulic actuator introduces unwanted behavior with both feedback control algorithms (SAC and LQR) when parametric changes are introduced for most earthquakes; for some earthquakes the hydraulic actuator worsened the nominal bridge responses. The observed behavior may be attributed to the dynamic force control present in the actuator model. These devices are usually mechanically stiff systems; the stiff columns make the force control very sensitive to parameters, especially when the force tracking is over a considerable bandwidth (Sivaselvan et al. 2008). Added compliance is suggested in Sivaselvan et al. (2008) to deal with this issue. Another potential reason for the worsening of responses by the actuation system is the force saturation imposed to the devices. Additionally, active control may not be the most recommended control solution for seismic control of large structures. These devices require high power in order to achieve high forces necessary to control seismically excited large structures. Power is likely to be unavailable during major extreme events, which would call for considerably large batteries to guarantee the functionality of the control scheme.

The passive-off scheme presents a very limited performance and lacks robustness. The passive-on presents a satisfactory performance for some parametric variations scenarios. However, it increased significantly the midspan RMS and peak displacements for some others. This poor performance is attributed to excessive stiffness introduced by the devices to the bridge ends. Results indicate that the lack of adjustability of the passive control leads to a sensitivity to parametric changes. The results contradict the idea that passive control is always beneficial; passive control may worsen responses of large structures where placement constraints exist.

Results indicate that semi-active control is a suitable alternative when controlling structures that have significant control placement constraints and are expected to have parametric variations. The optimal semi-active scheme reduces overall displacements and it is indeed robust provided the system is observable; this means the scheme requires a considerable amount of sensors to perform satisfactorily. Also, the optimal semi-active control increased midspan accelerations. The proposed semi-active adaptive controller with SAC is able to reduce overall seismic responses. The adaptive scheme holds performance well in face of parametric changes and it does not require observability to operate properly, allowing the adoption of a smaller amount of sensors.

7. CABLE-STAYED BRIDGES SEMI-ACTIVE ADAPTIVE CONTROL

In this section, semi-active adaptive control schemes are proposed to control a cable-stayed bridge considering parametric variations. The main objective of the control approach is to mitigate excessive response due to seismic excitations while providing a guaranteed level of robustness in face of parametric uncertainty. In the first portion of this section two adaptive schemes are developed, implemented and designed to control the cable-stayed bridge described in section 4.4 for a set of three major earthquakes, considering multi-support excitations and different angles of incidence. The performances of the adaptive schemes are compared to non-adaptive control before and after two parametric variations are introduced to the bridge. In the second portion of this section, the adaptive control schemes are implemented for the cable-stayed bridge considering earthquakes matched to the site design spectra, following AASHTO provisions. The performances of the adaptive schemes are compared to non-adaptive schemes considering the nominal structure and after two parametric variations are considered.

7.1. Control Scheme Design and Implementation

The semi-active adaptive control is developed by implementing two adaptive strategies to determine the control command to operate MR dampers with 1000kN maximum capacity. The control devices for all strategies are placed in the longitudinal direction (along the deck). There are a total of 24 devices, 4 between the deck and bent 1, 8 between the deck and pier 2, 8 between the deck and pier 3, and 4 between the deck and

pier 4. Fig. 7.1 gives the schematics of the placement distribution of the control devices in the cable-stayed bridge for the towers region.

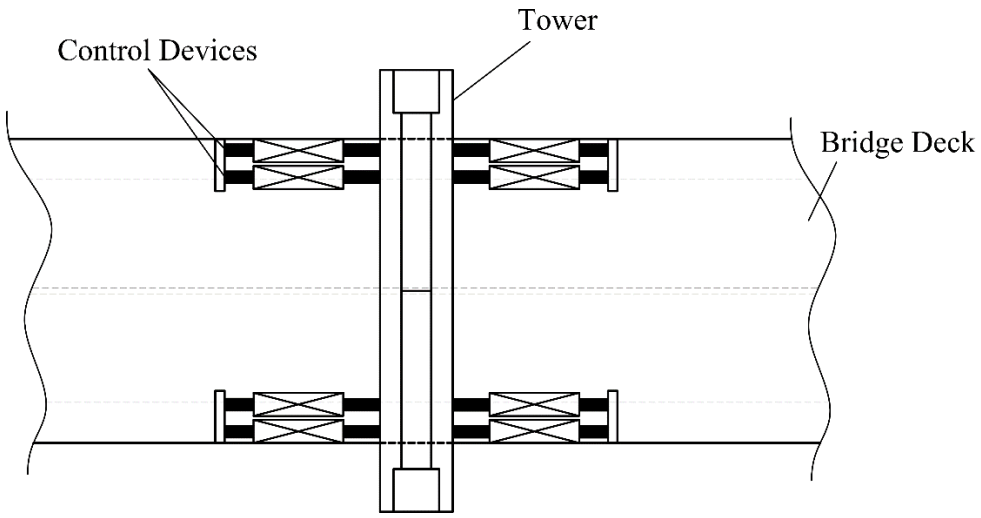

Fig. 7.1. Placement distribution of the control devices in the cable-stayed bridge.

Purely passive and non-adaptive semi-active control schemes are also implemented for comparison purposes. Purely passive cases are considered, where dampers are set to operate with maximum voltage (passive-on) and dampers set to operate with zero voltage (passive-off). The non-adaptive semi-active scheme is composed of resettable dampers operating with the same placement distribution and maximum capacity considered for the adaptive schemes. The dynamics models for the devices and parameters are presented in section 5.1. The adaptive schemes developed utilize the theoretical basis of SAC and Neuro-Fuzzy strategies. Two different scenarios of parametric variations are considered in order to assess the robustness of the control schemes: the deck mass is

increased in 5% and the stiffness of the deck and piers are reduced in 20%. The control approaches design and implementation are discussed in the following sections.

7.1.1. Simple Adaptive Control (SAC)

In the proposed approach, a reduced order model reference is considered for SAC implementation and the nodes to be tracked are shown in Fig. 7.2. The model reference is taken as the nominal bridge controlled by LQR optimal control considering full feedback and ideal actuators with no saturation. The longitudinal displacements and velocities of the midspan El Centro (1940) earthquake acting in the longitudinal direction for the uncontrolled bridge and model reference are given in Fig. 7.3. The figure shows that the optimal control reduces satisfactorily the midspan responses of the bridge. Tracking this behavior leads to reduction of midspan longitudinal responses. The gains for SAC obtained after implementation and design are:

$$\Gamma_e = 5 \times 10^7$$
$$\Gamma_x = 10^3$$
$$\Gamma_u = 10^3$$

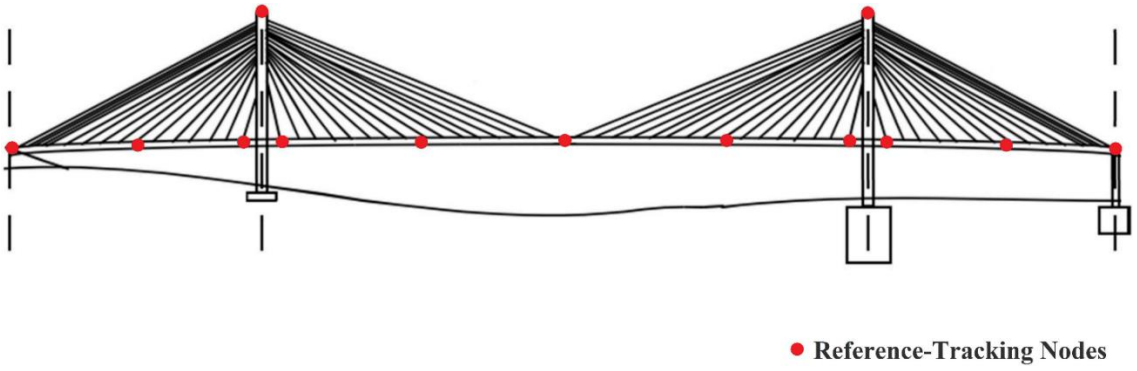

Fig. 7.2. Model reference cable-stayed bridge monitored nodes.

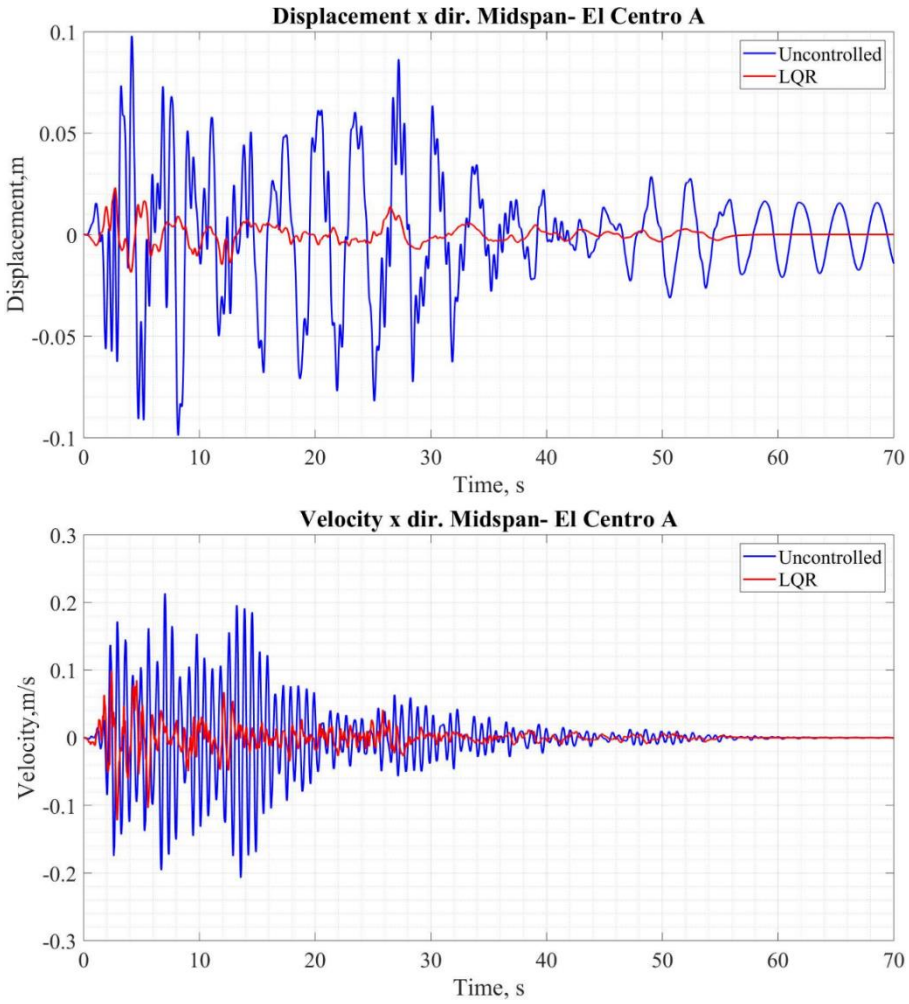

Fig. 7.3. Model reference midspan longitudinal displacements and velocities El Centro (1940) earthquake compared to the uncontrolled bridge response.

Fig. 7.4 displays the longitudinal midspan displacements for the SAC-controlled bridge and the uncontrolled for the different parametric scenarios considered. It is noticeable that the bridge controlled by SAC follows the behavior of the nominal controlled bridge while the uncontrolled bridge is more susceptible to the parametric changes introduced. The reference tracking is not perfect, which can be attributed to some loss in performance due to limitations on maximum forces and dynamics of the device. In

this preliminary assessment, the control scheme shows to be successful in reducing midspan displacements and tracking the model reference, therefore the design is considered satisfactory.

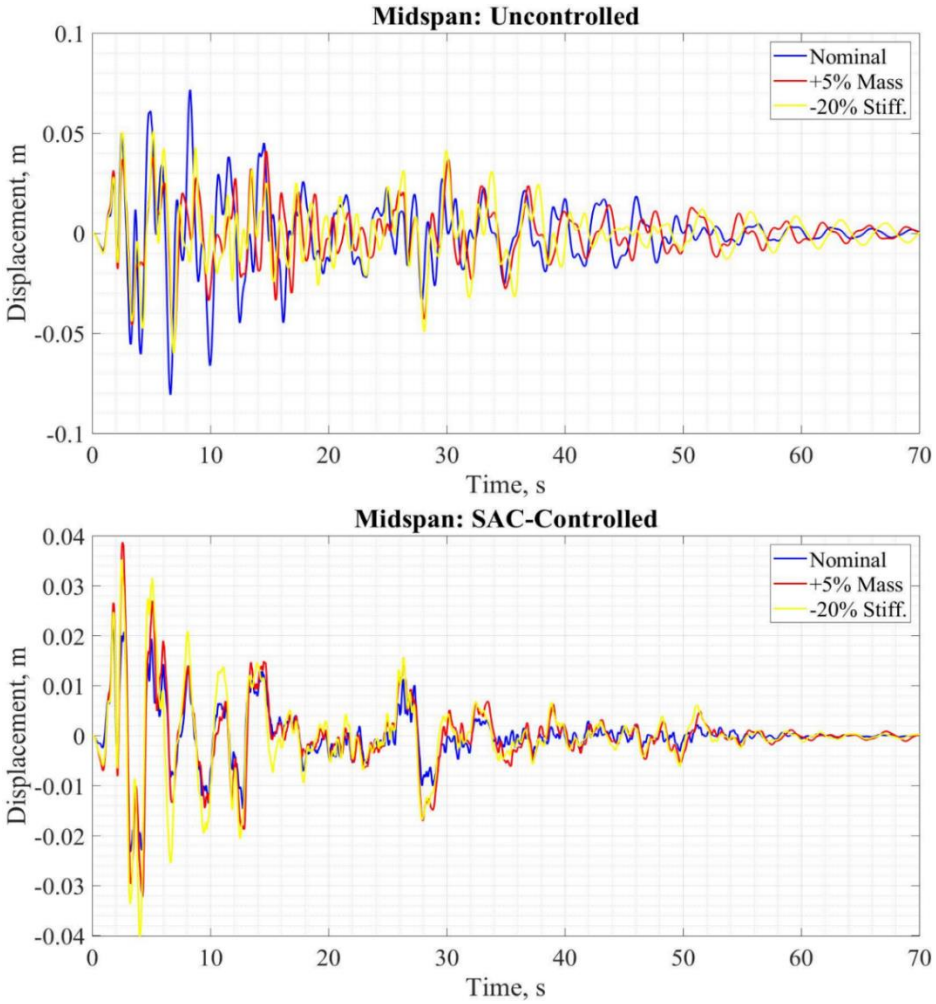

Fig. 7.4. Midspan longitudinal displacements and velocities El Centro (1940) earthquake for the uncontrolled and SAC-controlled.

7.1.2. Neuro-Fuzzy Adaptive Control

In the proposed approach, the target control is taken as the nominal bridge controlled by LQR with full feedback, as it is considered for SAC's model reference. The disturbance introduced to the target controller to be considered in training is a Gaussian white noise with 120s of duration. The inputs considered are the displacements and velocities from the same nodes monitored by SAC (refer to Fig. 7.2); the outputs are the command voltage of the MR dampers. After the target control data is collected an initial FIS is defined. Seven triangular-shaped membership functions are defined, as presented in Fig. 7.5.

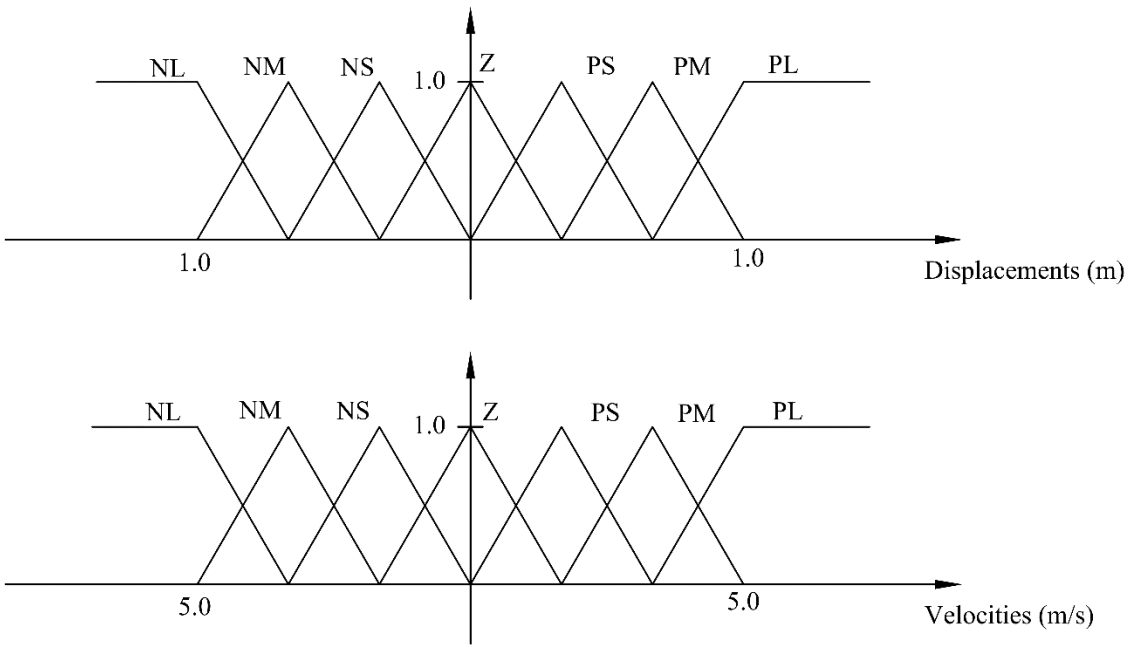

Fig. 7.5. Membership functions adopted for the inputs.

The fuzzy membership functions sets for the input variables (displacements and velocities of the monitored nodes) are:

a) NS = negative small

b) NM = negative medium

c) NL = negative large

d) Z = zero

e) PS = positive small

f) PM = positive medium

g) PL = positive large

The fuzzy membership functions for the output variable (voltage) are also triangular and vary from 0 to 10V. After the initial FIS is defined and the target controller inputs and outputs are obtained, the neural-networks learning process begins. The parameters of the FIS are adjusted until an acceptable predefined target error is reached.

7.2. Performance Criteria

The performance evaluation criteria adopted in this study are in their majority selected from the benchmark study (Caicedo et al. 2003). Criteria J_1, J_2, J_3, J_4, J_5 and J_6 evaluate the performance in terms of peak responses and are given by Equations (7.1)-(7.6), where the subscript *c* refers to the controlled case and the subscript *u* refers to the uncontrolled case. Criterion J_1 evaluates the performance in terms of peak base shear, J_2 in terms of peak deck shear, J_3 in terms of peak overturning moment, J_4 in terms of peak

deck moment, J_5 in terms of peak cable tension, and J_6 in terms of peak deck displacement at the abutments.

$$J_1 = \max\left\{\frac{\max|F_{bc}(t)|}{F_{bu}^{\max}}\right\} \tag{7.1}$$

$$J_2 = \max\left\{\frac{\max|F_{dc}(t)|}{F_{du}^{\max}}\right\} \tag{7.2}$$

$$J_3 = \max\left\{\frac{\max|M_{bc}(t)|}{M_{bu}^{\max}}\right\} \tag{7.3}$$

$$J_4 = \max\left\{\frac{\max|M_{dc}(t)|}{M_{du}^{\max}}\right\} \tag{7.4}$$

$$J_5 = \max\left\{\max\left[\frac{\left|T_{a,i}(t) - T_{\text{nominal},i}\right| / T_{\text{nominal},i}}{\max\left(\left|T_{a,i}(t) - T_{\text{nominal},i}\right| / T_{\text{nominal},i}\right)}\right]\right\} \tag{7.5}$$

$$J_6 = \max\left\{\frac{\max|x_{bc}(t)|}{x_{bu}^{\max}}\right\} \tag{7.6}$$

Criteria J_7, J_8, J_9 , J_{10} and J_{11} evaluate the performance in terms of normed responses as given by Equation (7.7). They are given by Equations (7.8)-(7.12), where the subscript *c* refers to the controlled response and the subscript *u* refers to the uncontrolled case. Criterion J_7 evaluates performance in terms of normed base shear, J_8 in terms of

normed deck shear, J_9 in terms of normed overturning moment, J_{10} in terms of normed deck moment, and J_{11} in terms of normed cable tension. The responses evaluated are in the longitudinal direction (*x* direction), where the most critical responses are observed.

$$\|\bullet\| \equiv \sqrt{\frac{1}{t_f}\int_0^{t_f} (\bullet)^2 dt} \tag{7.7}$$

$$J_7 = \max\left\{\frac{\max\|F_{bc}(t)\|}{\max\|F_{bu}(t)\|}\right\} \tag{7.8}$$

$$J_8 = \max\left\{\frac{\max\|F_{dc}(t)\|}{\max\|F_{du}(t)\|}\right\} \tag{7.9}$$

$$J_9 = \max\left\{\frac{\max\|M_{bc}(t)\|}{\max\|M_{bu}(t)\|}\right\} \tag{7.10}$$

$$J_{10} = \max\left\{\frac{\max\|M_{dc}(t)\|}{\max\|M_{du}(t)\|}\right\} \tag{7.11}$$

$$J_{11} = \max\left\{\max\left[\frac{\left\|T_{a,i}(t) - T_{\text{nominal},i}\right\| / T_{\text{nominal},i}}{\max\left(\left\|T_{a,i}(t) - T_{\text{nominal},i}\right\| / T_{\text{nominal},i}\right)}\right]\right\} \tag{7.12}$$

Criteria J_{12}, J_{14}, J_{16} and J_{17} evaluate the performance of the control approach. They are defined by Equations (7.13)-(7.16), where the subscript *c* refers to the controlled case

and the subscript *u* refers to the uncontrolled case. Criterion J_{12} evaluates the maximum force generated by the strategy normalized by the bridge weight (not including the foundations) W=510,000kN, J_{14} evaluates the effort of the control device, J_{16} is the number of devices employed, and J_{17} the number of sensors.

$$J_{12} = \max\left\{\frac{\max\left|f_{device}(t)\right|}{W}\right\} \tag{7.13}$$

$$J_{14} = \max\left\{\frac{\max\left|\dot{x}_{device}(t)\, f_{device}(t)\right|}{\max\left|\dot{x}_u^{\max} W\right|}\right\} \tag{7.14}$$

$$J_{16} = \text{number of devices} \tag{7.15}$$

$$J_{17} = \text{number of sensors} \tag{7.16}$$

7.3. Benchmark Earthquakes

In this portion of the study, the adaptive control schemes are implemented to control the cable-stayed bridge subjected to the earthquake records recommended by the benchmark for seismically excited cable-stayed bridges (Caicedo et al. 2003). The records considered are the significant events El Centro earthquake from 1940, Mexico City earthquake from 1985, and the Gebze earthquake from 1999; their acceleration time-histories are shown in Fig. 7.6. According to Caicedo et al. (2003), the Mexico City earthquake is chosen due to geological similarities between the region where the bridge is

located and Mexico City. The El Centro and Gebze earthquakes are chosen because they are both significant events that carry different characteristics.

Two different incidence angles of 15° and 45° are considered for each earthquake, taken from the longitudinal direction. To consider the effects of multiple support excitation, a delay in the ground motion is introduced for each bridge support. The arrival times for the motion for each support are described in Table 7.1. The multiple support excitation leads to an alteration in the formulation of the equation of motion for multi-degree of freedom structures presented in Equation (4.1) due to the relative motion between supports. The analytical formulation to consider this effect is presented in the next subsection.

Table 7.1: Incidence angle and arrival times of the earthquake records.

Incidence Angle	Arrival times for the Ground Motion (sec)			
	Location			
	Bent 1	Pier 1	Pier 2	Pier 3
15°	0	0.05	0.16	0.20
45°	0	0.03	0.12	0.15

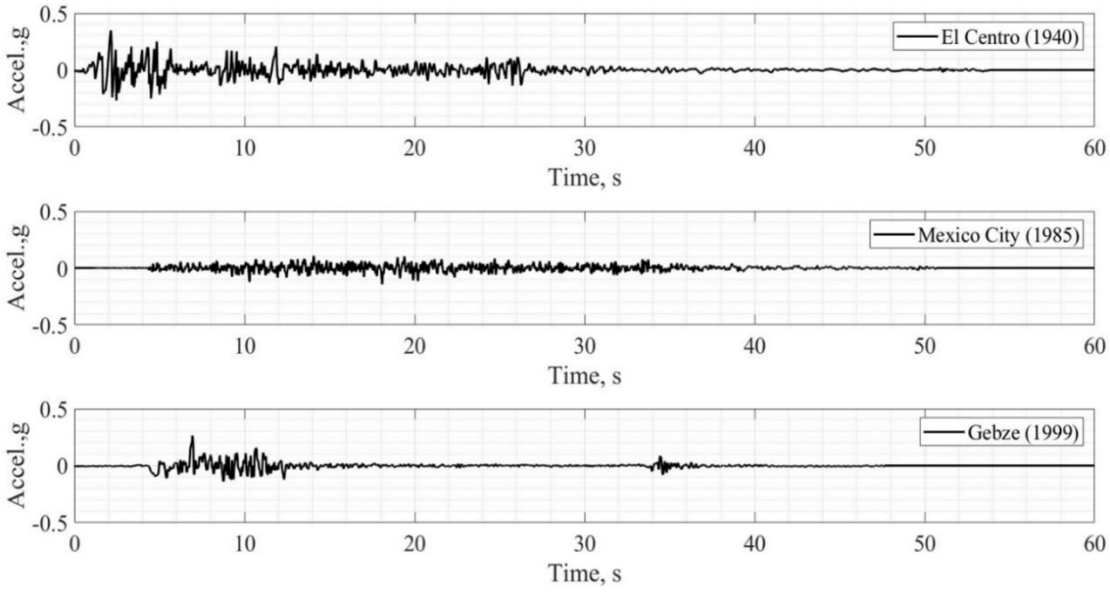

Fig. 7.6. Benchmark earthquakes acceleration time-histories.

7.3.1. Multiple Support Excitation

The ground motion experienced by cable-stayed bridges during the occurrence of an earthquake is likely to vary significantly from one support to another, given the size of their spans. In this section, the equation of motion formulation considering the prescribed ground motions that differ in arrival time and/or direction is presented, as described by Chopra (2012). The formulation of the equation of motion in case of multiple support excitation includes the DOFs for the supports and can be written in partitioned form:

$$\begin{bmatrix} \mathbf{M} & \mathbf{M}_g \\ \mathbf{M}_g^{\mathrm{T}} & \mathbf{M}_{gg} \end{bmatrix} \begin{Bmatrix} \ddot{\mathbf{x}}^{tot} \\ \ddot{\mathbf{x}}_g \end{Bmatrix} + \begin{bmatrix} \mathbf{C} & \mathbf{C}_g \\ \mathbf{C}_g^{\mathrm{T}} & \mathbf{C}_{gg} \end{bmatrix} \begin{Bmatrix} \dot{\mathbf{x}}^{tot} \\ \dot{\mathbf{x}}_g \end{Bmatrix} + \begin{bmatrix} \mathbf{K} & \mathbf{K}_g \\ \mathbf{K}_g^{\mathrm{T}} & \mathbf{K}_{gg} \end{bmatrix} \begin{Bmatrix} \mathbf{x}^{tot} \\ \mathbf{x}_g \end{Bmatrix} = \begin{Bmatrix} \mathbf{0} \\ \mathbf{p}_g(t) \end{Bmatrix} \tag{7.17}$$

In Equation (7.17), the subscript *g* refers to the support DOFs: $\mathbf{M_{gg}}$, $\mathbf{C_{gg}}$, $\mathbf{K_{gg}}$ are the mass, damping, and stiffness matrices correspondent to the supports, $\mathbf{M_g}$, $\mathbf{C_g}$, $\mathbf{K_g}$ matrices are the mass, damping and stiffness expressing the coupling effects in the structure DOFs due to motion of the supports, and $\mathbf{p_g}(t)$ is the vector of the support forces. The total displacement can be expressed as the sum of the displacements due to the ground motion and the structural deformations:

$$\begin{Bmatrix} \mathbf{x}^{\mathbf{tot}} \\ \mathbf{x_g} \end{Bmatrix} = \begin{Bmatrix} \mathbf{x}^{\mathbf{qs}} \\ \mathbf{x_g} \end{Bmatrix} + \begin{Bmatrix} \mathbf{x} \\ \mathbf{0} \end{Bmatrix} \tag{7.18}$$

$$\mathbf{x}^{\mathbf{qs}} = \left(-\mathbf{K}^{-1}\mathbf{K_g}\right)\mathbf{x_g} \tag{7.19}$$

$\mathbf{x}^{\mathbf{qs}}$ represents the structural displacements due to static application of the support displacements at each time instant. Since these displacements vary with time but are static in nature, $\mathbf{x}^{\mathbf{qs}}$ is called the quasi-static displacement vector. The term which multiplies the ground prescribed displacement in Equation (7.19) is called the influence matrix as given by Equation (7.23); it is obtained by inducing unit displacements to each support and checking the influence these displacements exert on structural displacements. Taking the first portion of the partitioned Equation of motion (7.17) and substituting the total displacement by the definition from Equation (7.18) leads to Equation (7.20). Rearrangement of the terms leads to Equation (7.21).

$$\mathbf{M}\ddot{\mathbf{x}}^{\mathbf{tot}} + \mathbf{M_g}\ddot{\mathbf{x}}_{\mathbf{g}} + \mathbf{C}\dot{\mathbf{x}}^{\mathbf{tot}} + \mathbf{C_g}\dot{\mathbf{x}}_{\mathbf{g}} + \mathbf{K}\mathbf{x}^{\mathbf{tot}} + \mathbf{K_g}\mathbf{x_g} = \mathbf{0} \tag{7.20}$$

$$\mathbf{M}\ddot{\mathbf{x}} + \mathbf{C}\dot{\mathbf{x}} + \mathbf{K}\mathbf{x} = -(\mathbf{M}\ddot{\mathbf{x}}^{qs} + \mathbf{M}_g\ddot{\mathbf{x}}_g + \mathbf{C}\dot{\mathbf{x}}^{qs} + \mathbf{C}_g\dot{\mathbf{x}}_g + \mathbf{K}\mathbf{x}^{qs} + \mathbf{K}_g\mathbf{x}_g) \quad (7.21)$$

Substitution of Equation (7.19) into Equation (7.21) leads to:

$$\mathbf{M}\ddot{\mathbf{x}} + \mathbf{C}\dot{\mathbf{x}} + \mathbf{K}\mathbf{x} = -(\mathbf{M}\iota + \mathbf{M}_g)\ddot{\mathbf{x}}_g - (\mathbf{C}\iota + \mathbf{C}_g)\dot{\mathbf{x}}_g \quad (7.22)$$

where $\iota = -\mathbf{K}^{-1}\mathbf{K}_g$ (7.23)

In the case where the mass matrix is diagonal, $\mathbf{M_g}$ is null. Additionally, the damping term is usually small when compared to the inertia term and may be dropped (Chopra 2012). This leads to a simplified version of the equation of motion considering multiple support excitations:

$$\mathbf{M}\ddot{\mathbf{x}} + \mathbf{C}\dot{\mathbf{x}} + \mathbf{K}\mathbf{x} = -\mathbf{M}\iota\ddot{\mathbf{x}}_g \quad (7.24)$$

After the nodal displacements and rotations of the structural elements are obtained, the elements forces can be determined by applying element stiffness properties, as displayed in Fig. 7.7 and the application of Equation (7.25). Fig. 7.8 gives some examples of stiffness coefficients.

$$\begin{Bmatrix} N_a \\ V_a \\ M_a \\ N_b \\ V_b \\ M_b \end{Bmatrix} = \begin{bmatrix} k_{11} & k_{12} & k_{13} & k_{14} & k_{15} & k_{16} \\ k_{21} & k_{22} & k_{23} & k_{24} & k_{25} & k_{26} \\ k_{31} & k_{32} & k_{33} & k_{34} & k_{35} & k_{36} \\ k_{41} & k_{42} & k_{43} & k_{44} & k_{45} & k_{46} \\ k_{51} & k_{52} & k_{53} & k_{54} & k_{55} & k_{56} \\ k_{61} & k_{62} & k_{63} & k_{64} & k_{65} & k_{66} \end{bmatrix} \begin{Bmatrix} x_a \\ y_a \\ \theta_a \\ x_b \\ y_b \\ \theta_b \end{Bmatrix} \tag{7.25}$$

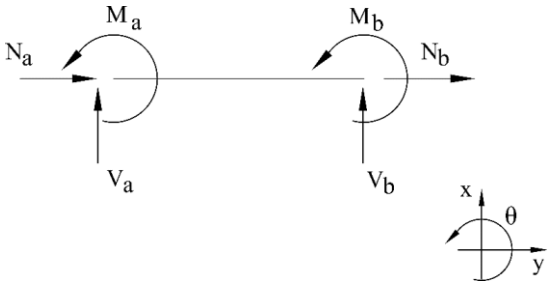

Fig. 7.7. Element forces considering in plane DOFs.

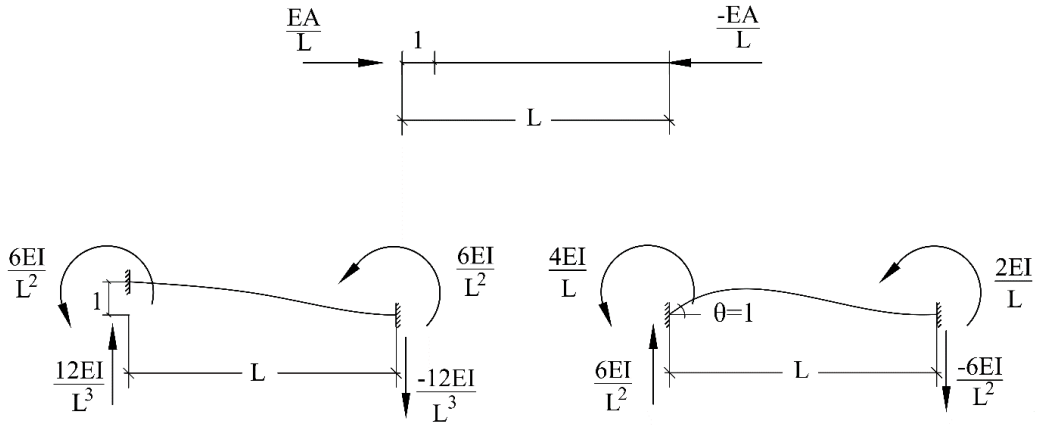

Fig. 7.8. Element stiffness coefficients for different types of imposed unit displacements.

7.3.2. Results and discussion

In this section are presented and discussed the results obtained after the bridge is subjected to the benchmark earthquake records El Centro, Mexico City and Gebze, considering angle of incidence of 15° and 45° and different arrival times. The control schemes considered are MR dampers behaving as fully passive devices; passive-on and passive-off; nonadaptive semi-active control with resettable devices, adaptive semi-active control with SAC and MR dampers (refer to section 7.1.1), and adaptive semi-active control with neuro-fuzzy control and MR dampers (refer to section 7.1.2). Three parametric scenarios are taken into consideration: nominal structure, bridge with 5% mass increase, and 20% stiffness reduction.

Table 7.2 gives the maximum value obtained for the performance criteria. Table 7.3 gives the standard deviation found for each performance criteria for all the scenarios analyzed. The supplemental and detailed results in terms of the performance criteria obtained for all earthquake records, angles of incidence, control schemes, and parametric variation scenarios are given in Appendix B.

Table 7.2: Performance criteria maximum values of each control scheme considering the parametric scenarios and earthquakes with different angles of incidence and arrival times.

Maximum Performance Criteria						
Criteria	Dir.	Passive-on	Passive-off	Resettable	SAC	Neuro-Fuzzy
J_1	x	2.4813	0.9530	0.9363	0.9357	1.0510
J_2	x	1.7653	1.3440	1.1314	1.0341	1.2136
J_3	x	2.4813	0.9530	0.9363	0.9357	1.0510
J_4	x	1.8627	1.1250	0.7872	0.7943	0.7614
J_5	-	1.4983	0.3251	0.3378	0.3197	0.6052
J_6	x	0.0098	0.0254	0.0195	0.0224	0.0161
J_7	x	3.8437	0.8908	1.0154	0.8402	1.6510
J_8	x	1.7704	0.8632	0.6909	0.6200	0.8622
J_9	x	3.8437	0.8908	1.0154	0.8402	1.6510
J_{10}	x	1.4863	0.8307	0.6631	0.5910	0.7366
J_{11}	-	0.2983	0.0469	0.0536	0.0444	0.1163
Max.		3.8437	1.3440	1.1314	1.0341	1.6510
Average		1.9401	0.7498	0.6897	0.6343	0.8832

Table 7.3: Performance criteria standard deviation of each control scheme among the parametric scenarios and earthquakes with different angles of incidence and arrival times.

Standard Deviation						
Value	Dir.	Passive-on	Passive-off	Resettable	SAC	Neuro-Fuzzy
J_1	x	0.5243	0.0888	0.0947	0.0877	0.1825
J_2	x	0.4721	0.2543	0.1853	0.1649	0.2364
J_3	x	0.5243	0.0888	0.0947	0.0877	0.1825
J_4	x	0.4436	0.1712	0.1063	0.1226	0.1660
J_5	-	0.3834	0.0487	0.0505	0.0441	0.1224
J_6	x	0.0030	0.0068	0.0049	0.0062	0.0045
J_7	x	1.0017	0.1323	0.1932	0.1288	0.4208
J_8	x	0.4959	0.1650	0.1193	0.0901	0.1966
J_9	x	1.0017	0.1323	0.1932	0.1288	0.4208
J_{10}	x	0.4018	0.1651	0.1171	0.0890	0.1833
J_{11}	-	0.0908	0.0081	0.0119	0.0092	0.0338
Max.		1.0017	0.2543	0.1932	0.1649	0.4208
Average		0.4857	0.1147	0.1065	0.0872	0.1954

Fig. 7.9 displays the maximum J_1 (peak base shear) for the control schemes considering different parametric scenarios and earthquake excitations. Fig. 7.10 displays the maximum J_5 (peak cable tension) for the control schemes considering different parametric scenarios and earthquake excitations. Fig. 7.11 displays the maximum J_7 (normed base shear) for the control schemes considering different parametric scenarios and earthquake excitations. Fig. 7.12 displays the maximum J_{10} (normed deck moment) for the control schemes considering different parametric scenarios and earthquake excitations. Fig. 7.13 gives the midspan longitudinal displacements due to earthquake El Centro with 15° angle of incidence, for all the control schemes considered. Fig. 7.14 gives the midspan longitudinal displacements due to earthquake Gebze with 15° angle of incidence, for all the control schemes considered.

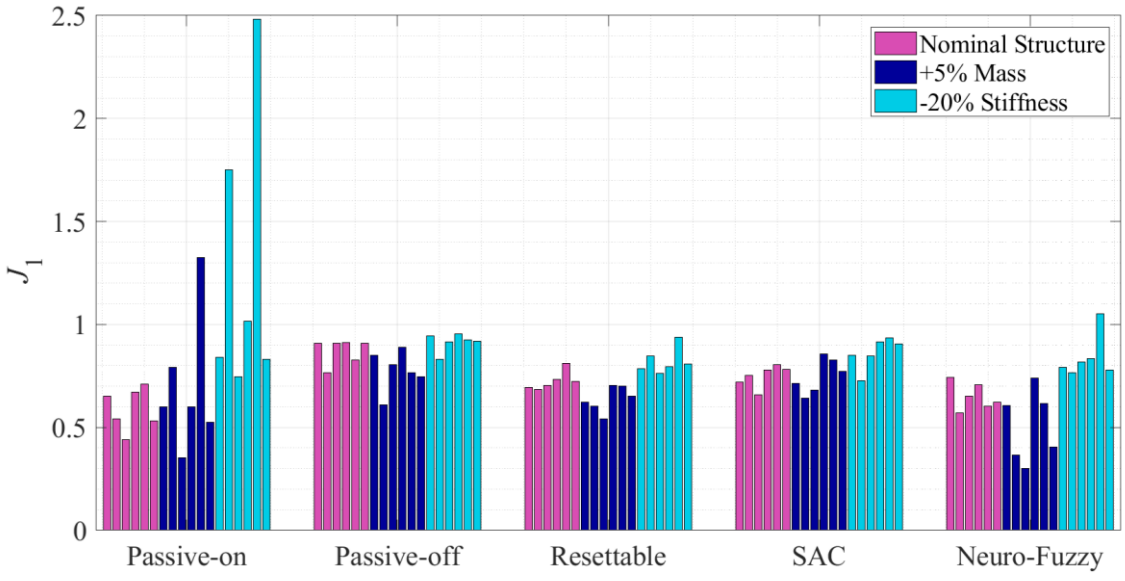

Fig. 7.9. Maximum J_1 (peak base shear) for earthquakes with different angles of incidence and arrival times, considering different parametric scenarios.

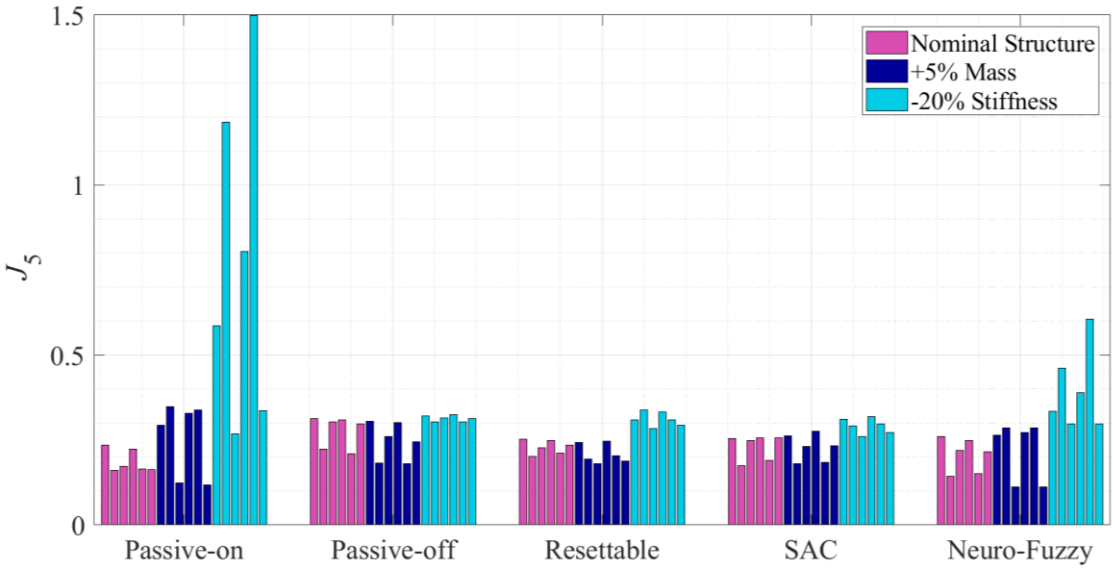

Fig. 7.10. Maximum J_5 (peak cable tension) for earthquakes with different angles of incidence and arrival times, considering different parametric scenarios.

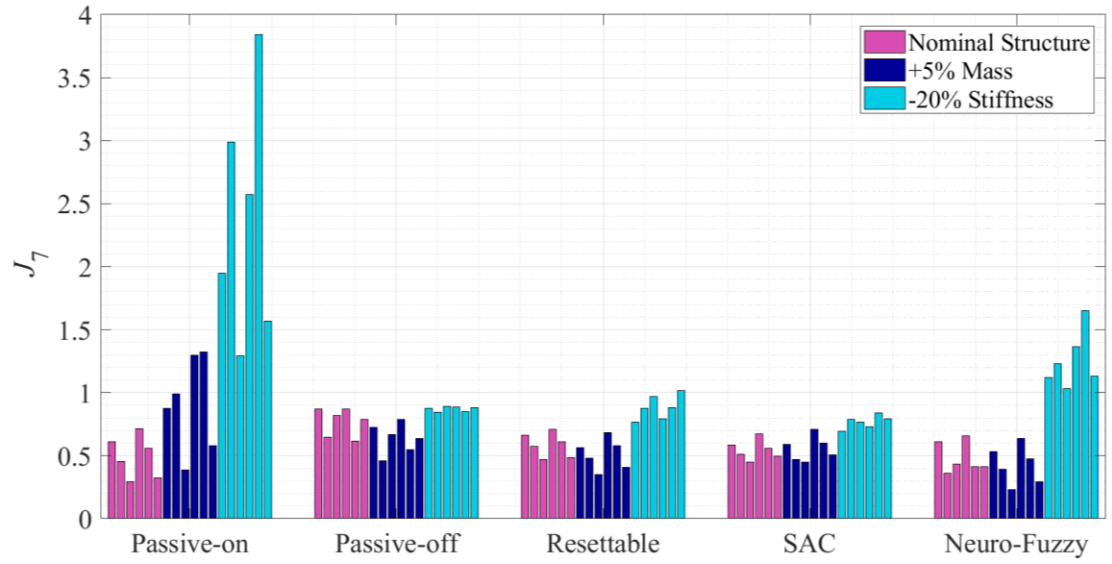

Fig. 7.11. Maximum J_7 (normed base shear) for earthquakes with different angles of incidence and arrival times, considering different parametric scenarios.

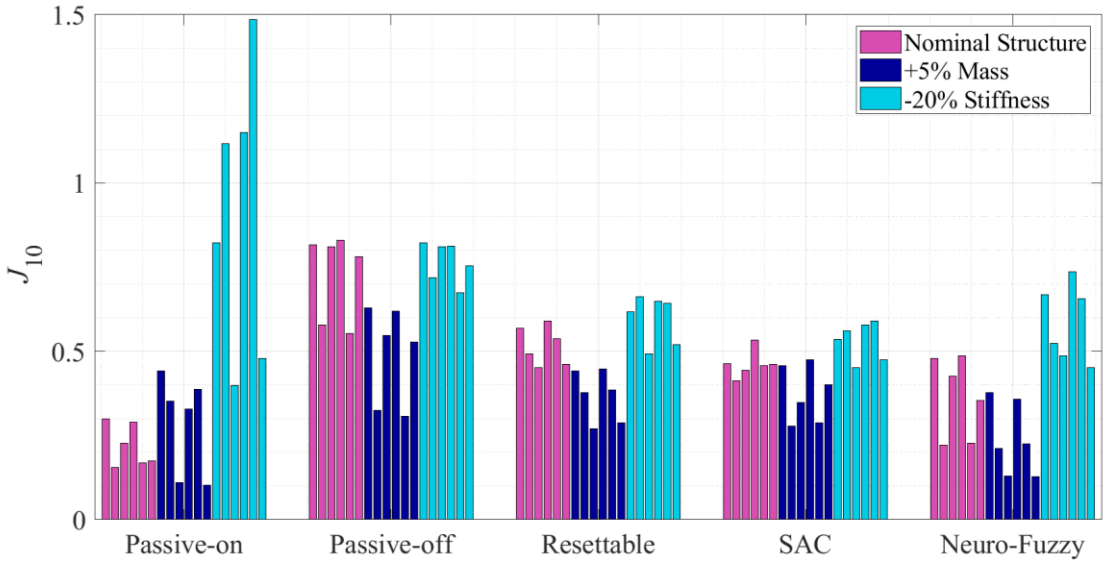

Fig. 7.12. Maximum J_{10} (normed deck moment) for earthquakes with different angles of incidence and arrival times, considering different parametric scenarios.

The bridge controlled by the passive-on case has a satisfactory performance for the nominal structure and the responses are very much attenuated. However, the performance of the control scheme deteriorates once the parameters are varied. The control scheme shows to be susceptible to parametric variations and not able to sustain overall performance when the parameters are varied. The bridge controlled by the passive-on scheme provided the largest peak and normed base and deck shear (J_1, J_3, J_7, J_9). The scheme reduces responses in terms of displacements really well, however the lack of adaptability shows that the passive scheme performance is not robust enough and depending on the parametric change it has the ability of deteriorating the seismic performance of the bridge.

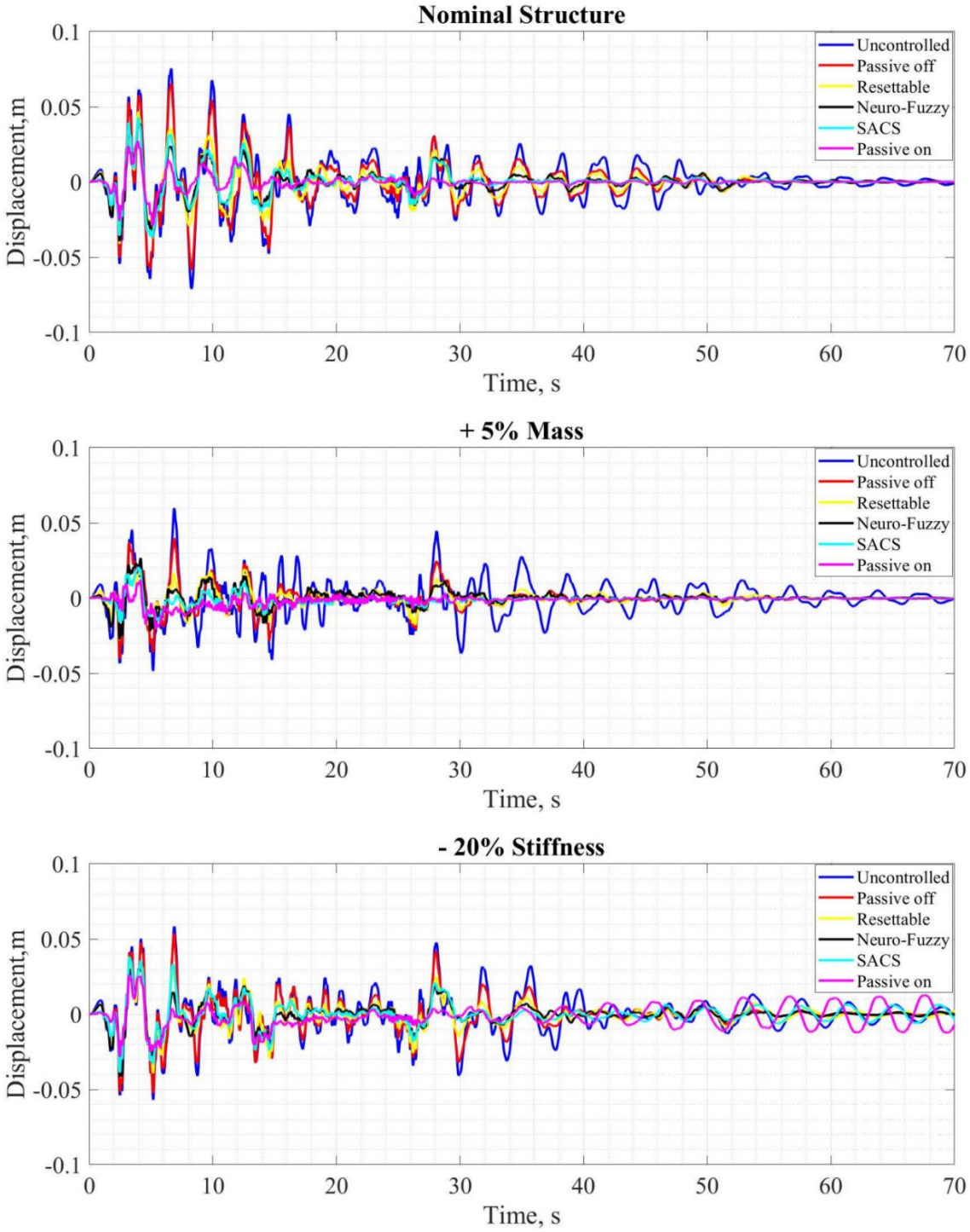

Fig. 7.13. Midspan longitudinal displacement considering different parametric scenarios for earthquake El Centro- 15° incidence.

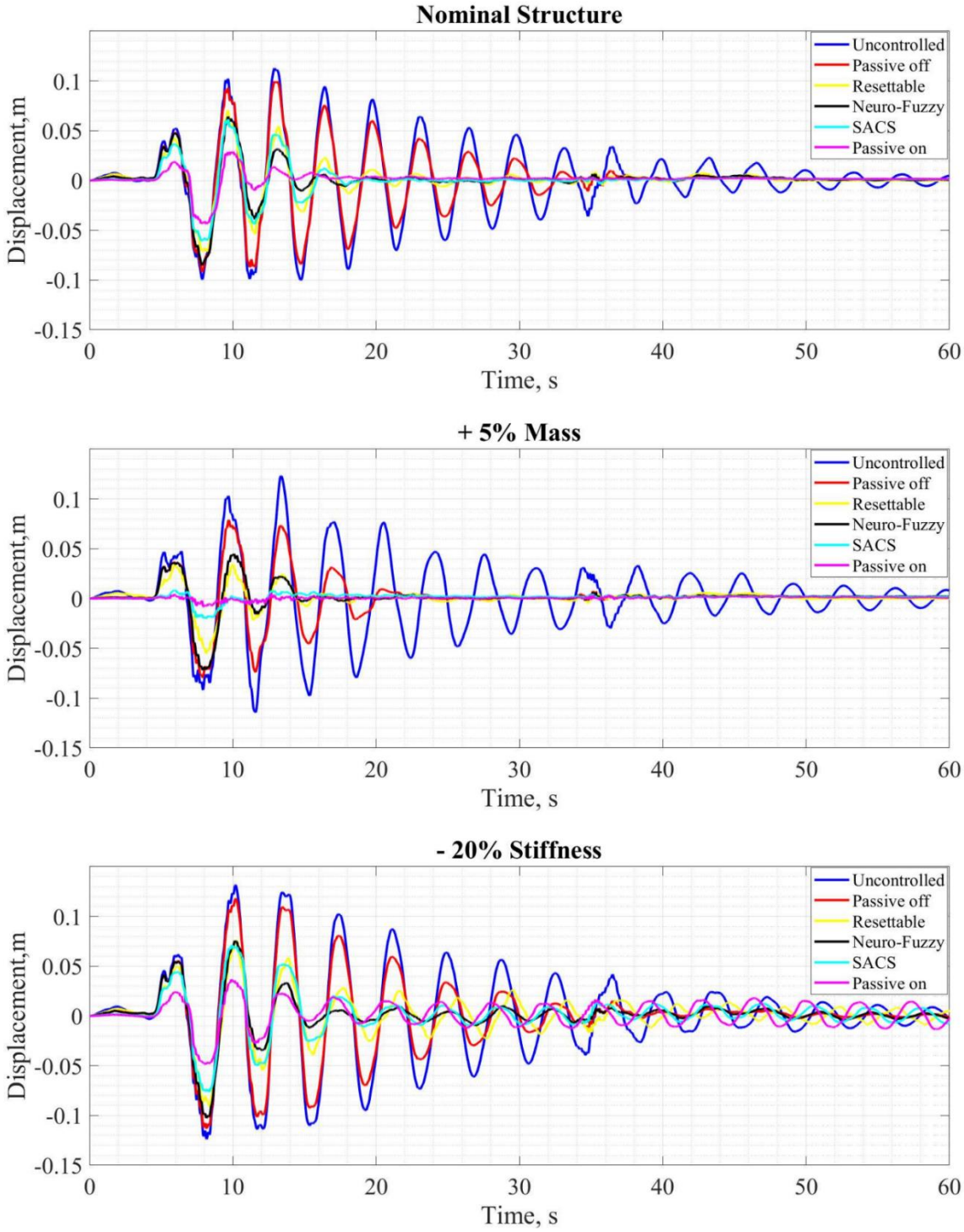

Fig. 7.14. Midspan longitudinal displacement considering different parametric scenarios for earthquake Gebze- 15° incidence.

On the other hand, the passive-off scheme sustains performance very well in face of the parametric changes, but the reduction in overall responses is not significant and the control scheme shows to have limited performance. The semi-active resettable devices give an overall successful reduction in responses and sustains performance better than the passive schemes. The scheme, however, is outperformed by SAC for most performance criteria evaluated. Neuro-fuzzy semi-active scheme is outperformed by the resettable scheme for some of the criteria evaluated. However, it shows enhanced performance when compared to the passive-off case and the scheme holds performance better than the passive-on scheme. Additionally, the scheme is considerably effective in reducing abutments and midspan displacements for all the parametric variations considered. The performance of the neuro-fuzzy controller may be further improved by changing the parameters of the control scheme and feedback conditions in order to improve its adaptability and consequently its robustness, and the resettable scheme does not have this advantage.

The semi-active adaptive control scheme controlled by SAC provide the best overall performance and least average variation. It can be concluded from the overall observation of the results that the control scheme is so far a suitable to control the cable-stayed bridge and sustain performance when in face of parametric variations and different earthquakes with different angles of incidence and times of arrival. The bridge is subjected to earthquakes spectral-matched to the design spectrum from AASHTO (2017), considering site conditions in the next subsection for further investigation.

7.4. Central US Earthquakes

In this section, the cable-stayed bridge is subjected to earthquakes representative of the Central US region. The control schemes previously evaluated are assessed considering local site conditions and time history analysis provisions from AASHTO (2017).

7.4.1. Central US Region Seismic Characterization

The cable-stayed bridge analyzed in this study is an existing bridge located between Missouri and Illinois, spanning the Mississippi River. This area is near to the New Madrid seismic zone, which is an intraplate deep-seated fault system located in the southern and Midwestern United States. The seismic zone stretches from Missouri and Illinois' border to Arkansas and Tennessee's and is about 70 km (45 miles) wide and about 200 km (125 miles) long. Fig. 7.15 shows the location of the fault system.

There is little evidence of the existence of the seismic zone in the surface, but there is evidence of these faults through earthquake activity. Most seismicity is localized between the depths of 5 to 25 km. There are two types of faults in the fault system, a strike-slip oriented to the northeast that runs from Marked Tree, AR to Caruthersville, MO, and a northwest trending reverse fault that rests below the New Madrid region. Material on the northwest side of the strike-slip fault moves northeast, and up the ramp (Department of Earth and Atmospheric Sciences 2016). Fig. 7.16 shows the schematics of the fault system.

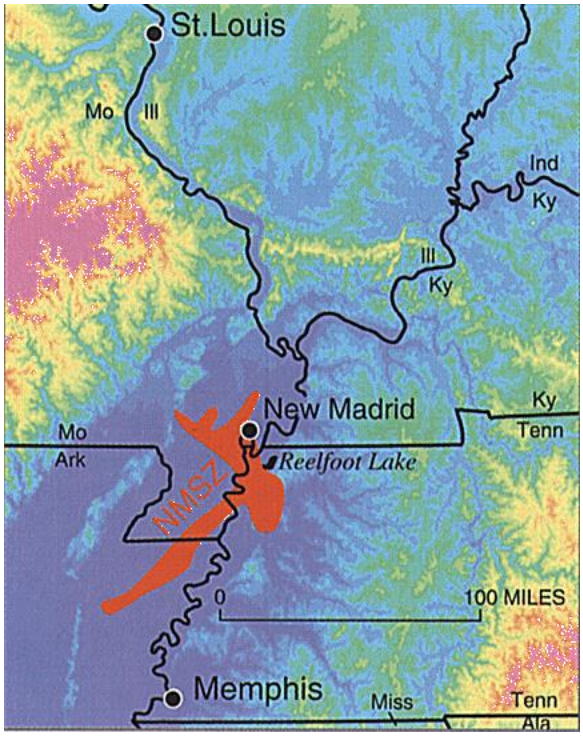

[https://pubs.usgs.gov/fs/1996/0200/]

Fig. 7.15: Location of the New Madrid Fault System.

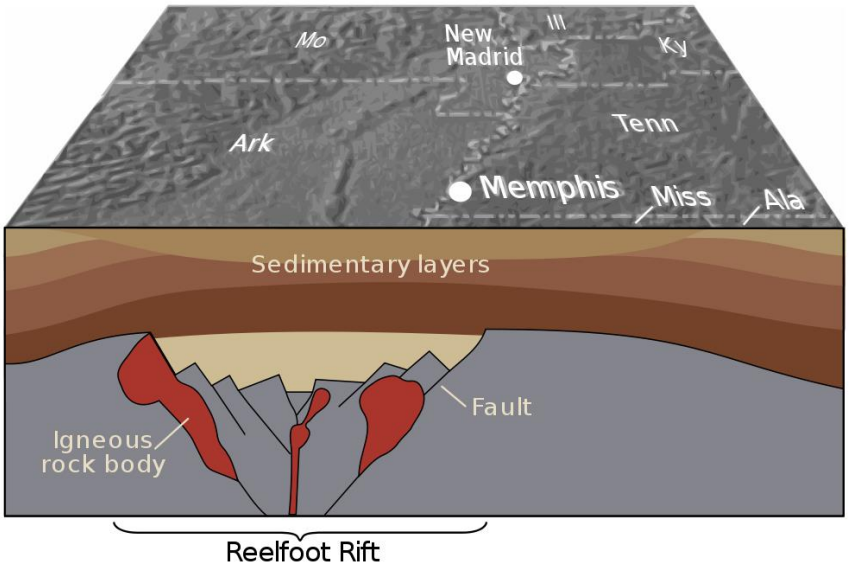

[https://pubs.usgs.gov/fs/1996/0200/]

Fig. 7.16: Schematics of New Madrid fault system, in Central US.

7.4.2. AASHTO (2017)

In the time history method, AASHTO (2017) recommends that the input acceleration have characteristics that are representative of the seismic environment and local site conditions. The following characteristics of the seismic environment in selecting time histories shall be considered: tectonic environment, magnitude, fault type, local site conditions and expected or design ground-motion characteristics. Response-spectrum compatible time histories must be used as developed from representative recorded motions. Where recorded time histories are used, it is necessary to scale the records to match the approximate level of the design response spectrum, using a time domain procedure, for example, as the study developed by Al Atik and Abrahamson (2010). Dominant earthquake information can be obtained from USGS website.

At least three time histories shall be used for each component of motion in representing the design earthquake, and all three orthogonal components (*x*, *y*, and *z*) of design motion shall be input simultaneously. The design actions shall be taken as the maximum response calculated for the three ground motions in each principal direction. If a minimum of seven time histories are used for each component of motion, the design actions may be taken as the mean response calculated for each principal direction.

7.4.2.1. Design Response Spectrum

The design response spectrum given by AASHTO (2017) has the format displayed in Fig. 7.17. The spectrum is calculated using the mapped peak ground acceleration

coefficients and spectral acceleration coefficients available in section 3.10.2, that must be scaled by the zero, short and long-period site factors F_{pga}, F_a, and F_v.

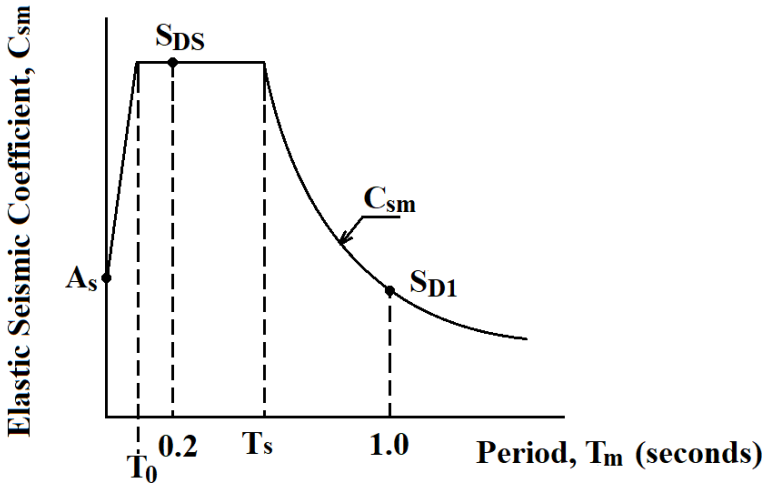

Fig. 7.17: AASHTO (2017) design response spectrum.

For periods smaller than T_0, the elastic seismic coefficient C_{sm} is taken as:

$$C_{sm} = A_s + (S_{DS} - A_S)(T_m / T_0) \tag{7.26}$$

$$A_s = F_{pga} PGA \tag{7.27}$$

$$S_{DS} = F_a S_s \tag{7.28}$$

$$T_s = \frac{S_{D1}}{S_{DS}} \tag{7.29}$$

$$T_0 = 0.2T_s \tag{7.30}$$

Where *PGA* is the peak ground acceleration coefficient on rock (Site Class B), S_s is the horizontal response spectral acceleration coefficient at 0.2-sec period on rock (Site Class B), T_m is the period of vibration of m^{th} mode, T_0 is the reference period used to define spectral shape, T_s is the corner period at which spectrum changes from being independent of period to being inversely proportional to period. For periods greater than or equal to T_0, and less than or equal to T_s:

$$C_{sm} = S_{DS} \tag{7.31}$$

For periods greater than T_s, the elastic seismic coefficient is taken as:

$$C_{sm} = S_{D1}/T_m \tag{7.32}$$

$$S_{D1} = F_v S_1 \tag{7.33}$$

Where S_1 is the horizontal response spectral acceleration coefficient at 1.0-sec period on rock (Site Class B). Based on the hazard maps available in AASHTO (2017) and the cable-stayed bridge location, the following coefficients are obtained:

$PGA = 36$ (%g)

$S_1 = 23$ (%g)

$S_s = 88$ (%g)

In order to determine the zero, short and long-period site factors it is necessary to find in which site class the soil profile falls into. Standard Penetration Test (SPT) blow counts may be used to classify sites from A through F. The simplified soil profile with SPT blow counts for the bridge site is found available in Applegate (2010).

The average SPT blow counts may be determined by as follows:

$$\overline{N} = \frac{\sum_{i=1}^{n} d_i}{\sum_{i=1}^{n} \frac{d_i}{N_i}} \tag{7.34}$$

Where d_i is the layer thickness between 0 and 100ft, and N_i is the SPT blow count of a layer, which may not exceed 100. For the cable-stayed bridge location profile:

$\overline{N} = 14.60 < 15 \rightarrow$ Site Class E

Given the Site Class, the following coefficients are obtained:

$F_{pga} = 1.10$

$F_a = 1.10$

$F_v = 3.00$

With all the coefficients determined, the design spectrum is built as shown in Fig. 7.18

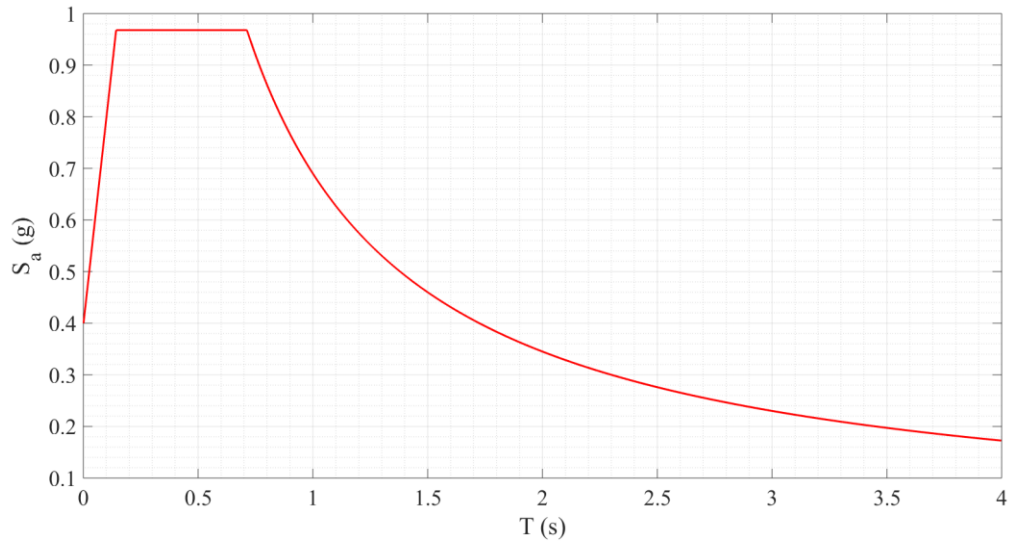

Fig. 7.18: Design Response Spectrum correspondent to the bridge's site.

7.4.2.2. Spectral Matching

Depending on the locality, it is common to have limitations to the recorded data set of time histories. According to AASHTO (2017) commentary, similarities in earthquake magnitudes and distance are especially important parameters because they have an influence on response spectral content, shape, duration, and motion characteristics. Where recorded time histories are used, AASHTO (2017) recommends to modify the records using time-domain response spectrum matching techniques instead of merely scaling the records. Scaling would involve purely multiplying the record by a constant factor to match the design response spectrum over a specific period range. Spectral matching modifies the frequency content of the record to match the design response spectrum for all periods of the spectrum.

It is important to point out though that there are some important debates involving the spectral matching process, although it is the usual approach method recommended in engineering practice. The method matches the entire time series to a design spectrum, so it is commonly argued that the record becomes an envelope for multiple earthquakes. It is supposed that the resultant time series overestimates the structural response. There are also large peaks that arise in the record after the spectral matching process that may be considered unrealistic. One advantage of adopting the method is that each compatible time series can be representative of about three scaled records in terms of variability of the mean of the nonlinear response of structures (Bazzurro and Luco 2006). This results in a reduction of the necessary number of records to be considered in design for a representative result (Al Atik and Abrahamson 2010).

The method developed by Lilhanand and Tseng (1987, 1988) is one of the spectral matching methods recommended by AASHTO (2017). Al Atik and Abrahamson (2010) propose improvements to the aforementioned method to solve some issues related to drift in resulting velocities and displacements time series. This approach is utilized in this study to perform spectral matching of selected time histories. It adjusts the time series in time domain adding wavelets to the initial time series. Although time domain spectral matching methods are more complex than frequency domain ones, they have the advantage of presenting good convergence and in most of the cases preserve the nonstationary character of the reference time series (Al Atik and Abrahamson 2010).

Frequency domain methods have the advantage of easily determining the frequencies present in a signal, but they present no time resolution due to Heisenberg's

Uncertainty Principle. The wavelet analysis is an attempt to overcome this issue by introducing scalable short waves that are shifted along the signal until enough information is obtained regarding its frequency and time content. A wavelet is a wave-shaped oscillation with zero mean. Unlike sinusoids, wavelets exist for finite durations.

The spectral matching method proposed by Al Atik and Abrahamson (2010) uses wavelets to modify the signal in order to make it compatible to the design spectrum, without changing the time of the peak response. Taking $a(t)$ as the initial acceleration time series, it is assumed the method modifies $a(t)$ in a way where its response spectrum matches the target spectrum (design spectrum) across the frequency range while maintaining its time characteristics. The difference between the target spectrum and the time-series spectrum is given by:

$$\Delta R_i = (Q_i - R_i)P_i \tag{7.35}$$

Where Q_i is the target spectral value, R_i is the time series spectral value, and P_i is equal to 1 if the peak response is positive and -1 if the peak response is negative. The objective is to find an adjustment time series $\delta a(t)$ such that the SDOF response from at time t_i is equal to ΔR_i:

$$\delta a(t) = \sum_{j=1}^{N} b_j f_j(t) \tag{7.36}$$

Where $f_j(t)$ is a set of adjustment functions, b_j is a set of amplitude for the adjustment functions and *N* is the number of frequencies to match. The acceleration response of $\delta a(t)$ for a frequency ω_i and damping β_i at time t_i is given by:

$$\delta R_i = \int_0^\infty \delta a(\tau) h_i(t_i - \tau) d\tau \tag{7.37}$$

Substituting in Equation (7.36) leads to:

$$\delta R_i = \sum_{j=1}^{N} b_j \int_0^\infty f_j(t) h_i(t_i - \tau) d\tau \tag{7.38}$$

Where τ is the integration time parameter and $h_i(t)$ is the acceleration impulse response function for a SDOF:

$$h_i(t) = \frac{-\omega_i}{\sqrt{1-\beta_i^2}} e^{(-\omega_i \beta_i t)}[(2\beta_i^2 - 1)\sin(\omega'_i t) - 2\beta_i\sqrt{1-\beta_i^2}\cos(\omega'_i t)] \tag{7.39}$$

$$\omega'_i = \omega_i \sqrt{1-\beta_i^2} \tag{7.40}$$

$$h_i(t) = 0 \text{ for } t < 0 \tag{7.41}$$

Defining c_{ij} as the response at time t_i for the i^{th} frequency and damping resulting from the adjustment function:

$$c_{ij} = \int_0^{t_i} f_j(\tau) h_i(t_i - \tau) d\tau \tag{7.42}$$

And substituting into Equation (7.38):

$$\delta R_i = \sum_{j=1}^{N} b_j c_{ij} \tag{7.43}$$

And since the response of the adjustment time series δR_i is the spectral misfit:

$$\Delta R_i = \sum_{j=1}^{N} b_j c_{ij} \tag{7.44}$$

The amplitude of each wavelet can be determined by:

$$\mathbf{b} = \mathbf{C}^{-1}\boldsymbol{\delta}\mathbf{R} \tag{7.45}$$

Where **C** is a square matrix with elements describing the amplitude of each SDOF response at the time the response needs to be adjusted, under the action of each wavelet. Given b_j, the adjustment time series for the first iteration is given by:

$$a_1(t) = a(t) + \gamma \delta a(t) \tag{7.46}$$

Where γ is a relaxation parameter (between 0 and 10) to damp the adjustments. In the second iteration, the algorithm is repeated using the adjusted time series in place of

$a_1(t)$. The iterations are continued until the desired accuracy is obtained (Al Atik and Abrahamson 2010). The improved tapered cosine wavelet proposed by Al Atik and Abrahamson (2010) is described by:

$$f_j(t) = \cos[\omega'_j(t - t_j + \Delta t_j)]\exp\left[-\left(\frac{t - t_j + \Delta t_j}{\gamma_j}\right)^2\right] \tag{7.47}$$

Where γ_j is a frequency dependent coefficient given by:

$$\gamma(f) = 1.178 f^{-0.93} \tag{7.48}$$

A flow chart with the detailed procedure for programming purposes can be found in Hancock et al. (2006), and more details regarding the spectral matching method described in this section can be found in Al Atik and Abrahamson (2010).

7.4.2.3. Earthquake Records for Central US

A set of 11 significant accelerations time histories that were recorded at stations near the bridge's location are selected and spectral-matched to AASHTO (2017) design response spectrum. The records are described in Table 7.4 and may be found in PEER Ground Motion Database (2013). The acceleration time-histories response spectra after spectral matching are displayed in Fig. 7.19.

Table 7.4: Earthquake records selected from PEER Ground Motion Database.

Event Name	Year	Station/ Location	Magnitude
Sullivan	2011	Carbondale, IL	5.89
Mineral	2011	Carbondale, IL	5.74
Sparks	2011	Carbondale, IL	5.68
Comal	2011	Carbondale, IL	4.71
Prairie Center	2004	Henderson Mound, MO	4.18
Shady Grove	2005	Henderson Mound, MO	4.25
Mt Carmel	2008	Henderson Mound, MO	4.64
Greenbrier	2011	Henderson Mound, MO	4.68
Kipawa	2000	Carbondale, IL	4.62
Au Sable Forks	2002	Carbondale, IL	4.99
Val de Bois	2010	Carbondale, IL	5.10

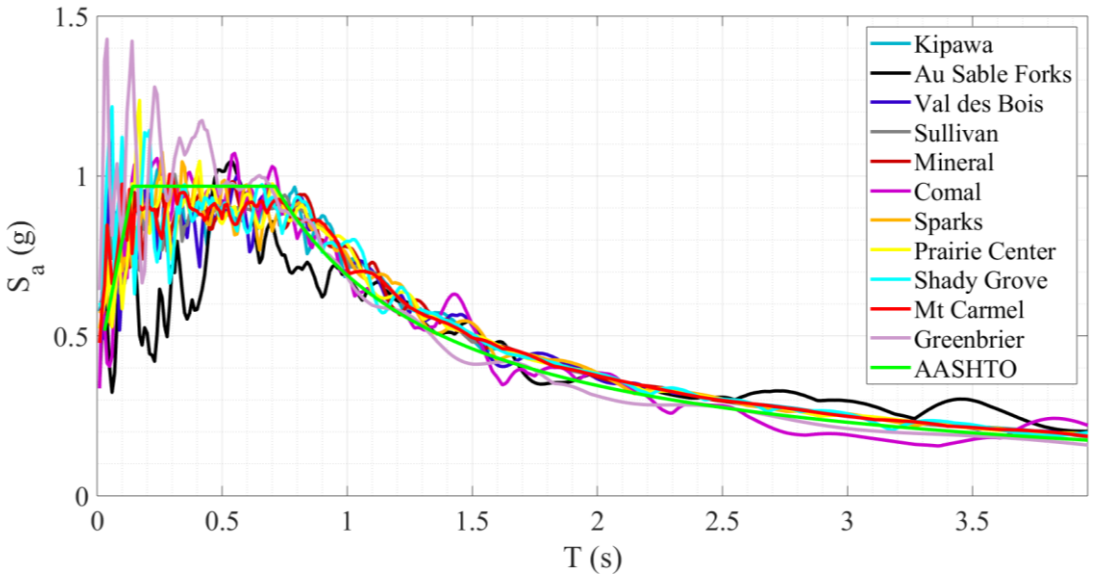

Fig. 7.19: Acceleration Response Spectra for the selected records after spectral matching.

7.4.3. Results and Discussion

In this section are presented and discussed the results obtained after the bridge is subjected to the spectral-matched earthquakes considering site conditions. The control schemes considered are MR dampers behaving as fully passive devices; passive-on and passive-off; nonadaptive semi-active control with resettable devices, adaptive semi-active control with SAC and MR dampers (refer to section 7.1.1), and adaptive semi-active control with neuro-fuzzy control and MR dampers (refer to section 7.1.2). Three parametric scenarios are taken into consideration: nominal structure, bridge with 5% mass increase, and 20% stiffness reduction.

Table 7.5 gives the maximum value obtained for the performance criteria. Table 7.6 gives the standard deviation obtained for the performance criteria among the parametric scenarios analyzed and earthquakes considered. Fig. 7.20 displays the maximum J_1 (peak deck shear) for the control schemes considering different parametric scenarios and earthquake excitations. Fig. 7.21 displays the maximum J_5 (peak cable tension) for the control schemes considering different parametric scenarios and earthquake excitations.

Fig. 7.22 displays the maximum J_7 (normed base shear) for the control schemes considering different parametric scenarios and earthquake excitations. Fig. 7.23 displays the maximum J_{10} (normed deck moment) for the control schemes considering different parametric scenarios and earthquake excitations. Fig. 7.24 displays the maximum J_{11} (normed cable tension) for the control schemes considering different parametric scenarios and earthquake excitations. Fig. 7.25 gives the midspan longitudinal displacements due to

earthquake Kipawa, for all the control schemes considered. Fig. 7.26 gives the midspan longitudinal displacements due to earthquake Mt Carmel, for all the control schemes considered. The supplemental and detailed results in terms of the performance criteria obtained for all earthquake records, control schemes, and parametric variation scenarios are given in Appendix B.

Table 7.5: Maximum values for all the performance criteria for the different control schemes, considering all the parametric scenarios and earthquake records.

Maximum Performance Criteria						
Value	Dir.	Passive-on	Passive-off	Resettable	SAC	Neuro-Fuzzy
J_1	x	1.0380	1.0500	1.1382	1.0030	1.0671
J_2	x	0.9552	1.3026	1.0094	1.0413	0.9265
J_3	x	1.0380	1.0500	1.1382	1.0030	1.0671
J_4	x	1.3383	1.2639	1.4436	1.0980	1.2030
J_5	-	0.4080	0.3318	0.3189	0.3092	0.3344
J_6	x	0.0445	0.0655	0.0485	0.0458	0.0514
J_7	x	1.4126	0.9448	0.8819	1.1513	1.0792
J_8	x	0.7572	0.9954	0.6435	0.5972	0.6377
J_9	x	1.4126	0.9448	0.8819	1.1513	1.0792
J_{10}	x	0.6871	0.9609	0.6570	0.5810	0.6631
J_{11}	-	0.0858	0.0481	0.0450	0.0622	0.0564
J_{12}	x	0.0020	0.0004	0.0020	0.0020	0.0020
J_{14}	-	0.0020	0.0002	0.0010	0.0014	0.0012
J_{16}	-	24	24	24	24	24
J_{17}	-	0	0	13	13	26
Max		1.413	1.264	1.444	1.151	1.203
Average		0.653	0.601	0.551	0.546	0.561

Table 7.6: Standard deviation among the performance criteria for the different control schemes, considering all the parametric scenarios and earthquake records.

Standard Deviation						
Value	Dir.	Passive-on	Passive-off	Resettable	SAC	Neuro-Fuzzy
J_1	x	0.1780	0.0666	0.1614	0.1459	0.1649
J_2	x	0.1660	0.1837	0.1924	0.1783	0.1860
J_3	x	0.1780	0.0666	0.1614	0.1459	0.1649
J_4	x	0.2130	0.1460	0.2088	0.2053	0.2298
J_5	-	0.0625	0.0251	0.0503	0.0544	0.0635
J_6	x	0.0093	0.0093	0.0086	0.0088	0.0109
J_7	x	0.3480	0.0929	0.1554	0.2310	0.2279
J_8	x	0.1295	0.1025	0.1081	0.1003	0.1310
J_9	x	0.3480	0.0929	0.1554	0.2310	0.2279
J_{10}	x	0.1393	0.0996	0.1171	0.1157	0.1533
J_{11}	-	0.0226	0.0050	0.0087	0.0141	0.0132
Max		0.348	0.184	0.209	0.231	0.230
Average		0.163	0.081	0.121	0.130	0.143

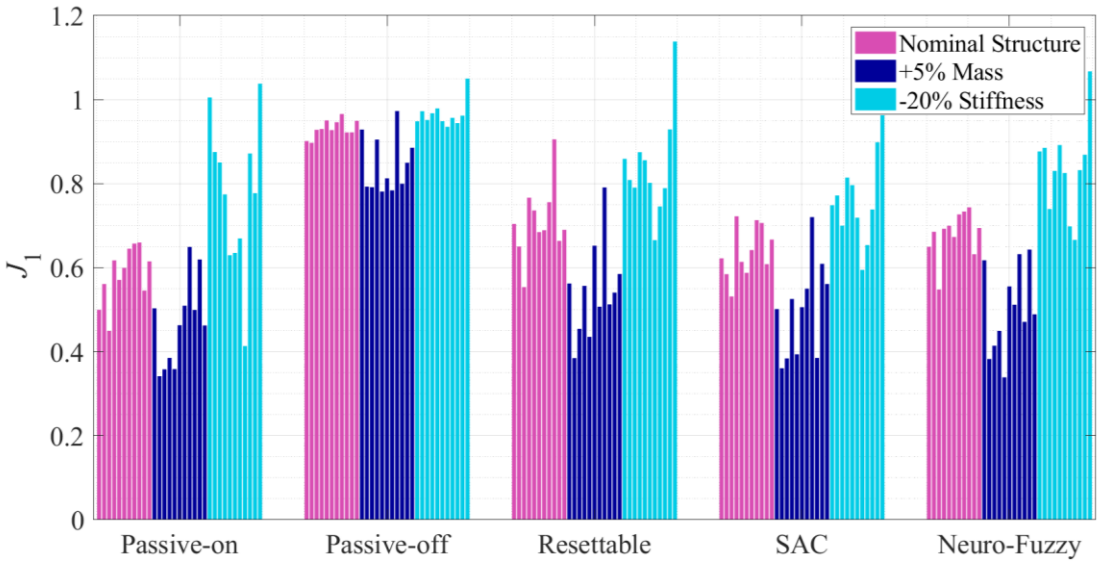

Fig. 7.20. Maximum J_1 (peak base shear) for different spectral-matched earthquakes, considering different parametric scenarios.

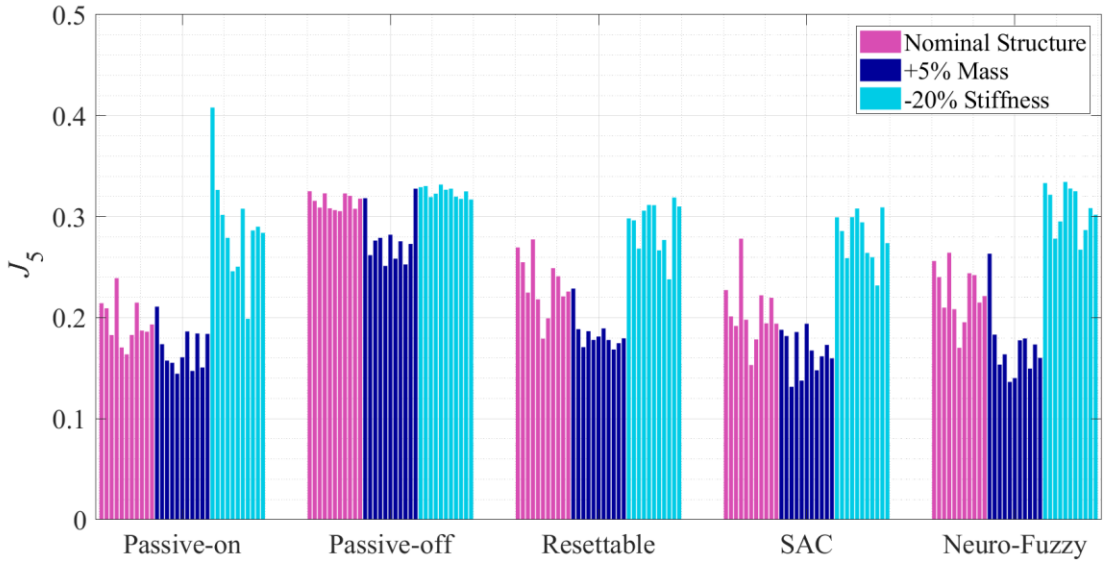

Fig. 7.21. Maximum J_5 (peak cable tension) for different spectral-matched earthquakes, considering different parametric scenarios.

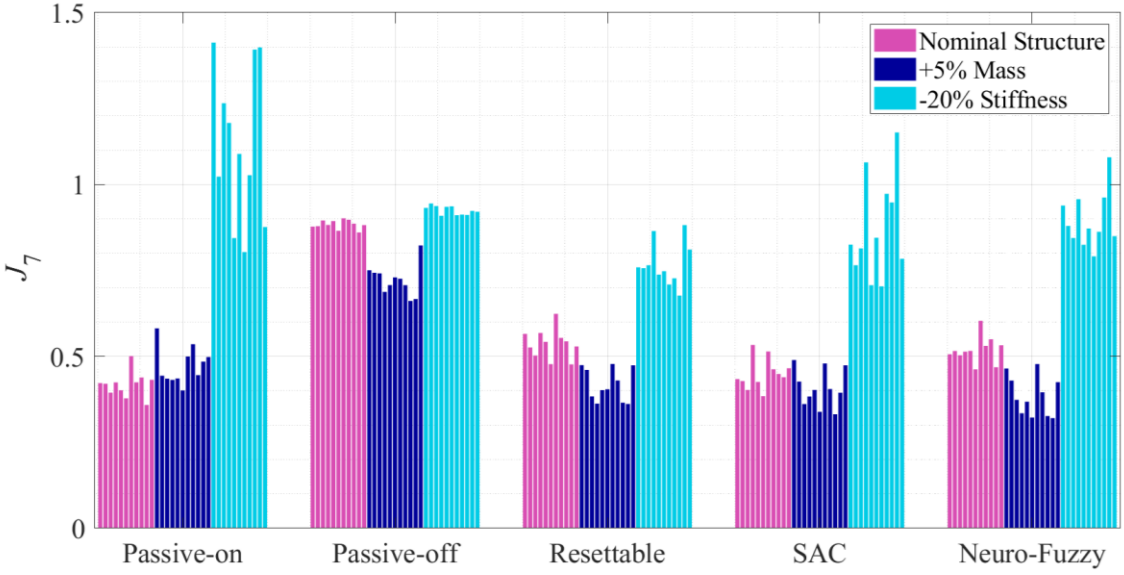

Fig. 7.22. Maximum J_7 (normed base shear) for different spectral-matched earthquakes, considering different parametric scenarios.

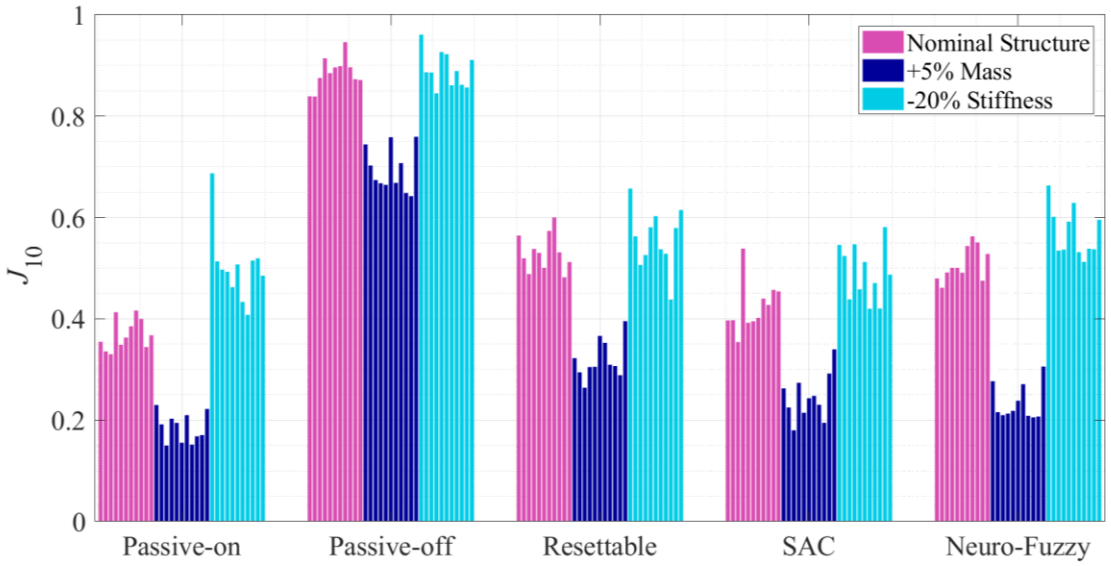

Fig. 7.23. Maximum J_{10} (normed deck moment) for different spectral-matched earthquakes, considering different parametric scenarios.

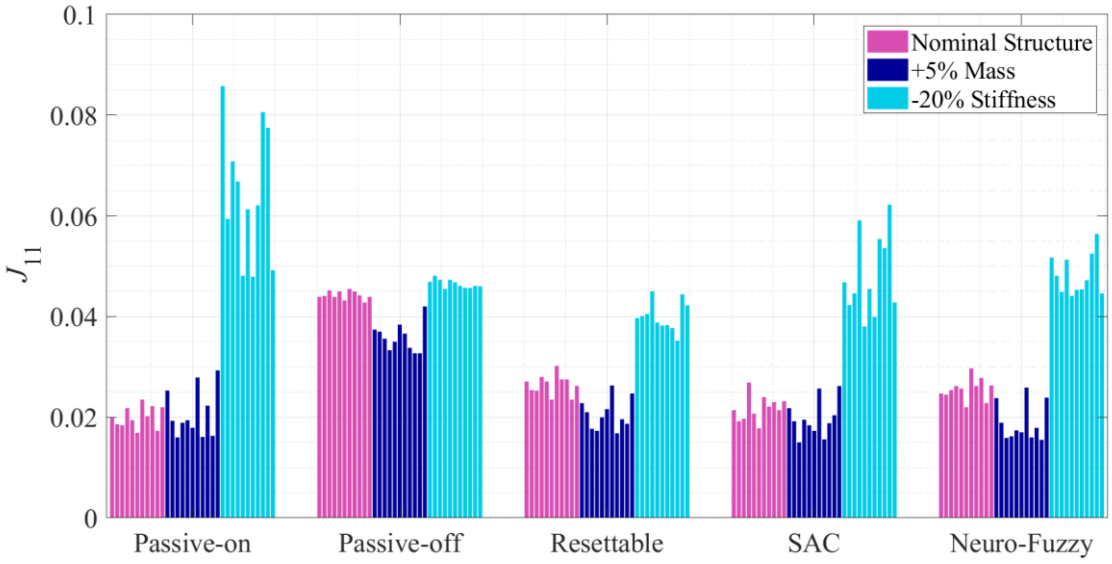

Fig. 7.24. Maximum J_{11} (normed cable tension) for different spectral-matched earthquakes, considering different parametric scenarios.

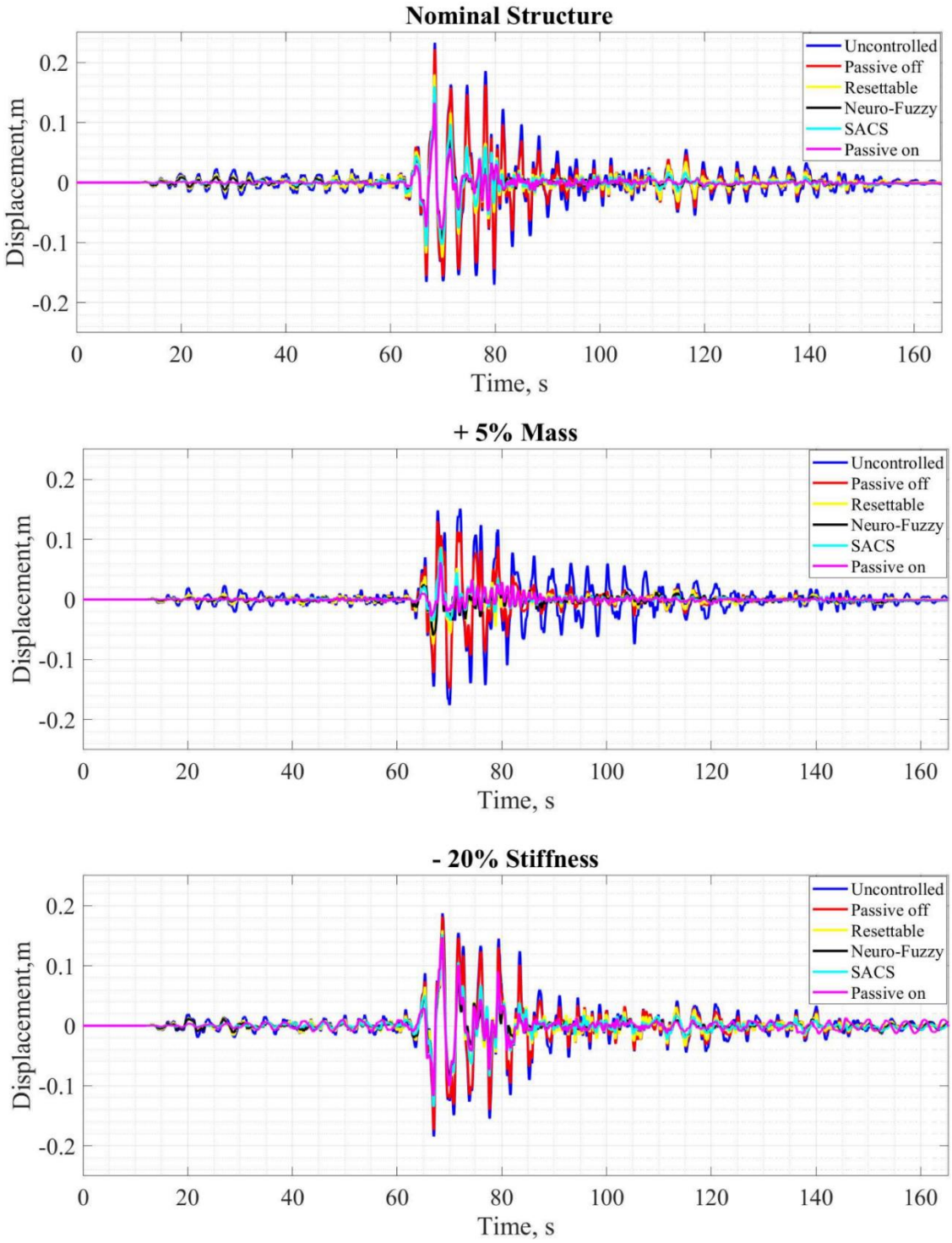

Fig. 7.25. Midspan displacement considering different parametric scenarios for earthquake Kipawa.

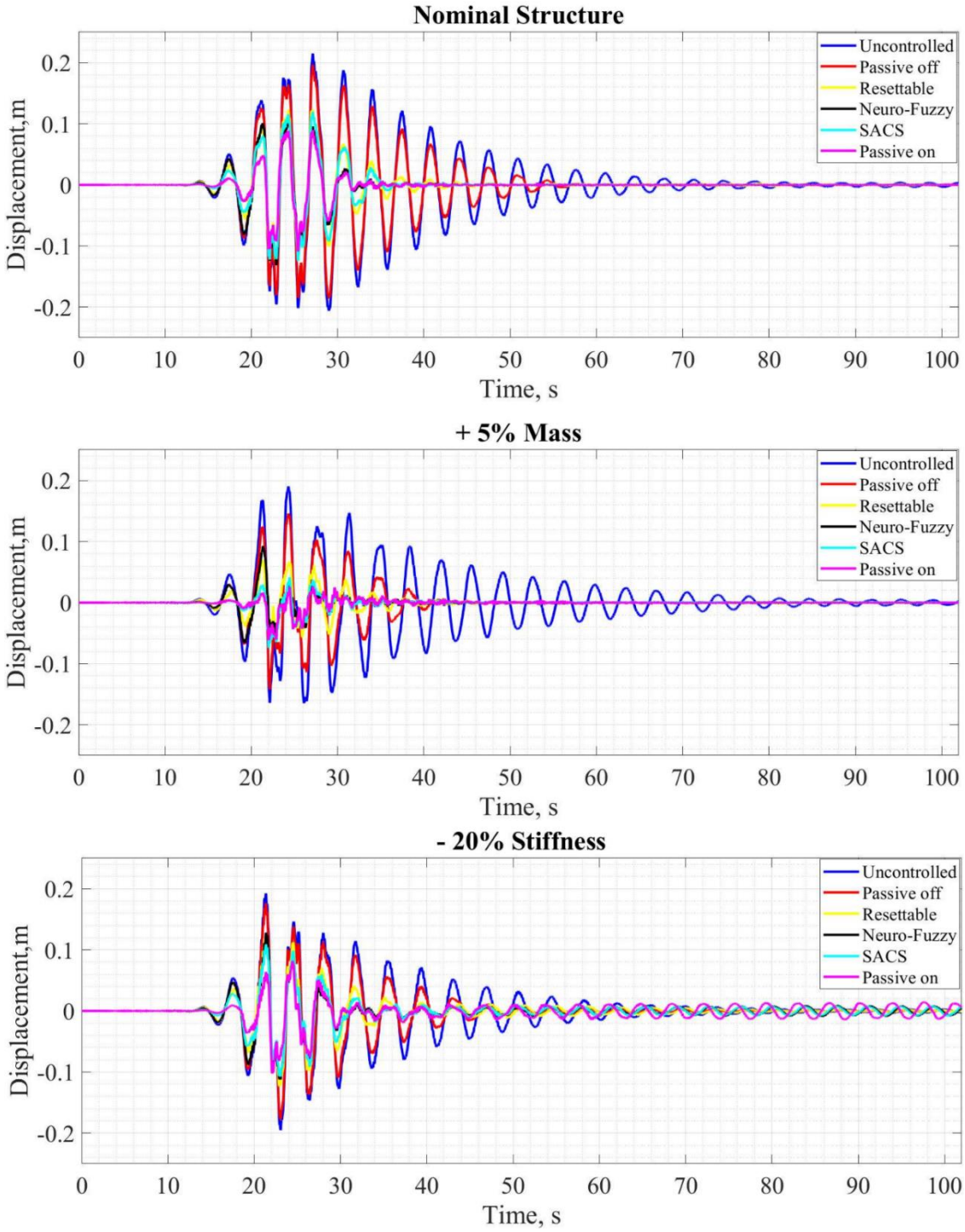

Fig. 7.26. Midspan displacement considering different parametric scenarios for earthquake Mt Carmel.

In order to understand and interpret further the results, probability density functions (PDF) are obtained for each control scheme considering the performance criteria. The normal distribution fitting of a curve can be justified by the Central Limit theorem, which states that the sum of independent samples from any distribution with a certain mean and variance tends to the normal distribution for an infinity sized sample. Ina simplified explanation, it can be state that probability density functions provide a relative likelihood that the value of a random variable equals a certain value. Considering σ is the standard deviation and μ is the mean:

$$y = \frac{1}{\sigma\sqrt{2\pi}} e^{-\frac{(x-\mu)^2}{2\sigma^2}}, \text{ for } x \in \mathbb{R} \tag{7.49}$$

Fig. 7.27 gives the probability density function for passive-on, passive-off, semi-active resettable, SAC and neuro-fuzzy schemes in terms of peak base shear (J_1). Fig. 7.28 gives the probability density function for passive-on, passive-off, semi-active resettable, SAC and neuro-fuzzy schemes in terms of peak cable tension (J_5). Fig. 7.29 gives the probability density function for passive-on, passive-off, semi-active resettable, SAC and neuro-fuzzy schemes in terms of normed base shear (J_7). Fig. 7.30 gives the cumulative probability density function for passive-on, passive-off, semi-active resettable, SAC and neuro-fuzzy schemes in terms of normed deck moment (J_{10}). Fig. 7.31 gives the cumulative probability density function for passive-on, passive-off, semi-active resettable, SAC and neuro-fuzzy schemes in terms of normed cable tension (J_{11}).

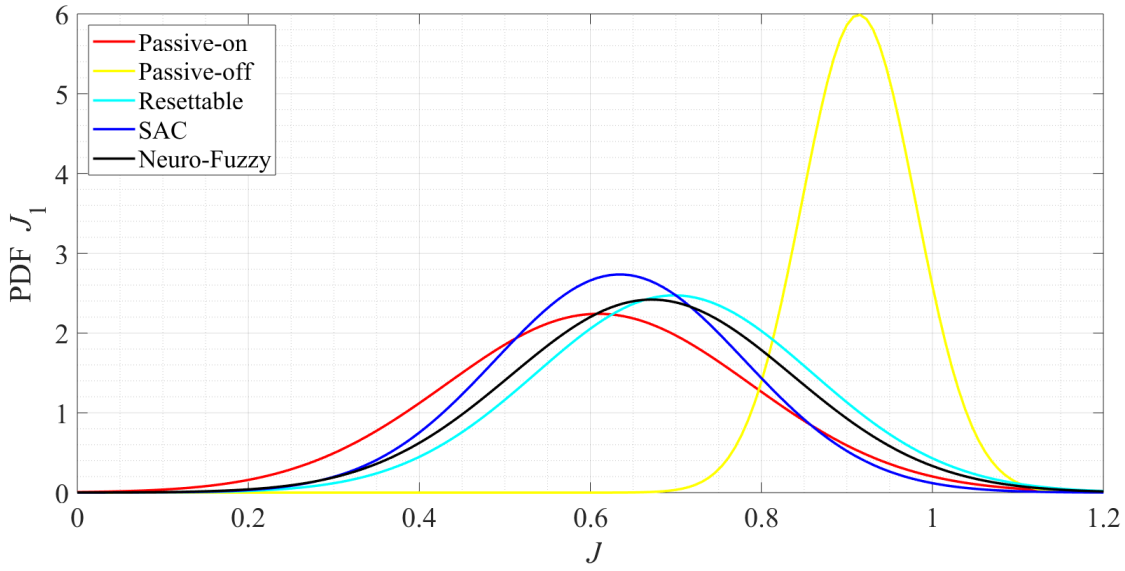

Fig. 7.27. Cumulative probability density function for all the control schemes- peak base shear criteria (J_1).

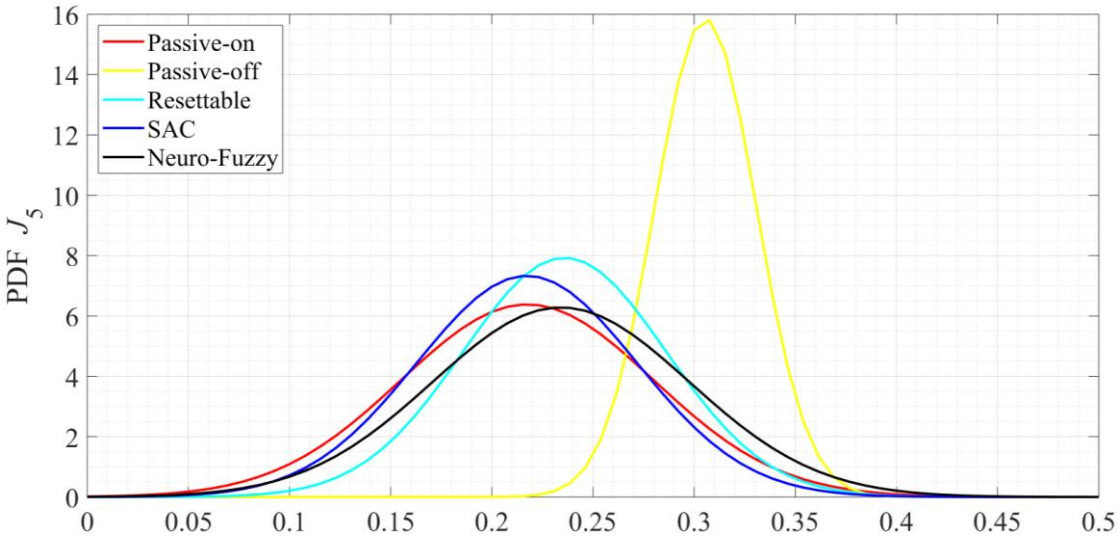

Fig. 7.28. Cumulative probability density function for all the control schemes- peak cable tension criteria (J_5).

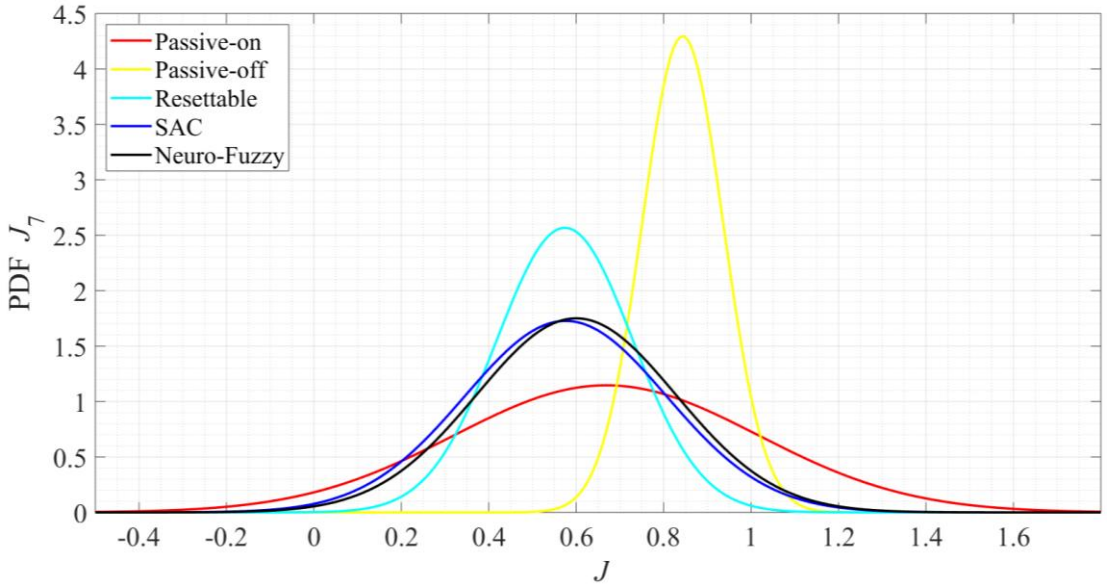

Fig. 7.29. Cumulative probability density function for all the control schemes- normed base shear criteria (J_7).

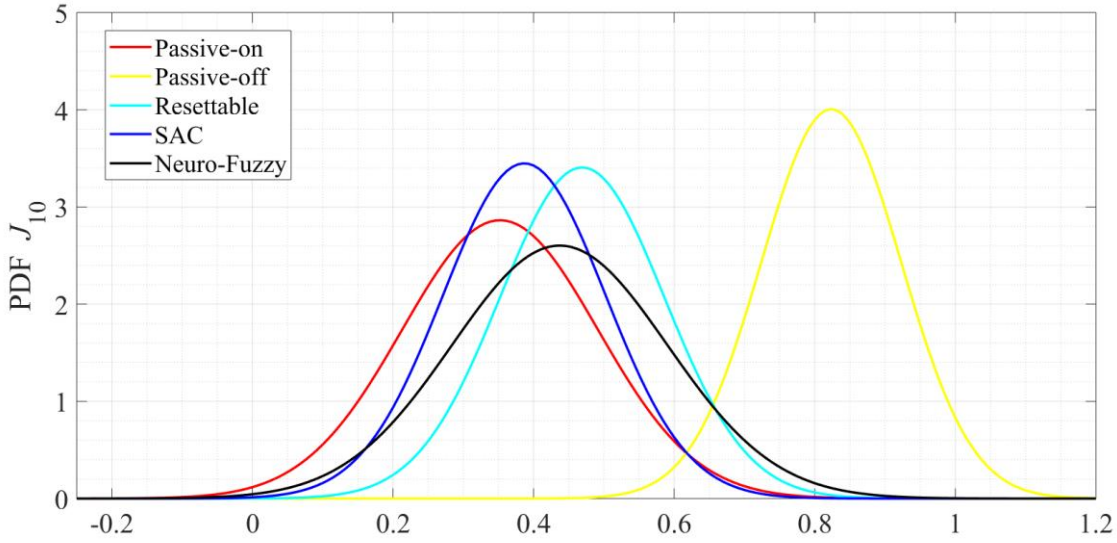

Fig. 7.30. Cumulative density probability density function for all the control schemes- normed deck moment criteria (J_{10}).

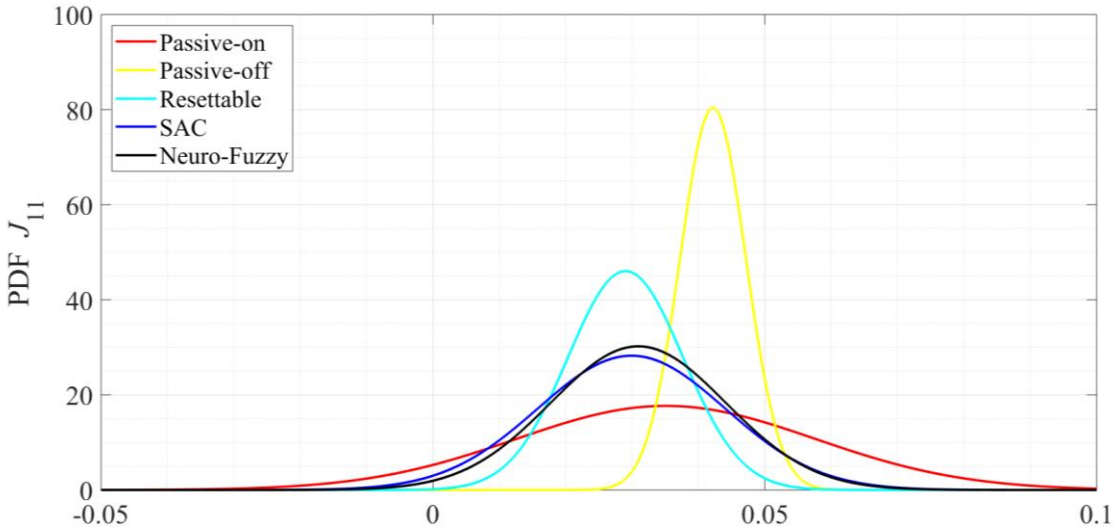

Fig. 7.31. Cumulative density probability density function for all the control schemes-normed cable tension criteria (J_{11}).

For the set of earthquakes representative of the Central US site, the bridge controlled by the passive-on case presents a satisfactory performance for the nominal structure, similarly to what is observed for the benchmark earthquakes. However, once the parameters are changed, the performance of the control scheme deteriorates. The scheme presents the maximum values for performance criteria related to peak cable tension, normed base shear, normed base moment and normed cable tension (J_5, J_7, J_9, J_{11}). The control scheme shows to be susceptible to parametric variations and not able to sustain overall performance when the parameters are changed. The scheme presents the greatest standard deviation for performance criteria related to peak base shear, peak base moment, normed base shear, normed base moment and normed cable tension (J_1, J_3, J_7, J_9, J_{11}). The passive-off scheme sustains performance well and it gives the least standard deviation for peak base shear, peak deck moment, normed base shear, normed base moment, normed

deck moment and normed cable tension (J_1, J_4, J_7, J_9, J_{10}, J_{11}). However, the control scheme does not reduce overall responses significantly. The scheme presents the maximum values for performance criteria related to peak deck shear, abutment displacements, normed deck shear and normed deck moment (J_2, J_6, J_8, J_{10}).

The semi-active neuro-fuzzy control displays enhanced performance when compared to the passive-off case and for peak response in comparison to the resettable scheme. The scheme, however, presents greater standard deviation values for many performance criteria, such as peak deck moment, peak cable tension, abutment displacements, normed deck shear and normed base moment (J_4, J_5, J_6, J_8, J_9). The scheme is especially effective in reducing abutments and midspan displacements for all the parametric variations considered. As aforementioned, the performance of the controller may be further improved by changing the membership functions shape and quantity or by considering acceleration feedback instead of velocity/displacement. The semi-active resettable devices give an overall successful reduction in normed responses and sustains performance well for most criteria. The scheme provides the best performance for reduction in normed base shear, normed base moment and normed cable tension (J_7, J_9, J_{11}). However, presents the maximum values for performance criteria related to peak base shear, peak base moment and peak deck moment (J_1, J_3, J_4). The scheme sustains performance well in particular when considering normed responses. The scheme is the control solution that provides the least average variation. The semi-active adaptive control scheme controlled by SAC gives an overall successful reduction in both peak and normed responses and sustains performance for most criteria. The scheme provides the best

performance for reduction in peak base shear, peak base moment, peak deck moment, cable tension, normed deck shear and normed deck moment (J_1, J_3, J_4, J_5, J_8, J_{10}). The scheme sustains performance well in for most peak and normed responses.

The passive schemes have the advantage of not requiring sensors, but again they cannot provide guaranteed robustness and have the potential to worsen the performance of the bridge. Among the semi-active approaches, SAC and resettable allows for the least number of sensors. The neuro-fuzzy control requires velocity and displacement feedback to present smaller training errors, which leads to a greater amount of sensors. In terms of peak control force, the semi-active control and the passive-on schemes reached the maximum capacity of the devices of 1000kN. The passive-off case, therefore gives the least maximum control force, since it is the only case where the device is not reaching its maximum capacity. This can explain why the control solution provides limited performance when it comes to mitigation of excessive seismic induced responses. The scheme that requires the maximum effort is the passive-on, followed by SAC, neuro-fuzzy, resettable and passive-off. Achieving the required control effort is not a problem provided the approach adopted is semi-active, which is operated with low power requirements and is essentially resistive.

8. CONCLUSIONS AND FUTURE WORK

In this research, adaptive control is presented as an alternative to control bridge structures, given adaptive schemes' ability to calculate control gains that vary over time based on sensed responses and sustain performance in face of parametric variations. Parametric variations occur throughout bridges service life as a result of temperature variations, cracking, localized damage and fatigue. Existing bridges parameters are difficult to estimate precisely, which can lead to control schemes performing unsatisfactorily depending on how sensitive they are to parametric changes. The goal of this research is to develop, implement, design and assess adaptive control schemes to mitigate excessive response of bridges under varying parametric conditions.

The main objectives of this research are to develop adaptive control schemes based on the concepts of the simple adaptive control and the neural-fuzzy control, and investigate their effectiveness in reducing excessive dynamic responses of bridge structures; implement, design and evaluate the performance of the developed control in face to parametric changes whilst considering different types of structural configurations and realistic operation conditions; investigate the importance and sensitivity of structural modeling considerations for control design and implementation on bridge structures.

In sections 1, 2 and 3 are presented the introduction, background, motivation, significance, objectives and overview of the research. In section 4, bridges dynamic analysis, structural characterization and modeling assumptions are presented and discussed. Model reduction techniques are presented, implemented and validated for the

cable-stayed bridge. These structures are generally substantial in size and structurally complex, and as a consequence many simplifications are necessary to guarantee the analyses are computationally feasible. Excessively complex models and calculations demand computation capacities that may surpass what would be cost-effective, as it would require massive computational and human resources to process and interpret a considerably large amount of data. Section 5 discusses and presents the theory necessary for the development of structural control where the theoretical basis for implementation and design of the control strategies and design considered in this research are presented and discussed.

In section 6, adaptive control approaches are developed to control two different highway bridges. In section 6.1, it is conducted an initial investigation where the control scheme is implemented and designed aiming to mitigate seismic responses of a three-span highway bridge considering realistic implementation. The main control strategy implemented in this portion of the research is based in the SAC algorithm. There are sensors measuring displacements at both abutments and 4 control devices acting in the transverse direction are attached to each bridge ends and abutments, totalizing 8 devices. The model reference is taken as the bridge considering parameters from the nominal structure with a 50% reduction in displacements. To guarantee performance, the gains of the controller are tuned considering ideal active devices, with no saturation of control forces. Then, hydraulic actuators and MR dampers are considered as devices controlled by SAC. The bridge is subjected to a set of three significant historical earthquake records, and the performance of the controller is compared to the performance of passive devices.

The robustness of the control scheme is assessed by implementing 20% stiffness reduction to both piers. Observation of the results obtained in the analysis leads to the conclusion that the adaptive strategy is successful in mitigation of seismic responses. Additionally, the adaptive technique is the least affected by the reduction in stiffness when compared to the non-adaptive.

Following the initial investigation, a parametric study is conducted in section (6.2) considering a two-span skewed highway bridge. An adaptive control scheme is developed, designed and implemented to provide control command for MR dampers and hydraulic actuators installed at the bridge ends. The scheme is assessed by subjecting the bridge to set of 11 earthquakes, while stiffness and mass parameters are varied systematically. Both mass and stiffness values are varied systematically in order to map how the proposed control approach sustains performance. The performance of the adaptive semi-active control scheme is compared to non-adaptive passive control and optimal control, taking into account the effects of noise and device dynamics. In the proposed scheme, a reduced order model reference is considered. The possibility of taking a model reference of lower order than the actual structure is one of the advantages of implementing SAC algorithm for large structures. In the model reference chosen for this parametric study, selected nodes are set to have zero displacements. This model reference leads the controller to induce the bridge to a stationary position as fast as possible in the occurrence of a major extreme event.

A total of 16 control devices are placed between abutments and the bridge's deck controlling the transverse and longitudinal direction (8 at each bridge end). The main

devices considered are MR dampers and hydraulic actuators. MR dampers working with no external power (passive-off) and with constant maximum external power (passive-on) are also considered. A total of 10 sensors measuring displacements are considered for the SAC scheme. A LQR+LQE operating with 10 sensors is examined in this study for comparison purposes. As the total of 10 sensors measuring displacements, leads to a non-observable system which indicates that the estimator reconstruction of the states is not accurate. An observable system composed of LQR+LQE operating with a total of 41 sensors measuring displacements is also considered. White noise is introduced to the measured outputs given that such measurements are likely to be imperfect.

The hydraulic actuator introduces unwanted behavior with both control algorithms (SAC and LQR) for many parametric scenarios cases as well in terms of all performance criteria. The accelerations are particularly worsened by LQR. This behavior can be attributed to the dynamic force control present in the actuator model, since they are usually mechanically stiff systems. The stiff columns make the force control very sensitive to parameters, especially when there is force tracking over a considerable bandwidth (Sivaselvan et al. 2008). Added compliance is suggested in Sivaselvan et al. (2008) to deal with this issue. Another potential reason for the worsening of responses by the actuation system is the force saturation imposed to the devices. However, when it comes to civil structures, the energy requirements present in the actuation system indicate that large batteries are necessary to guarantee operational conditions, complicating the implementation of this control solution. The results indicate that semi-active control is a more suitable alternative when controlling large structures subjected to extreme events

that have significant control placement constraints and are expected to experience parametric variations or which parameters are difficult to predict. Passive schemes do not sustain performance and for some cases increase midspan responses significantly. The optimal semi-active scheme reduces overall displacements; however, the scheme requires a considerable amount of sensors to perform satisfactorily and increases accelerations. The proposed adaptive controller with SAC holds performance well in face of parametric changes, reduces overall seismic response and allows the adoption of a small amount of sensors.

In section 7, semi-active adaptive control schemes are proposed to control a cable-stayed bridge considering parametric variations. The main objective of the control approach is to mitigate excessive response due to seismic excitations while providing a guaranteed level of robustness when in face of parametric variations. Model reduction is performed following section 4 considerations. For the semi-active SAC scheme, the model reference is taken as the bridge controlled by LQR optimal control considering full-feedback and ideal actuators with no saturation. A reduced order model reference is considered. For the semi-active neuro-fuzzy adaptive scheme, the target controller considers also the bridge as controlled by optimal LQR with full feedback scheme. The input for the neuro-fuzzy control utilized for training are the displacements and velocities from the same nodes monitored by SAC. Seven triangular-shaped membership functions are defined. After the initial FIS and the target controller input and output are obtained, the fuzzy scheme parameters are adjusted by neural-networks.

Initially, the two adaptive schemes are implemented to control the cable-stayed bridge for a set of three major earthquakes, considering multi-support excitations and different angles of incidence. The controllers' performance is compared to non-adaptive control schemes, before and after two parametric variations are introduced to the structure. The semi-active resettable devices give an overall successful reduction in responses and sustains performance better than the passive schemes. The scheme, however, is outperformed by SAC for most performance criteria evaluated. Neuro-fuzzy semi-active scheme is outperformed by the resettable scheme for some of the criteria evaluated. However, it shows enhanced performance when compared to the passive-off case and the scheme holds performance better than the passive-on scheme. Additionally, the scheme is considerably effective in reducing abutments and midspan displacements for all the parametric variations considered. The performance of the neuro-fuzzy controller may be further improved by changing the parameters of the control scheme and feedback conditions in order to improve its adaptability and consequently its robustness, and the resettable scheme does not have this advantage. The semi-active adaptive control scheme controlled by SAC provide the best overall performance and least average variation.

Lastly, earthquakes matched to the site design spectra following AASHTO (2017) provisions are introduced to the cable-stayed bridge. The adaptive methods are again compared to non-adaptive schemes before and after two parametric variations are considered. For the set of earthquakes representative of the Central US site, the bridge controlled by the passive-on case presents a satisfactory performance for the nominal structure, similarly to what is observed for the benchmark earthquakes. However, once the

parameters are changed, the performance of the control scheme deteriorates. The control scheme shows to be susceptible to parametric variations and not able to sustain overall performance when the parameters are changed. The passive-off scheme sustains performance well; however, the control scheme does not reduce overall responses significantly. The neuro-fuzzy semi- control displays enhanced performance in comparison to the passive-off case and for peak response in comparison to the resettable scheme, especially when it comes to reducing abutments and midspan displacements. The scheme, however, presents greater standard deviation values for many performance criteria and does not hold performance as desired. The performance of the controller may be further improved by changing the membership functions shape and quantity, or by considering acceleration feedback instead of velocity/displacement. The semi-active adaptive control scheme controlled by SAC gives an overall successful reduction in both peak and normed responses, sustaining performance for most criteria. The scheme sustains performance well considering both peak and normed responses. It is advisable that the strategy is implemented along with semi-active devices, which are reactive devices and can be operated with small batteries. Implementation of SAC with active devices would require massive amounts of power to operate.

Passive control has the potential to introduce unwanted behavior and lead the controlled structure to perform worse than the uncontrolled. This is a reality especially for control of bridges, where control placement constraints are common and the introduced damping is not uniform. Implementation of a controller that does not present enough robustness/dependability requires complex instrumentation and model identification of

the existing structure, to guarantee the control strategy remains effective. The adaptive schemes that are proposed in this research come as a viable alternative solution to this problem and provide bridge control the necessary robustness. The implementation of a control approach that is cost effective, dependable, predictable and effective may lead to the possibility of accounting for this control solution in design, allowing for more flexible but safe structures. Additionally, a control approach that is dependable and robust has the potential to guarantee performance limits and impact how structures are designed in the future. It can be concluded from the investigations performed in this research, that the developed adaptive control approaches are suitable to control large bridge structures and guarantee performance considering parametric variations and realistic operational conditions. The approaches allow for a reduced quantity of sensors, which is cost-effective and less complicated to build. Additionally, they performed well for earthquakes with different characteristics, frequency content, and when in the presence measuring of noise.

For future work it is recommended the investigation of efficient ways to automate the model reference choice for SAC. This step shows to be especially challenging for large-sized structural configurations. The size of the model turns the monitoring of the nodes and trial and error design of gains particularly difficult. Automation of this process would facilitate greatly the determination of the controller parameters. It is also recommended to revisit the training process for the neuro-fuzzy based scheme. The control approach ended up being susceptible to the variation of earthquake record shapes and parameters. As aforementioned, the performance of the controller may be further improved by changing membership functions shape and quantity or by considering

acceleration feedback instead of velocity/displacement. Future studies may consider the influence of material nonlinearities and soil-structure interaction in the adaptive control of bridge structures. In this work, the damping is assumed to remain the same throughout all the parametric variation scenarios. As a suggestion for future work, damping variation and adaptive control robustness when in face of damping variation can also be considered. Adaptive strategies as a solution to mitigate wind induced vibrations may also be explored, as well as experimental validation. A reliability analysis of the control schemes would be of great value to bridge designers, as would random variation of structural parameters.

REFERENCES

Agrawal, A., Tan, P., Nagarajaiah, S., and Zhang, J. (2009). "Benchmark structural control problem for a seismically excited highway bridge-Part I: Phase I Problem definition." *Structural control & health monitoring* (16):509–529.

Al Atik, L., and Abrahamson, N. (2010). "An improved method for nonstationary spectral matching." *Earthquake Spectra* 26 (3):601-617.

American Association of State Highway and Transportation Officials, AASHTO. (2017). *Bridge Design Specifications- LRFD*. Eighth ed. Washington, D.C.

Applegate, K. N. (2010). *Evaluation of liquefaction-induced lateral spreading in the midwest*. M.S. in Civil Engineering Thesis, Civil, Architectural and Environmental Engineering, Missouri University of Science and Technology.

Arnold, W. F. , and Laub, A. J. (1984). "Generalized eigenproblem algorithms and software for algebraic Riccati equations." *Proceedings of the IEEE* 72 (12):1746-1754.

Barkana, I. (1987). "Parallel feedforward and simplified adaptive control." *International Journal of Adaptive Control and Signal Processing* 1 (2):95-109.

Barkana, I. (2005). "Gain conditions and convergence of simple adaptive control." *International Journal of Adaptive Control and Signal Processing* 19 (1):13-40.

Barkana, I. (2008). "A modified invariance principle and gain convergence in adaptive control." *IEEE 25th Convention of Electrical and Electronics Engineers in Israel*, Eilat, Israel, 800-804.

Barkana, I. (2013). "Extensions in adaptive model tracking with mitigated passivity conditions." *Chinese Journal of Aeronautics* 26 (1):136-150.

Barkana, I. (2014). "Simple adaptive control - a stable direct model reference adaptive control methodology - brief survey." *International Journal of Adaptive Control and Signal Processing* 28 (7-8):567-603.

Barkana, I. (2016a). "Adaptive Control? But is so Simple!" *Journal of Intelligent & Robotic Systems* 83 (1):3-34.

Barkana, I. (2016b). "Parallel Feedforward and Simple Adaptive Control of Flexible Structures: First-Order Pole Instead of Collocated Velocity Sensors?" *Journal of aerospace engineering* 29 (2):04015039.

Barkana, I. (2016c). "Robustness and perfect tracking in simple adaptive control." *International Journal of Adaptive Control and Signal Processing* 30 (8-10):1118-1151.

Barkana, I., and Guez, A. (1990). "Simple adaptive control for a class of non-linear systems with application to robotics." *International Journal of Control* 52 (1):77-79.

Barkana, I., and Kaufman, H. (1993). "Simple adaptive control of large flexible space structures." *IEEE Transactions on Aerospace and Electronic Systems* 29 (4):1137-1149.

Barroso, L. R., Chase, J. G., and Hunt, S. (2003). "Resettable smart dampers for multi-level seismic hazard mitigation of steel moment frames." *Journal of Structural Control* 10 (1):41-58.

Battista, Ronaldo C., and Pfeil, Michèle S. (2000). "Reduction of vortex-induced oscillations of Rio–Niterói bridge by dynamic control devices." *Journal of Wind Engineering and Industrial Aerodynamics* 84 (3):273-288.

Bazzurro, P., and Luco, N. (2006). "Do Scaled and Spectrum-Matched near-Source Records Produce Biased Nonlinear Structural Responses." *Proceedings of the 8th U.S. National Conference on Earthquake Engineering*, San Francisco, CA.

Bitaraf, M., Barroso, L. R., and Hurlebaus, S. (2010). "Adaptive control to mitigate damage impact on structural response." *Journal of intelligent material systems and structures* 21 (6):607-619.

Bitaraf, M., and Hurlebaus, S. (2013). "Semi-active adaptive control of seismically excited 20-story nonlinear building." *Engineering Structures* 56:2107-2118.

Bitaraf, M., Hurlebaus, S., and Barroso, L. R. (2012). "Active and Semi-active Adaptive Control for Undamaged and Damaged Building Structures Under Seismic Load." *Computer-aided civil and infrastructure engineering* 27 (1):48-64.

Caicedo, J. M., and Dyke, S. J. (2004). "Implementation of a SHM method on a numerical model of a cable-stayed bridge." *Proceedings of the 2004 American Control Conference*, Boston, MA, 4213-4218 vol.5.

Caicedo, J. M., Dyke, S. J., Moon, S. J., Bergman, L. A., Turan, G., and Hague, S. (2003). "Phase II benchmark control problem for seismic response of cable-stayed bridges." *Journal of Structural Control* 10 (3-4):137-168.

Chopra, A. K. (2012). *Dynamics of Structures: Theory and Applications to Earthquake Engineering*. Third ed. New Jersey, NY: Prentice Hall.

Chu, S. (2009). "Application of real-time adaptive identification technique on damage detection and structural health monitoring." *Structural control & health monitoring* 16 (2):154-177.

Chung, R. M. (1996). *January 17, 1995 Hyogoken-Nanbu (Kobe) earthquake: Performance of structures, lifelines, and fire protection systems (NIST SP 901)*. National Institute of Standards and Technology (NIST SP 901), Gaithersburg, MD.

de Silva, C. W. (2015). *Sensors and Actuators: Engineering System Instrumentation*. Second ed. Boca Raton, FL: CRC Press.

Department of Earth and Atmospheric Sciences, Saint Louis University. (2016). "Saint Louis University Earthquake Center." <http://www.eas.slu.edu/Earthquake_Center/> (June 24th, 2018).

Dicleli, M. , Mansour, M. Y. , and Constantinou, M. C. . (2005). "Efficiency of Seismic Isolation for Seismic Retrofitting of Heavy Substructured Bridges." *Journal of Bridge Engineering* 10 (4):429-441.

Dormand, J. R., and Prince, P. J. (1980). "A family of embedded Runge-Kutta formulae." *Journal of Computational and Applied Mathematics* 6 (1):19-26.

Dyke, S. J., Spencer Jr, B. F., Quast, P., and Sain, M. K. (1995). "Role of control-structure interaction in protective system design." *Journal of Engineering Mechanics* 121 (2):322-338.

Erkus, B., Abé, M., and Fujino, Y. (2002). "Investigation of semi-active control for seismic protection of elevated highway bridges." *Engineering Structures* 24 (3):281-293.

Gamota, D. R., and Filisko, F. E. (1991). "Dynamic mechanical studies of electrorheological materials: Moderate frequencies." *Journal of Rheology* 35 (3):399-425.

Gattulli, V., and Romeo, F. (2000). "Integrated procedure for identification and control of MDOF structures." *Journal of Engineering Mechanics* 126 (7):730.

Hancock, J., Watson-Lamprey, J., Abrahamson, N. A., Bommer, J. J., Markatis, A., McCoyh, E., and Mendis, R. (2006). "An improved method of matching response spectra of recorded earthquake ground motion using wavelets." *Journal of Earthquake Engineering* 10 (sup001):67-89.

Jabbari, F., and Bobrow, J. E. (2002). "Vibration suppression with resettable device." *Journal of Engineering Mechanics* 128.

Jang, J. S. R., Sun, C. T., and Mizutani, E. (1997). *Neuro-fuzzy and Soft Computing: A Computational Approach to Learning and Machine Intelligence*. First ed. New Jersey, NY: Prentice Hall.

Javanbakht, M. (2016). "Application of simple adaptive control to an MR damper-based control system for seismically excited nonlinear buildings." *Smart Structures and Systems* 18 (6):1251-1267.

Jung, H. J. (2004). "State-of-the-art of semiactive control systems using MR fluid dampers in civil engineering applications." *Structural Engineering and Mechanics* 17:493-526.

Jung, H. J., Spencer, B. F., and Lee, I. W. (2003). "Control of seismically excited cable-stayed bridge employing magnetorheological fluid dampers." *Journal of Structural Engineering* 129 (7):873.

Kidder, R. L. (1973). "Reduction of structural frequency equations." *AIAA Journal* 11 (6):892-892.

Lilhanand, K., and Tseng, W. S. (1987). "Generation of synthetic time histories compatible with multiple-damping design response spectra." *Transactions of the 9th international conference on structural mechanics in reactor technology*, Lausanne, Switzerland.

Lilhanand, K., and Tseng, W. S. (1988). "Development and application of realistic earthquake time histories compatible with multiple-damping design spectra." *Proceedings of the 9th world conference on earthquake engineering*, 819-824.

Lu, Lyan-Ywan. (2009). "A theoretical study on piezoelectric smart isolation system for seismic protection of equipment in near-fault areas." *Journal of intelligent material systems and structures* 20 (2):217-232.

Makris, N., and Zhang, J. (2004). "Seismic response analysis of a highway overcrossing equipped with elastomeric bearings and fluid dampers." *Journal of Structural Engineering* 130 (6):830-845.

Mamdani, E. H., and Assilian, S. (1999). "An experiment in linguistic synthesis with a fuzzy logic controller." *International Journal of Human-Computer Studies* 51 (2):135-147.

Ningsu, L. (1999). "Decentralized model reference control of flexible cable-stayed beam structures." *Proceedings of the 1999 American Control Conference*, San Diego, CA., 3817-20.

Ok, S. Y., Kim, D. S., Park, K. S., and Koh, H. M. (2007). "Semi-active fuzzy control of cable-stayed bridges using magneto-rheological dampers." *Engineering structures* 29 (5):776-788.

PEER Ground Motion Database. (2013). "NGA East- Central & Eastern North-America " <https://ngawest2.berkeley.edu/spectras/> (June 25th, 2018).

Qu, Z. Q. (2013). *Model order reduction techniques with applications in finite element analysis*. First ed: Springer London.

Saaed, T. E., Nikolakopoulos, G. , Jonasson, J. E., and Hedlund, H. . (2015). "A state-of-the-art review of structural control systems." *Journal of Vibration and Control* 21 (5):919-937.

Schurter, K. C., and Roschke, P. N. (2001a). "Neuro-fuzzy control of structures using acceleration feedback." *Smart Materials and Structures* 10 (4):770.

Schurter, K. C., and Roschke, P. N. (2001b). "Neuro-fuzzy control of structures using magnetorheological dampers." *Proceedings of the 2001 American Control Conference*, Arlington, VA, 2001, 1097-1102 vol.2.

Sivaselvan, M. V., Reinhorn, A. M., Shao, X., and Weinreber, S. (2008). "Dynamic force control with hydraulic actuators using added compliance and displacement compensation." *Earthquake Engineering & Structural Dynamics* 37 (15):1785-1800.

Sobel, K., Kaufman, H., and Mabius, L. (1982). "Implicit adaptive control for a class of MIMO systems." *IEEE Transactions on Aerospace and Electronic Systems* AES-18 (5):576-590.

Sommerville, P. (1997). *Develop suites of time histories*. SAC Joint Venture Steel Project Phase II Report, Woodward-Clyde Federal Services, Pasadena, CA.

Spencer, B. F., and Nagarajaiah, S. (2003). "State of the Art of Structural Control." *Journal of Structural Engineering* 129 (7):845-856.

Spencer, B. F., and Sain, M. K. (1997). "Controlling buildings: a new frontier in feedback." *IEEE Control Systems Magazine* 17 (6):19-35.

Spencer Jr, B. F., Dyke, S. J. , Sain, M. K., and Carlson, J. D. F. . (1997). "Phenomenological model for magnetorheological dampers." *Journal of Engineering Mechanics* 123 (3):230-238.

Stanway, R., Sproston, J. L., and Stevens, N. G. (1985). "Non-Linear Identification of an Electro-Rheological Vibration Damper." *IFAC Proceedings Volumes* 18 (5):195-200.

Sugeno, M. (1985). *Industrial Applications of Fuzzy Control*. First ed. North-Holland: Elsevier Science Ltd.

Tan, P., and Agrawal, A. K. (2009). "Benchmark structural control problem for a seismically excited highway bridge—Part II: Phase I Sample control designs." *Structural Control and Health Monitoring* 16 (5):530-548.

The MathWorks, Inc. (2017a). *MATLAB.* v. R2017b. Natick, MA.

The MathWorks, Inc. (2017b). *SIMULINK*. v. R2017b. Natick, MA.

Tsang, H. H., Su, R. K. L., and Chandler, A. M. (2006). "Simplified inverse dynamics models for MR fluid dampers." *Engineering structures* 28 (3):327-341.

Ubertini, F, and Materazzi, AL. (2009). "Reliability of multiple tuned mass dampers for bridge flutter control." *Proceedings of the 5th European & African Conference on Wind Engineering (EACWE 5), June*, 19-23.

Ulrich, S., and Sasiadek, J. Z. (2014). "Decentralized simple adaptive control of nonlinear systems." *International Journal of Adaptive Control and Signal Processing* 28 (7-8):750-763.

United States Geological Survey, USGS. (1999). "USGS Online Publications Directory." <https://pubs.usgs.gov/dds/dds-29/screens/> (September 16th, 2018).

Venanzi, I., Fravolini, M. L., and Ierimonti, L. (2017). "Multi-model robust adaptive control of tall buildings." *Meccanica* 52 (13):3237–3253.

Wen, Y. (1976). "Method for random vibration of hysteretic systems." *Journal of the Engineering Mechanics Division* 102 (2):249-263.

Wilson, J. C., and Gravelle, W. (1991). "Modelling of a cable-stayed bridge for dynamic analysis." *Earthquake Engineering & Structural Dynamics* 20 (8):707-721.

Xu, Y. L. (2008). "Integrated vibration control and health monitoring of building structures using semi-active friction dampers: Part I-methodology." *Engineering structures* 30 (7):1789-1801.

Yang, G., Spencer, Jr B. F., Carlson, J. D., and Sain, M. K. (2002). "Large-scale MR fluid dampers: modeling and dynamic performance considerations." *Engineering Structures* 24:309-323.

APPENDIX A

SUPPLEMENTARY RESULTS FOR SECTION 6

Two-span Highway Bridge- Active Control

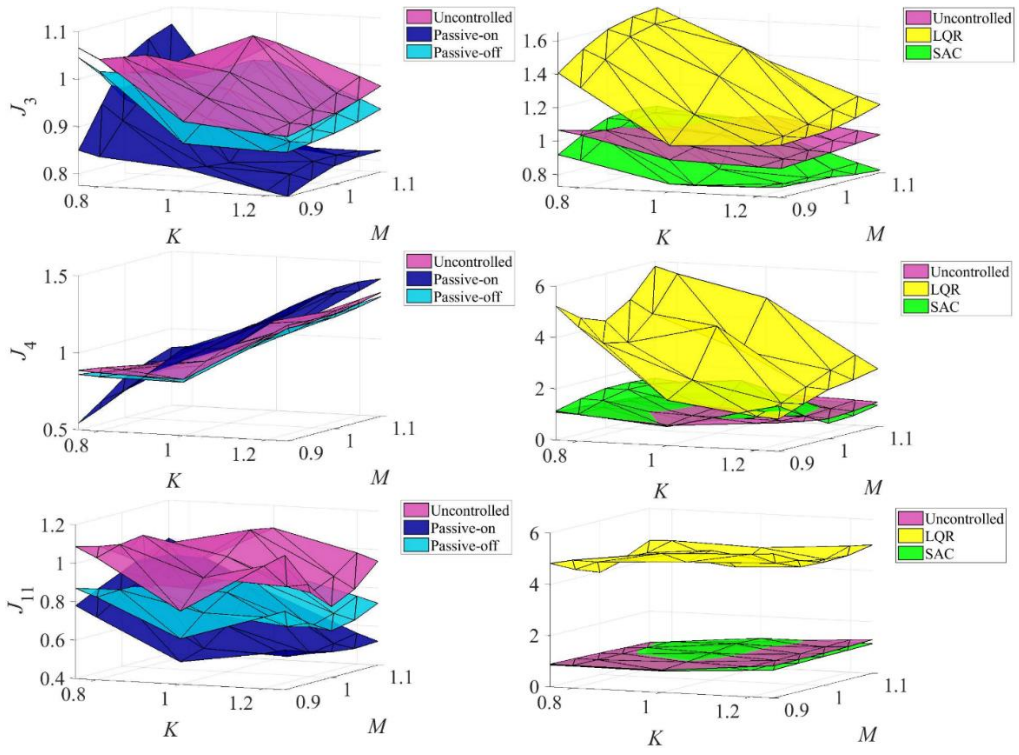

Fig. A.1: Maximum J_3, J_4 and J_{11} for different mass and stiffness ratios: Duzce.

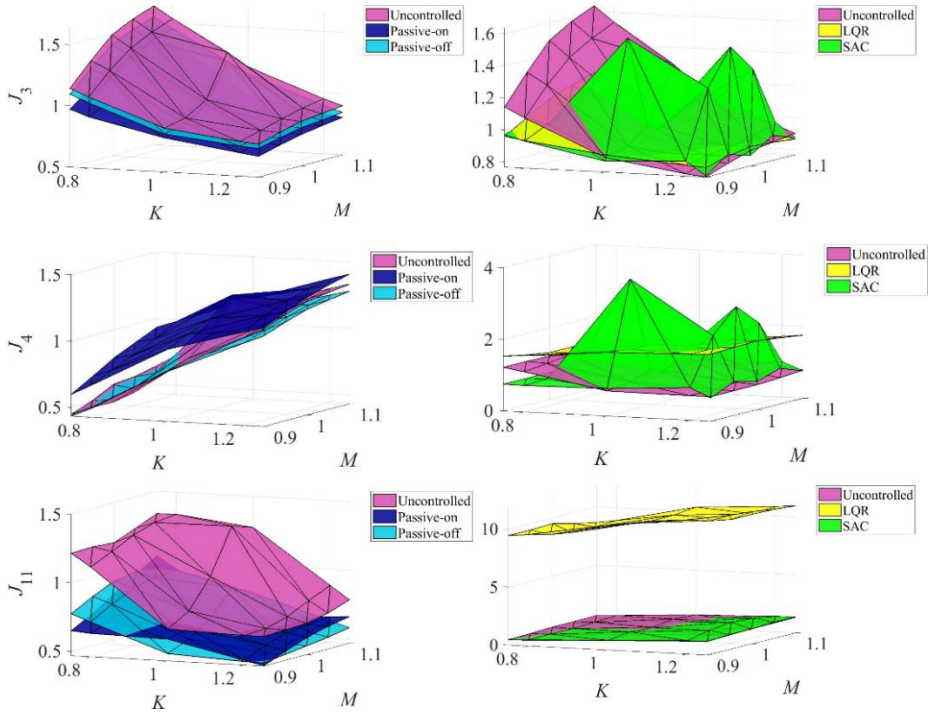

Fig. A.2: Maximum J_3, J_4 and J_{11} for different mass and stiffness ratios: Imperial Valley.

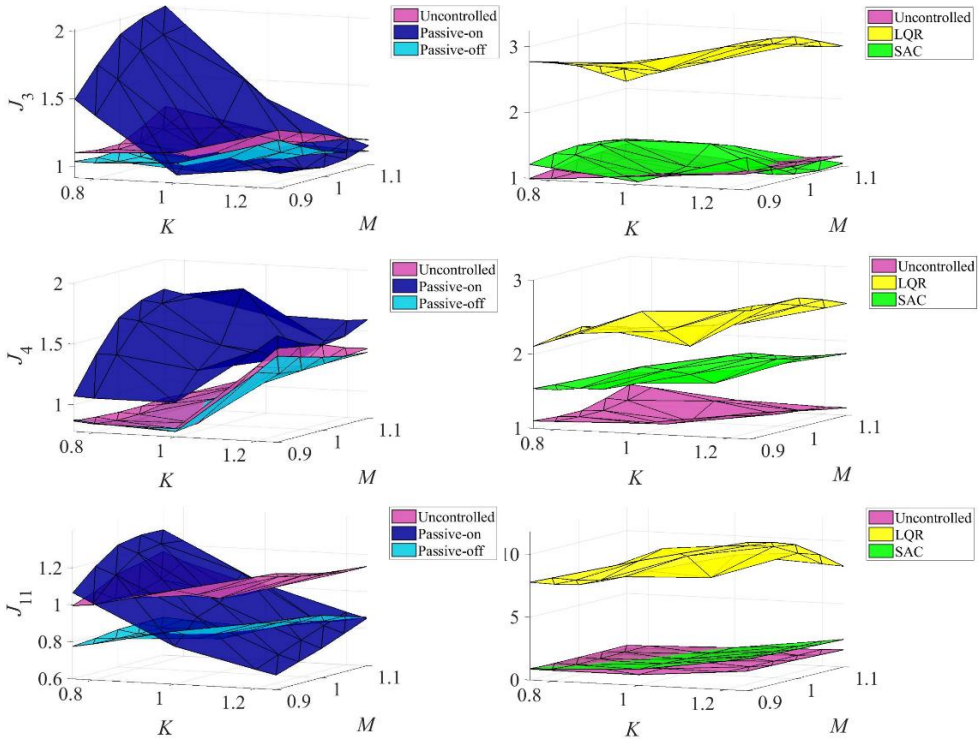

Fig. A.3: Maximum J_3, J_4 and J_{11} for different mass and stiffness ratios: Kobe.

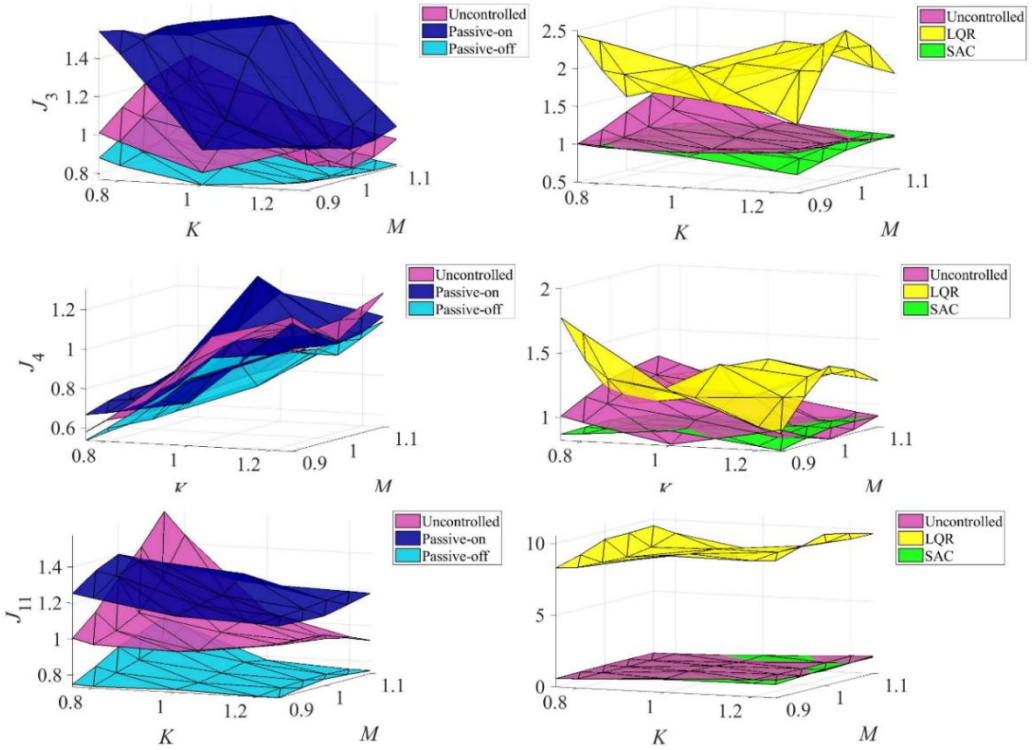

Fig. A.4: Maximum J_3, J_4 and J_{11} for different mass and stiffness ratios: Landers.

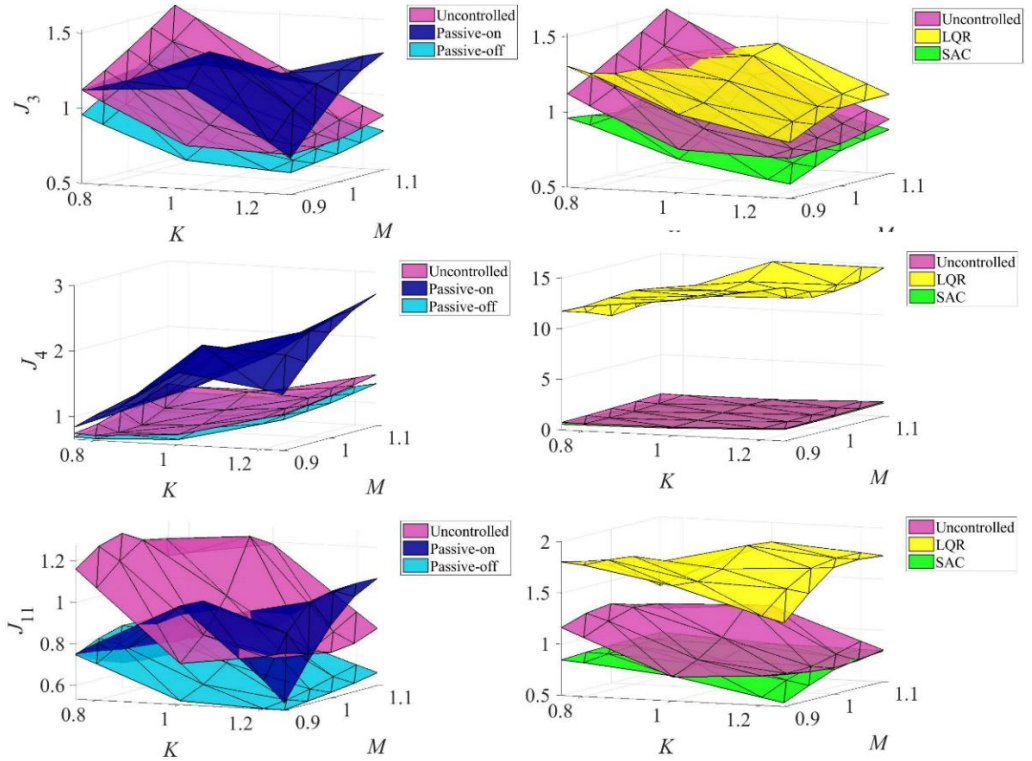

Fig. A.5: Maximum J_3, J_4 and J_{11} for different mass and stiffness ratios: Loma Prieta.

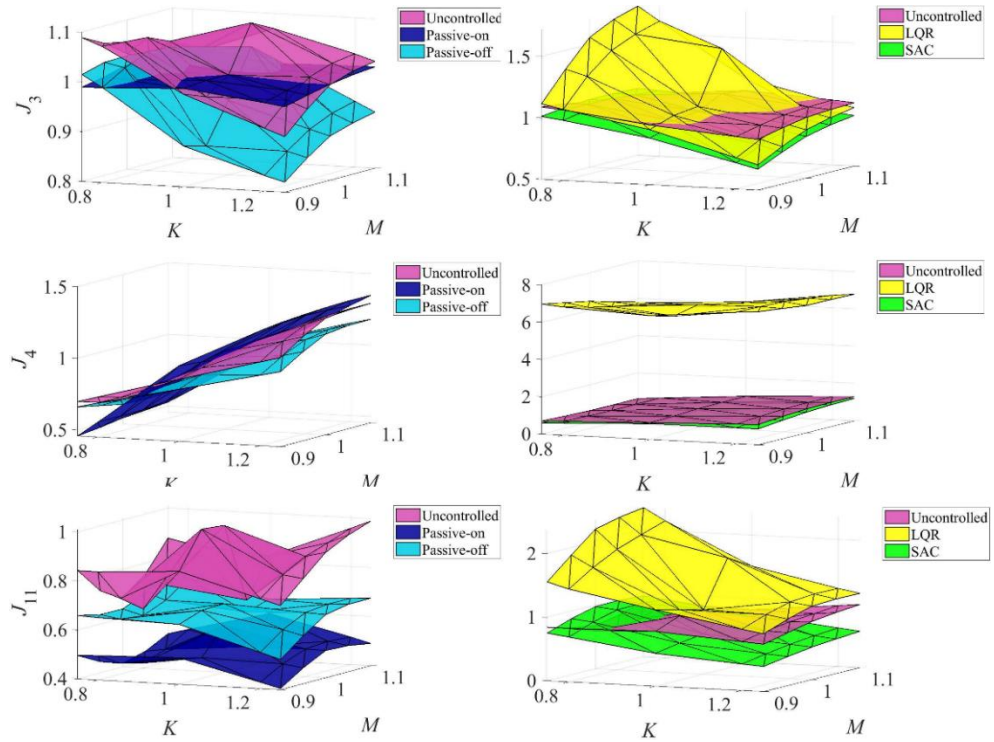

Fig. A.6: Maximum J_3, J_4 and J_{11} for different mass and stiffness ratios: North Palm Springs.

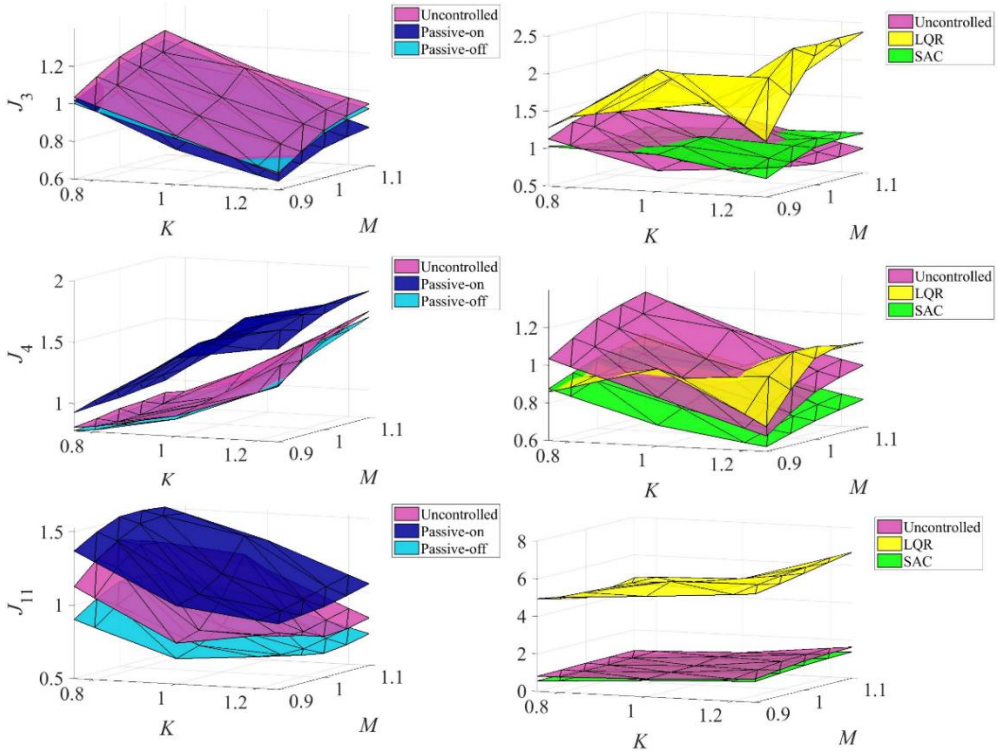

Fig. A.7: Maximum J_3, J_4 and J_{11} for different mass and stiffness ratios: Northridge.

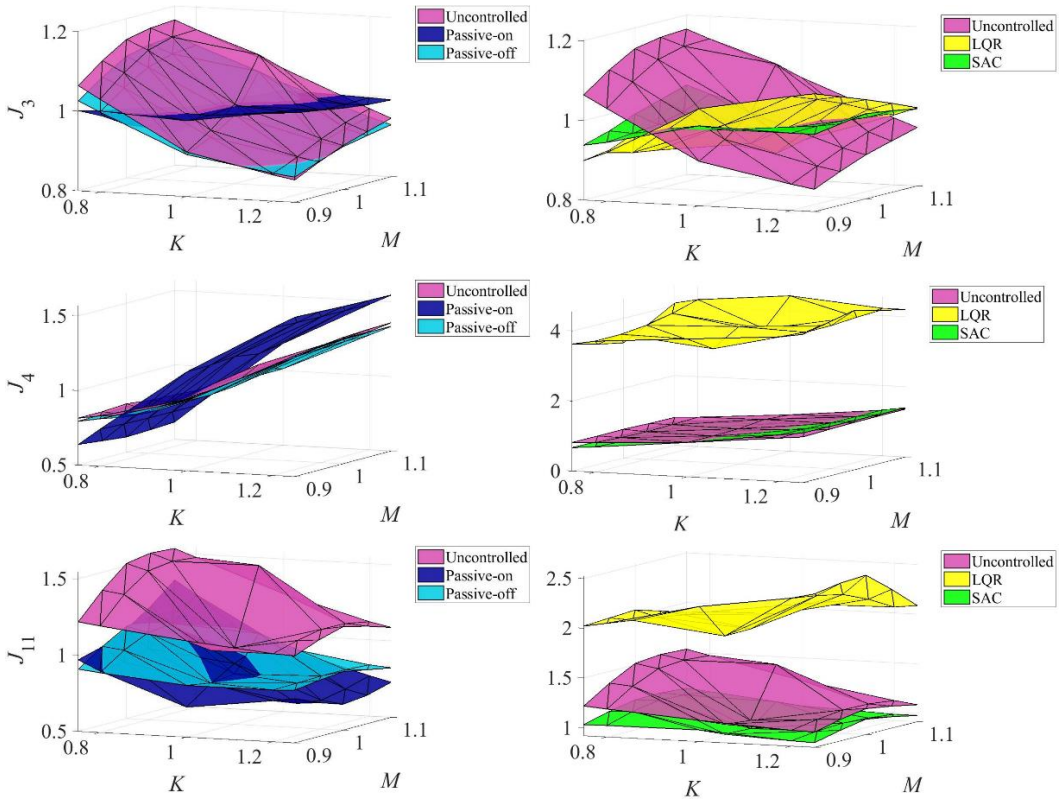

Fig. A.8: Maximum J_3, J_4 and J_{11} for different mass and stiffness ratios: Petrolia.

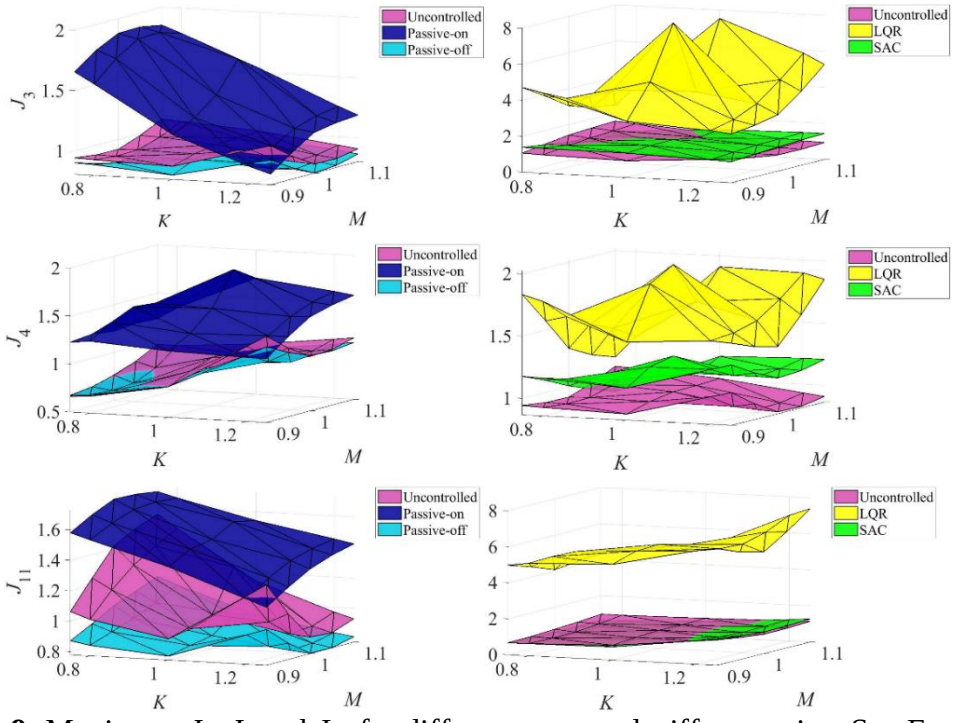

Fig. A.9: Maximum J_3, J_4 and J_{11} for different mass and stiffness ratios: San Fernando.

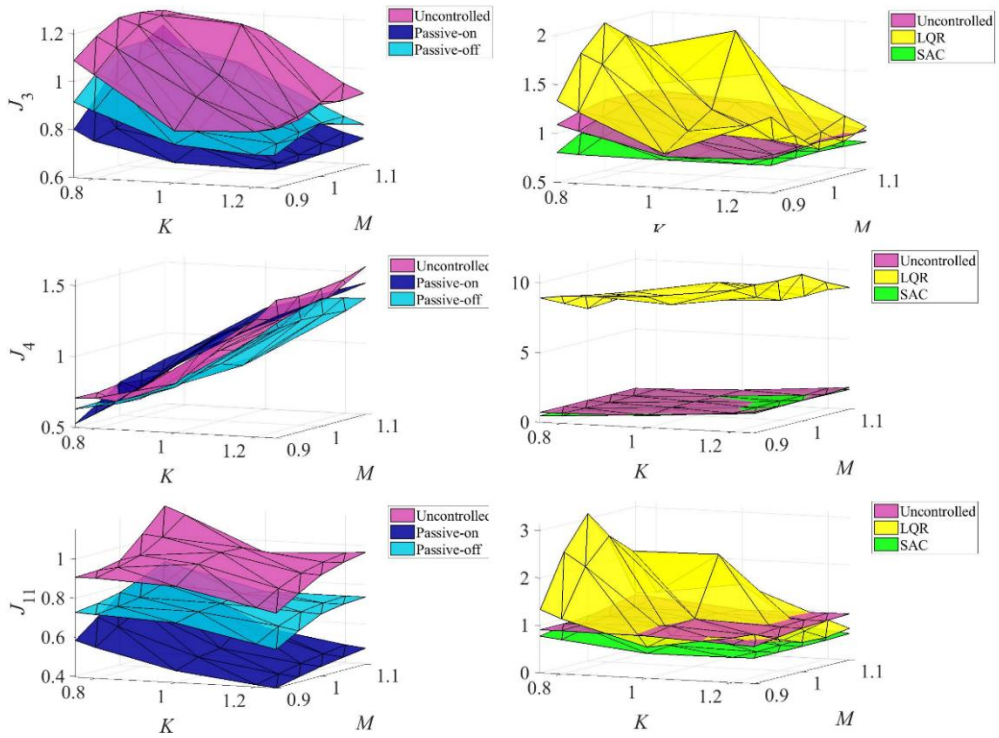

Fig. A.10: Maximum J_3, J_4 and J_{11} for different mass and stiffness ratios: Superstition Hills.

Two-span Highway Bridge- Semi-Active Control

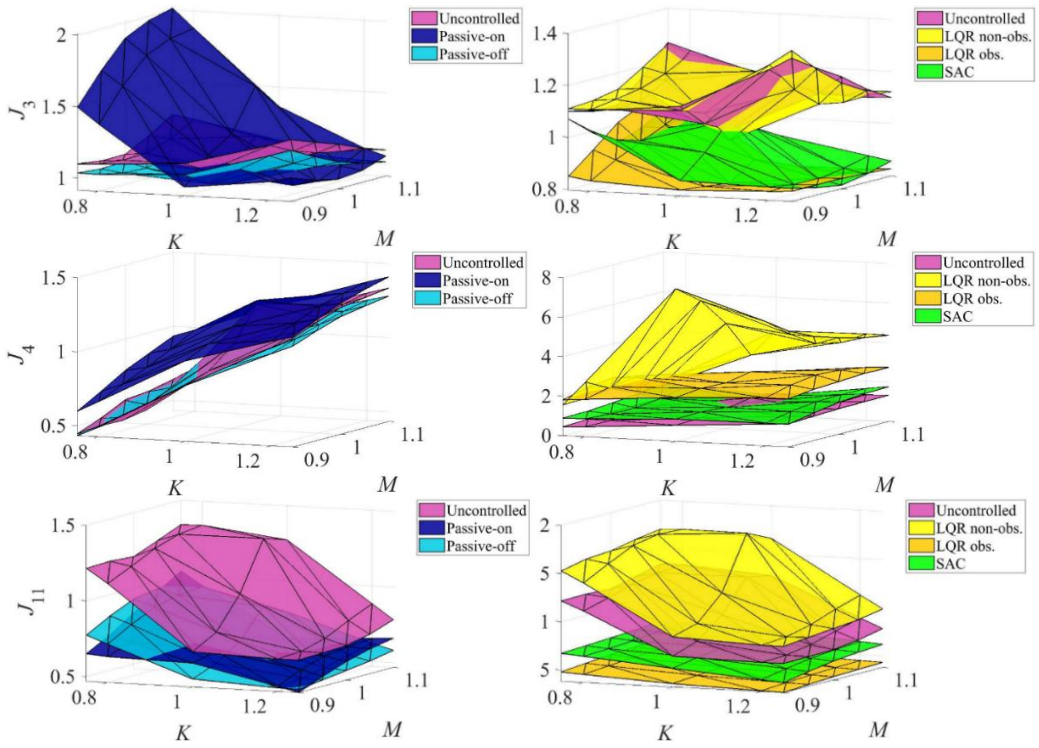

Fig. A.11: Maximum J_3, J_4 and J_{11} for different mass and stiffness ratios: Duzce.

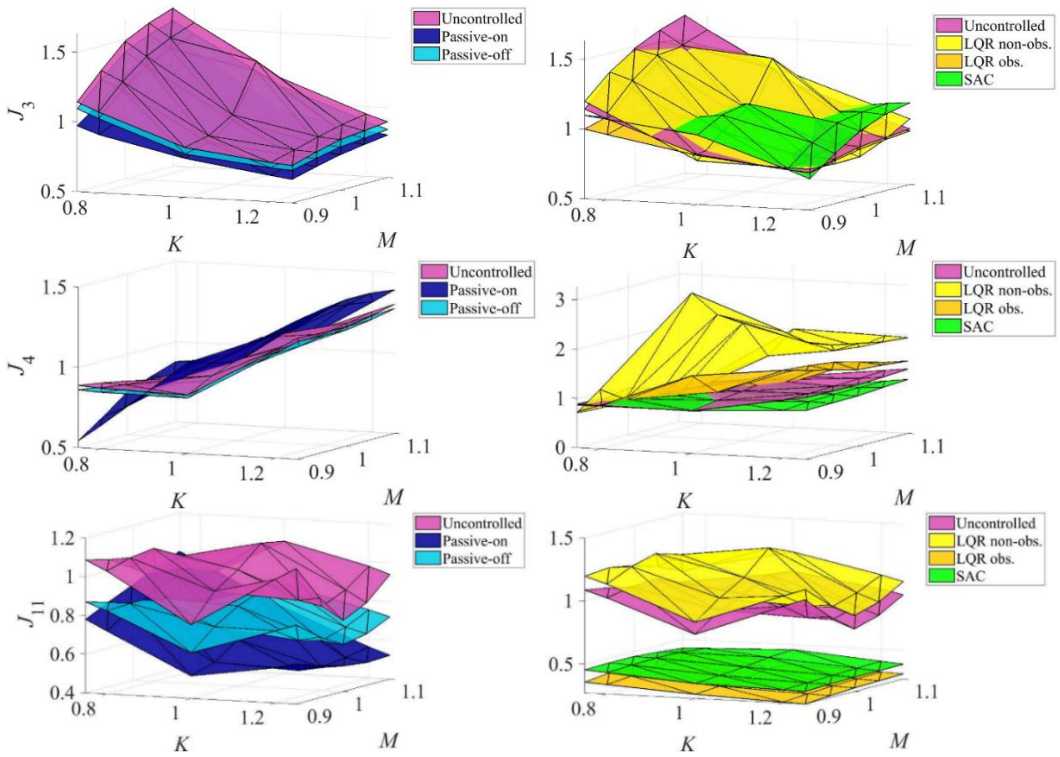

Fig. A.12: Maximum J_3, J_4 and J_{11} for different mass and stiffness ratios: Imperial Valley.

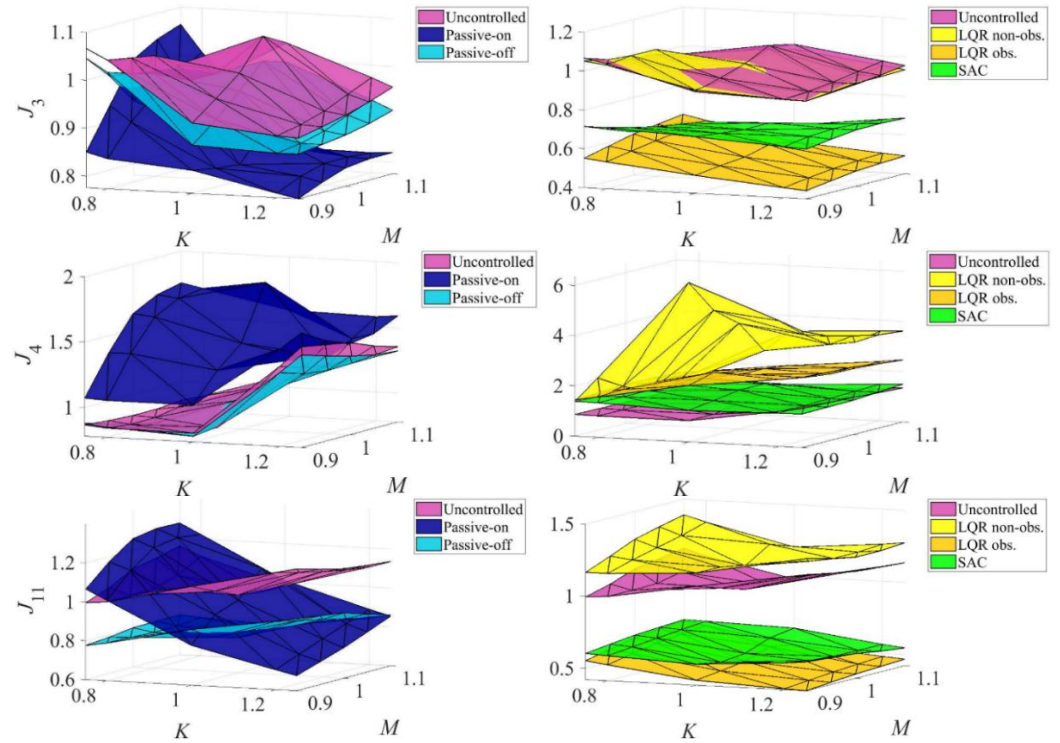

Fig. A.13: Maximum J_3, J_4 and J_{11} for different mass and stiffness ratios: Kobe.

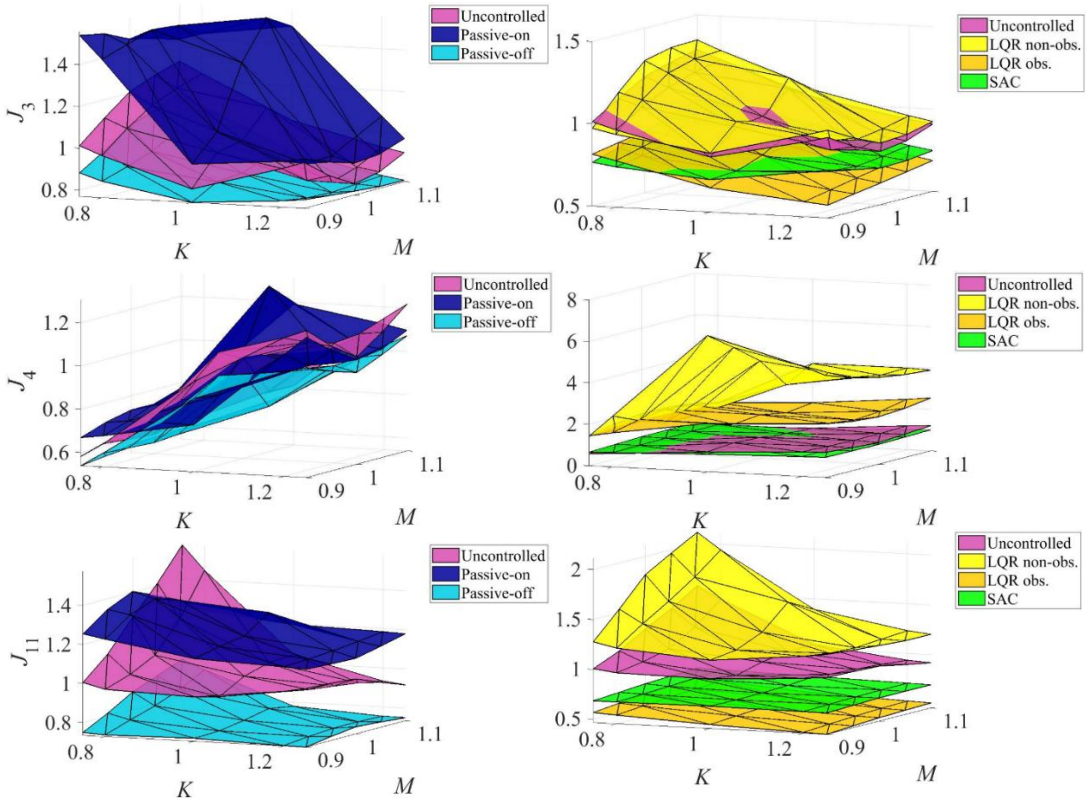

Fig. A.14: Maximum J_3, J_4 and J_{11} for different mass and stiffness ratios: Landers.

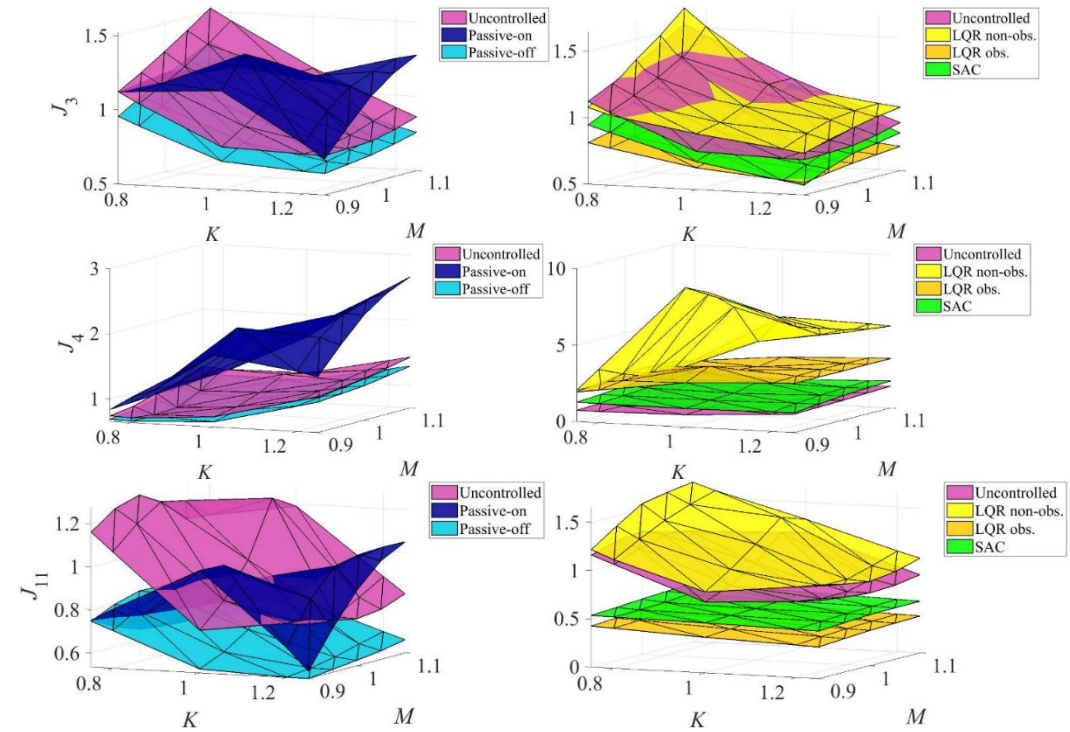

Fig. A.15: Maximum J_3, J_4 and J_{11} for different mass and stiffness ratios: Loma Prieta.

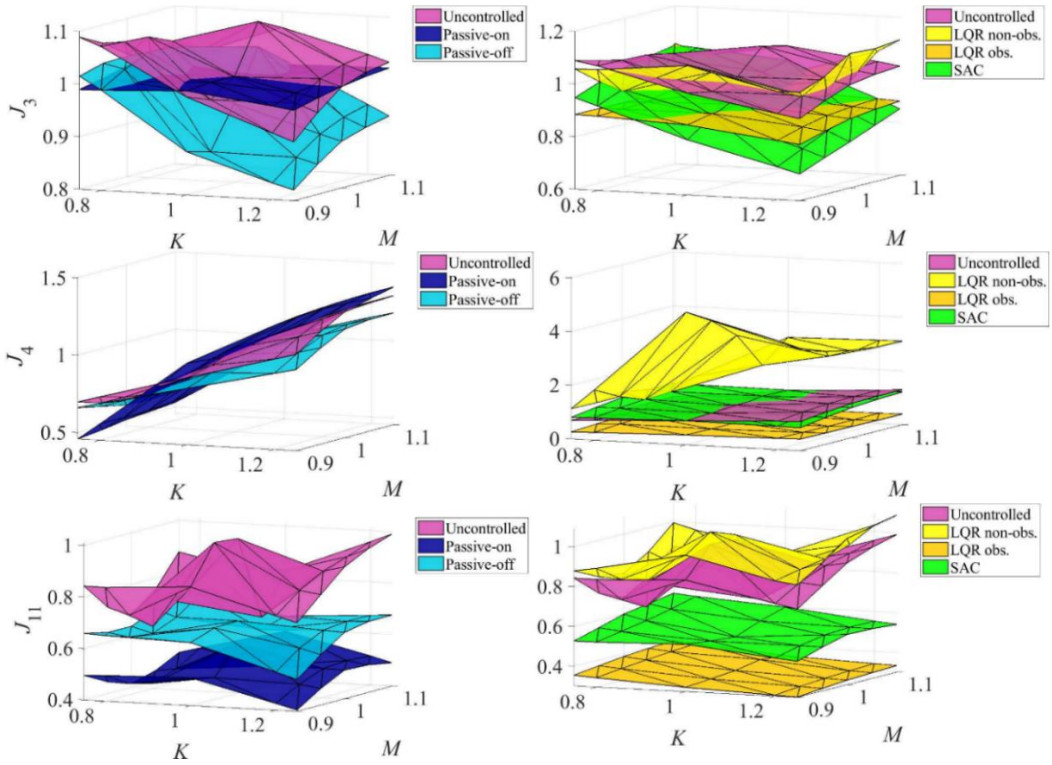

Fig. A.16: Maximum J_3, J_4 and J_{11} for different mass and stiffness ratios: North Palm Springs.

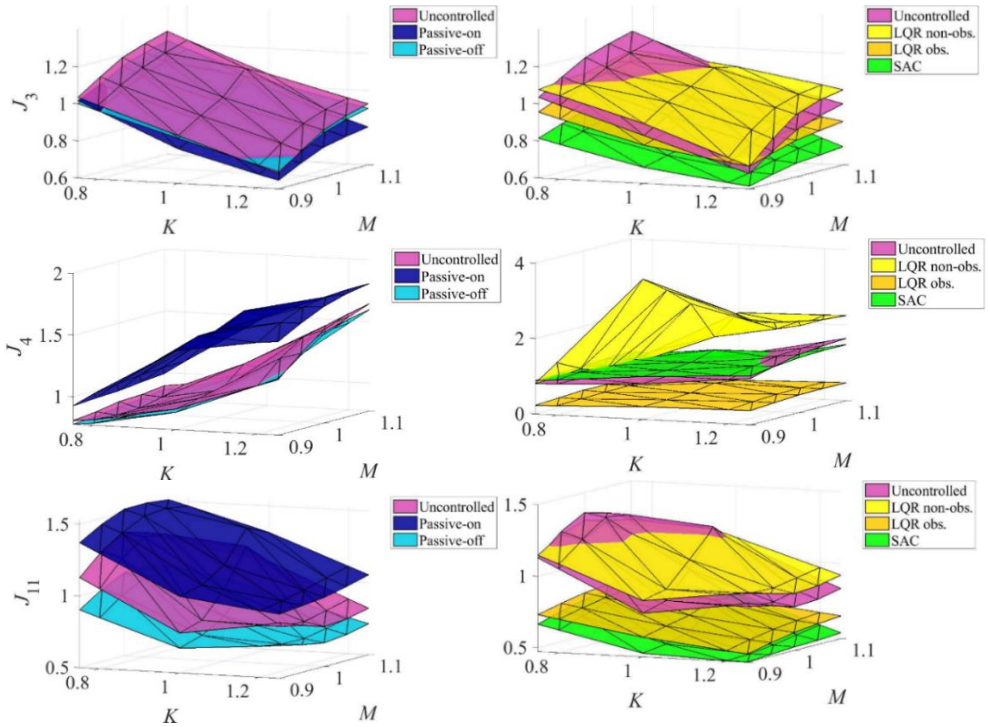

Fig. A.17: Maximum J_3, J_4 and J_{11} for different mass and stiffness ratios: Northridge.

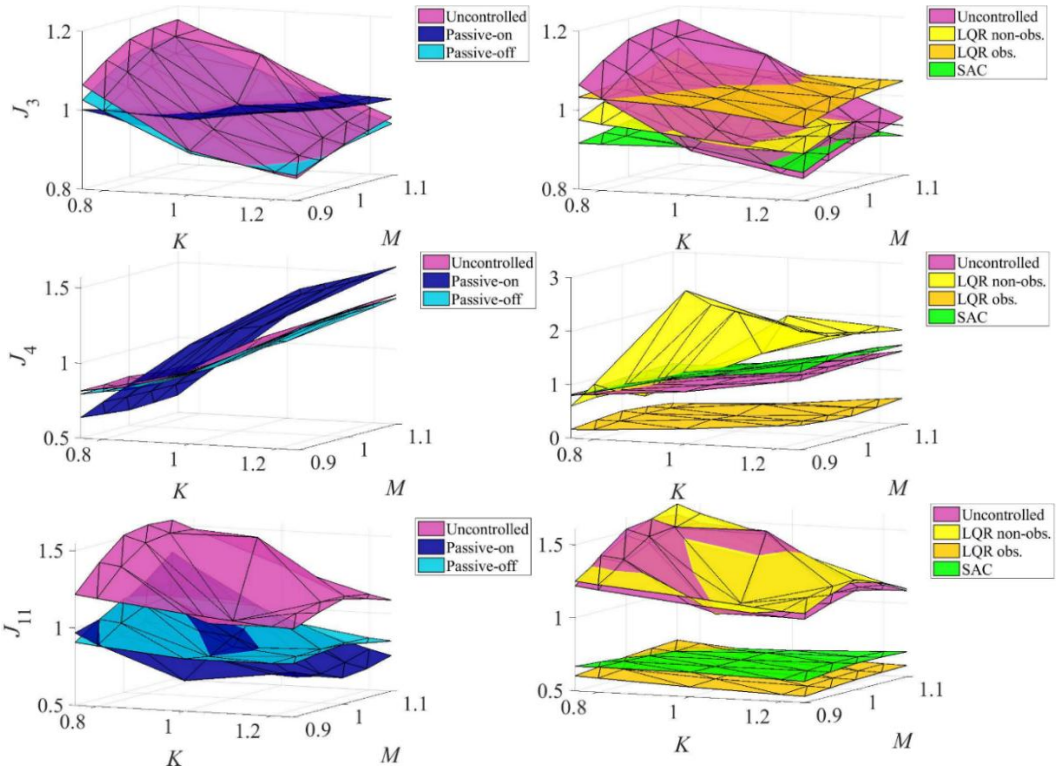

Fig. A.18: Maximum J_3, J_4 and J_{11} for different mass and stiffness ratios: Petrolia.

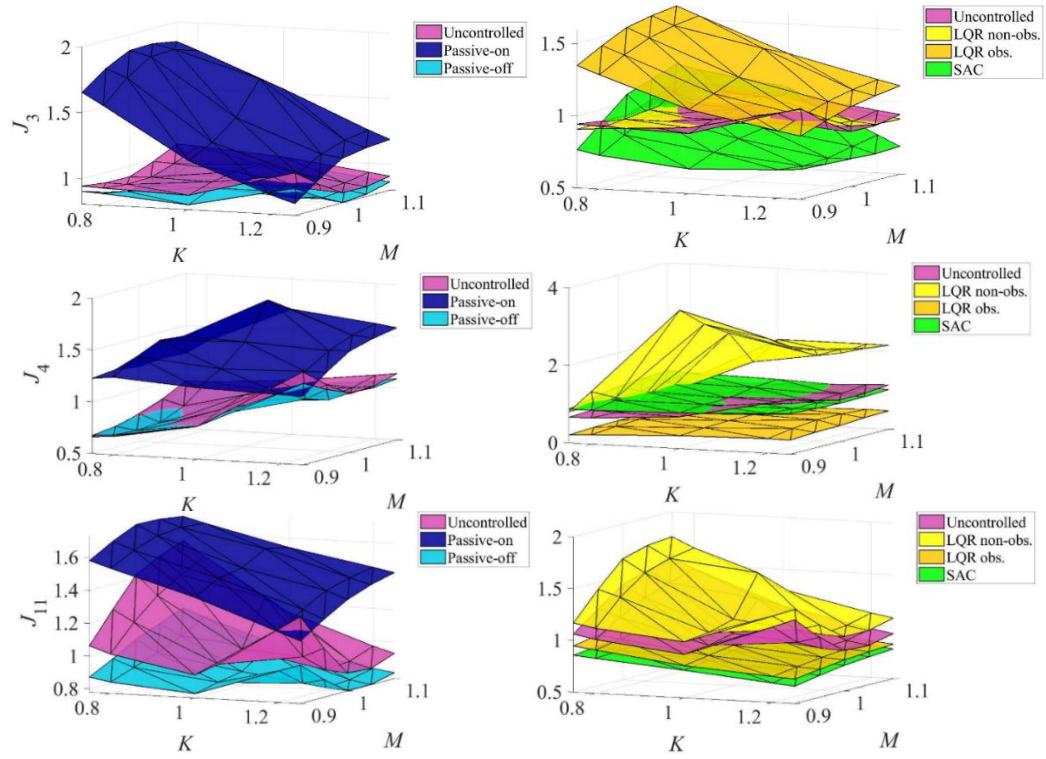

Fig. A.19: Maximum J_3, J_4 and J_{11} for different mass and stiffness ratios: San Fernando.

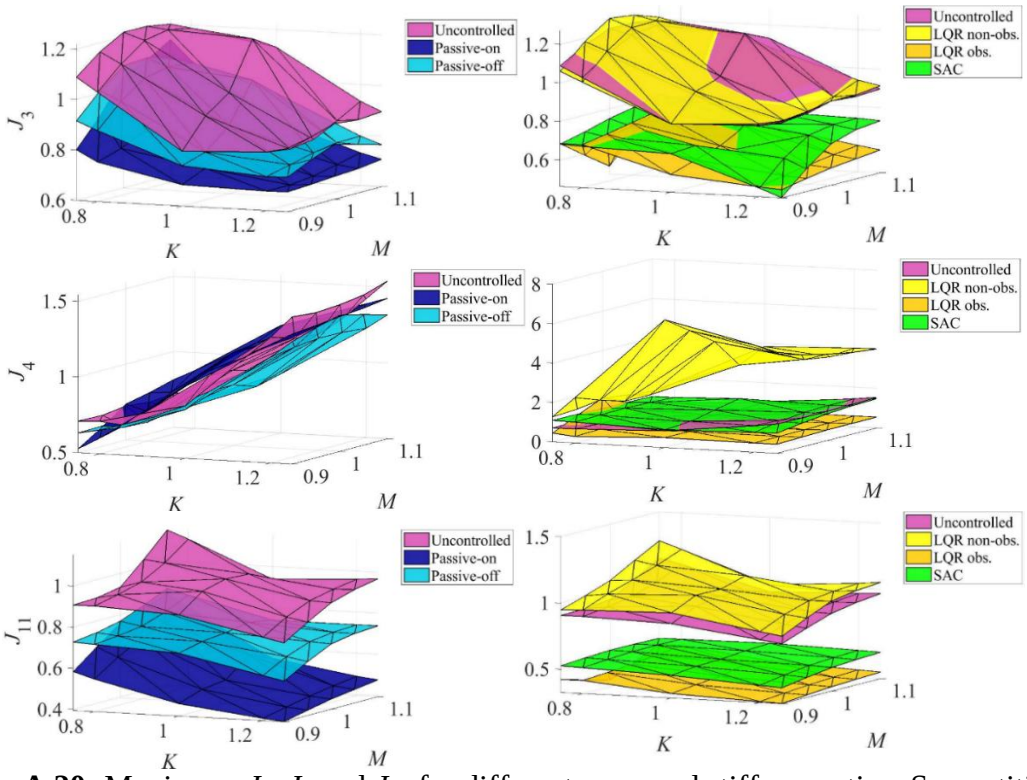

Fig. A.20: Maximum J_3, J_4 and J_{11} for different mass and stiffness ratios: Superstition Hills.

APPENDIX B

SUPPLEMENTARY RESULTS FOR SECTION 7

Cable-Stayed Bridge- Benchmark Earthquakes

Table B.1: Maximum values for all the performance criteria for the passive-on-controlled nominal structure.

Nominal Structure: Passive-on										
Crit.		15° Incidence			45° Incidence			Max	Min	Var
		El Centro	Mexico	Gebze	El Centro	Mexico	Gebze			
J_1	x	0.651	0.543	0.440	0.671	0.710	0.531	0.710	0.440	0.270
J_2	x	0.407	0.255	0.458	0.415	0.334	0.247	0.458	0.247	0.210
J_3	x	0.651	0.543	0.440	0.671	0.710	0.531	0.710	0.440	0.270
J_4	x	0.477	0.277	0.373	0.332	0.270	0.373	0.477	0.270	0.207
J_5	-	0.235	0.161	0.172	0.223	0.166	0.162	0.235	0.161	0.074
J_6	x	0.008	0.001	0.010	0.007	0.002	0.007	0.010	0.001	0.009
J_7	x	0.611	0.458	0.294	0.715	0.560	0.325	0.715	0.294	0.421
J_8	x	0.338	0.200	0.228	0.312	0.213	0.193	0.338	0.193	0.146
J_9	x	0.611	0.458	0.294	0.715	0.560	0.325	0.715	0.294	0.421
J_{10}	x	0.299	0.156	0.227	0.289	0.170	0.175	0.299	0.156	0.143
J_{11}	-	0.027	0.020	0.014	0.027	0.020	0.013	0.027	0.013	0.014
J_{12}	x	0.002	0.002	0.002	0.002	0.002	0.002	0.002	0.002	0.000
J_{14}	-	0.001	0.001	0.001	0.001	0.000	0.001	0.001	0.000	0.001
J_{16}	-	24	24	24	24	24	24	24	24	0
J_{17}	-	-	-	-	-	-	-	-	-	-

Table B.2: Maximum values for all the performance criteria for the passive-on-controlled structure with 5% added masses.

+5% Mass: Passive-on										
Crit.		15° Incidence			45° Incidence			Max	Min	Var
		El Centro	Mexico	Gebze	El Centro	Mexico	Gebze			
J_1	x	0.598	0.793	0.352	0.600	1.325	0.524	1.325	0.352	0.972
J_2	x	0.861	0.560	0.182	0.636	0.869	0.149	0.869	0.149	0.720
J_3	x	0.598	0.793	0.352	0.600	1.325	0.524	1.325	0.352	0.972
J_4	x	0.682	0.521	0.128	0.454	0.540	0.175	0.682	0.128	0.554
J_5	-	0.293	0.348	0.124	0.329	0.339	0.118	0.348	0.118	0.229
J_6	x	0.006	0.002	0.003	0.006	0.002	0.004	0.006	0.002	0.004
J_7	x	0.876	0.989	0.388	1.295	1.325	0.582	1.325	0.388	0.937
J_8	x	0.761	0.651	0.189	0.544	0.726	0.159	0.761	0.159	0.602
J_9	x	0.876	0.989	0.388	1.295	1.325	0.582	1.325	0.388	0.937
J_{10}	x	0.442	0.352	0.111	0.329	0.387	0.103	0.442	0.103	0.339
J_{11}	-	0.058	0.047	0.015	0.048	0.048	0.014	0.058	0.014	0.043
J_{12}	x	0.002	0.002	0.002	0.002	0.002	0.002	0.002	0.002	0.000
J_{14}	-	0.001	0.002	0.001	0.001	0.001	0.001	0.002	0.001	0.001
J_{16}	-	24	24	24	24	24	24	24	24	0
J_{17}	-	-	-	-	-	-	-	-	-	-

Table B.3: Maximum values for all the performance criteria for the passive-on-controlled structure with 20% stiffness reduction.

-20% Stiffness: Passive-on										
Crit.		15° Incidence			45° Incidence			Max	Min	Var
		El Centro	Mexico	Gebze	El Centro	Mexico	Gebze			
J_1	x	0.842	1.750	0.747	1.015	2.481	0.830	2.481	0.747	1.735
J_2	x	0.590	1.382	0.368	1.519	1.765	0.462	1.765	0.368	1.397
J_3	x	0.842	1.750	0.747	1.015	2.481	0.830	2.481	0.747	1.735
J_4	x	0.977	1.211	0.324	1.135	1.863	0.422	1.863	0.324	1.539
J_5	-	0.586	1.186	0.268	0.804	1.498	0.337	1.498	0.268	1.231
J_6	x	0.008	0.002	0.010	0.008	0.001	0.007	0.010	0.001	0.009
J_7	x	1.948	2.986	1.294	2.573	3.844	1.570	3.844	1.294	2.550
J_8	x	1.048	1.363	0.462	1.519	1.770	0.570	1.770	0.462	1.308
J_9	x	1.948	2.986	1.294	2.573	3.844	1.570	3.844	1.294	2.550
J_{10}	x	0.822	1.117	0.399	1.150	1.486	0.480	1.486	0.399	1.087
J_{11}	-	0.177	0.230	0.073	0.243	0.298	0.090	0.298	0.073	0.225
J_{12}	x	0.002	0.002	0.002	0.002	0.002	0.002	0.002	0.002	0.000
J_{14}	-	0.003	0.002	0.001	0.002	0.003	0.002	0.003	0.001	0.002
J_{16}	-	24	24	24	24	24	24	24	24	0
J_{17}	-	-	-	-	-	-	-	-	-	-

Table B.4: Maximum values for all the performance criteria for the passive-off-controlled nominal structure.

Nominal Structure: Passive-off										
Crit.		15° Incidence			45° Incidence			Max	Min	Var
		El Centro	Mexico	Gebze	El Centro	Mexico	Gebze			
J_1	x	0.910	0.766	0.910	0.912	0.827	0.910	0.912	0.766	0.145
J_2	x	0.939	0.645	1.062	0.744	0.527	0.668	1.062	0.527	0.535
J_3	x	0.910	0.766	0.910	0.912	0.827	0.910	0.912	0.766	0.145
J_4	x	0.900	0.746	0.917	0.925	0.771	0.893	0.925	0.746	0.179
J_5	-	0.313	0.224	0.304	0.309	0.209	0.297	0.313	0.209	0.103
J_6	x	0.013	0.005	0.021	0.012	0.004	0.016	0.021	0.004	0.017
J_7	x	0.871	0.649	0.820	0.873	0.618	0.791	0.873	0.618	0.256
J_8	x	0.863	0.588	0.844	0.815	0.535	0.801	0.863	0.535	0.328
J_9	x	0.871	0.649	0.820	0.873	0.618	0.791	0.873	0.618	0.256
J_{10}	x	0.817	0.579	0.811	0.831	0.553	0.781	0.831	0.553	0.277
J_{11}	-	0.045	0.031	0.041	0.044	0.029	0.039	0.045	0.029	0.016
J_{12}	x	0.000	0.000	0.000	0.000	0.000	0.000	0.000	0.000	0.000
J_{14}	-	0.000	0.000	0.000	0.000	0.000	0.000	0.000	0.000	0.000
J_{16}	-	24	24	24	24	24	24	24	24	0
J_{17}	-	-	-	-	-	-	-	-	-	-

Table B.5: Maximum values for all the performance criteria for the passive-off-controlled structure with 5% added masses.

+5% Mass: Passive-off										
Crit.		15° Incidence			45° Incidence			Max	Min	Var
		El Centro	Mexico	Gebze	El Centro	Mexico	Gebze			
J_1	x	0.851	0.611	0.805	0.889	0.767	0.748	0.889	0.611	0.278
J_2	x	0.939	0.390	0.651	0.633	0.405	0.507	0.939	0.390	0.549
J_3	x	0.851	0.611	0.805	0.889	0.767	0.748	0.889	0.611	0.278
J_4	x	0.796	0.419	0.637	0.829	0.420	0.675	0.829	0.419	0.410
J_5	-	0.306	0.182	0.260	0.302	0.181	0.245	0.306	0.181	0.126
J_6	x	0.011	0.003	0.018	0.011	0.002	0.015	0.018	0.002	0.016
J_7	x	0.724	0.463	0.669	0.788	0.546	0.638	0.788	0.463	0.325
J_8	x	0.669	0.356	0.551	0.626	0.333	0.521	0.669	0.333	0.336
J_9	x	0.724	0.463	0.669	0.788	0.546	0.638	0.788	0.463	0.325
J_{10}	x	0.630	0.326	0.546	0.618	0.307	0.528	0.630	0.307	0.322
J_{11}	-	0.040	0.023	0.032	0.039	0.024	0.030	0.040	0.023	0.016
J_{12}	x	0.000	0.000	0.000	0.000	0.000	0.000	0.000	0.000	0.000
J_{14}	-	0.000	0.000	0.000	0.000	0.000	0.000	0.000	0.000	0.000
J_{16}	-	24	24	24	24	24	24	24	24	0
J_{17}	-	-	-	-	-	-	-	-	-	-

Table B.6: Maximum values for all the performance criteria for the passive-off-controlled structure with 20% stiffness reduction.

-20% Stiffness: Passive-off										
Crit		15° Incidence			45° Incidence			Max	Min	Var
		El Centro	Mexico	Gebze	El Centro	Mexico	Gebze			
J_1	x	0.944	0.832	0.917	0.953	0.924	0.920	0.953	0.832	0.121
J_2	x	0.671	0.579	1.081	1.344	0.629	0.899	1.344	0.579	0.765
J_3	x	0.944	0.832	0.917	0.953	0.924	0.920	0.953	0.832	0.121
J_4	x	1.125	0.780	0.815	0.844	0.693	0.840	1.125	0.693	0.433
J_5	-	0.320	0.304	0.315	0.325	0.304	0.312	0.325	0.304	0.022
J_6	x	0.014	0.005	0.025	0.013	0.004	0.020	0.025	0.004	0.021
J_7	x	0.876	0.843	0.891	0.887	0.849	0.880	0.891	0.843	0.048
J_8	x	0.816	0.710	0.819	0.823	0.673	0.788	0.823	0.673	0.150
J_9	x	0.876	0.843	0.891	0.887	0.849	0.880	0.891	0.843	0.048
J_{10}	x	0.823	0.719	0.811	0.813	0.675	0.753	0.823	0.675	0.148
J_{11}	-	0.047	0.046	0.045	0.047	0.045	0.044	0.047	0.044	0.003
J_{12}	x	0.000	0.000	0.000	0.000	0.000	0.000	0.000	0.000	0.000
J_{14}	-	0.000	0.000	0.000	0.000	0.000	0.000	0.000	0.000	0.000
J_{16}	-	24	24	24	24	24	24	24	24	0
J_{17}	-	-	-	-	-	-	-	-	-	-

Table B.7: Maximum values for all the performance criteria for the resettable-controlled nominal structure.

Nominal Structure: Resettable										
Crit		15° Incidence			45° Incidence			Max	Min	Var
		El Centro	Mexico	Gebze	El Centro	Mexico	Gebze			
J_1	x	0.695	0.683	0.705	0.734	0.812	0.722	0.812	0.683	0.129
J_2	x	0.571	0.608	0.580	0.598	0.660	0.615	0.660	0.571	0.089
J_3	x	0.695	0.683	0.705	0.734	0.812	0.722	0.812	0.683	0.129
J_4	x	0.627	0.629	0.610	0.537	0.703	0.687	0.703	0.537	0.166
J_5	-	0.253	0.201	0.227	0.248	0.211	0.235	0.253	0.201	0.051
J_6	x	0.011	0.005	0.016	0.010	0.004	0.013	0.016	0.004	0.012
J_7	x	0.665	0.574	0.468	0.712	0.611	0.488	0.712	0.468	0.244
J_8	x	0.588	0.499	0.431	0.600	0.528	0.471	0.600	0.431	0.170
J_9	x	0.665	0.574	0.468	0.712	0.611	0.488	0.712	0.468	0.244
J_{10}	x	0.568	0.493	0.453	0.589	0.537	0.462	0.589	0.453	0.137
J_{11}	-	0.036	0.027	0.023	0.037	0.029	0.024	0.037	0.023	0.014
J_{12}	x	0.002	0.001	0.002	0.002	0.001	0.002	0.002	0.001	0.001
J_{14}	-	0.001	0.000	0.000	0.000	0.000	0.000	0.001	0.000	0.001
J_{16}	-	24	24	24	24	24	24	24	24	0
J_{17}	-	13	13	13	13	13	13	13	13	0

Table B.8: Maximum values for all the performance criteria for the resettable-controlled structure with 5% added masses.

+5% Mass: Resettable										
Crit		15° Incidence			45° Incidence			Max	Min	Var
		El Centro	Mexico	Gebze	El Centro	Mexico	Gebze			
J_1	x	0.622	0.604	0.540	0.705	0.702	0.652	0.705	0.540	0.165
J_2	x	0.435	0.372	0.464	0.422	0.436	0.314	0.464	0.314	0.150
J_3	x	0.622	0.604	0.540	0.705	0.702	0.652	0.705	0.540	0.165
J_4	x	0.489	0.487	0.466	0.507	0.466	0.494	0.507	0.466	0.042
J_5	-	0.242	0.193	0.181	0.247	0.204	0.187	0.247	0.181	0.065
J_6	x	0.008	0.003	0.012	0.009	0.003	0.010	0.012	0.003	0.009
J_7	x	0.566	0.482	0.350	0.683	0.581	0.408	0.683	0.350	0.333
J_8	x	0.455	0.388	0.270	0.503	0.405	0.280	0.503	0.270	0.233
J_9	x	0.566	0.482	0.350	0.683	0.581	0.408	0.683	0.350	0.333
J_{10}	x	0.442	0.378	0.269	0.448	0.385	0.287	0.448	0.269	0.179
J_{11}	-	0.033	0.024	0.017	0.033	0.025	0.018	0.033	0.017	0.016
J_{12}	x	0.002	0.001	0.002	0.002	0.000	0.002	0.002	0.000	0.002
J_{14}	-	0.001	0.000	0.001	0.000	0.000	0.001	0.001	0.000	0.001
J_{16}	-	24	24	24	24	24	24	24	24	0
J_{17}	-	13	13	13	13	13	13	13	13	0

Table B.9: Maximum values for all the performance criteria for the resettable-controlled structure with 20% stiffness reduction.

-20% Stiffness: Resettable										
Crit		15° Incidence			45° Incidence			Max	Min	Var
		El Centro	Mexico	Gebze	El Centro	Mexico	Gebze			
J_1	x	0.787	0.845	0.764	0.795	0.936	0.809	0.936	0.764	0.172
J_2	x	0.522	0.582	0.845	1.131	0.635	0.564	1.131	0.522	0.609
J_3	x	0.787	0.845	0.764	0.795	0.936	0.809	0.936	0.764	0.172
J_4	x	0.716	0.684	0.513	0.787	0.585	0.755	0.787	0.513	0.274
J_5	-	0.310	0.338	0.284	0.333	0.308	0.294	0.338	0.284	0.054
J_6	x	0.011	0.004	0.020	0.011	0.004	0.016	0.020	0.004	0.016
J_7	x	0.768	0.878	0.973	0.791	0.881	1.015	1.015	0.768	0.247
J_8	x	0.624	0.655	0.508	0.691	0.630	0.499	0.691	0.499	0.192
J_9	x	0.768	0.878	0.973	0.791	0.881	1.015	1.015	0.768	0.247
J_{10}	x	0.617	0.663	0.493	0.649	0.642	0.520	0.663	0.493	0.170
J_{11}	-	0.046	0.049	0.051	0.046	0.047	0.054	0.054	0.046	0.008
J_{12}	x	0.002	0.001	0.002	0.002	0.001	0.002	0.002	0.001	0.001
J_{14}	-	0.002	0.001	0.001	0.001	0.000	0.001	0.002	0.000	0.002
J_{16}	-	24	24	24	24	24	24	24	24	0
J_{17}	-	13	13	13	13	13	13	13	13	0

Table B.10: Maximum values for all the performance criteria for the SAC-controlled nominal structure.

Nominal Structure: SAC										
Crit		15° Incidence			45° Incidence			Max	Min	Var
		El Centro	Mexico	Gebze	El Centro	Mexico	Gebze			
J_1	x	0.721	0.751	0.658	0.778	0.804	0.781	0.804	0.658	0.147
J_2	x	0.532	0.635	0.707	0.539	0.495	0.592	0.707	0.495	0.212
J_3	x	0.721	0.751	0.658	0.778	0.804	0.781	0.804	0.658	0.147
J_4	x	0.506	0.633	0.724	0.577	0.737	0.791	0.791	0.506	0.286
J_5	-	0.254	0.175	0.248	0.256	0.191	0.256	0.256	0.175	0.081
J_6	x	0.011	0.005	0.020	0.010	0.004	0.016	0.020	0.004	0.016
J_7	x	0.584	0.511	0.451	0.672	0.560	0.498	0.672	0.451	0.221
J_8	x	0.484	0.419	0.422	0.515	0.437	0.492	0.515	0.419	0.096
J_9	x	0.584	0.511	0.451	0.672	0.560	0.498	0.672	0.451	0.221
J_{10}	x	0.463	0.412	0.444	0.533	0.457	0.461	0.533	0.412	0.122
J_{11}	-	0.032	0.024	0.021	0.034	0.025	0.023	0.034	0.021	0.013
J_{12}	x	0.002	0.001	0.002	0.002	0.001	0.002	0.002	0.001	0.001
J_{14}	-	0.001	0.000	0.000	0.000	0.000	0.000	0.001	0.000	0.001
J_{16}	-	24	24	24	24	24	24	24	24	0
J_{17}	-	13	13	13	13	13	13	13	13	0

Table B.11: Maximum values for all the performance criteria for the SAC-controlled structure with 5% added masses.

+5% Mass: SAC										
Crit		15° Incidence			45° Incidence			Max	Min	Var
		El Centro	Mexico	Gebze	El Centro	Mexico	Gebze			
J_1	x	0.712	0.643	0.682	0.857	0.828	0.774	0.857	0.643	0.214
J_2	x	0.688	0.314	0.509	0.603	0.386	0.480	0.688	0.314	0.374
J_3	x	0.712	0.643	0.682	0.857	0.828	0.774	0.857	0.643	0.214
J_4	x	0.574	0.400	0.565	0.543	0.410	0.719	0.719	0.400	0.319
J_5	-	0.263	0.180	0.232	0.276	0.185	0.233	0.276	0.180	0.096
J_6	x	0.007	0.003	0.016	0.008	0.003	0.015	0.016	0.003	0.013
J_7	x	0.591	0.470	0.451	0.710	0.598	0.505	0.710	0.451	0.259
J_8	x	0.523	0.296	0.347	0.539	0.325	0.393	0.539	0.296	0.243
J_9	x	0.591	0.470	0.451	0.710	0.598	0.505	0.710	0.451	0.259
J_{10}	x	0.457	0.278	0.349	0.475	0.287	0.400	0.475	0.278	0.197
J_{11}	-	0.037	0.022	0.021	0.037	0.023	0.023	0.037	0.021	0.017
J_{12}	x	0.001	0.000	0.001	0.001	0.000	0.001	0.001	0.000	0.001
J_{14}	-	0.001	0.000	0.000	0.000	0.000	0.000	0.001	0.000	0.000
J_{16}	-	24	24	24	24	24	24	24	24	0
J_{17}	-	13	13	13	13	13	13	13	13	0

Table B.12: Maximum values for all the performance criteria for the SAC-controlled structure with 20% stiffness reduction.

-20% Stiffness: SAC										
Crit		15° Incidence			45° Incidence			Max	Min	Var
		El Centro	Mexico	Gebze	El Centro	Mexico	Gebze			
J_1	x	0.850	0.728	0.849	0.917	0.936	0.904	0.936	0.728	0.208
J_2	x	0.542	0.469	0.733	1.034	0.525	0.806	1.034	0.469	0.565
J_3	x	0.850	0.728	0.849	0.917	0.936	0.904	0.936	0.728	0.208
J_4	x	0.761	0.642	0.662	0.794	0.770	0.592	0.794	0.592	0.202
J_5	-	0.311	0.292	0.261	0.320	0.298	0.273	0.320	0.261	0.059
J_6	x	0.011	0.004	0.022	0.012	0.004	0.019	0.022	0.004	0.018
J_7	x	0.696	0.788	0.766	0.733	0.840	0.792	0.840	0.696	0.145
J_8	x	0.568	0.535	0.462	0.620	0.583	0.465	0.620	0.462	0.158
J_9	x	0.696	0.788	0.766	0.733	0.840	0.792	0.840	0.696	0.145
J_{10}	x	0.536	0.562	0.451	0.578	0.591	0.475	0.591	0.451	0.140
J_{11}	-	0.044	0.043	0.040	0.044	0.044	0.041	0.044	0.040	0.005
J_{12}	x	0.002	0.001	0.002	0.002	0.001	0.002	0.002	0.001	0.001
J_{14}	-	0.002	0.001	0.001	0.001	0.000	0.000	0.002	0.000	0.002
J_{16}	-	24	24	24	24	24	24	24	24	0
J_{17}	-	13	13	13	13	13	13	13	13	0

Table B.13: Maximum values for all the performance criteria for the neuro-fuzzy-controlled nominal structure.

Nominal Structure: Neuro-Fuzzy										
Crit		15° Incidence			45° Incidence			Max	Min	Var
		El Centro	Mexico	Gebze	El Centro	Mexico	Gebze			
J_1	x	0.742	0.572	0.651	0.709	0.604	0.621	0.742	0.572	0.170
J_2	x	0.737	0.343	0.660	0.454	0.286	0.406	0.737	0.286	0.451
J_3	x	0.742	0.572	0.651	0.709	0.604	0.621	0.742	0.572	0.170
J_4	x	0.477	0.326	0.597	0.565	0.332	0.564	0.597	0.326	0.270
J_5	-	0.261	0.144	0.219	0.249	0.152	0.215	0.261	0.144	0.117
J_6	x	0.010	0.002	0.014	0.009	0.002	0.010	0.014	0.002	0.012
J_7	x	0.611	0.363	0.433	0.658	0.415	0.411	0.658	0.363	0.295
J_8	x	0.499	0.248	0.403	0.468	0.235	0.364	0.499	0.235	0.264
J_9	x	0.611	0.363	0.433	0.658	0.415	0.411	0.658	0.363	0.295
J_{10}	x	0.478	0.222	0.425	0.488	0.227	0.353	0.488	0.222	0.266
J_{11}	-	0.032	0.018	0.021	0.031	0.019	0.019	0.032	0.018	0.013
J_{12}	x	0.002	0.001	0.002	0.002	0.001	0.002	0.002	0.001	0.001
J_{14}	-	0.001	0.000	0.000	0.000	0.000	0.000	0.001	0.000	0.001
J_{16}	-	24	24	24	24	24	24	24	24	0
J_{17}	-	26	26	26	26	26	26	26	26	0

Table B.14: Maximum values for all the performance criteria for the neuro-fuzzy-controlled structure with 5% added masses.

+5% Mass: Neuro-Fuzzy										
Crit		15° Incidence			45° Incidence			Max	Min	Var
		El Centro	Mexico	Gebze	El Centro	Mexico	Gebze			
J_1	x	0.606	0.364	0.300	0.739	0.616	0.404	0.739	0.300	0.439
J_2	x	0.659	0.472	0.199	0.686	0.489	0.160	0.686	0.160	0.527
J_3	x	0.606	0.364	0.300	0.739	0.616	0.404	0.739	0.300	0.439
J_4	x	0.553	0.286	0.198	0.436	0.374	0.294	0.553	0.198	0.355
J_5	-	0.264	0.287	0.112	0.273	0.285	0.113	0.287	0.112	0.175
J_6	x	0.005	0.002	0.005	0.007	0.002	0.005	0.007	0.002	0.005
J_7	x	0.536	0.392	0.234	0.635	0.478	0.294	0.635	0.234	0.401
J_8	x	0.566	0.379	0.154	0.549	0.405	0.156	0.566	0.154	0.412
J_9	x	0.536	0.392	0.234	0.635	0.478	0.294	0.635	0.234	0.401
J_{10}	x	0.378	0.211	0.129	0.358	0.225	0.127	0.378	0.127	0.252
J_{11}	-	0.044	0.033	0.013	0.043	0.032	0.014	0.044	0.013	0.031
J_{12}	x	0.001	0.001	0.001	0.001	0.001	0.001	0.001	0.001	0.001
J_{14}	-	0.001	0.001	0.000	0.000	0.000	0.000	0.001	0.000	0.001
J_{16}	-	24	24	24	24	24	24	24	24	0
J_{17}	-	26	26	26	26	26	26	26	26	0

Table B.15: Maximum values for all the performance criteria for the neuro-fuzzy-controlled structure with 20% stiffness reduction.

-20% Stiffness: Neuro-Fuzzy										
Crit		15° Incidence			45° Incidence			Max	Min	Var
		El Centro	Mexico	Gebze	El Centro	Mexico	Gebze			
J_1	x	0.793	0.767	0.816	0.836	1.051	0.780	1.051	0.767	0.284
J_2	x	0.538	0.431	0.597	1.214	0.506	0.558	1.214	0.431	0.782
J_3	x	0.793	0.767	0.816	0.836	1.051	0.780	1.051	0.767	0.284
J_4	x	0.761	0.624	0.521	0.752	0.705	0.524	0.761	0.521	0.241
J_5	-	0.334	0.461	0.297	0.390	0.605	0.297	0.605	0.297	0.308
J_6	x	0.010	0.003	0.016	0.010	0.002	0.012	0.016	0.002	0.014
J_7	x	1.122	1.231	1.034	1.365	1.651	1.129	1.651	1.034	0.617
J_8	x	0.725	0.567	0.493	0.862	0.758	0.458	0.862	0.458	0.405
J_9	x	1.122	1.231	1.034	1.365	1.651	1.129	1.651	1.034	0.617
J_{10}	x	0.669	0.524	0.487	0.737	0.656	0.451	0.737	0.451	0.286
J_{11}	-	0.090	0.086	0.055	0.116	0.116	0.061	0.116	0.055	0.062
J_{12}	x	0.002	0.001	0.002	0.002	0.001	0.002	0.002	0.001	0.001
J_{14}	-	0.002	0.001	0.000	0.001	0.001	0.001	0.002	0.000	0.001
J_{16}	-	24	24	24	24	24	24	24	24	0
J_{17}	-	26	26	26	26	26	26	26	26	0

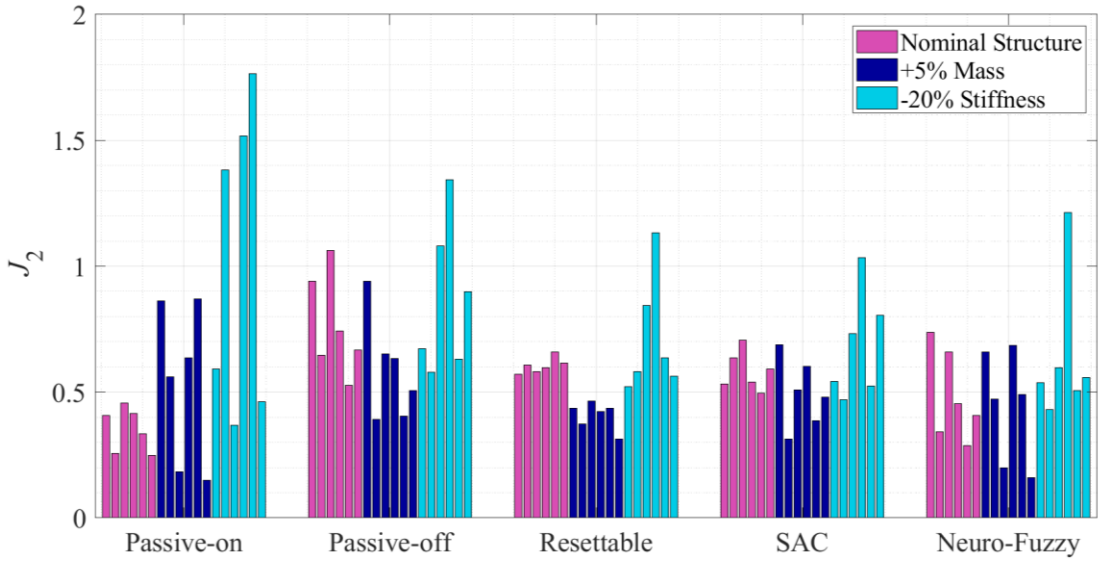

Fig. B.1: Maximum J_2 (peak deck shear) for the control schemes considering different parametric configurations and earthquake excitations.

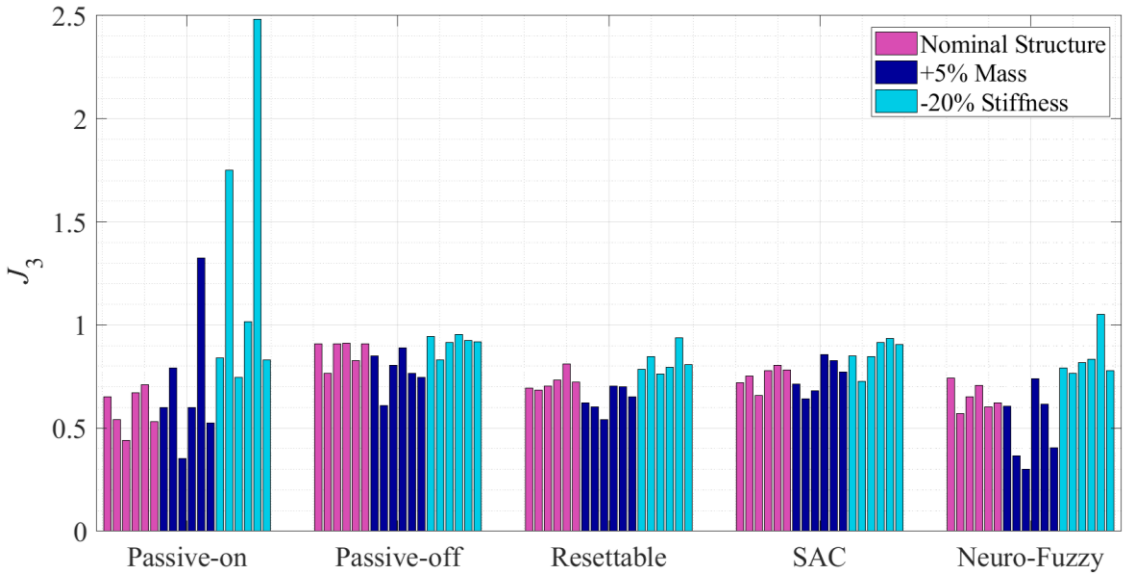

Fig. B.2: Maximum J_3 (peak base moment) for the control schemes considering different parametric configurations and earthquake excitations.

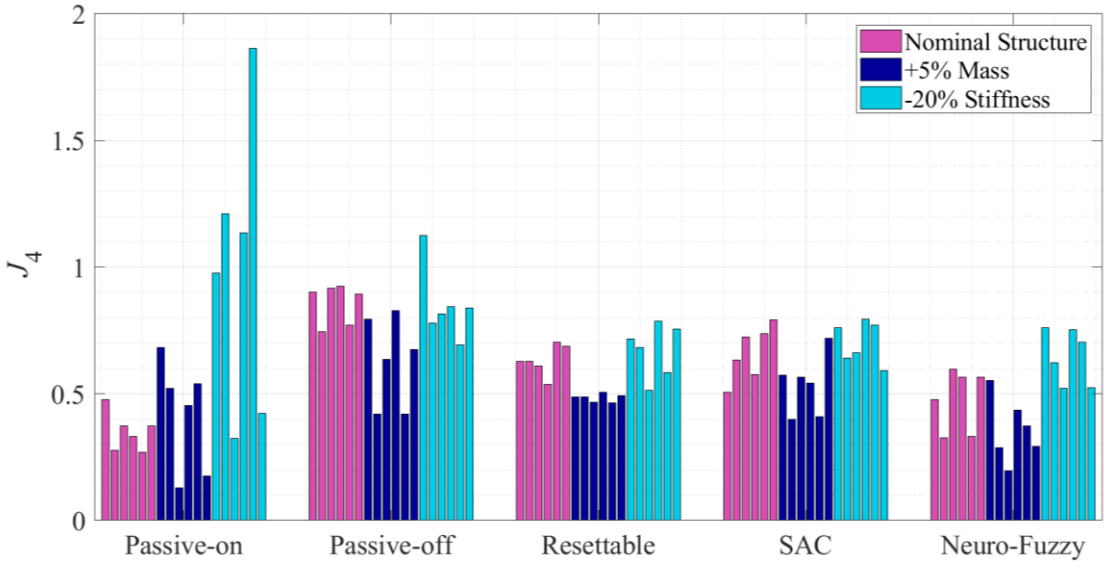

Fig. B.3: Maximum J_4 (peak deck moment) for the control schemes considering different parametric configurations and earthquake excitations.

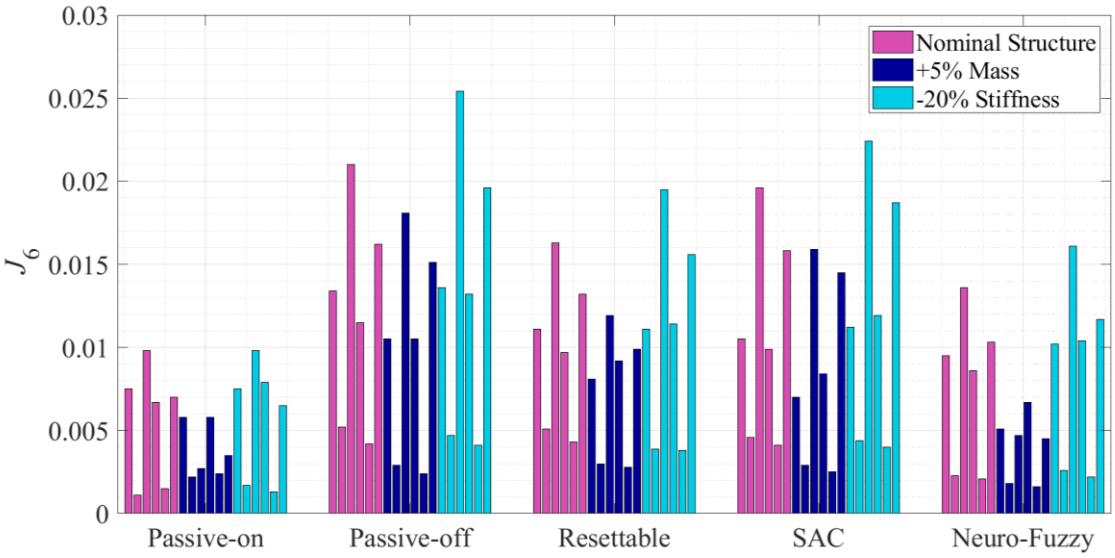

Fig. B.4: Maximum J_6 (peak abutment displacement) for the control schemes considering different parametric configurations and earthquake excitations.

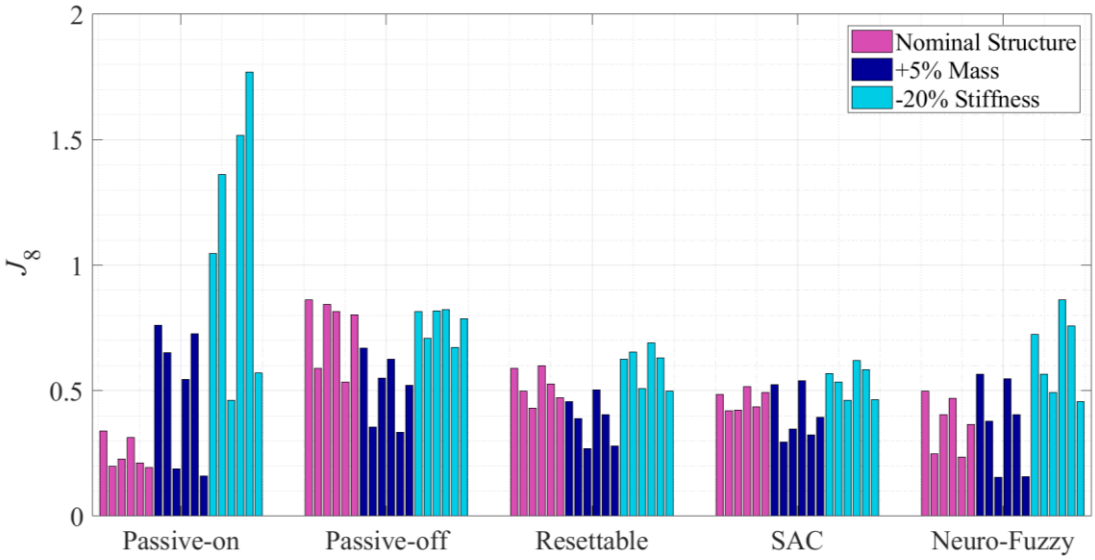

Fig. B.5: Maximum J_8 (normed deck shear) for the control schemes considering different parametric configurations and earthquake excitations.

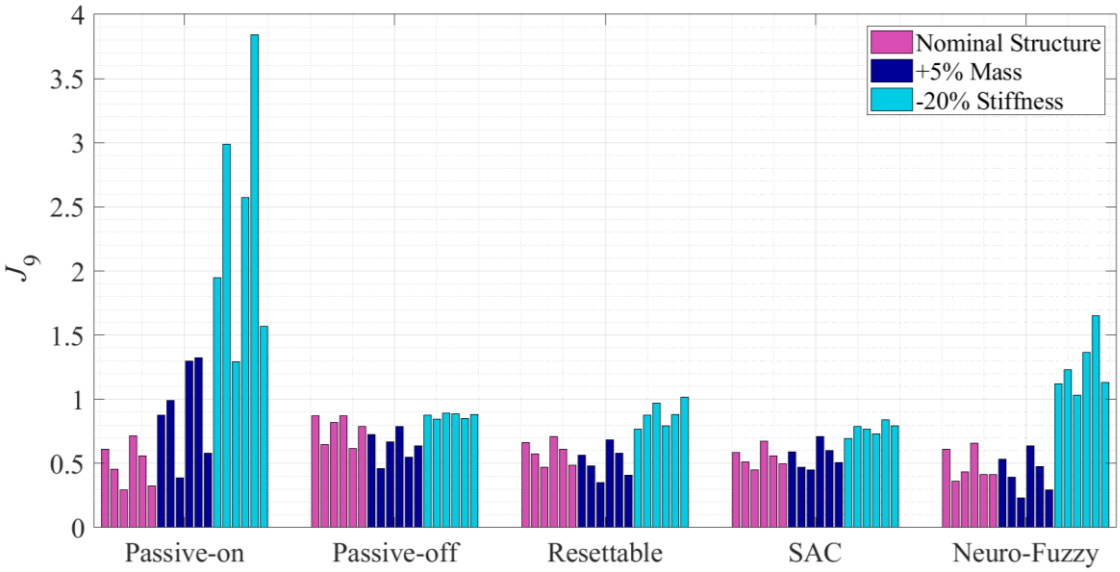

Fig. B.6: Maximum J_9 (normed base moment) for the control schemes considering different parametric configurations and earthquake excitations.

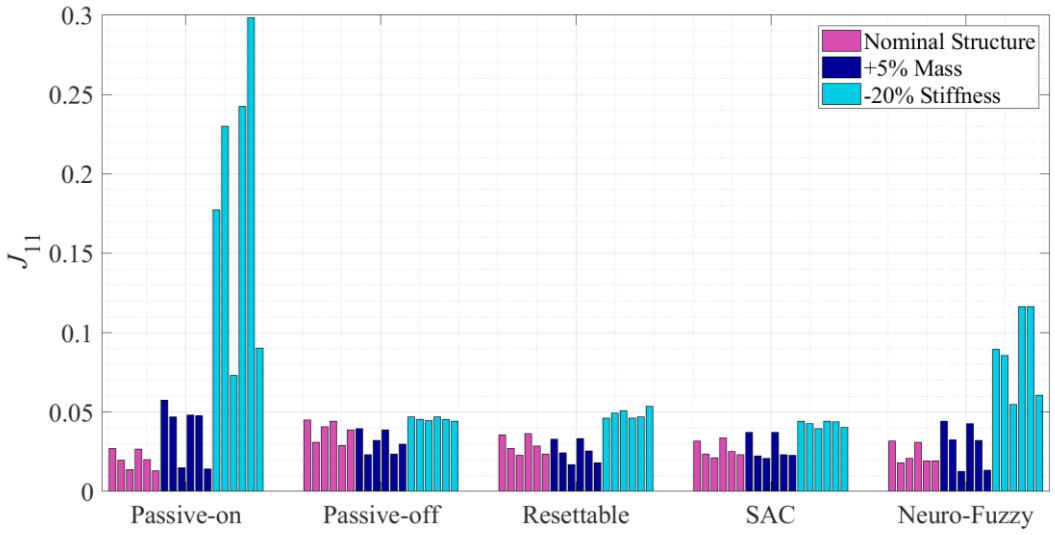

Fig. B.7: Maximum J_{11} (normed cable tension) for the control schemes considering different parametric configurations and earthquake excitations.

Cable-Stayed Bridge- Central US Earthquakes

Table B.16: Maximum values for all the performance criteria for the passive-on-controlled nominal structure.

Nominal Structure: Passive-on											
Crit.	Kipawa	Au Sable Forks	Val des Bois	Sullivan	Mineral	Sparks	Comal	Prairie Center	Green brier	Mt Carmel	Shady Grove
J_1	0.500	0.561	0.450	0.617	0.571	0.599	0.645	0.657	0.660	0.546	0.615
J_2	0.444	0.556	0.538	0.674	0.384	0.486	0.464	0.545	0.724	0.487	0.612
J_3	0.500	0.561	0.450	0.617	0.571	0.599	0.645	0.657	0.660	0.546	0.615
J_4	0.518	0.440	0.560	0.701	0.412	0.545	0.402	0.534	0.544	0.498	0.415
J_5	0.214	0.209	0.183	0.239	0.171	0.164	0.183	0.215	0.187	0.186	0.193
J_6	0.020	0.039	0.027	0.025	0.023	0.034	0.024	0.028	0.024	0.025	0.027
J_7	0.422	0.420	0.395	0.424	0.401	0.378	0.501	0.424	0.439	0.359	0.432
J_8	0.307	0.327	0.372	0.373	0.350	0.347	0.445	0.449	0.442	0.286	0.409
J_9	0.422	0.420	0.395	0.424	0.401	0.378	0.501	0.424	0.439	0.359	0.432
J_{10}	0.355	0.336	0.330	0.413	0.349	0.363	0.385	0.416	0.400	0.344	0.368
J_{11}	0.020	0.019	0.018	0.022	0.019	0.017	0.024	0.020	0.022	0.017	0.022
J_{12}	0.002	0.002	0.002	0.002	0.002	0.002	0.002	0.002	0.002	0.002	0.002
J_{14}	0.0004	0.0004	0.0005	0.0006	0.0004	0.0004	0.0005	0.0005	0.0004	0.0005	0.0007
J_{16}	24	24	24	24	24	24	24	24	24	24	24
J_{17}	0	0	0	0	0	0	0	0	0	0	0

Table B.17: Maximum values for all the performance criteria for the passive-on-controlled structure with 5% added masses.

+5% Mass: Passive-on											
Crit.	Kipawa	Au Sable Forks	Val des Bois	Sullivan	Mineral	Sparks	Comal	Prairie Center	Green brier	Mt Carmel	Shady Grove
J_1	0.503	0.342	0.358	0.385	0.359	0.463	0.510	0.649	0.499	0.620	0.462
J_2	0.323	0.395	0.341	0.245	0.328	0.227	0.407	0.214	0.339	0.685	0.337
J_3	0.503	0.342	0.358	0.385	0.359	0.463	0.510	0.649	0.499	0.620	0.462
J_4	0.250	0.279	0.226	0.220	0.316	0.325	0.307	0.297	0.185	0.346	0.267
J_5	0.211	0.174	0.158	0.155	0.145	0.161	0.186	0.147	0.184	0.151	0.184
J_6	0.010	0.027	0.013	0.014	0.016	0.013	0.013	0.011	0.012	0.018	0.011
J_7	0.581	0.444	0.435	0.432	0.436	0.401	0.500	0.536	0.445	0.485	0.498
J_8	0.306	0.268	0.211	0.266	0.251	0.248	0.328	0.202	0.242	0.263	0.342
J_9	0.581	0.444	0.435	0.432	0.436	0.401	0.500	0.536	0.445	0.485	0.498
J_{10}	0.230	0.192	0.150	0.203	0.195	0.155	0.210	0.152	0.168	0.171	0.222
J_{11}	0.025	0.019	0.016	0.019	0.019	0.018	0.028	0.016	0.022	0.016	0.029
J_{12}	0.002	0.002	0.002	0.002	0.002	0.002	0.002	0.002	0.002	0.002	0.002
J_{14}	0.0006	0.0004	0.0006	0.0009	0.0005	0.0005	0.0006	0.0008	0.0006	0.0008	0.0009
J_{16}	24	24	24	24	24	24	24	24	24	24	24
J_{17}	0	0	0	0	0	0	0	0	0	0	0

Table B.18: Maximum values for all the performance criteria for the passive-on-controlled structure with 20% stiffness reduction.

-20% Stiffness: Passive-on											
Crit.	Kipawa	Au Sable Forks	Val des Bois	Sullivan	Mineral	Sparks	Comal	Prairie Center	Green brier	Mt Carmel	Shady Grove
J_1	1.005	0.875	0.850	0.774	0.630	0.635	0.670	0.414	0.872	0.777	1.038
J_2	0.761	0.476	0.321	0.466	0.399	0.574	0.531	0.955	0.454	0.365	0.650
J_3	1.005	0.875	0.850	0.774	0.630	0.635	0.670	0.414	0.872	0.777	1.038
J_4	0.595	0.745	0.634	0.672	0.495	0.467	0.463	0.464	0.447	0.448	1.338
J_5	0.408	0.327	0.302	0.279	0.246	0.251	0.308	0.199	0.286	0.290	0.284
J_6	0.028	0.045	0.031	0.041	0.031	0.034	0.018	0.033	0.023	0.025	0.034
J_7	1.413	1.023	1.237	1.179	0.844	1.089	0.803	1.027	1.393	1.399	0.876
J_8	0.757	0.525	0.482	0.548	0.463	0.536	0.470	0.505	0.592	0.574	0.467
J_9	1.413	1.023	1.237	1.179	0.844	1.089	0.803	1.027	1.393	1.399	0.876
J_{10}	0.687	0.513	0.497	0.493	0.462	0.507	0.433	0.408	0.515	0.519	0.485
J_{11}	0.086	0.059	0.071	0.067	0.048	0.061	0.048	0.062	0.081	0.078	0.049
J_{12}	0.002	0.002	0.002	0.002	0.002	0.002	0.002	0.002	0.002	0.002	0.002
J_{14}	0.001	0.002	0.002	0.002	0.002	0.001	0.001	0.001	0.002	0.001	0.001
J_{16}	24	24	24	24	24	24	24	24	24	24	24
J_{17}	0	0	0	0	0	0	0	0	0	0	0

Table B.19: Maximum values for all the performance criteria for the passive-off-controlled nominal structure.

Nominal Structure: Passive-off											
Crit.	Kipawa	Au Sable Forks	Val des Bois	Sullivan	Mineral	Sparks	Comal	Prairie Center	Green brier	Mt Carmel	Shady Grove
J_1	0.901	0.897	0.928	0.930	0.951	0.928	0.946	0.966	0.922	0.922	0.950
J_2	1.030	0.753	0.869	0.939	0.773	0.821	0.858	1.071	1.206	0.809	0.861
J_3	0.901	0.897	0.928	0.930	0.951	0.928	0.946	0.966	0.922	0.922	0.950
J_4	0.738	0.850	0.964	1.264	1.062	0.990	0.878	0.903	0.941	0.796	1.017
J_5	0.325	0.316	0.309	0.323	0.308	0.307	0.305	0.323	0.321	0.308	0.318
J_6	0.039	0.061	0.054	0.042	0.057	0.055	0.045	0.057	0.034	0.044	0.053
J_7	0.878	0.879	0.895	0.882	0.894	0.865	0.902	0.897	0.886	0.861	0.882
J_8	0.849	0.796	0.891	0.840	0.882	0.844	0.890	0.995	0.888	0.828	0.862
J_9	0.878	0.879	0.895	0.882	0.894	0.865	0.902	0.897	0.886	0.861	0.882
J_{10}	0.839	0.839	0.875	0.914	0.885	0.896	0.899	0.946	0.897	0.873	0.871
J_{11}	0.044	0.044	0.045	0.044	0.045	0.043	0.046	0.045	0.044	0.043	0.044
J_{12}	0.0003	0.0003	0.0003	0.0003	0.0003	0.0003	0.0003	0.0004	0.0003	0.0003	0.0003
J_{14}	0.0001	0.0001	0.0001	0.0001	0.0001	0.0001	0.0001	0.0001	0.0001	0.0001	0.0002
J_{16}	24	24	24	24	24	24	24	24	24	24	24
J_{17}	0	0	0	0	0	0	0	0	0	0	0

Table B.20: Maximum values for all the performance criteria for the passive-off-controlled structure with 5% added masses.

+5% Mass: Passive-off											
Crit.	Kipawa	Au Sable Forks	Val des Bois	Sullivan	Mineral	Sparks	Comal	Prairie Center	Green brier	Mt Carmel	Shady Grove
J_1	0.929	0.793	0.792	0.905	0.781	0.813	0.784	0.973	0.800	0.850	0.885
J_2	0.838	0.723	0.801	0.530	0.918	0.661	0.686	0.635	0.869	0.749	0.910
J_3	0.929	0.793	0.792	0.905	0.781	0.813	0.784	0.973	0.800	0.850	0.885
J_4	0.890	0.926	0.826	0.684	0.889	0.850	0.764	0.656	0.665	0.889	0.733
J_5	0.318	0.262	0.276	0.279	0.251	0.282	0.258	0.276	0.253	0.273	0.328
J_6	0.037	0.054	0.047	0.047	0.035	0.037	0.034	0.043	0.039	0.034	0.038
J_7	0.751	0.743	0.741	0.688	0.707	0.730	0.726	0.707	0.661	0.667	0.823
J_8	0.725	0.668	0.684	0.592	0.645	0.750	0.694	0.693	0.685	0.628	0.818
J_9	0.751	0.743	0.741	0.688	0.707	0.730	0.726	0.707	0.661	0.667	0.823
J_{10}	0.744	0.703	0.674	0.667	0.664	0.758	0.668	0.707	0.648	0.642	0.759
J_{11}	0.037	0.037	0.036	0.033	0.035	0.038	0.037	0.034	0.033	0.033	0.042
J_{12}	0.0003	0.0003	0.0003	0.0003	0.0003	0.0003	0.0003	0.0003	0.0003	0.0003	0.0003
J_{14}	0.0001	0.0001	0.0001	0.0001	0.0001	0.0001	0.0001	0.0001	0.0001	0.0001	0.0001
J_{16}	24	24	24	24	24	24	24	24	24	24	24
J_{17}	0	0	0	0	0	0	0	0	0	0	0

Table B.21: Maximum values for all the performance criteria for the passive-off-controlled structure with 20% stiffness reduction.

-20% Stiffness: Passive-off											
Crit.	Kipawa	Au Sable Forks	Val des Bois	Sullivan	Mineral	Sparks	Comal	Prairie Center	Green brier	Mt Carmel	Shady Grove
J_1	0.948	0.972	0.952	0.967	0.979	0.949	0.935	0.957	0.944	0.962	1.050
J_2	1.219	0.720	1.303	0.799	0.993	1.153	0.846	1.106	1.075	0.736	1.059
J_3	0.948	0.972	0.952	0.967	0.979	0.949	0.935	0.957	0.944	0.962	1.050
J_4	1.139	1.088	1.111	0.918	1.062	1.025	0.852	0.788	0.889	0.879	1.120
J_5	0.329	0.330	0.319	0.323	0.332	0.327	0.328	0.320	0.318	0.325	0.317
J_6	0.040	0.059	0.061	0.066	0.045	0.052	0.042	0.060	0.044	0.040	0.040
J_7	0.932	0.945	0.937	0.909	0.935	0.937	0.911	0.912	0.912	0.923	0.921
J_8	0.952	0.863	0.826	0.887	0.875	0.963	0.875	0.855	0.876	0.829	0.890
J_9	0.932	0.945	0.937	0.909	0.935	0.937	0.911	0.912	0.912	0.923	0.921
J_{10}	0.961	0.887	0.886	0.845	0.927	0.922	0.861	0.889	0.862	0.856	0.911
J_{11}	0.047	0.048	0.047	0.046	0.047	0.047	0.046	0.046	0.046	0.046	0.046
J_{12}	0.0003	0.0003	0.0003	0.0003	0.0003	0.0003	0.0003	0.0003	0.0003	0.0003	0.0003
J_{14}	0.0001	0.0001	0.0001	0.0002	0.0001	0.0001	0.0001	0.0001	0.0001	0.0001	0.0001
J_{16}	24	24	24	24	24	24	24	24	24	24	24
J_{17}	0	0	0	0	0	0	0	0	0	0	0

Table B.22: Maximum values for all the performance criteria for the resettable-controlled nominal structure.

Nominal Structure: Resettable											
Crit.	Kipawa	Au Sable Forks	Val des Bois	Sullivan	Mineral	Sparks	Comal	Prairie Center	Green brier	Mt Carmel	Shady Grove
J_1	0.704	0.650	0.554	0.767	0.736	0.685	0.689	0.756	0.905	0.664	0.690
J_2	0.645	0.732	0.699	0.996	0.557	0.494	0.690	0.832	1.009	0.578	0.565
J_3	0.704	0.650	0.554	0.767	0.736	0.685	0.689	0.756	0.905	0.664	0.690
J_4	0.726	0.667	0.756	0.792	0.742	0.685	0.549	0.689	0.772	0.536	0.583
J_5	0.270	0.255	0.225	0.278	0.218	0.179	0.199	0.249	0.241	0.221	0.226
J_6	0.030	0.047	0.032	0.034	0.036	0.040	0.028	0.037	0.027	0.030	0.033
J_7	0.565	0.526	0.503	0.568	0.542	0.478	0.624	0.554	0.544	0.477	0.529
J_8	0.539	0.486	0.534	0.558	0.544	0.494	0.620	0.592	0.580	0.469	0.498
J_9	0.565	0.526	0.503	0.568	0.542	0.478	0.624	0.554	0.544	0.477	0.529
J_{10}	0.564	0.519	0.488	0.538	0.530	0.501	0.574	0.600	0.531	0.482	0.512
J_{11}	0.027	0.025	0.025	0.028	0.027	0.024	0.030	0.028	0.028	0.024	0.026
J_{12}	0.002	0.002	0.002	0.002	0.002	0.002	0.002	0.002	0.002	0.002	0.002
J_{14}	0.0006	0.0004	0.0005	0.0006	0.0004	0.0004	0.0004	0.0005	0.0004	0.0005	0.0007
J_{16}	24	24	24	24	24	24	24	24	24	24	24
J_{17}	13	13	13	13	13	13	13	13	13	13	13

Table B.23: Maximum values for all the performance criteria for the resettable-controlled structure with 5% added masses.

+5% Mass: Resettable											
Crit.	Kipawa	Au Sable Forks	Val des Bois	Sullivan	Mineral	Sparks	Comal	Prairie Center	Green brier	Mt Carmel	Shady Grove
J_1	0.562	0.385	0.454	0.557	0.435	0.652	0.507	0.791	0.513	0.541	0.585
J_2	0.208	0.325	0.334	0.392	0.485	0.443	0.367	0.364	0.424	0.387	0.473
J_3	0.562	0.385	0.454	0.557	0.435	0.652	0.507	0.791	0.513	0.541	0.585
J_4	0.343	0.451	0.391	0.427	0.498	0.494	0.421	0.431	0.350	0.333	0.428
J_5	0.229	0.189	0.171	0.187	0.178	0.181	0.189	0.178	0.169	0.175	0.180
J_6	0.018	0.028	0.021	0.026	0.023	0.025	0.019	0.023	0.018	0.019	0.025
J_7	0.474	0.461	0.384	0.363	0.402	0.404	0.478	0.430	0.365	0.362	0.474
J_8	0.301	0.297	0.283	0.331	0.314	0.427	0.400	0.330	0.321	0.343	0.394
J_9	0.474	0.461	0.384	0.363	0.402	0.404	0.478	0.430	0.365	0.362	0.474
J_{10}	0.322	0.294	0.264	0.305	0.305	0.366	0.353	0.309	0.307	0.289	0.395
J_{11}	0.023	0.021	0.018	0.017	0.020	0.022	0.026	0.017	0.020	0.019	0.025
J_{12}	0.002	0.002	0.002	0.002	0.002	0.002	0.002	0.002	0.002	0.002	0.002
J_{14}	0.0005	0.0003	0.0007	0.0006	0.0004	0.0004	0.0004	0.0005	0.0003	0.0006	0.0006
J_{16}	24	24	24	24	24	24	24	24	24	24	24
J_{17}	13	13	13	13	13	13	13	13	13	13	13

Table B.24: Maximum values for all the performance criteria for the resettable-controlled structure with 20% stiffness reduction.

-20% Stiffness: Resettable											
Crit.	Kipawa	Au Sable Forks	Val des Bois	Sullivan	Mineral	Sparks	Comal	Prairie Center	Green brier	Mt Carmel	Shady Grove
J_1	0.859	0.809	0.791	0.875	0.856	0.802	0.666	0.746	0.789	0.929	1.138
J_2	0.712	0.632	0.420	0.522	0.611	0.779	0.556	0.672	0.470	0.562	0.899
J_3	0.859	0.809	0.791	0.875	0.856	0.802	0.666	0.746	0.789	0.929	1.138
J_4	0.715	0.804	0.569	0.773	0.680	0.537	0.483	0.592	0.486	0.618	1.444
J_5	0.298	0.296	0.268	0.306	0.312	0.311	0.267	0.277	0.238	0.319	0.310
J_6	0.030	0.049	0.038	0.048	0.036	0.038	0.025	0.040	0.025	0.026	0.042
J_7	0.759	0.757	0.765	0.865	0.738	0.748	0.709	0.727	0.677	0.882	0.811
J_8	0.644	0.534	0.450	0.484	0.569	0.618	0.548	0.513	0.459	0.577	0.554
J_9	0.759	0.757	0.765	0.865	0.738	0.748	0.709	0.727	0.677	0.882	0.811
J_{10}	0.657	0.563	0.506	0.526	0.581	0.603	0.537	0.529	0.438	0.579	0.615
J_{11}	0.040	0.040	0.041	0.045	0.039	0.038	0.038	0.038	0.035	0.044	0.042
J_{12}	0.002	0.002	0.002	0.002	0.002	0.002	0.002	0.002	0.002	0.002	0.002
J_{14}	0.0006	0.0008	0.0006	0.0007	0.0006	0.0005	0.0004	0.0004	0.0010	0.0008	0.0007
J_{16}	24	24	24	24	24	24	24	24	24	24	24
J_{17}	13	13	13	13	13	13	13	13	13	13	13

Table B.25: Maximum values for all the performance criteria for the SAC-controlled nominal structure.

Nominal Structure: SAC											
Crit.	Kipawa	Au Sable Forks	Val des Bois	Sullivan	Mineral	Sparks	Comal	Prairie Center	Green brier	Mt Carmel	Shady Grove
J_1	0.622	0.585	0.532	0.722	0.614	0.588	0.642	0.713	0.706	0.608	0.667
J_2	0.503	0.576	0.528	0.691	0.323	0.512	0.540	0.677	1.041	0.559	0.477
J_3	0.622	0.585	0.532	0.722	0.614	0.588	0.642	0.713	0.706	0.608	0.667
J_4	0.643	0.650	0.452	0.903	0.546	0.575	0.424	0.529	0.544	0.597	0.570
J_5	0.227	0.201	0.192	0.278	0.198	0.153	0.179	0.222	0.194	0.220	0.194
J_6	0.023	0.041	0.026	0.030	0.027	0.034	0.025	0.030	0.026	0.030	0.030
J_7	0.434	0.428	0.402	0.533	0.426	0.384	0.514	0.463	0.449	0.439	0.465
J_8	0.366	0.358	0.388	0.516	0.380	0.359	0.439	0.527	0.481	0.410	0.448
J_9	0.434	0.428	0.402	0.533	0.426	0.384	0.514	0.463	0.449	0.439	0.465
J_{10}	0.397	0.397	0.354	0.539	0.392	0.395	0.402	0.440	0.427	0.457	0.454
J_{11}	0.021	0.019	0.020	0.027	0.021	0.018	0.024	0.022	0.023	0.021	0.023
J_{12}	0.002	0.002	0.002	0.002	0.002	0.002	0.002	0.002	0.002	0.002	0.002
J_{14}	0.0005	0.0004	0.0006	0.0008	0.0004	0.0004	0.0005	0.0004	0.0004	0.0004	0.0007
J_{16}	24	24	24	24	24	24	24	24	24	24	24
J_{17}	13	13	13	13	13	13	13	13	13	13	13

Table B.26: Maximum values for all the performance criteria for the SAC-controlled structure with 5% added masses.

+5% Mass: SAC											
Crit.	Kipawa	Au Sable Forks	Val des Bois	Sullivan	Mineral	Sparks	Comal	Prairie Center	Green brier	Mt Carmel	Shady Grove
J_1	0.502	0.361	0.384	0.525	0.394	0.506	0.550	0.720	0.385	0.609	0.561
J_2	0.252	0.569	0.309	0.325	0.431	0.291	0.295	0.256	0.482	0.516	0.505
J_3	0.502	0.361	0.384	0.525	0.394	0.506	0.550	0.720	0.385	0.609	0.561
J_4	0.418	0.283	0.222	0.308	0.268	0.340	0.379	0.349	0.230	0.505	0.410
J_5	0.188	0.182	0.132	0.186	0.138	0.194	0.168	0.148	0.162	0.173	0.160
J_6	0.014	0.020	0.013	0.016	0.020	0.017	0.012	0.017	0.017	0.016	0.018
J_7	0.489	0.427	0.361	0.383	0.402	0.339	0.479	0.405	0.332	0.394	0.474
J_8	0.298	0.282	0.232	0.297	0.257	0.283	0.319	0.237	0.268	0.309	0.422
J_9	0.489	0.427	0.361	0.383	0.402	0.339	0.479	0.405	0.332	0.394	0.474
J_{10}	0.263	0.225	0.180	0.274	0.215	0.243	0.248	0.230	0.195	0.292	0.340
J_{11}	0.022	0.019	0.015	0.020	0.018	0.017	0.026	0.016	0.019	0.020	0.026
J_{12}	0.002	0.002	0.002	0.002	0.002	0.002	0.002	0.002	0.002	0.002	0.002
J_{14}	0.0008	0.0004	0.0005	0.0010	0.0006	0.0006	0.0005	0.0009	0.0006	0.0008	0.0012
J_{16}	24	24	24	24	24	24	24	24	24	24	24
J_{17}	13	13	13	13	13	13	13	13	13	13	13

Table B.27: Maximum values for all the performance criteria for the SAC-controlled structure with 20% stiffness reduction.

-20% Stiffness: SAC											
Crit.	Kipawa	Au Sable Forks	Val des Bois	Sullivan	Mineral	Sparks	Comal	Prairie Center	Green brier	Mt Carmel	Shady Grove
J_1	0.749	0.772	0.700	0.814	0.796	0.719	0.595	0.654	0.739	0.898	1.003
J_2	0.981	0.628	0.482	0.527	0.442	0.581	0.575	0.770	0.446	0.506	0.502
J_3	0.749	0.772	0.700	0.814	0.796	0.719	0.595	0.654	0.739	0.898	1.003
J_4	0.557	1.098	0.530	0.773	0.577	0.469	0.438	0.568	0.403	0.662	1.023
J_5	0.299	0.286	0.259	0.300	0.308	0.294	0.264	0.260	0.232	0.309	0.274
J_6	0.027	0.044	0.033	0.046	0.032	0.034	0.022	0.034	0.022	0.024	0.036
J_7	0.825	0.765	0.814	1.064	0.707	0.845	0.704	0.973	0.948	1.151	0.784
J_8	0.597	0.481	0.395	0.516	0.432	0.539	0.444	0.470	0.442	0.575	0.436
J_9	0.825	0.765	0.814	1.064	0.707	0.845	0.704	0.973	0.948	1.151	0.784
J_{10}	0.546	0.524	0.438	0.547	0.458	0.512	0.420	0.471	0.420	0.581	0.487
J_{11}	0.047	0.042	0.045	0.059	0.038	0.046	0.040	0.055	0.054	0.062	0.043
J_{12}	0.002	0.002	0.002	0.002	0.002	0.002	0.002	0.002	0.002	0.002	0.002
J_{14}	0.0011	0.0014	0.0011	0.0007	0.0012	0.0008	0.0007	0.0005	0.0012	0.0008	0.0012
J_{16}	24	24	24	24	24	24	24	24	24	24	24
J_{17}	13	13	13	13	13	13	13	13	13	13	13

Table B.28: Maximum values for all the performance criteria for the neuro-fuzzy-controlled nominal structure.

Nominal Structure: Neuro-Fuzzy											
Crit.	Kipawa	Au Sable Forks	Val des Bois	Sullivan	Mineral	Sparks	Comal	Prairie Center	Green brier	Mt Carmel	Shady Grove
J_1	0.650	0.685	0.548	0.693	0.700	0.673	0.727	0.734	0.744	0.632	0.695
J_2	0.716	0.718	0.719	0.825	0.386	0.594	0.547	0.815	0.860	0.577	0.565
J_3	0.650	0.685	0.548	0.693	0.700	0.673	0.727	0.734	0.744	0.632	0.695
J_4	0.524	0.573	0.726	0.729	0.619	0.985	0.579	0.757	0.941	0.569	0.613
J_5	0.256	0.240	0.210	0.264	0.208	0.170	0.196	0.244	0.242	0.215	0.221
J_6	0.026	0.048	0.030	0.030	0.032	0.040	0.029	0.036	0.027	0.029	0.032
J_7	0.506	0.516	0.503	0.514	0.516	0.462	0.603	0.531	0.550	0.468	0.532
J_8	0.511	0.475	0.523	0.501	0.488	0.451	0.580	0.570	0.591	0.448	0.508
J_9	0.506	0.516	0.503	0.514	0.516	0.462	0.603	0.531	0.550	0.468	0.532
J_{10}	0.480	0.461	0.491	0.501	0.501	0.491	0.544	0.563	0.551	0.475	0.528
J_{11}	0.025	0.025	0.025	0.026	0.026	0.022	0.030	0.026	0.028	0.023	0.026
J_{12}	0.002	0.002	0.002	0.002	0.002	0.002	0.002	0.002	0.002	0.002	0.002
J_{14}	0.0003	0.0003	0.0004	0.0006	0.0004	0.0004	0.0003	0.0004	0.0004	0.0004	0.0006
J_{16}	24	24	24	24	24	24	24	24	24	24	24
J_{17}	26	26	26	26	26	26	26	26	26	26	26

Table B.29: Maximum values for all the performance criteria for the neuro-fuzzy-controlled structure with 5% added masses.

+5% Mass: Neuro-Fuzzy											
Crit.	Kipawa	Au Sable Forks	Val des Bois	Sullivan	Mineral	Sparks	Comal	Prairie Center	Green brier	Mt Carmel	Shady Grove
J_1	0.618	0.383	0.414	0.450	0.339	0.555	0.512	0.632	0.471	0.643	0.489
J_2	0.346	0.596	0.428	0.364	0.349	0.303	0.379	0.255	0.384	0.387	0.392
J_3	0.618	0.383	0.414	0.450	0.339	0.555	0.512	0.632	0.471	0.643	0.489
J_4	0.336	0.291	0.245	0.268	0.258	0.381	0.371	0.339	0.278	0.381	0.483
J_5	0.263	0.183	0.154	0.164	0.136	0.140	0.178	0.179	0.150	0.173	0.160
J_6	0.013	0.028	0.017	0.014	0.016	0.015	0.014	0.014	0.017	0.017	0.016
J_7	0.465	0.430	0.374	0.335	0.368	0.322	0.478	0.395	0.327	0.320	0.425
J_8	0.321	0.300	0.246	0.269	0.257	0.276	0.337	0.253	0.250	0.219	0.357
J_9	0.465	0.430	0.374	0.335	0.368	0.322	0.478	0.395	0.327	0.320	0.425
J_{10}	0.277	0.216	0.210	0.213	0.218	0.238	0.271	0.209	0.205	0.207	0.306
J_{11}	0.024	0.019	0.016	0.016	0.017	0.017	0.026	0.016	0.018	0.016	0.024
J_{12}	0.002	0.002	0.002	0.002	0.002	0.002	0.002	0.002	0.002	0.002	0.002
J_{14}	0.0005	0.0003	0.0004	0.0007	0.0003	0.0003	0.0003	0.0005	0.0004	0.0006	0.0004
J_{16}	24	24	24	24	24	24	24	24	24	24	24
J_{17}	26	26	26	26	26	26	26	26	26	26	26

Table B.30: Maximum values for all the performance criteria for the neuro-fuzzy-controlled structure with 20% stiffness reduction.

-20% Stiffness: Neuro-Fuzzy											
Crit.	Kipawa	Au Sable Forks	Val des Bois	Sullivan	Mineral	Sparks	Comal	Prairie Center	Green brier	Mt Carmel	Shady Grove
J_1	0.877	0.885	0.740	0.830	0.892	0.825	0.698	0.666	0.832	0.869	1.067
J_2	0.858	0.927	0.703	0.728	0.618	0.691	0.584	0.725	0.727	0.520	0.687
J_3	0.877	0.885	0.740	0.830	0.892	0.825	0.698	0.666	0.832	0.869	1.067
J_4	0.760	0.735	0.574	0.889	0.699	0.566	0.704	0.608	0.514	0.555	1.203
J_5	0.333	0.322	0.278	0.295	0.334	0.328	0.325	0.267	0.287	0.308	0.302
J_6	0.030	0.051	0.040	0.047	0.036	0.037	0.023	0.038	0.027	0.022	0.040
J_7	0.939	0.879	0.844	0.957	0.825	0.872	0.791	0.863	0.962	1.079	0.850
J_8	0.601	0.580	0.502	0.526	0.580	0.638	0.536	0.544	0.551	0.572	0.520
J_9	0.939	0.879	0.844	0.957	0.825	0.872	0.791	0.863	0.962	1.079	0.850
J_{10}	0.663	0.601	0.535	0.537	0.592	0.629	0.532	0.512	0.538	0.537	0.595
J_{11}	0.052	0.048	0.045	0.051	0.044	0.045	0.045	0.047	0.053	0.056	0.045
J_{12}	0.002	0.002	0.002	0.002	0.002	0.002	0.002	0.002	0.002	0.002	0.002
J_{14}	0.0006	0.0012	0.0005	0.0007	0.0005	0.0005	0.0004	0.0003	0.0011	0.0007	0.0007
J_{16}	24	24	24	24	24	24	24	24	24	24	24
J_{17}	26	26	26	26	26	26	26	26	26	26	26

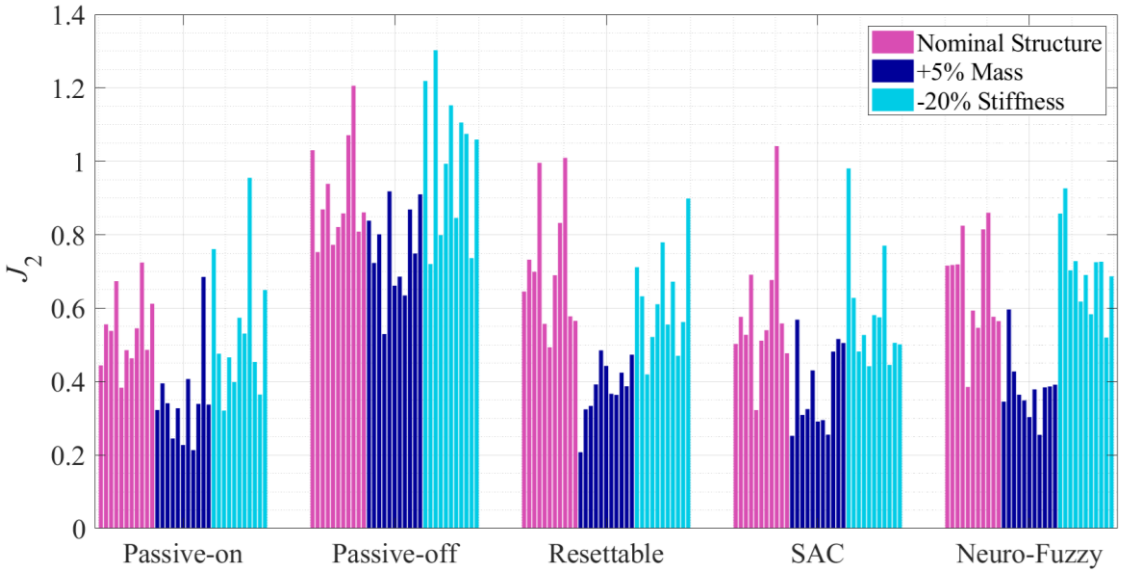

Fig. B.8: Maximum J_2 (peak deck shear) for the control schemes considering different parametric configurations and earthquake excitations.

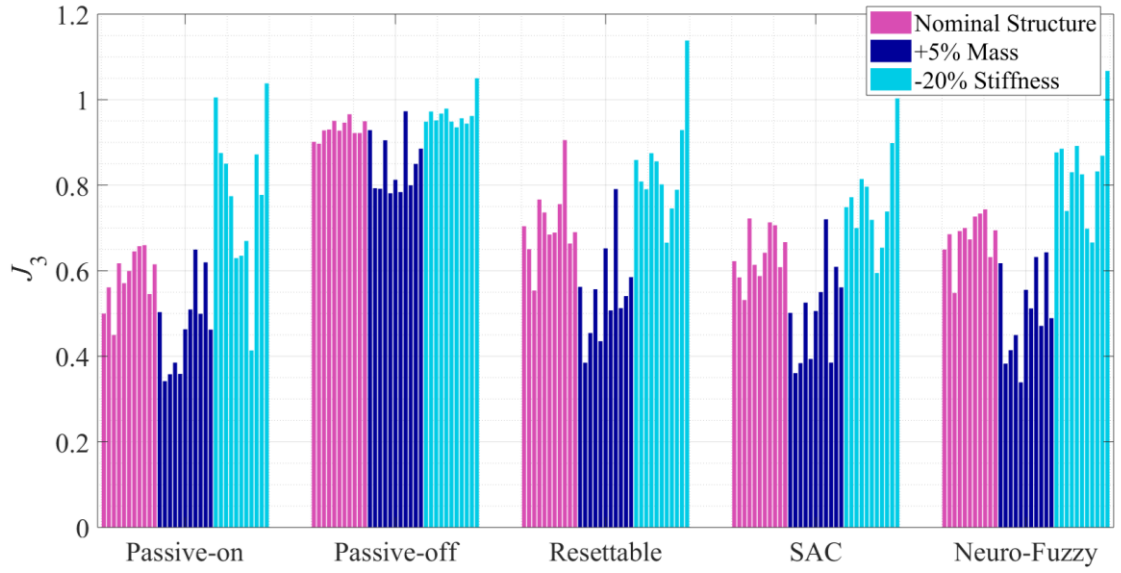

Fig. B.9: Maximum J_3 (peak base moment) for the control schemes considering different parametric configurations and earthquake excitations.

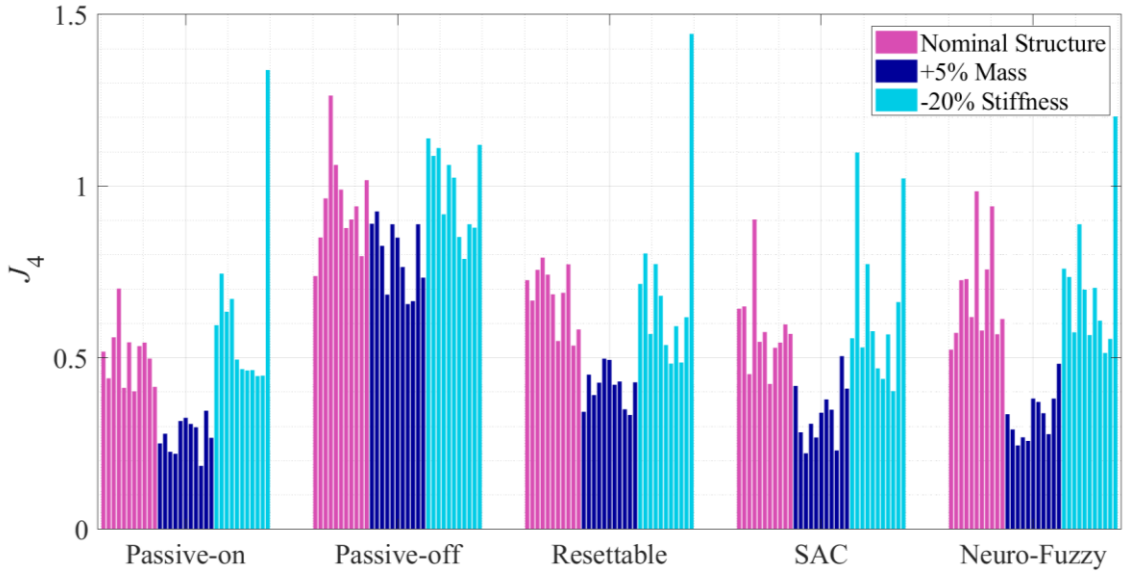

Fig. B.10: Maximum J_4 (peak deck moment) for the control schemes considering different parametric configurations and earthquake excitations.

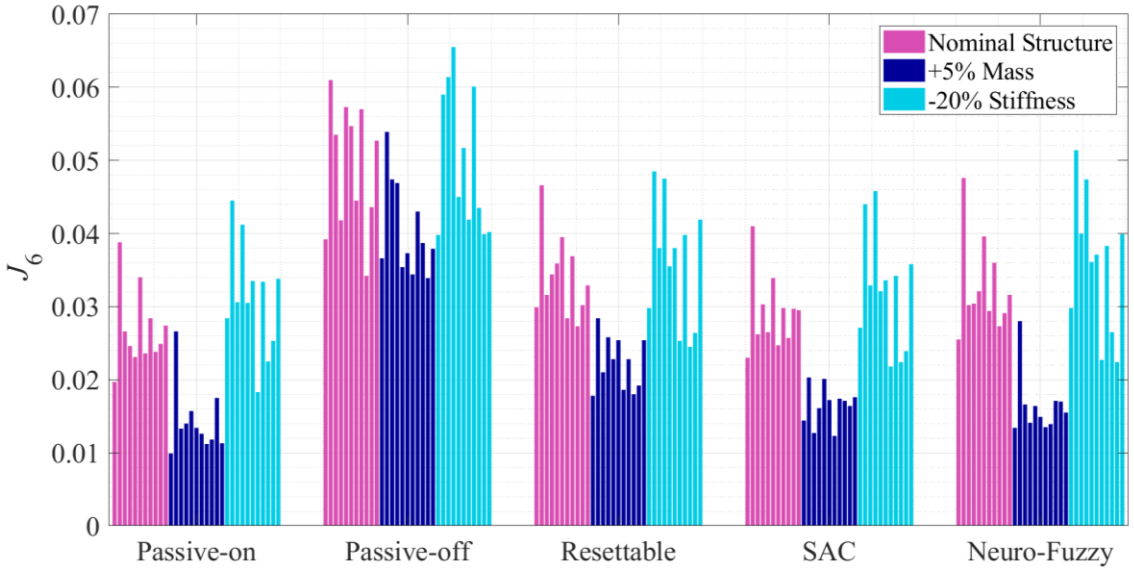

Fig. B.11: Maximum J_6 (peak abutment displacement) for the control schemes considering different parametric configurations and earthquake excitations.

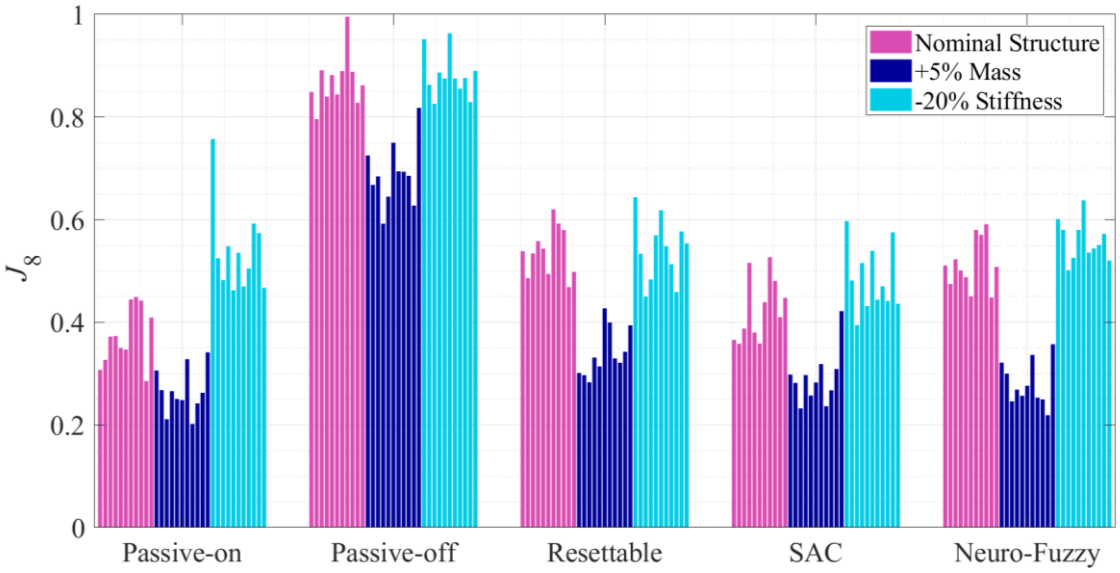

Fig. B.12: Maximum J_8 (normed deck shear) for the control schemes considering different parametric configurations and earthquake excitations.

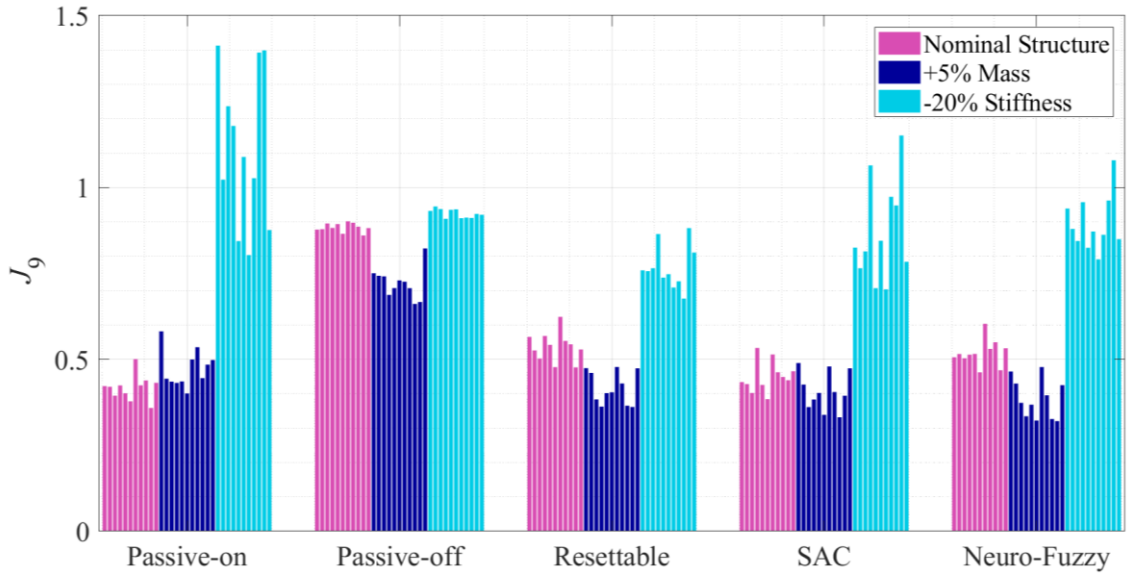

Fig. B.13: Maximum J_9 (normed base moment) for the control schemes considering different parametric configurations and earthquake excitations.

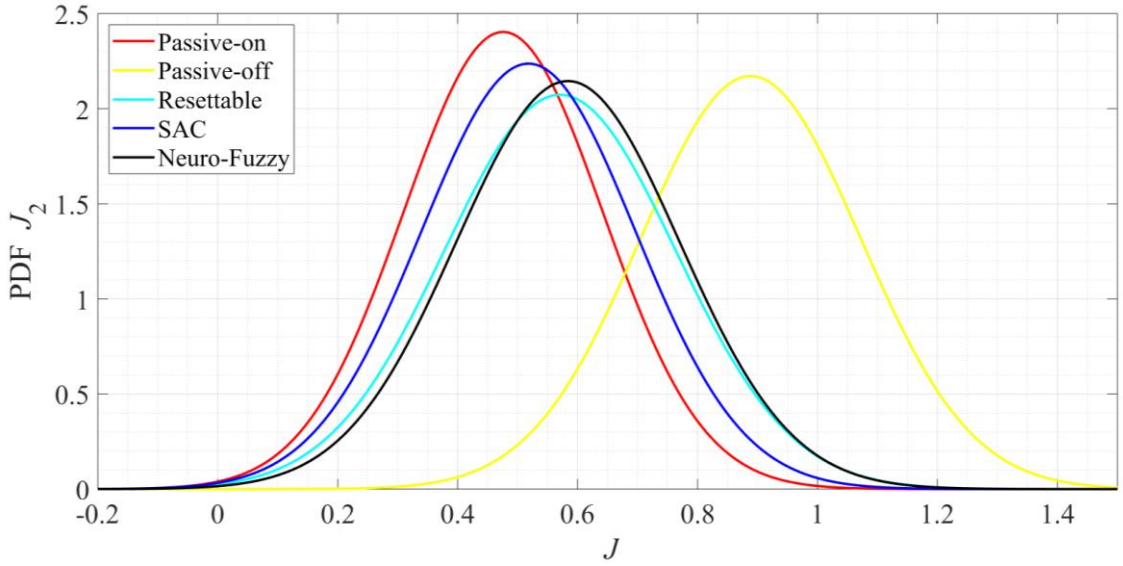

Fig. B.14: Probability density function for all the control schemes- peak deck shear (J_2).

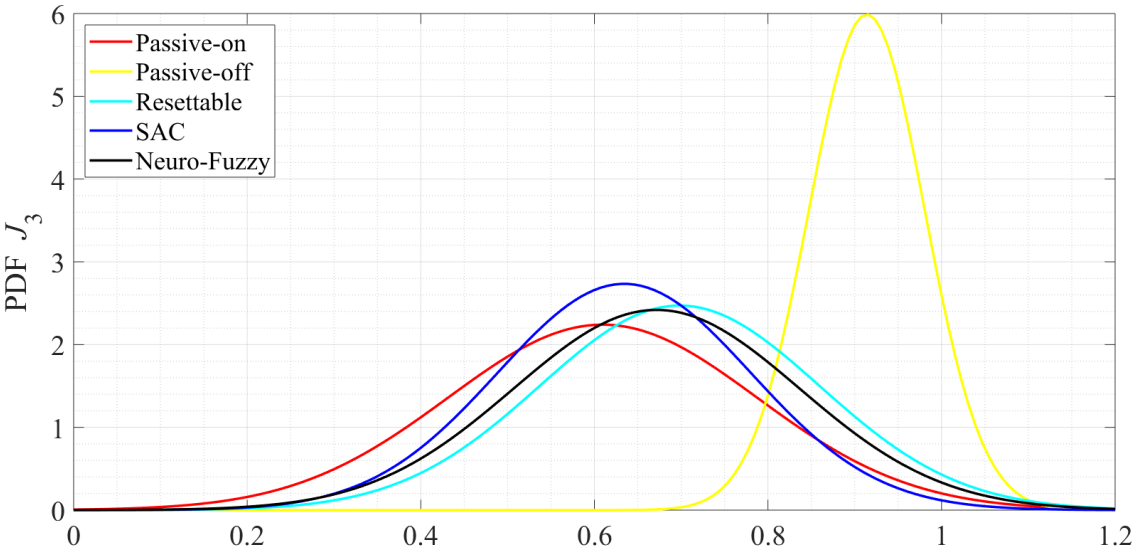

Fig. B.15: Probability density function for all the control schemes- peak base moment (J_3).

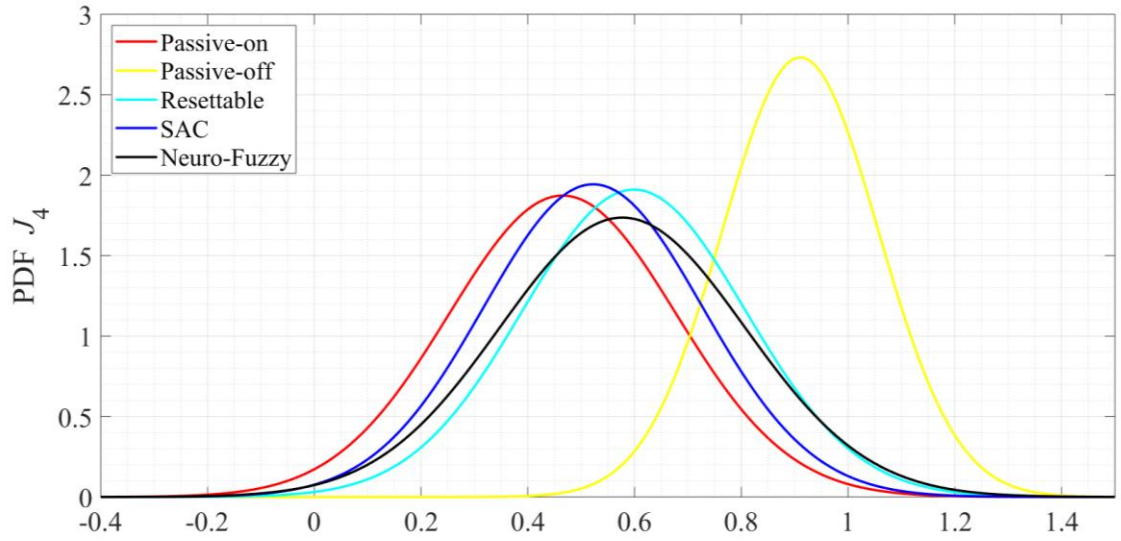

Fig. B.16: Probability density function for all the control schemes- peak deck moment (J_4).

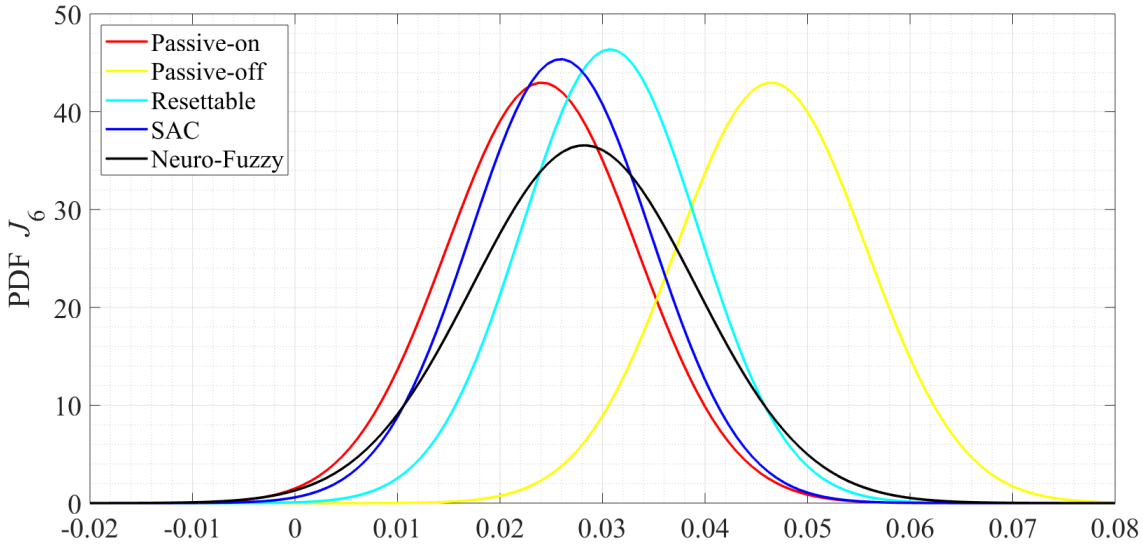

Fig. B.17: Probability density function for all the control schemes- normed deck shear (J_8).

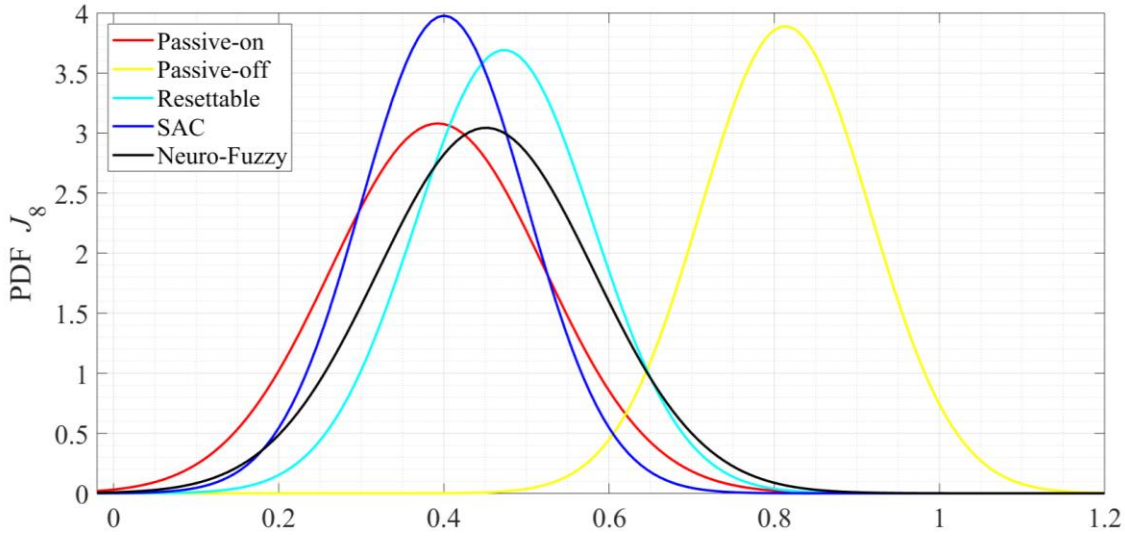

Fig. B.18: Probability density function for all the control schemes- normed deck shear (J_8).

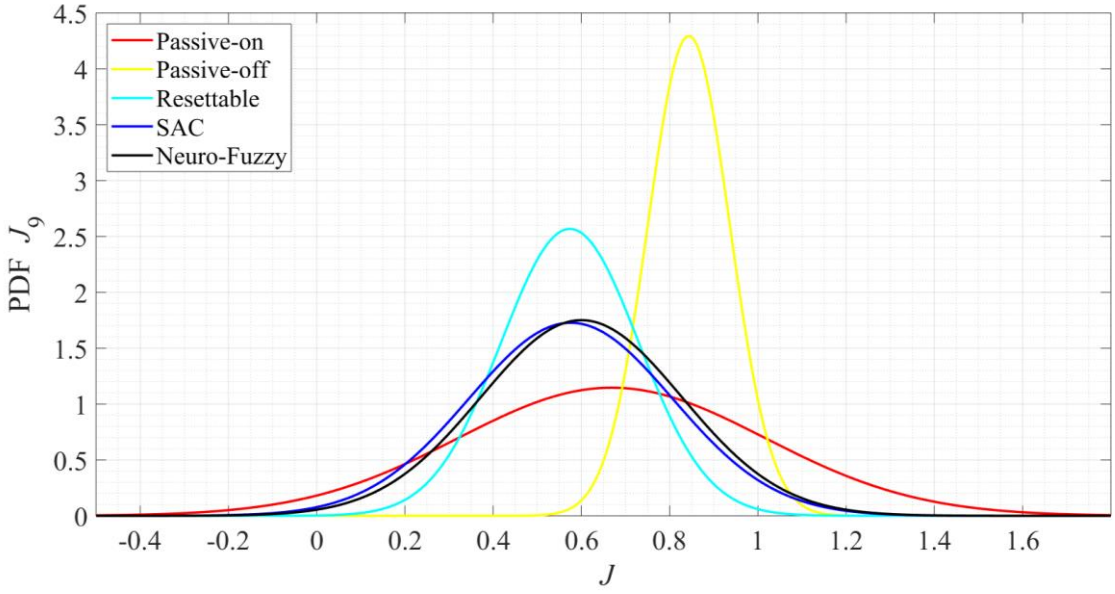

Fig. B.19: Probability density function for all the control schemes- normed base moment (J_9).